EFFECT OF ALUMINA/GNP HYBRID NANOREINFORCEMENT ON WETTING AND MECHANICAL PROPERTIES OF ADHESIVELY BONDED ALUMINIUM ALLOY WITH EPOXY

MOHAMAD SYAIFUL IZWAN BIN ALIES

MASTER OF SCIENCE

UNIVERSITI MALAYSIA PAHANG
AL-SULTAN ABDULLAH

UNIVERSITI MALAYSIA PAHANG AL-SULTAN ABDULLAH

DECLARATION OF THESIS AND COPYRIGHT

Author's Full Name : MOHAMAD SYAIFUL IZWAN BIN ALIES
Date of Birth : 9th AUGUST 1994
Title : EFFECT OF ALUMINA/GNP HYBRID NANOREINFORCEMENT ON WETTING AND MECHANICAL PROPERTIES OF ADHESIVELY BONDED ALUMINIUM ALLOY WITH EPOXY
Academic Session : SEMESTER II 2023/2024

I declare that this thesis is classified as:

☐ CONFIDENTIAL (Contains confidential information under the Official Secret Act 1997)*
☐ RESTRICTED (Contains restricted information as specified by the organization where research was done)*
☒ OPEN ACCESS I agree that my thesis to be published as online open access (Full Text)

I acknowledge that Universiti Malaysia Pahang Al-Sultan Abdullah reserves the following rights:

1. The Thesis is the Property of Universiti Malaysia Pahang Al-Sultan Abdullah
2. The Library of Universiti Malaysia Pahang Al-Sultan Abdullah has the right to make copies of the thesis for the purpose of research only.
3. The Library has the right to make copies of the thesis for academic exchange.

Certified by:

(Student's Signature)

DR. NUR ZALIKHA BINTI KHALIL
PENSYARAH KANAN
FAKULTI TEKNOLOGI KEJURUTERAAN
MEKANIKAL DAN AUTOMOTIF
UNIVERSITI MALAYSIA PAHANG
TEL: 09-431 6191

(Supervisor's Signature)

New IC/Passport Number
Date: 12/6/2024

DR. NUR ZALIKHA BINTI KHALIL
Name of Supervisor
Date: 12/6/2024

NOTE : * If the thesis is CONFIDENTIAL or RESTRICTED, please attach a thesis declaration letter.

THESIS DECLARATION LETTER (OPTIONAL)

Librarian,
Universiti Malaysia Pahang Al-Sultan Abdullah,
Lebuh Persiaran Tun Khalil Yaakob,
26300, Gambang, Kuantan, Pahang.

Dear Sir,

CLASSIFICATION OF THESIS AS RESTRICTED

Please be informed that the following thesis is classified as RESTRICTED for a period of three (3) years from the date of this letter. The reasons for this classification are as listed below.

Author's Name
Thesis Title

Reasons (i)

(ii)

(iii)

Thank you.

Yours faithfully,

____
(Supervisor's Signature)

Date:

Stamp:

Note: This letter should be written by the supervisor and addressed to the Librarian, *Universiti Malaysia Pahang Al-Sultan Abdullah* with its copy attached to the thesis.

اونيۏرسيتي مليسيا ڤهڠ السلطان عبدالله
UNIVERSITI MALAYSIA PAHANG
AL-SULTAN ABDULLAH

SUPERVISOR’S DECLARATION

I/We* hereby declare that I/We* have checked this thesis/project* and in my/our* opinion, this thesis/project* is adequate in terms of scope and quality for the award of the degree of *Doctor of Philosophy/ Master of Science.

DR. NUR ZALIKHA BINTI KHALIL
PENSYARAH KANAN
FAKULTI TEKNOLOGI KEJURUTERAAN
MEKANIKAL DAN AUTOMOTIF
UNIVERSITI MALAYSIA PAHANG
TEL: 09-431 6191

(Supervisor’s Signature)

Full Name : DR. NUR ZALIKHA BINTI KHALIL
Position : SENIOR LECTURER
Date : 12/6/2024

Fraunhofer
IFAM
Wiener Str. 12 · 28359 Bremen
Germany

(Co-supervisor’s Signature)

Full Name : DR.HOLGER FRICKE
Position : HEAD OF DEPARTMENT FOR ADHESIVE BONDING TECHNOLOGY AT FRAUN HOFER IFAM, GERMANY
Date : 12/6/2024

اونيۏرسيتي مليسيا ڤهڠ السلطان عبدالله
UNIVERSITI MALAYSIA PAHANG
AL-SULTAN ABDULLAH

STUDENT’S DECLARATION

I hereby declare that the work in this thesis is based on my original work except for quotations and citations which have been duly acknowledged. I also declare that it has not been previously or concurrently submitted for any other degree at Universiti Malaysia Pahang Al-Sultan Abdullah or any other institutions.

(Student’s Signature)

Full Name : MOHAMAD SYAIFUL IZWAN BIN ALIES
ID Number : MMF19006
Date : 12/6/2024

EFFECT OF ALUMINA/GNP HYBRID NANOREINFORCEMENT ON WETTING AND MECHANICAL PROPERTIES OF ADHESIVELY BONDED ALUMINIUM ALLOY WITH EPOXY

MOHAMAD SYAIFUL IZWAN BIN ALIES

Thesis submitted in fulfillment of the requirements
for the award of the degree of
Master of Science

Faculty of Mechanical and Automotive Engineering Technology

UNIVERSITI MALAYSIA PAHANG AL-SULTAN ABDULLAH

JUNE 2024

ACKNOWLEDGEMENTS

First and foremost, all praise and gratitude to Almighty God for giving me good health and the strength throughout completing my project successfully. Many people lend their hands to me throughout this very valuable and priceless journey and there is no word to describe their contribution and time spent to help me to complete this project. Sincerely from the bottom of my heart, I would like to send my upmost gratitude and thanks each one of them and apologies for any mistake or behaviour on my side.

I am grateful and like to express my sincere gratefulness to my supervisor. Dr Nur Zalikha binti Khalil as well as my co-supervisor Dr. Holger Fricke for their prodigious ideas, invaluable guidance, continuous encouragement and unbroken support who she has been the main drive throughout this master degree project until my research study has been done successfully. I am very thankful for her tolerance and patience of my naïve mistakes and her full commitment and cooperation during my research study. All her sacrifice will be very much appreciated.

I also wish to express my sincere thanks to all the lecturers, laboratory staffs of Faculty of Mechanical and Automotive Engineering Technology, Universiti Malaysia Pahang Al Sultan Abdullah, especially to Mr Zulkarnain, Mr Khairul, Mr Rozikin and Puan Saadah for their guidance and permission on the usage of the equipment and facilities for my project in order to be completed.

Finally, and most importantly, I acknowledge my sincere indebtedness and gratitude to my parents, Mr. Alies Bin Hj. Ibrahim and Puan Che Munah Binti Che Mat and also my siblings for their love and sacrifices throughout my life who gave me relentless support in terms of time, financially, emotionally and morally for me to complete my studies. Literally, I would not be here writing this without them. I would like to thanks my fellow friends who encouraged me and giving me motivation and moral support to me throughout my years of studies until it is completely done.

Thank you.

ABSTRAK

Pengukuhan nanopartikel hibrid telah menunjukkan peningkatan ketara dalam kekuatan ikatan berbanding dengan komposit polimer dengan penguatan nanopartikel tunggal. Walau bagaimanapun, pada ketika ini hasil eksperimen agak terhad dan penyelidikan mengenai kesan parameter kandungan berat nano-penguatan dan gabungan nisbah berat kepada kekuatan penggabungan pelekat perekat belum dibincangkan secara komprehensif. Dalam kajian ini, kesan penguatan nano hibrid alumina / GNP pada tingkah laku basah, sifat tarikan dan tingkah laku patah telah dikaji. Hubungan antara sifat-sifat itu juga dikaji. Dalam kajian semasa, perekat epoksi yang dimodifikasi dengan pelbagai kandungan nanopartikel (0.5, 1.0, 1.5 dan 2.0 wt%) dan pelbagai kombinasi nisbah berat (10:0, 7:3, 5:5, 3:7 dan 0:10 alumina: GNP) telah dibuat menjadi spesimen ASTM E8 dan digunakan dalam specimen ASTM D1002. Untuk kekuatan tarik spesimen ASTM E8, peningkatan tertinggi (64.75%) ditunjukkan pada kandungan nanopartikel hybrid pada 1.5 wt%, dengan korelasi terkuat (R = 0.52) antara nisbah GNP dan kekuatan tarik. Sementara itu, untuk perpanjangan patah, peningkatan maksimum (130.77%) diperhatikan pada 1.5 wt% kandungan nanopartikel hibrid, dengan nilai korelasi R = 0.65 antara nisbah berat alumina dan perpanjangan patah. Dalam sendi gunting lap, peningkatan kekuatan dan perpanjangan patah yang paling tinggi berlaku dengan kandungan nanopartikel hibrid pada 1.5 wt% dengan masing – masing mencatatkan peningkatan sehingga 15.13% dan 10.53% berbanding dengan spesimen dengan perekat yang tidak diubah suai. Hubungan adalah paling kuat pada beban ini untuk kedua-dua kekuatan (R = 0.89) dan pemanjangan (R = 0.78). Sehingga 1.5 wt% kandungan nanopartikel hibrid, peningkatan nisbah berat alumina meningkatkan tingkah laku basah, dengan kawasan penyebaran meningkat sebanyak 309%. Kesan ini paling ketara pada 0.5 wt% kandungan nanopartikel hibrid. Pada 1.5 wt% kandungan nanopartikel hibrid, mekanisma kegagalan menunjukkan interaksi sinergis yang optimal antara nanopartikel alumina dan nanopartikel GNP. Hubungan positif antara kekuatan pemotongan dan kawasan penyebaran diperhatikan pada beban yang lebih tinggi, dengan korelasi terbaik pada 2.0 wt% kandungan nanopartikel hibrid. Walau bagaimanapun, penambahbaikan sifat memuncak pada 1.0 wt% kandungan nanopartikel hibrid. Ringkasnya, perekat dengan pengukuhan nanopartikel hibrid Alumina / GNP pada 1.5 wt% kandungan nanopartikel hibrid menunjukkan keseimbangan yang optimal dari sifat tarikan yang dipertingkatkan, kekuatan pemotongan, perpanjangan keretakan, tingkah laku basah, dan interaksi kegagalan. Walaupun pada 2.0 wt% kandungan nanopartikel hibrid menunjukkan korelasi sifat-keupayaan yang baik, peningkatan keseluruhan adalah marginal di luar 1.0 wt% muatan alumina / GNP pengukuhan hibrid. Oleh itu, 1.0 wt% alumina / GNP hibrid pengukuhan menunjukkan kandungan nanopartikel hibrid yang optimal dan 7: 3 nisbah berat gabungan nano hibrid Alumina / GNP.

ABSTRACT

Hybrid nanoparticle reinforcement has demonstrated a significant increment in bonding strength compared to polymer composites with a single nano reinforcement. However, experimental results are rather limited and investigation regarding the parametric effects of nano-reinforcement weight content and weight ratio combinations on the joining strength of adhesive joining not yet been discussed comprehensively. To date, the effects of Alumina/GNP hybrid nano reinforcement on wetting behavior, tensile properties and fracture behavior have been studied. The correlation of that properties was studied as well. In current study, epoxy adhesive modified with various nanoparticle content (0.5, 1.0, 1.5 and 2.0 wt%) and various weight ratio combination (10:0, 7:3, 5:5, 3:7 and 0:10 Alumina:GNP) have been fabricated into ASTM E8 and ASTM D1002 specimens. For the tensile strength of the ASTM E8 specimen, the highest improvement (64.75%) was demonstrated at 1.5 wt% loading, with the strongest correlation (R=0.52) between GNP ratio and tensile strength. Meanwhile, for fracture elongation, the maximum increment (130.77%) was observed at 1.5 wt% loading, with the correlation value of R=0.65 between alumina weight ratio and fracture elongation. In lap shear joints, the highest increases in strength and fracture elongation occurred with 1.5 wt% hybrid nanoreinforcement content with increment up to 15.13% and 10.53% respectively as compared to specimen with unmodified adhesive. Correlations were strongest at this loading for both strength (R=0.89) and elongation (R=0.78). Up to 1.5wt%, increased of alumina weight ratio improved wettability, with spread area rising by 309%. The effect was most pronounced at 0.5 wt%. At 1.5 wt% loading, failure mechanisms showed optimal synergistic interactions between alumina and GNP nanoparticles. A positive relationship between shear strength and spread area was noted at higher loadings, with the best correlation at 2.0 wt%. However, property improvements peaked at 1.0wt%. In summary, the adhesive with 1.5 wt% Alumina/GNP hybrid nanoparticle reinforcement demonstrated the optimal balance of enhanced tensile properties, shear strength, fracture elongation, wettability, and failure interactions. While 2.0 wt% exhibited good property-wettability correlations, the overall improvements were marginal beyond 1.0 wt% loading of alumina/GNP hybrid nanoreinforcement. Therefore, 1.0 wt% alumina/GNP hybrid nanoreinforcement seems to be the optimal hybrid nanoparticle concentration and 7:3 weight ratio combination of Alumina/GNP hybrid nano reinforcement.

TABLE OF CONTENT

LIST OF TABLES

LIST OF FIGURES

LIST OF SYMBOLS

Θ	Angle
Ø	Diameter
σ	Tensile strength
τ	Shear strength
Δl	Fracture elongation
t_A	Thickness adhesive
°C	Degree Celsius
l	Height
A	Spread area
A_i	Initial spread area
A_f	Final spread area
t	Curing time
h	Drop height
R	Radius
%	Percent
Wt%	Nanoparticle content

LIST OF ABBREVIATIONS

AA7075	Aluminium alloy 7075
AF	Adhesive fracture
AG	Silver flakes
AL_2O_3	Aluminum oxide
ALUC	Alumina calcined fumed
ASTM	American society for testing and materials
C_2H_5OH	Ethanol
$CaCO_3$	Calcium carbonate
CB	Carbon black
CF	Cohesive fracture
CNF	Carbon nanofiber
CNT	Carbon nanotube
Cps	Centipoise
EG	Expended graphite flakes
FESEM	Field emission scanning electron microscopy
FE_2O_3	Iron oxide black
GNP	Graphene nanoplatelets
HNT	Halloysite
KHz	Kilo hertz
MAM	Methymethacrylate-butylacrylate-methylmethacrylate
MGP	Multi-graphene platelets
MGOH	Magnesium hydroxide
MPa	Mega pascal
MWCNT	Multi-walled carbon nanotube
OM	Optical microscope
POSS	Polyhedral oligomeric silsesquioxanes
PVA	Polyvinyl alcohol
RGO	Reduced graphene oxide
SBM	Styrene-butadiene-methyl methacrylate
SLJ	Single lap joint
SiC	Silicon carbide

SiO_2	Silicon oxide
SWCNT	Single-walled carbon nanotube
TiO_2	Titanium dioxide
Zr	Zirconium

LIST OF APPENDICES

CHAPTER 1

INTRODUCTION

1.1 Research background

Adhesive joining is a process that uses adhesives to join at least two or more substrates together (Wei et al., 2024; Zhou and Chen, 2024). In recent years, the use of adhesives has gained popularity due to their flexibility in joining similar and dissimilar materials such as metal to metal, metal to composite and composite to plastic materials (Vlasov et al., 2023). Additionally, adhesives require fewer processing requirements, leading to low-cost manufacturing compared to conventional joining techniques such as mechanical fastening, welding and soldering (Jojibabu, Zhang, and Prusty, 2020). Furthermore, adhesively joined materials also possess a high strength-to-weight ratio, allowing for a wider surface area attachment. This characteristic improves the ability of the joint to flex, absorb force and transmit the rest of it across the surface area, contributing to a more uniform stress distribution throughout the bonding area (Kong and Khalil, 2022; Otorgust et al., 2017). These advantages have enabled adhesive joining to be widely utilised in various industrial applications such as aircraft (Jojibabu, Zhang, Rider, et al., 2020; Kong and Khalil, 2022), automotive (Wei et al., 2024), marine (Hentinen, 2021), construction (Vallée and Albiez, 2021) and electronics (Nassiet et al., 2021).

As mentioned earlier, adhesive joining is a preferred joining technique in various industries, including automotive and aerospace primarily due to its ability to join dissimilar materials. This allows for joining multiple lightweight materials to meet ecological and government standards, contributing to the reduction of carbon footprint (Queval et al., 2024). Aluminum alloy is widely used in the automotive and aerospace industries due to its advantageous properties. The automobile industry relies on aluminum alloys for their excellent formability, low weight, high resistance to corrosion, ductility, and high fuel economy (Ouyang and Chen, 2023). This ability to join dissimilar materials is a significant advantage of adhesive bonding over traditional joining methods, providing manufacturers with a wider range of materials to work with.

However, adhesive joining suffers from low mechanical properties due to weaker polymer adhesive properties compared to the adherends they join, resulting in premature failure at the joining ends/edges (Alies and Khalil, 2022; Khalil et al., 2019). To address this issue, several approaches have been proposed. Among the available methods, the reinforcement of nanoparticles into polymer adhesives has gained significant attention due to several advantages (Jojibabu et al., 2016). Previously studies have demonstrated that the addition of a single nanofiller enhances the performance of adhesive itself by promoting stress transfer and ensuring uniform stress distribution within the polymer matrix (Khalil et al., 2019). The presence of nanofillers has also been shown to facilitate penetration into small gaps or voids on the adherend surface, leading to an increase in the mechanical strength of the joining components through interlocking. In a previous investigation conducted by Khalil et al. (2019), the addition of 1.5wt% of alumina into epoxy adhesive demonstrated a shear strength improvement of up to 54.2% compared to the pristine adhesive counterpart. In another study, Chavooshian et al. (2017) reported that the inclusion of 1.5wt% of SiC into acrylic adhesive demonstrated an enhancement of shear strength up to 17.8% compared to unmodified adhesive. These improvements have been attributed to the efficient stress transfer mechanism between the nanofiller and polymer matrix, thereby improving mechanical properties and the joining strength (Çakır, 2023). Moreover, it was also proposed that the nanofillers contribute to the toughening mechanism for the adhesive-adherends interphase through nanoparticles breakage, bridging, crack deviation and pull-out mechanisms (Ahmadi, 2019).

Meanwhile, in recent years, there has been an increasing trend of combining two or more nanofillers of different composition into polymeric materials (Kesavulu and Mohanty, 2019). These innovations stem from the prospect of obtaining distinct yet desirable characteristic in the resultant composite materials, which are difficult to achieve with the utilisation of single nano reinforcement alone. Hybrid nanoparticle reinforcement has demonstrated a significant increment in bonding strength compared to polymer composites with a single nano reinforcement. Regarding adhesive joining, it has been reported that the addition of 0.5 wt% hybrid ozone-functionalised carbon nanotube/ Styrene-Butadiene-Methyl methacrylate (OZ-CNT/SBM) with a 10:3 weight ratio combination into epoxy adhesive demonstrated an improvement in shear strength up to 112.0% and 32.0% compared to pristine adhesive and a single SBM counterpart respectively (Jojibabu et al., 2020a). This improvement was attributed to the presence of more surface contact area between the nanofiller and epoxy as well as the surface (Osman et al., 2021) in the polymer composite, leading to a more efficient mechanical interlocking due to improved interfacial adhesion. Meanwhile, Razavi et al. (2018a) demonstrated that the inclusion of 0.8 wt% hybrid SiC/MWCNT nanofiller at a 1:1 weight ratio combination into epoxy adhesive resulted in an improvement in shear strength of aluminium/epoxy composite joints up to 28.3% compared to joining specimens with unmodified epoxy. This improvement was attributed to the plastic deformation around microcracks and the uniform distribution of the nanofiller. Subramanian et al. (2016) reported that the inclusion of 0.5 wt% hybrid polydopamine (PDA)/MWCNT at a 2:1 weight ratio combination recorded an improvement in shear strength up to 28.3% compared to the pristine adhesive. This improvement was due to the better interaction among nanoparticles and between nanoparticles and the aluminium substrate surface, leading to a remarkable improvement in joining strength.

Wetting behaviour, on the other hand, also plays an important role in the joining strength and failure mode of the adhesive joints (Cui et al., 2020). In essence, appropriate wetting is crucial to allow for sufficient spreading of the adhesive onto the adherend. Sufficient wetting of the adhesive generally results in a more uniform bond line thickness, leading to subsequent higher bonding performance (Ahmadi, 2019). For instance, Khalil et al. (2019) reported improved wetting behaviour in adhesive joining utilising epoxy adhesive with alumina nanoparticle. Meanwhile, Dorigato and Pegoretti, (2011) reported that the incorporation of calcined alumina (AluC) enhanced the wettability between the adhesive and substrate with a contact angle of 56.0°, which had a favourable impact on the joining performance. Dorigato et al. (2010) reported that the addition of Zirconia nanoparticles (Zr) into epoxy adhesive significantly reduced the equilibrium contact angle values up to 76.0° due to better interfacial wettability between the adhesive and substrate, resulting in a higher bonding efficiency of up to 59.74MPa.

1.2 Problem statement

From these literatures, it appears that the use of hybrid nanoparticles in polymer adhesives has shown significant potential for achieving superior bonding performance compared to their unmodified and single nano-reinforced adhesive counterparts (Jojibabu et al., 2020b; Kesavulu and Mohanty, 2020) due to several strengthening mechanisms. Nevertheless, to date, experimental results are rather limited and investigation regarding the parametric effects of nano-reinforcement weight content and weight ratio combinations on the joining strength of adhesive joining have not yet been comprehensively reported. Furthermore, to the best of the author's knowledge, the investigation regarding the correlation between hybrid nano-reinforcement, wetting behaviour, tensile properties and fracture behaviour has not yet been reported comprehensively. Therefore, there is a need to address this issue by systematically investigating the effect of hybrid nano-reinforcement on these elements to gain a holistic understanding of the behaviour of adhesive joining.

1.3 Research objectives

To address the aforementioned concern, in this thesis, a systematic investigation has been carried out with the following objectives:

i. To study the effect of Alumina/GNP hybrid nano reinforcement on wetting behaviour of epoxy adhesive and correlate these findings with the tensile and fracture properties of the adhesive.

ii. To assess the impact of varying Alumina/GNP hybrid nano reinforcement content and weight ratio combination on the tensile properties (shear strength and fracture elongation) of single lap joint specimens (ASTM D1002) and ASTM E8 specimen.

iii. To explore and correlate the effect of Alumina/GNP hybrid nano reinforcement on the fracture behaviour and surface morphology of the tested specimen.

1.4 Research scopes

The aim of this study was to investigate the effect of Alumina/GNP hybrid nano reinforcement on the adhesion and mechanical properties of epoxy adhesive. Therefore, the scope of current work would be limited to the:

i. Surface treatment of Aluminium Alloy 7075-T6 as adherend (Abrasive blasting).

ii. Synthesis of alumina/GNP hybrid nano adhesive with various nanoparticle contents (0.0, 0.5, 1.0, 1.5 and 2.0 wt%) and weight ratio combinations (10:0, 7:3, 5:5, 3:7 and 0:10) using magnetic stirrer.

iii. Wetting behaviour analysis (Spread area) of alumina/GNP hybrid nano adhesive by using spreading test setup.

iv. Mechanical properties evaluation of SLJ Specimen and tensile test bulk specimen with Alumina/GNP hybrid nano adhesive by using tensile testing machine.

v. Microstructural characterisation analysis of alumina/GNP hybrid nano adhesive with various concentrations and weight ratio combinations by using Field Emission Scanning Electron Microscopic (FESEM) and open-source software (ImageJ).

1.5 Thesis overview

The present thesis is organized into five subsections in the following ways:

Chapter 1, or also known as the introduction, provides a detailed discussion on the research background, problem statement, research objective and research scope.

In chapter 2, an extensive literature review is presented, encompassing various aspects such as introduction of adhesive bonding, different type of joining and engineering adhesives, practical applications of adhesive bonding in an industrial context, stress concentration behaviour in single lap joint specimens, techniques for enhancing the strength of adhesive joining, wetting characteristics of nano-reinforced adhesives, fracture behaviour of joining specimens, and the utilization of Pearson’s correlation matrix and heatmap analysis for data analysis.

Chapter 3 provides detailed information about the experimental work conducted for this research. In this study, Alumina/GNP hybrid nano reinforcement with various concentrations (0.0, 1.0, 1.5, and 2.0 wt%) and weight ratio combinations (10:0, 7:3, 5:5, 3:7, and 0:10) were incorporated into epoxy adhesive. This chapter also covers the synthesis method of the Alumina/GNP hybrid nano adhesive, the preparation of bulk and single joint specimens, and the analytical methods used for the specimens.

In Chapter 4, a detailed analysis of the experiment results from the current study is presented and discussed. This analysis includes scanning electron microscope (SEM) examination of nanoparticle, specifically Alumina and Graphene Nanoplatelets (GNP), along with an evaluation of the morphology and profilometry of the surface treated adherend for Aluminium Alloy 7075-T6. Additionally, the chapter provides a comprehensive discussion on the impact of the Alumina/GNP hybrid nano reinforcement on wetting (spread ability). The effect hybrid nano reinforcement on tensile properties, such as tensile strength and fracture elongation, for both bulk and joining specimens were examined. Furthermore, the chapter explores the relationships between Alumina nanoparticle and GNP to the spread area, tensile and shear properties, as well as the fracture behaviour of joining specimens. The utilization of a Pearsons correlation matrix and heatmap analysis for a comprehensive investigation of these correlations is discussed as well.

In Chapter 5, an overview of the key findings for each relationship is provided, primarily based on the Pearson correlation matrix. This section also details the most optimal formulation for the hybrid nanoparticle within the context of the current study, and offers suggestions for potential future enhancements.

.

CHAPTER 2

LITERATURE REVIEW

2.1 Introduction

The purpose of this chapter was to provide an overview of the literature reviews and past research related to the scope of the current work. This chapter delved into topics such as adhesive bonding, types of joining, engineering adhesives, application of adhesive bonding, stress concentration in single lap joint specimen, strength improvement techniques in adhesive joining, wetting characteristic of nano reinforced adhesive and summary of literature findings.

2.2 Adhesive bonding

Adhesives are utilised for joining and assembling two or more structural components. Adhesive joining is usually preferred for materials that are non-metal weldable, allowing for the joining of metals to plastics, glass and many other material combinations. This method offers significant advantages over other joining methods, including the ability to quickly attach similar / dissimilar substrate such as such as metal-to-metal, plastic, glass and other material combinations (Hu et al., 2013). Adhesive bonding offers a uniform stress transfer mechanism, thereby reducing stress concentration on the bonded materials (Shang et al., 2019). Adhesive bonding also provides a continuous and larger joining area (Shang et al., 2019), thereby distributing force more efficiently. These advantages have made adhesive bonding preferred joining technique in numerous applications, including automotive (Wei et al., 2024), marine (Kong et al., 2021), space and aerospace industries (Akpinar et al., 2017).

While adhesive joining is advantageous, it comes with certain limitations. These include the requirement of surface preparation before joining (Zhang et al., 2023), longer bonding time and the presence of defects in the joint (Zhou and Chen, 2024). Perhaps, more importantly the primary concern with adhesive bonding is its limitation of strength as compared to conventional joining techniques such as welding and mechanical fastening. This will be discussed in detail in section 2.6.

2.3 Type of joining

When designing adhesive bonding applications, joint design optimisation is a crucial consideration that needs careful attention. Adhesive joints do not impose geometric restrictions on their mechanical binders. During the design phase, it is essential to give special attention to the potential effects of shock and mechanical vibration, especially in applications that involve dynamic bonds. When proposing a common design, installation, manufacturing processes and economic considerations must also be taken into account. In this section, the most widely used joining geometry and design would be discussed.

2.3.1 Butt joint

A butt joint is the simplest structure, which is formed by joining two adherends that are generally in line. There are several advantages when using a butt joint, including ease of manufacture, not requiring any special tools or equipment and being strong enough for most applications. However, butt joints are not as strong as other types of joints, can be challenging to align properly and may not be completely hidden once assembled. Butt joints are commonly used in framing and other construction projects.

2.3.2 Scarf joint

A scarf joint is an overlapping joint where the angle (θ) between the adhesive layer axis and the adherend axis (with the same width and thickness) is greater than 0° (butt joint) and less than 90° (Yousef et al., 2022). This method requires the use of relatively thick adhesive layers at least 10 mm thick (Duncan, 2010). Scarf joint is one of the most widely used adhesive joining techniques because the bonding structure can maintain a uniform thickness throughout the joint (Dilger, 2010). It also has the ability to transfer loads more efficiently and provides higher strength than the single lap joint counterpart (Liao et al., 2013). However, it is important to note that the bonded area of a scarf joint needs to be machined, making the manufacturing of joints more challenging (Barbosa et al., 2018). Despite this, the scarf joint is widely used in structural technology.

2.3.3 T-joint

T-joints are formed when two pieces intersect at a 90° angle, creating a structure resembling the letter 'T'. T-joints are simple and easy to design, requiring little or no edge preparation (Mathers, 2002). These joints are commonly used in thin-walled structures such as wind turbine blades, aircraft wings and fuselage (Wagih et al., 2022). However, when used in primary structures, bonded T-joints may require some reinforcement to stabilise the joint such as small components or mechanical fasteners (pins or bolts) for stronger bonding performance and safety (Dahmen et al., 2020; Wagih et al., 2022). It is important to note that such reinforcement can increase both fabrication costs and the final weight of the structure.

2.3.4 Single lap joint (SLJ)

Single lap joints provide a simple means of joining two materials via an overlapping bond (Lempke, 2013). This type of joint is used in various processes, including soldering, brazing, spot welding and adhesive bonding (Richardson et al., 1994). Single lap joints are particularly popular in the aerospace industry due to their low weight and the absence of stress concentration points associated with drill holes (Natu et al., 2019). However, the single lap joint is an asymmetrical structure. The joining structure will bend during loading due to load eccentricity, resulting in high peel stresses at the edges of the adhesive layer (Duncan, 2010). Table 2.1 summarises the differences in types of joining designs.

In the engineering industry, the widely used type of joint is the SLJ. In this research study, the same type of joining technique was used because it is easier to manufacture and provides a strong bonded construction. Shear loading of the adhesive is considered the most effective method of adhesive loading. When tested at the joining level, the SLJ allows for obtaining an estimation of the adhesives' shear properties; however, it is more suited for the study of the combined performance of the substrates, adhesive and joint geometry (Carbas et al., 2021). Among other joining techniques, the SLJ with metallic or composite adherends is the most prevalent configuration due to its simplicity of geometry and low cost (Carbas et al., 2021).

Table 2.1 Type of joining

Type of joining	Advantages	Disadvantages	Application	Reference
Butt joint 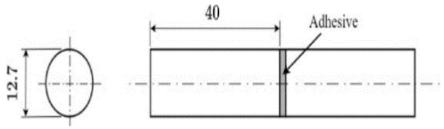	Simple and straight forward design geometry	- Relatively low strength compared to other joining geometry - Can be difficult to align properly	Framing and other construction projects	(Carbas et al., 2021)
Scarf joint 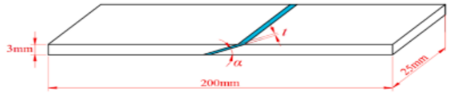	Uniform thickness throughout the joint	Complex manufacturing process	Structural technology	(Barbosa et al., 2018; Dilger, 2010; Duncan, 2010; Liao et al., 2013)
T-joint 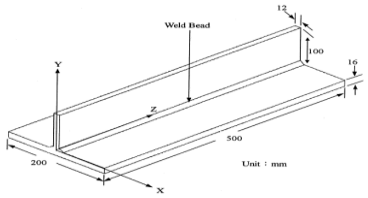	- Simple and easy design - Required little/ no edge preparation	Required reinforcing components	- Aircraft wings and fuselage - Wind turbine blades	(Dahmen et al., 2020; Wagih et al., 2022)
Single lap joint (SLJ) 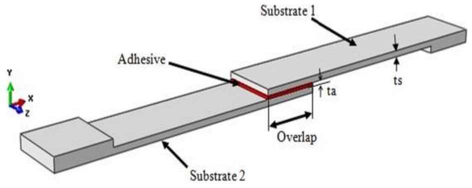	Low cost and simple geometry design	The joining structure will bend during loading due to load eccentricity	Aerospace industry	(Djebbar et al., 2022; Lempke, 2013; Natu et al., 2019)

2.4 Engineering adhesive

2.4.1 Epoxy adhesive

The most commonly used adhesives in a variety of engineering applications are epoxy adhesive. There are several types of epoxy adhesive that are commonly available, usually as one- or two-component systems. One-component epoxies can be applied in the field without using heat (Li et al., 2020), while two-component epoxies, especially cold-curable adhesives, can be cured at room temperature after mixing different components (Cruz et al., 2021). The preferred mechanical characteristics of epoxy adhesive such as high modulus and strength (Cavezza et al., 2020; Razavi et al., 2018) as well as excellent chemical and heat resistance, have been taken into consideration (Deng et al., 2008). However, due to their inherent brittleness and high cross-link density (Jojibabu, Zhang and Prusty, 2020), most cured epoxy adhesives exhibit low fracture toughness, poor resistance to crack initiation and propagation and inferior impact strength (Jojibabu et al., 2020a). In addition, due to their strong adhesion strength, corrosion resistance, chemical resistance and high mechanical strength, epoxy adhesives can be utilised in various applications such as coatings, structural adhesives and flooring tiles (Kesavulu and Mohanty, 2020; Kumar et al., 2019).

2.4.2 Acrylic adhesive

Acrylic adhesive is a common structural adhesive in the market, which is characterised as a viscoelastic material that exhibits properties of both liquids and solids simultaneously. Before and after application, acrylic adhesive maintains a permanent surface stickiness (Czech and Milker, 2003). Various types of acrylic adhesive exist, including toughened acrylic, cyanoacrylate, anaerobic adhesive and UV-curing acrylic adhesive. In practice, polymerization begins when the components are mixed together. As acrylates polymerization progresses, the elastomer precipitates out as very fine particles (approximately 1μm in diameter), simultaneously undergoing graft polymerization with the acrylate (Chavooshian et al., 2017). Acrylic adhesives do not require precise activator measurement, curing quickly at room temperature with a wide range of substrates. The cured adhesive exhibits excellent peel resistance and properties across a broad temperature range (Tutunchi et al., 2016). Moreover, acrylic adhesives offer excellent transparency, weather resistance and heat resistance. They can exhibit various properties such as soft segments, hard segments and functional groups based on the monomer composition (Seok et al., 2022). However, a disadvantage of using acrylic adhesive is that it allows substrates to be easily separated under low pressure without leaving a residue (Lee et al., 2019). Despite this drawback, acrylic adhesives are widely used in the manufacture of tapes, graphic films, display products and medical devices (Lee et al., 2019).

2.4.3 Hot-melts adhesive

Hot-melt adhesives are available in rod, sheet and powder forms, offering a convenient method for assembling small components with light loads. In this method, the rod is heated using a hot gun until it melts, and the melted adhesive is then applied to a component. Upon cooling, the adhesive solidifies, creating a bond between the two surfaces. Hot-melt adhesives consist of three major components: a polymer for mechanical strength, a tackifier for promoting wetting and tack, and wax to reduce viscosity and cost. Antioxidants are commonly added to minimise thermal degradation and oxidation (Robertson et al., 2021). Due to their ability to enable high-speed manufacturing process, hot-melts adhesives are widely used (Kalish et al., 2015). They form a strong bond quickly upon cooling, are compatible with most materials, and are clean and simple to handle. However, hot-melt adhesives have a disadvantage of limited heat resistance and strength (Karakaya et al., 2020). Despite this drawback, they are widely used in food packaging (Jaén et al., 2022), footwear and book-binding (Chu et al., 2020).

2.4.4 Solvent-based adhesive

Solvent-based adhesive is a type of adhesive applied to two surfaces with a solvent solution. It is commonly used as a high-strength contact adhesive in shoe manufacturing and for installing liners on outerwear (Petrie, 2015). The solvent evaporates, leaving a sticky film that adheres to the surfaces. However, these adhesives are difficult to thoroughly remove from non-paper substrates, often leaving adhesive residue that complicates cleaning. Given the increasing market demand for environmentally friendly products that can be cleanly removed from the substrate during domestic or industrial cleaning processes (Czech, 2006), solvent-based adhesives face a disadvantage. The cost of these adhesives is influenced by the use of solvents, which are employed to reduce viscosity and provide good coating properties. The evaporated solvent must be recovered or treated after the adhesive application. As solvents are primarily petrochemical in nature, they are subject to the high price and volatility associated with crude oil (Petrie, 2015). Common applications of solvent-based adhesives include self-adhesive tapes, labels, sign and marking films, protective films as well as in dermal dosage systems for pharmaceutical applications and in biomedical electrodes (Kim et al., 2022).

Table 2.2 summarises various types of engineering adhesives. In the current study, epoxy adhesive was chosen due to its widespread availability, common usage, and ease of accessibility in the market. Epoxy adhesive is an ideal choice for bonding materials that are difficult to bond with other adhesives, including metals, ceramics and composites. It is also effective for bonding materials with different coefficients of thermal expansion, addressing a challenge that can cause stress and eventual failure in other types of adhesives. Because of its high mechanical strength and durability, epoxy adhesives are commonly used as structural adhesives in aerospace, electronics, civil and packaging applications (Jojibabu et al., 2020). Epoxy adhesive has wide range of applications, including the coatings, structural adhesives, flooring tiles and various other purposes (Kesavulu and Mohanty, 2020; Kumar et al., 2019). Epoxy adhesive offers several advantages over other types of adhesives. It exhibits excellent chemical resistance, high strength and good resistance to heat and moisture. Its ability to fill gaps and voids between materials adds to its versatility for various applications. Epoxy adhesive is relatively easy to process and can be used in a range of temperatures and humidity levels. It can be applied using various methods, including brush, spray, roller or injection. Moreover, it cures quickly, enhancing production efficiency and reducing assembly time. In summary, epoxy adhesive stands out as a strong, versatile and user-friendly adhesive, making it an excellent choice for bonding materials that pose challenges for other adhesives. Its high strength, chemical resistance, gap-filling ability, ease of processing and quick curing time collectively contributes to its efficiency and effectiveness in diverse applications, especially in production environments.

Table 2.2 Type of engineering adhesive

Adhesive	Advantages	Disadvantages	Applications	Reference
Epoxy	- High modulus and strength - Excellent chemical and heat resistance	- Low fracture toughness - Poor resistance to crack initiation and propagation, and inferior impact strength.	- Coatings - Adhesives, flooring tiles	(Li et al., 2020;Cruz et al., 2021;Cavezza et al., 2020; Razavi, Neisiany, et al., 2018;Deng et al.,2008;Jojibabu et al., 2020;Kesavulu and Mohanty, 2020; Kumar et al., 2019)
Acrylic	Do not require exact measuring of the activator	Easily separated under weak pressure	Used as tapes, graphic films, display products and medical products	(Czech et al., 2017;Tutunchi et al., 2016;Seok et al., 2022; Lee et al., 2019)
Hot melts	Easy to handle	Limited heat resistance and strength	Food packaging, food wear and book-binding	(Robertson et al., 2021;Kalish et al., 2015;Karakaya et al.,2020;Jaén et al., 2022;Chu et al., 2020)
Solvent-based	High strength adhesive	Leaving traces of adhesive residue on the substrate	Pharmaceutical applications	(Czech, 2006; Kim et al., 2022; Petrie, 2015)

2.5 Application of adhesive bonding in industries

The used of polymer adhesive has been increasingly utilized as structural adhesives in many industrial applications due to their advantages for example flexibility (Vlasov et al., 2023), fewer processing requirements, leading to low-cost manufacturing (Jojibabu, Zhang, and Prusty, 2020) and possess a high strength-to-weight ratio, allowing for a wider surface area attachment (Kong and Khalil, 2022; Otorgust et al., 2017) as discussed earlier in section 1.1.

The diverse characteristics of polymer adhesive and its versatility make it suitable for various industrial applications. Figure 2.1 depicts a forecast of trends in joining processes using different methods. According to the figure, it is evident that after the year 2030, there will be a high demand for adhesives in joining materials due to the possibility of manufacturing lightweight materials.

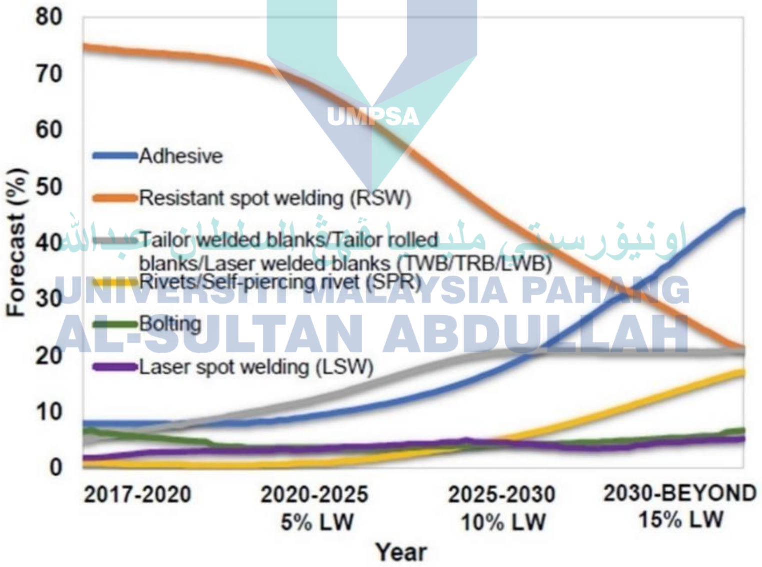

Figure 2.1 Replotted forecast of joining process. LW: Light weighting

Source : CAR Research – Automotive Technology Roadmaps (2017)

2.5.1 Aircraft and spacecraft application

Adhesive bonding has been a prevalent practice in assembling major aircraft structures for over 50 years and remains widely used in contemporary aircraft projects (Higgins, 2000). Epoxy, phenolic or acrylic adhesives are commonly used for structural bonding in aircraft structures. This method is primarily employed to reinforce structures and prevent buckling by attaching stringers to fuselage and wing skins. Additionally, adhesive bonding is instrumental in fabricating flight control components such as elevators, ailerons, spoilers as well as in constructing rigid and lightweight metal honeycomb structures enclosed in metal skin (Higgins, 2000). Figure 2.2 illustrates the use of aluminium honeycomb and adhesive bonding in joining metal to metal within aircraft structures. Given the high cost of composites used in aircraft parts and structures, frequent replacement of damaged structures with new ones is not economically viable.

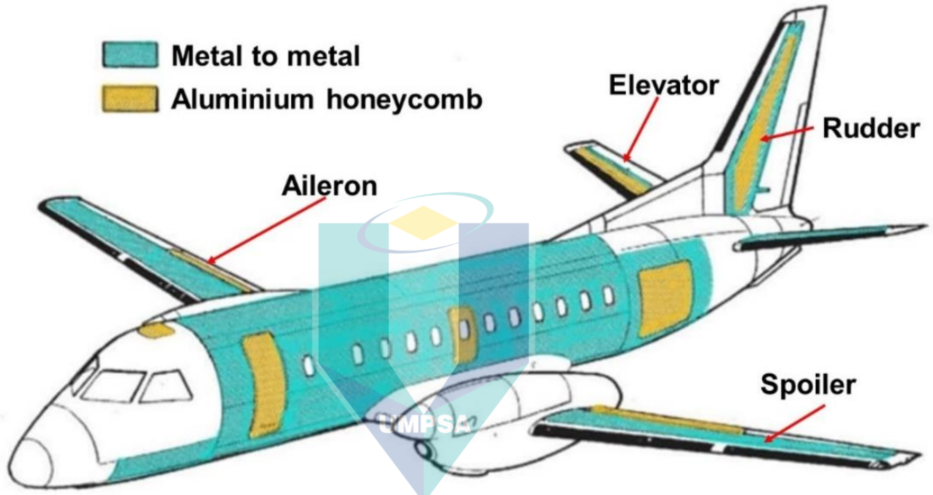

Figure 2.2 Application of adhesive bonding in aircraft

Source : Hart-Smith (2021)

2.5.2 Automotive application

Automotive parts such as roof, doors and engine covers are increasingly crafted from materials such as aluminium alloys, fibre-reinforced plastics and other alloys rather than the traditional steel. Figure 2.3 shows that the widespread application of adhesive bonding in the automotive industry, particularly in modern cars. Adhesives are frequently used in the automotive sector due to the limitations of traditional joining techniques such as riveting, bolting and threading, which may cause stress concentration at threaded holes when combining different materials. Adhesive bonding, which creates a continuous bond rather than a localised point of contact, provides greater joint rigidity compared to mechanical fasteners or spot welds. This results in a more even distribution of stress over a larger area. In some cases, a hybrid joining method is employed to enhance the strength and rigidity of bonded parts. After applying the adhesive between parts and sheets, additional joining processes such as spot welding or mechanical joining (e.g., riveting or clinching) must be carried out while the adhesive is still uncured (Dilger, 2021). A well-designed joint in this context offers good energy absorption, vibration damping and noise dampening properties. Besides sealing the joint against moisture and dirt ingress, the adhesive serves a dual purpose in enabling the joining of dissimilar or incompatible materials. This is achievable because the adhesive layer prevents intimate contact, mitigating the risk of galvanic corrosion. Figure 2.4 shows the use of adhesive bonding in a specific automotive part with a specific purpose.

Figure 2.3 Application of adhesive bonding in modern car

Source : Dilger (2021)

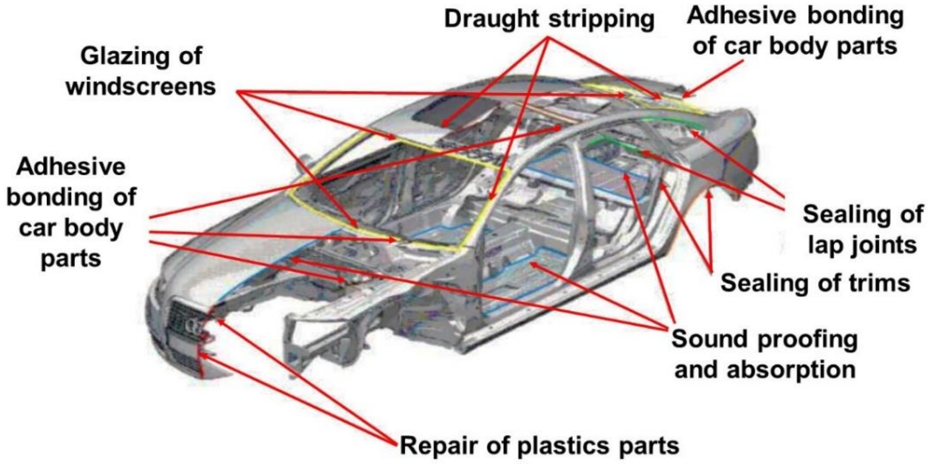

Figure 2.4 The uses of adhesive bonding in specific part of automotive

2.5.3 Naval and marine application

In marine applications, adhesive joining is gaining popularity, particularly in structural joints between significant components such as the hull and deck, stiffeners and hull shell, and bulkheads (Hentinen, 2021). Various materials are used in maritime applications, and adhesive joints often involve two FRP parts (polyester, vinyl ester or epoxy matrix) or a combination of FRP and aluminium. The primary goal of using adhesive bonds, particularly acrylic adhesive, is to prevent water (moisture) from penetrating the bonded region (Marquardt, 2020). Figure 2.5 shows the widespread application of adhesive bonding in marine applications, particularly in boats. Adhesive bonding of windshield and other glass adhesive bonding is becoming increasingly common in maritime applications, particularly in recreational boats. Moreover, glass-FRP joints, glass-aluminium joints, and adhesive bonding of acrylic windows are also feasible.

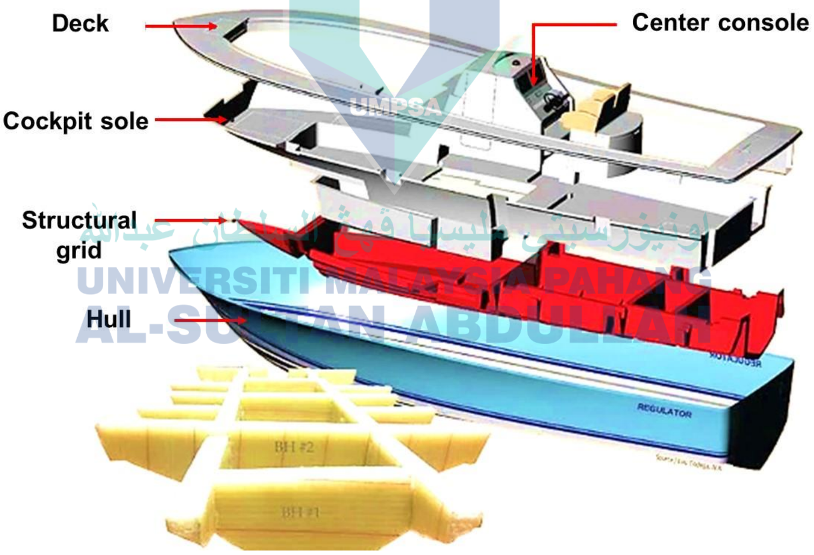

Figure 2.5 Application of adhesive bonding in boat

2.5.4 Electronic application

Joining and sealing similar and dissimilar materials with a wide variety of physicochemical properties is crucial for electronic assembly and package fabrication (Nassiet et al., 2021). Adhesive bonding is applied in electronic industry processes such as Surface Mount Technology (SMT), Printed Circuit Board (PCB) assembly, die attach, flip-chip technology, encapsulation, display devices, microelectromechanical systems (MEMS), and power electronics packaging (Nassiet et al., 2021). Printed Circuit Boards (PCBs) utilise adhesive bonding materials for surface mount components, wire tacking, conformal coatings and encapsulation of electronic components (Gould, 2004). Figure 2.6 shows that the use of adhesives in electronic components. Surface mount acts as a processing aid, holding a part in place during permanent soldering onto another surface. It also helps to relieve stress during the soldering process, preventing premature failure of electrical connections. Structural adhesives are used to secure wire bonding in areas prone to vibration. Adhesives are also used for encapsulating and potting electric components.

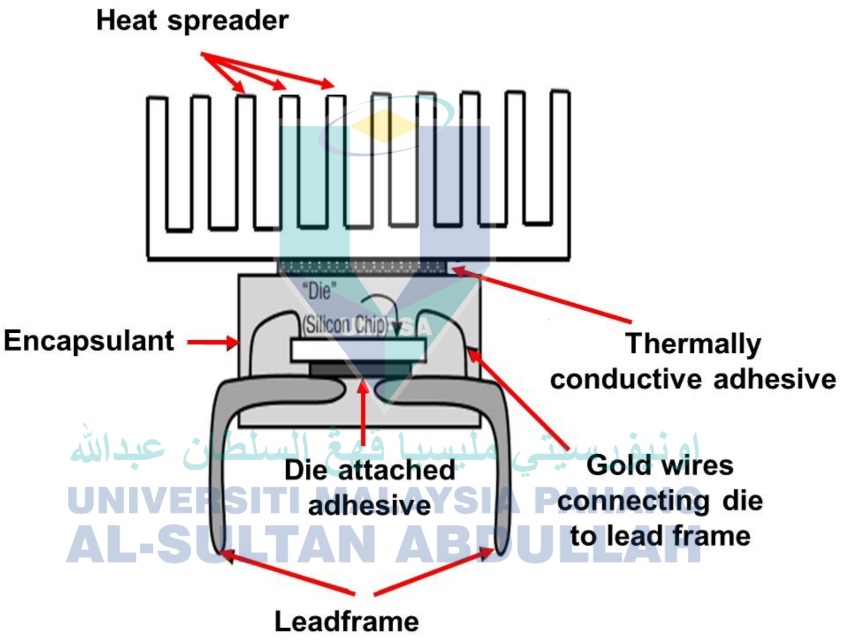

Figure 2.6 Application of adhesive bonding in electronic component
Source : Pocius (2021)

2.5.5 Construction application

Adhesives play a crucial role in construction and civil engineering due to their ability to bond large surfaces, accommodate thick joints and facilitate the joining of different materials such as steel to concrete and components with complex forms (Moussa et al., 2012). Various types of adhesives, including polyurethanes, epoxies and MS polymers, are suitable for construction and each is designed for specific purposes. Structural or semi-structural adhesive joining is commonly used in bridge construction, facilitating connections between segments of concrete bridges, concrete bridge decks and steel girders or joints of steel trusses as shown in Figure 2.7.

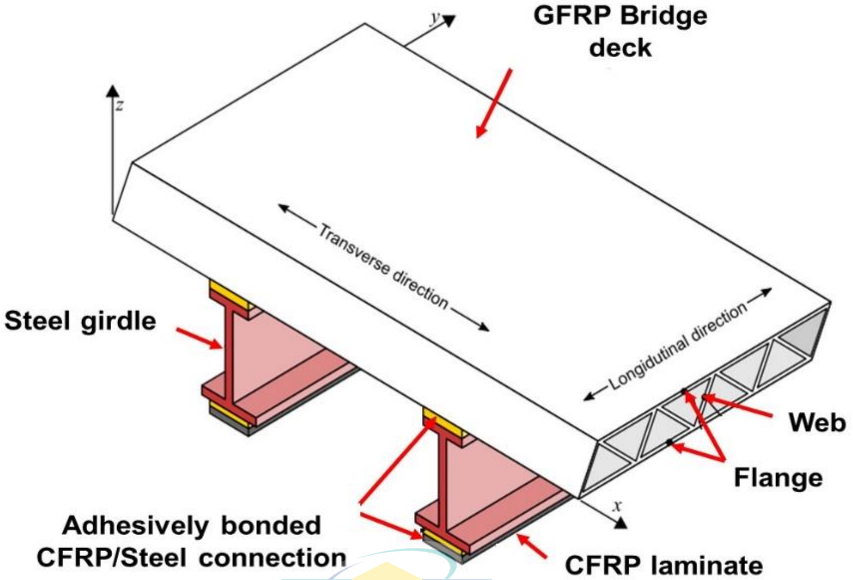

Figure 2.7 Application of adhesive bonding in concrete bridges
Source : Heshmati et al., (2016)

Cold-curing epoxy adhesives are often used for these applications (Messler, 2004; Moussa et al., 2012). In addition, traditional materials like cement, plaster, and natural adhesives find use in bonding and sealing for applications such as ceramic tiles, wall erection and decoration (Camacho et al., 2020). Interior design also benefits from adhesive bonding, with applications including carpet installation, countertop lamination, and attaching laminates and veneers to furniture for decorative purposes. Construction adhesives are suitable for both outdoor and indoor use, adhering to a wide range of surfaces. When water and vapour impermeability is required, universal adhesive tape is appropriate for sealing joints, edges, connections, cracks and overlapping panels. Applications include glass roof structures, skylights, attics, air conditioning and ventilation systems, plumbing pipes, chimneys and corrugated roofing sheets (Jucienė and Dobilaitė, 2021). Figure 2.8 depicts the use of adhesive bonding in building construction.

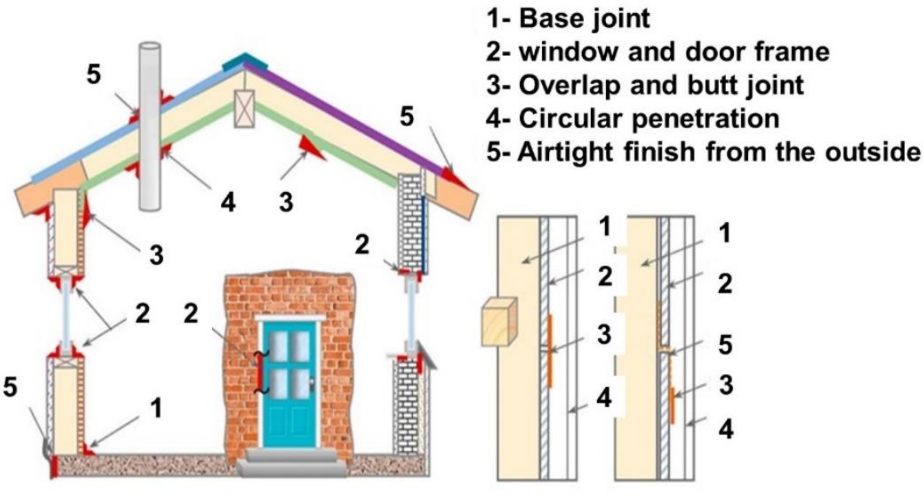

Figure 2.8 Application of adhesive bonding in a building shell airtight
Source : Jucienė and Dobilaitė (2021)

2.6 Stress concentration of single lap joint specimen

As briefly mentioned in Section 1.1, adhesive bonding suffers from poor mechanical properties when compared to other joining methods (Pawlik et al., 2020; Gupta and Veeranjaneyulu, 2017), which is attributed to the premature joint failure at the ends of the joint due to stress concentration at overlapping edges (Tutunchi et al., 2016). In general, when a load is applied to the single lap joint specimen, stresses are distributed across the joint. However, the distribution of stresses is not uniform, where certain areas of the joint may experience higher stresses than others. This phenomenon is known as stress concentration (Mottaghian and Taheri, 2022). The stress concentration value is typically higher at the edges of the overlap region and gradually decreases in the middle overlap of single lap joint, where the material is bent and the load is transferred abruptly, resulting in low joining performance of the specimens as shown in Figure 2.9. In addition, a bending moment occurs in the overlapping area due to eccentric loading since this joint type is subjected to tensile stress (Shishesaz and Hosseini, 2020). This bending moment causes peel stresses to develop at both edges of the joint overlap area.

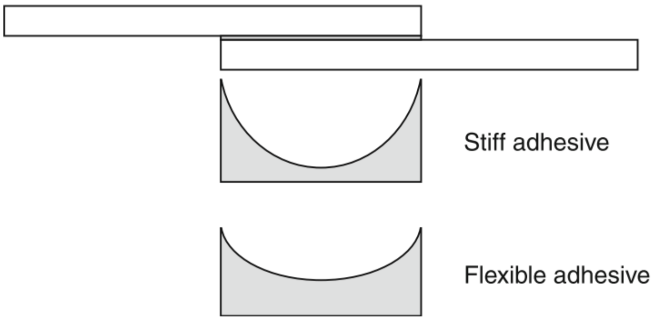

Figure 2.9 Illustration of stress concentration for single lap joint specimen
Source : Lucas F M Silva (2011)

According to Yang (2015), shear stress and peel stress concentrations are generated prominently at the overlap ends, while shear/peel stress distributions are symmetrical along the lap length direction. Nevertheless, peel stress is less than shear stress. The stress analysis along the bonded region in a single lap joint specimen is shown in Figure 2.10. Figures 2.10 (a) and (b) illustrate the shear stress and peel stress concentration respectively of a single lap joint specimen in the mid-surface of the adhesive layer. Peel stress is lower than shear stress despite the clear creation of shear stress and peel stress at the overlap ends, and their distributions are symmetrical along the lap length direction. For these reasons, the primary element affecting joint strength is shear stress.

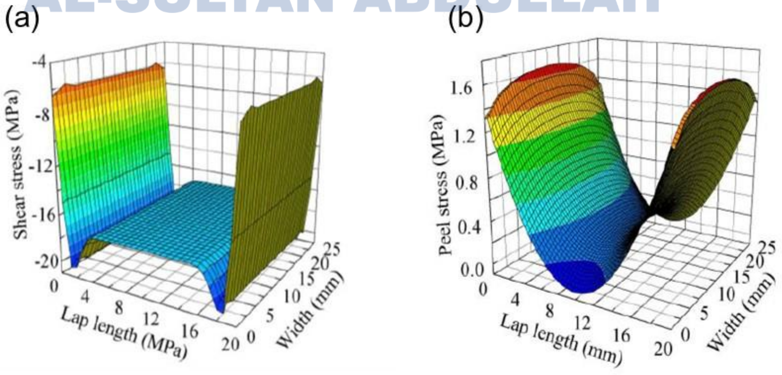

Figure 2.10 Stress analysis of single lap joint specimen (a) Shear stress and (b) Peel stress
Source : Yang (2015)

To address this issue, researchers utilize various techniques such as geometrical modifications, adherend surface treatments, and adhesive modifications, which are discussed in detail in section 2.7.

2.7 Strength improvement techniques in adhesive joining

There are several approaches to minimise the stress concentration that affects the joining strength of SLJ specimens. These include geometrical modification (Grant et al., 2009; Lang and Mallick, 1998), adherend surface treatment (Correia et al., 2018) and adhesive modification (Dorigato and Pegoretti, 2011; Tutunchi et al., 2015a; Zhai et al., 2008; Jojibabu et al., 2020; Kesavulu and Mohanty, 2020; Shadlou et al., 2014) as summarised in Figure 2.11. Firstly, geometrical modification generally involves the alteration of components in the joining such as adherends, adhesive, both adherend and adhesive, and the joining specimens itself. Meanwhile, adherend surface treatment involves the alteration of surface morphology of the adherend with several methods such as sanding, grit blasting, laser treatment, etching and anodization. Finally, adhesive modification involves two methods: the inclusion of single-phase nano reinforcement and hybrid-phase nano reinforcement with various types and sizes of nanofillers. These approaches would be described in detail in the following subsections.

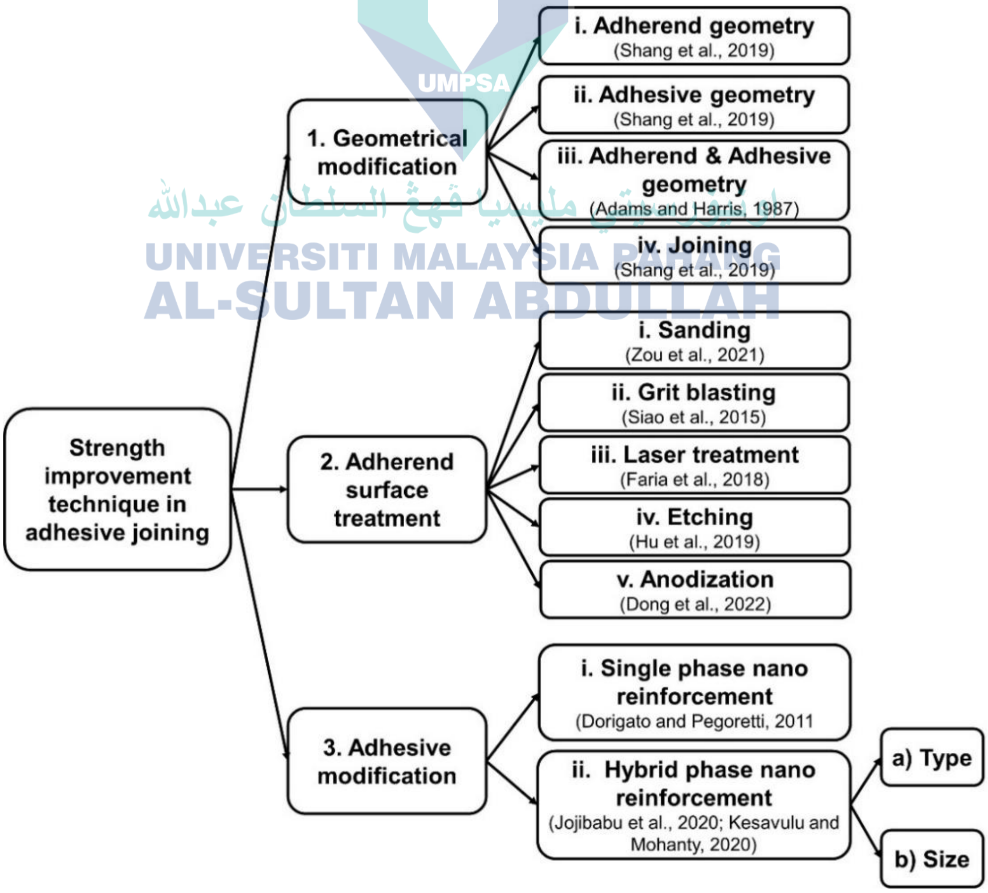

Figure 2.11 Methods for improving joining strength in adhesive joining

2.7.1 Geometrical modification

The modification of geometry is one of the methods to minimise stress concentration in adhesive joining. It generally includes the modification of adherend (Shang et al., 2019), the modification of adhesive (Shang et al., 2019) or a combination of both adherend and adhesive modification (Adams and Harris, 1987) as well as joining modification (Shang et al., 2019). Table 2.3 shows the improvement techniques, which are geometrical modifications to minimise stress concentration. For example, adherend modification can reduce stress concentration by producing the reverse bend joint. The reverse bend joint produces a bending moment in the substrate opposite to that occurring in the conventional single lap joint. According to Razavi et al. (2018), the reverse moment diminishes the maximum peel stress and leads to uniform shear stress through the adhesive layer. A study by Shang et al. (2019) found that the reverse bent configuration was more effective in improving joint strength when a brittle adhesive was used with aluminium substrates. The reverse bent joint adherend modification is not suitable for thick adherends due to angle considerations that are important in reverse bent modification. Meanwhile, areas of excessive adhesive that are squeezed out of the overlap area during the joining process can be modified to form a spew fillet. This is also one of the approaches to reduce stress concentration in SLJ specimens. Lang and Mallick (1998) studied the effect of spew geometries (i.e., full and semi- triangular, full and half circular, full oval and square, and arched type) on the stress distribution across the bond line at the bonding surface of joints with sheet moulding compound adherends. All spew geometries types provided a high percent reduction in maximum stresses. Rispler et al. (2000) reported that peeling stress was reduced by up to 66.0% by improving the shape of fillet shape in double-sided CFRP/titanium bond specimens. The formation and shaping of the spew fillet, along with an increase in its size, can create a smoother transition in the joint geometry and significantly reduce the stress concentrations. The spew fillet increases the load-carrying capacity of the joint and decreases the stress concentration (Doru et al., 2014). In addition, the spew fillet plays an important role in reducing peak adhesive stresses through both load transfer before the overlap area and the elimination of stress concentration at the end of the overlap area (Crocombe and Adams, 1981). Controlling and manufacturing the adhesive fillet is difficult since the adhesive fillet is just squeezed out form the overlap area (Han et al., 2020).

Table 2.3 Improvement techniques to minimize the stress concentration by geometrical modification

Methods		**Advantages**	**Challenges**	**Strengthening mechanism**	**Strength improvement (%)**
Geometrical modification	Adherend modification - Reversed bend joint 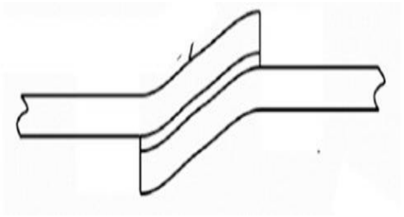 (Razavi et al., 2018; Shang et al., 2019)	Reverse bend joint more effective when using brittle adhesive (Campilho et al., 2011)	Required proper amplitude to achieve best joining performance (Campilho et al., 2011)	Reverse moment diminished the maximum peel stress and lead to uniform shear stress through adhesive layer. (Razavi, Esmaeili, et al., 2018)	+70.0 (Razavi et al., 2018; Shang et al., 2019)
	Adhesive modification - Round spew fillet 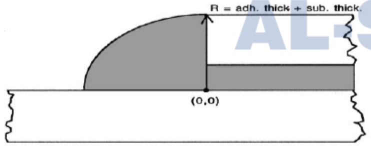 (Lang and Mallick 1998)	Spew fillet provide more uniform stress distribution and load transfer region (Shang et al., 2019)	Difficult to control and manufacture of adhesive fillet (Shang et al., 2019)	The formation shaping spew fillet and increasing its size can create a smoother transition in the joint geometry (Lucas F M Silva, 2011)	+66.0 (Rispler et al., 2000)

Table 2.3 Continued

	Methods	**Advantages**	**Challenges**	**Strengthening mechanism**	**Strength improvement (%)**
Geometrical modification	Adherend and adhesive modification • Inside tapers and adhesive fillet 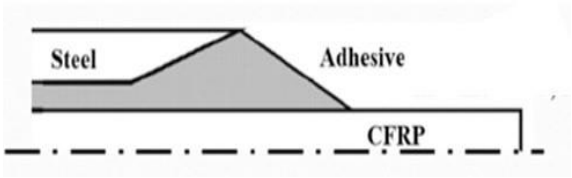 (Shang et al., 2019)	Greater increase in joint strength	Complex design and not possible to realize in practice (Lucas F M Silva, 2011)	Provide smoother transition in joint geometry (Shang et al., 2019)	+40.0 (Silva and Öchsner, 2008)
	Joining 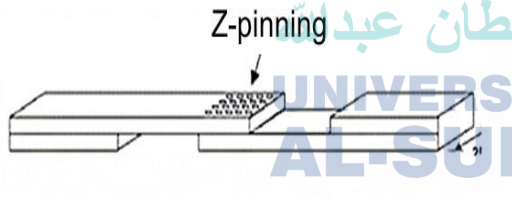 (Chang et al., 2000)	Z-pinning use very small number of pins that provided increasing ultimate transverse strength (M. Li et al., 2016)	Only effective on the thick composite materials (M. Li et al., 2016)	From unstable joint debonding in the absence of pins to stable debonding in the presence of pins (Shang et al., 2019)	+41.0 (Chang et al., 2000)

2.7.2 Adherend surface treatment

Surface treatment is one of the factors that significantly affects joining strength (Lucas et al., 2009). Surface treatment for metallic materials can involve either mechanical treatment (i.e., grinding, sanding, grit blasting, laser treatment) or chemical treatment (i.e., acid etching and anodizing) as shown in Table 2.4. Mechanical treatment increases the surface roughness of the substrate to provide better wetting of the adhesive and a larger surface area. This contributes on a macroscopic level as mechanical forces between the substrate and the adhesive also promotes adhesion. These types of interactions are introduced by changes in surface morphology, with the adhesive penetrating into cavities, voids or pores on the irregular surface to form a mechanical bond (Molitor et al., 2001). Meanwhile, chemical treatment (i.e., acid etching and anodizing) improves the ability of the surface to form chemical bonds with the polymeric adhesive, providing functional groups (e.g., silanes, hydroxides) that are compatible with the chosen adhesive and/or increasing the density of these functional groups. According to Balos et al. (2020), mechanical roughening of the surface adherent by using grit blasting or mechanical abrasion contributes to the improvement of joining strength. Grit blasting is preferred over other methods due to its simplicity, significantly reduced waste generation and cost-effectiveness in surface treatment (Gude et al., 2013). However, it is important to note that abrasive blasting can generate hazardous dust, fumes and noise that that may pose risks to the operator and people nearby. Inhaling the dust and fumes can lead to respiratory problems, while the noise may result in hearing loss.

Meanwhile, Saleema et al. (2012) investigated aluminium A6061 immersed in a 0.1M sodium hydroxide (NaOH) solution for 30 minutes and then rinsed ultrasonically with deionized water to stop the chemical reaction between the adherend and the solution. The etching process resulted in a micro-rough surface, leading to a 60.0% improvement in adhesion strength compared to pristine conditions. The etching process also removed weak surface oxide layers from aluminium alloys, resulting in a scalloped surface morphology (Hu et al., 2019). The etching solution is highly toxic and hazardous during operation and the waste can be harmful if the solution is released into water supplies (Ebnesajjad, 2014). According to Dong et al. (2022), aluminium substrates that undergo an anodization process demonstrated a 36.82% improvement in joining performance due to the presence of a microgroove structure. The anodization process can modify the chemical composition or morphological features of the aluminium substrate surface to improve adhesion performance. However, obtaining an ideal oxide film for better adhesion properties is challenging since optimising anodizing parameters for different types of aluminium proves to be quite challenging.

Table 2.4 Improvement techniques to minimize the stress concentration for mechanical and chemical treatment

	Methods	**Advantages**	**Challenges**	**Strengthening mechanism**	**Strength improvement (%)**
Mechanical treatment	Sanding 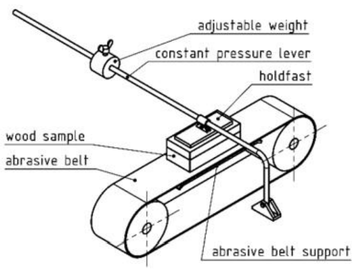 (Sydor et al., 2021)	Removing the material that increase surface energy by changing surface topography	Take long time to sand the material into desired condition	Increases the surface roughness of the substrate to provide better wetting of the adhesive and a larger surface area (Zou et al., 2021)	+22.2 (Zou et al., 2021)
	Abrasive blasting 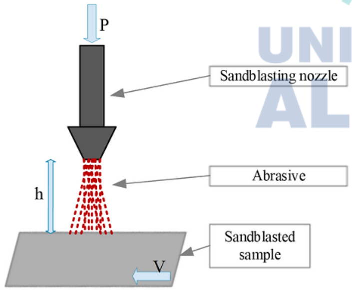 (Miturska-Barańska et al., 2021)	-Increase the surface roughness - Simple method and significantly less waste generation (Gude et al., 2013)	Residual can cause air pollution	Mechanical interlocking (Miturska-Barańska et al., 2021)	+262.8 (Miturska-Barańska et al., 2021)

Table 2.4 Continued

Methods		Advantages	Challenges	Strengthening mechanism	Strength improvement (%)
	Laser treatment 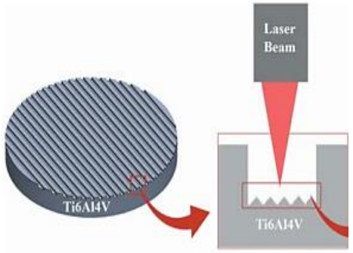 (Faria et al., 2018)	Offers excellent scope of tailoring the surface microstructure (Shoja and Reza, 2011)	Generate of toxic fumes in polymer ablation	Mechanical roughening (Balos et al., 2020)	+6.8 (Wan et al., 2021)
Chemical treatment	Etching 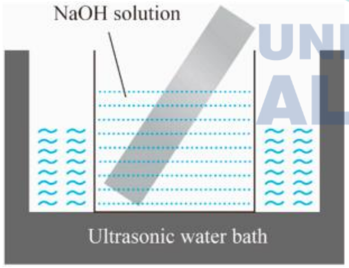 (Hu et al., 2019)	Provide micro rough surface by immersed the substrate in chemical solution depending on etching time (Saleema et al., 2012)	Very toxic and hazardous during operation and the waste is harmful (Ebnesajjad, 2014)	Remove passive oxide layer and allowed formation of hydroxide layers (Hu et al., 2019)	+60.0 (Saleema et al., 2012)

Table 2.4 Continued

Methods		**Advantages**	**Challenges**	**Strengthening mechanism**	**Strength Improvement (%)**
Chemical treatment	Anodization 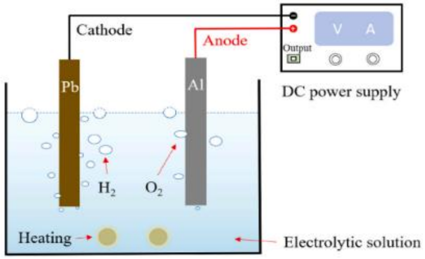 (Dong et al., 2022)	Improve the surface natural ability to oxidation and present the microgroove structure	Difficult to obtain the ideal oxide film for better adhesion, optimizing anodizing parameter for different material type (Dong et al., 2022)	Provide anodized layer which good corrosion resistance and useful adhesion characteristic	+36.8 (Dong et al., 2022)

2.7.3 Adhesive modification

Another approach to reduce stress concentration in a single lap joint specimen is to modify the adhesive by integrating filler reinforcement as shown in Table 2.5. Various types of filler reinforcement, including type, size and geometry, exist. Filler reinforcement can improve the mechanical properties of the adhesive, with both size and type enhancing the superior properties of the matrix. Macro, micro or nanosized fillers exhibit different properties and effects compared to their bulk form (Necati Ataberk, 2020). Particles of sizes on the nanometer scale, typically ranging from 1 to 100 nanometers, are called nanoparticles. Nanoparticles exhibits unique properties compared to larger sized particle of the same materials due to their small size and high surface area -to-volume ratio (Ahmadi, 2019; Carolan et al., 2023; Taylor, 2011). Dispersion of nanofillers into the polymer matrix is widely favoured compared to macro or micro fillers for reinforcement because of their favourable properties, including ease processing and higher property enhancement at 1% to 5% volume fraction (Kartik Shubham et al., 2019; Landowski et al., 2017). Adhesive modification can be achieved with single-phase nano-reinforcement and hybrid reinforcement involving type, size and/or geometry of nanofillers. The improvement in joining strength occurs through several mechanisms, including mechanical interlocking, efficient stress transfer and homogeneous distribution of nanoparticles. The greatest challenges in producing polymer nanocomposites are finding an effective method to control the dispersion of nanoparticles in the polymer matrix (Landowski et al., 2017). An excessive amount of nanoparticles causes the agglomeration of nanoparticles in the polymer matrix, which facilitates crack initiation and propagation (Kesavulu and Mohanty, 2020). The presence of voids and porosities, mechanical air entrapment during preparation and gas created due to chemical reactions during the curing process may also causes a reduction in the strength performance of the nano adhesive (Ahmadi, 2019). The existing voids in epoxy adhesive can make it easier for cracks to propagate through the void and increase the fracture path, thus dissipating energy and resulting in low tensile strength (Shah et al., 2020).

Table 2.5 Improvement techniques to minimize the stress concentration by adhesive modification

Methods		**Advantages**	**Challenges**	**Strengthening mechanism**
Adhesive modification	Single phase nano reinforcement (Dorigato and Pegoretti, 2011; Tutunchi et al., 2015a; Zhai et al., 2008)	Versatile (Kim et al., 2020)	Homogeneous Dispersion (Çakır, 2023; Korayem et al., 2017; J. Wei et al., 2015)	Mechanical interlocking, efficient stress transfer and homogeneous distribution of nanoparticle (Guo et al., 2017; Kaboorani and Riedl, 2012; Tutunchi et al., 2015a)(Kaboorani and Riedl, 2012; Tutunchi et al., 2015a)
	Hybrid nano reinforcement (Jojibabu et al., 2020; Kesavulu and Mohanty, 2020; Shadlou et al., 2014)			Chemical interaction of functional group and reduce agglomeration (Yang et al., 2011)

2.7.3.1 Single-phase nanoparticle reinforcement

2.7.3.1.1 The usage of single nano reinforcement in bulk specimens

In recent years, significant works have been devoted to improve the properties of polymeric adhesives utilised in adhesive joining by reinforcing them with nanoparticles. In this subsection, the results of nanoparticle inclusion into adhesive joining and its mechanisms were briefly summarised. Some types of commercially available nanoparticles exhibit one or more unique physical properties that cannot be achieved at macro level such as carbon-based materials (i.e., Carbon nanotube (CNT), carbon nanofibers (CNF) and graphene nanoplatelets (GNP)), metal-based materials (i.e., alumina (Al_2O_3), zirconia (ZrO_2) and silver (Ag)), and other nanomaterials (i.e., nano clays and nano silicas (SiO_2)) (Shadlou et al., 2014). For example, the addition of carbon-based nanoparticles to the polymer matrix improves mechanical, electrical and thermal properties (Osman et al., 2021; Rathore et al., 2016; Shin et al., 2021). In addition, the incorporation of metal-based nanoparticles into the polymer matrix improves several properties such as electrical, mechanical, optical and magnetic properties (Dorigato et al., 2010; Gorbatkina et al., 2007; Zhai et al., 2006). Other nanofillers like nanoclays show promising results in enhancing gas permeation barrier properties and mechanical properties (Khalili et al., 2010; Otorgust et al., 2017).

The structure and properties of the interfacial polymer layer are closely related to the interfacial interaction between nanoparticles and the polymer matrix (Guo et al., 2017). Efficient stress transfer between nanoparticles and the polymer matrix plays an important role in improving the mechanical properties of nano adhesives. Local stress can be easily transferred onto the tougher particle, resulting in larger plastic deformation when the nanoparticle comes into contact with the polymer matrix, thus increasing the strength performance of the nano adhesive (Kaboorani and Riedl, 2012).

Obtaining a high interfacial interaction between nanoparticles and the polymer matrix is essential. High interfacial interaction and good stress transfer across the interface can be achieved by introducing covalent bonds between the matrix and the nanoparticles (i.e., carbon-based nanoparticle). Nanoparticles undergo functionalization/modification to achieve chemical interactions with the polymer matrix, which subsequently alter the mechanical properties of the nano adhesive (Salom et al., 2018). This is because if the surface chemistry of the nanoparticle is attractive to the polymer matrix, surface functional groups of the nanoparticle could either react with the polymer molecules or have good compatibility with them, strengthening the interface interactions. Conversely, if the surface chemistry of the inorganic nanoparticle is repulsive to the polymer matrix, the surface functional groups of the filler could neither react with the polymer molecules nor have good compatibility with them, resulting in weakened interface interactions.

Based on the literature studies, the inclusion of nanoparticles into polymer adhesive significantly increases strength performance. Osman et al. (2021) reported a 6.50% improvement in the tensile strength of nano adhesive with 1.0 wt% alumina inclusion compared to pristine epoxy. This improvement is attributed to alumina nanoparticles being able to twist and tilt crack directions, hence increasing the strength of the nano adhesive. Meanwhile, Park et al. (2009) demonstrated a 22.0% increase in strength performance when 1.0 wt% carbon black (CB) reinforcement was used in epoxy adhesive compared to unmodified epoxy. The improvement in tensile strength is due to the uniform dispersion of nanoparticles into the epoxy adhesive. Zhang et al. (2019) demonstrated that the addition of CNT into a two-part epoxy adhesive resulted in a significant increment of strength performance up to 26.80% compared to the pristine epoxy at 2.0 wt% CNT nanoparticle content. This improvement is attributed to the excellent individual dispersion of CNT and their tendency to form a network throughout the polymer matrix during the curing process. Chavooshian et al. (2017) demonstrated a 17.80% increase in strength performance when 1.5 wt% SiC nanoparticle content was used in epoxy adhesive compared to unmodified epoxy. The improvement in the strength performance of the nano adhesive is due to efficient stress transfer between SiC and the polymer matrix. In this case, the local stress can be more easily transferred onto the joined particles, which leads to a larger local plastic deformation of the matrix. The end result is higher joint strength when the particles are in intimate contact with the polymer matrix.

While the addition of a small amount of nanoparticles into polymer adhesive significantly improves the mechanical performance of nano adhesives, there is a limit to the number of nanoparticles that can be dispersed into the polymer matrix (Meguid and Sun, 2004). Excessive addition of nanoparticles into the polymer matrix increases viscosity, causing non-uniform distribution of nanoparticles within the polymer matrix. This can significantly reduce the properties of nano adhesives (Tutunchi et al., 2015b). Furthermore, an excessive amount of nanoparticles causes the agglomeration of nanoparticles in the polymer matrix, which facilitates crack initiation and propagation (Kesavulu and Mohanty, 2020). The presence of voids and porosities may also cause a reduction in the strength performance of nano adhesives (Ahmadi, 2019). The presence of voids results from several possible factors such as mechanical air entrapment during preparation and gas created due to chemical reaction during the curing process. The existing voids in epoxy adhesive can make it easier for cracks to propagate through the void, increase the fracture path and results in dissipated energy, leading to low tensile strength (Shah et al., 2020).

However, in a different study, Tang et al. (2013) investigated the effect of a 2.0 wt% inclusion of multi-walled carbon nanotubes (MWCNT) into epoxy adhesive, where a significant decrease in strength performance of up to 3.90% was observed compared to specimens with pristine epoxy. The reduction in strength performance was attributed to the unstable crack propagation, exhibiting the characteristic of stick-slip mode crack propagation. Salom et al. (2018) demonstrated that the addition of 6.0 wt% graphene nanoplatelets (GNP) into epoxy adhesive resulted in an 18.50% decrease in strength performance compared to unmodified epoxy. Agglomeration of nanoparticles and weak interfacial adhesion between nanoparticles and the polymer matrix resulted in the reduction of strength performance. Osman et al. (2021) reported a 15.0% decrease in the tensile strength of nano adhesive with 1.0 wt% GNP compared to pristine epoxy. The high surface area and van der Waals force make GNP more prone to agglomeration in the polymer matrix, acting as stress concentrations where cracks can easily initiate.

It is also worth noting that the dispersion stability of nanoparticles into the polymer matrix affects the mechanical properties of nano adhesives (Kaboorani and Riedl, 2012). A homogeneous distribution of nanoparticles is often desired as it helps to achieve good stress transfer between the nanoparticles and the polymer matrix, resulting in a more uniform stress distribution and better strength performance. Poor dispersion of nanoparticles in the polymer matrix could significantly reduce the properties of the polymer matrix. The quality of dispersion is assumed based on the performance of the nano adhesive; when better properties are achieved, it can be translated into a stable dispersion of nanoparticles within the polymer matrix (Korayem et al., 2017). However, achieving a uniform nanoparticle dispersion in a polymer matrix is quite challenging due to strong van der Waals attractions. Essentially, van der Waals forces between nanoparticles are weak intermolecular attractions; however, at the nanoscale, they tend to be substantial due to the large surface area of the nanoparticles (Jojibabu et al., 2020b). This makes it easy for them to agglomerate in the polymer matrix, where agglomerations can act as stress concentrations that weaken the nano adhesive. Therefore, cracks can be easily initiated (Osman et al., 2021).

Figure 2.12 summarises the trend of results for nano adhesive strength performance and Table 2.6 provides a summary of various bulk nano adhesive strength performances based on different types of adhesives (i.e., epoxy, acrylic, polyurethane, etc.) and various type of nanoparticles (i.e., alumina, GNP, SiC, MWCNT, etc.) for the dog bone specimens. Based on the literature studies, it was noted that nanoparticle content was typically kept around 2.0 wt% in order to minimise possible nanofiller agglomeration (Osman et al., 2021) and viscosity issues (Tutunchi et al., 2015b).

In conclusion, the addition of nanoparticles to polymer adhesive can lead to different trends in strength, either improvement or decrement. The improvement in strength is attributed to several mechanisms, including efficient stress transfer, crack deviation by nanoparticles and the formation of a network through good dispersion of nanoparticles. Excessive nanoparticle addition to the polymer matrix has a negative effect on strength performance. The decrement in strength performance is due to mechanisms such as nanoparticle agglomeration and unstable crack propagation. It is crucial to note that a stable and homogeneous dispersion of nanoparticles in the polymer matrix is important to reduce nanoparticle agglomeration. Furthermore, there are inconsistent trends in the strength performance of nano adhesives, especially with GNP reinforcement. Therefore, further investigation is needed to elucidate the effect of GNP and nano reinforcement in the polymer matrix on adhesive strength performance.

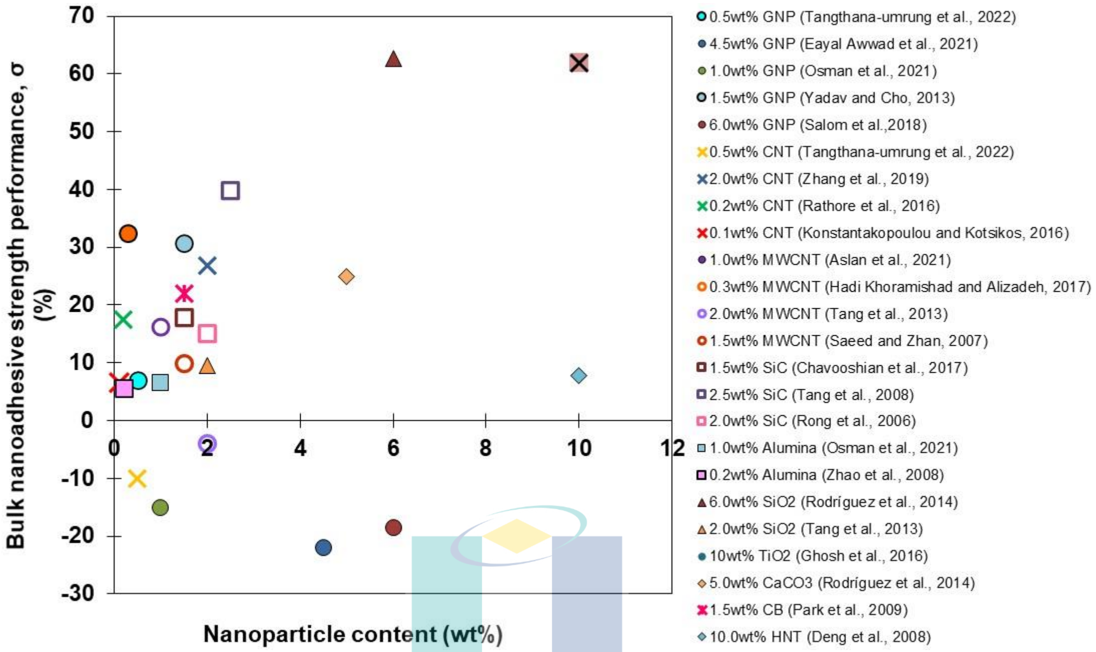

Figure 2.12 Bulk nano adhesive strength with single nanoparticle

Table 2.6 Bulk nano adhesive strength with single nanoparticle

Nanofiller	**Nanoparticle content (wt%)**	**Adhesive**	**Strength performance (%)**	**Mechanism**	**Reference**
MWCNT	1.5	Polyimide	+9.8	Delay the initiation micro crack and propagation by bridging of embedded MWCNT	(Saeed and Zhan, 2007)
	0.3	Epoxy	+32.4	N/A	(Khoramishad and Alizadeh, 2017)
	0.5		+7.5		(Khashaba et al., 2014)
	1.0		+12.7		(Yang et al., 2011)
	1.0		+16.3		(Aslan et al., 2021)
	2.0		-3.9	Unstable crack propagation	(Tang et al., 2013)
Alumina	0.2		+5.7	Pull-out	(Zhao et al., 2008)
	1.0		+6.5	Twist and tilt the crack direction	(Osman et al., 2021)
CNT	0.1		+6.6	N/A	(Konstantakopoulou and Kotsikos, 2016)
	0.2		+17.4		(Rathore et al., 2016)
	0.5		-10.0	Poor dispersion	(Tangthana-umrung et al., 2022)
	2.0		+26.8	Excellent dispersion and tend to form network	(Zhang et al., 2019)

Table 2.6 Continued

Nanofiller	**Nanoparticle content (wt%)**	**Adhesive**	**Strength performance (%)**	**Mechanism**	**Reference**
SiC	1.5	Epoxy	+17.8	Efficient stress transfer	(Chavooshian et al., 2017)
	2.0		+15.10	N/A	(Rong et al., 2006)
	2.5		+39.8		(Tang et al., 2008)
TiO_2	10.0		+62.0		(Ghosh et al., 2016)
CB	1.5		+22.0	Uniform dispersion	(Park et al., 2009)
CNF	0.5		+22.4	N/A	(Zhang et al., 2019)
Cu	15.0		+15.0	Cu resisted to deformation the epoxy	(Necati Ataberk, 2020)
RGO	0.03		+8.2	N/A	(Tang et al., 2013)
	1.0		-15.0	Agglomeration	(Osman et al., 2021)
HNT (Halloysite nanotube)	10.0		+7.7	Bridging	(Deng et al., 2008)
SiO_2	2.0		+11.5	Unstable crack propagation	(Tang, Wan, Peng, et al., 2013)
GNP	0.1		+2.1	Pull-out and debonding	(Quan et al., 2018)
	1.0		-15.0	Agglomeration	(Osman et al., 2021)

Table 2.6 Continued

Nanofiller	Nanoparticle content (wt%)	Adhesive	Strength performance (%)	Mechanism	Reference
GNP	0.5	Epoxy	+7.0	Good interfacial interaction and well dispersion	(Tangthana-umrung et al., 2022)
	4.5		-22.0	Aggregation and agglomeration	(Eayal Awwad et al., 2021)
	6.0		-18.5	Agglomeration	(Salom et al., 2018)
	1.5	Polyurethane	+30.7	Efficient stress transfer	(Yadav and Cho, 2013)
SiO_2	6.0		+62.6	N/A	(Rodríguez et al., 2014)
$CaCO_3$	5.0		+15.0		

‘(+)’: Increment of bulk single nano adhesive strength, ‘(-)’: Decrement of bulk single nano adhesive strength

2.7.3.1.2 The usage of single nano reinforcement in adhesive joining

The enhancement of the mechanical performance of epoxy adhesives can be directly related to the improved shear strength of the joined specimens. The presence of small amounts of nanofillers may enhance the interfacial adhesion properties of the nano adhesive-adherend. It has been reported that due to the tiny dimensions of nanofillers, they can penetrate into small voids on the adherend surface, thus enhancing joint strength through mechanical interlocking (Yadollahi et al., 2015). Efficient stress transfer between the nanofiller and polymer plays a crucial role in improving adhesion strength. Local stress can be easily transferred onto the joined particles, leading to a larger local plastic deformation of the matrix when the particles are in close contact with the polymer (Kaboorani and Riedl, 2012; Tutunchi et al., 2015a). The dependence of the tensile and shear strength of nano-reinforced adhesive on the nanofiller content can be attributed to the following factors: as the number of adhesively joined points increases, the cohesive strength of the adhesive also increases, resulting in a higher mechanical strength of the interface. This is due to the ability of nanofillers to fill any microscopic gaps present in the adhesive, resulting from their dispersion, and mechanical interlocking due to the extensive contact regions between the fillers and the adhesive.

Previously, Tutunchi et al. (2016) demonstrated that the addition of 1.5 wt% alumina nanoparticles into acrylic adhesive resulted in an increase in joining strength of up to 43.0% compared to its pristine adhesive. The higher joining strength is mainly due to intimate contact of the particles with the polymer matrix. The author also reported that the introduction of nanoparticles led to better interfacial wettability and chemical compatibility between the adhesive and the substrate, positively contributing to the shear resistance of the joints. Aradhana et al. (2018) demonstrated that the addition of 1.0 wt% carbon nanotube (CNT) nanoparticles into epoxy adhesive resulted in an increment of joining strength of up to 48.2% compared to its pristine adhesive, which was attributed to the higher interaction of CNTs with epoxy resin owing to their high aspect ratio. Dorigato et al. (2010) demonstrated that the addition of 1.0 wt% zirconia (Zr) nanoparticles into epoxy adhesive resulted in an increase in joining strength of up to 60.0% compared to pristine adhesive counterparts, although the presence of nanoparticle agglomerates had detrimental effects on the mechanical behaviour of the joints. It is also possible that the increase in adhesive viscosity at elevated filler contents produced a nonoptimal distribution of the adhesive in overlapping joint regions. Gültekin et al. (2016) demonstrated that the addition of 1.0 wt% graphene nanoplatelet (GNP) nanoparticles into epoxy adhesive resulted in an increment in joining strength of up to 16.8% compared to that of pristine adhesive due to homogeneous distribution of nanoparticles significantly increasing joining strength. According to Gorbatkina et al. (2007), the addition of 2.0 wt% alumina into epoxy adhesive resulted in an improvement in joining strength of up to 9% when compared to pristine adhesive. This improvement is attributed to the presence of a small amount of nanoparticle increasing the interfacial strength, thus increasing the joining strength. While in the case of alumina nanoparticle, the interfacial strength is not inferior to that of joints compared to pristine adhesive.

However, it appears that there is a limit to the number of dispersed nanoparticles, beyond which a drop in properties is observed. Once the nanoparticles fully fill the gaps and porosities as well as all the contact points are established, further addition of nanoparticles cannot interact effectively within the adhesive; consequently, poor matrix infiltration occurs (Chavooshian et al., 2017). Excessive loading of nanoparticle is one of the reasons why the joining strength significantly reduces. According to Meguid and Sun (2004), the inclusion of nanoparticles into polymer adhesive has a limited amount. The excessive amount of nanoparticles tends to make the nanoparticles easily agglomerate due to strong van der Waals force between nanoparticles (Jojibabu et al., 2020b). Agglomeration of nanoparticle acts as a stress concentration and facilitates crack initiation and propagation.

In a different work, Prolongo et al. (2010) demonstrated that the addition of 1.0wt% CNF into epoxy adhesive resulted in a decrement in joining strength up to 6% compared to pristine adhesive. Joining strength also strongly depends on the surface treatment applied to the composite (Prolongo et al., 2010). Higher strength was obtained for the composite treated by plasma due to higher wettability of the adhesives on these surfaces. Although the surface energy of grit blasted adherend is not significantly modified, the measured lap shear strength is quite high. This must be related to the increase in roughness generated. It is worth noting that the failure mode of these joints, the adherends of which were treated by grit-blasting, was totally cohesive in the substrate. This means that the strength of the composite adherends is lower than the adhesive strength. Khalili et al. (2010) demonstrated that the addition of 5.0 wt% nanoclay into epoxy adhesive resulted in a decrement in joining strength of up to 18% compared to pristine adhesive counterparts due to poor adhesion hindering the proper wetting of the adherend surface.

In conclusion, the inclusion of nanofiller into the polymer matrix leads to different trends of strength improvement or decrement in adhesive joining. The improvement in joining strength is due to several mechanisms, including mechanical interlocking, efficient stress transfer and homogeneous distribution of nanoparticles. Meanwhile, the excessive loading of nanoparticles results in a decrement in strength performance due to mechanisms such as agglomeration and poor matrix infiltration. The strength performance decrement mechanism includes poor adhesion and dependence on the type of surface treatment. From Figure 2.13 and Table 2.7, it was noted that most of the nano reinforcement loadings were below 2.0 wt% nanoparticle content in order to minimise possible agglomeration (Osman et al., 2021) and high viscosity (Tutunchi et al., 2015b). Therefore, further investigation is needed to elucidate the effect of GNP and nano-reinforcement on the strength performance of joining specimens.

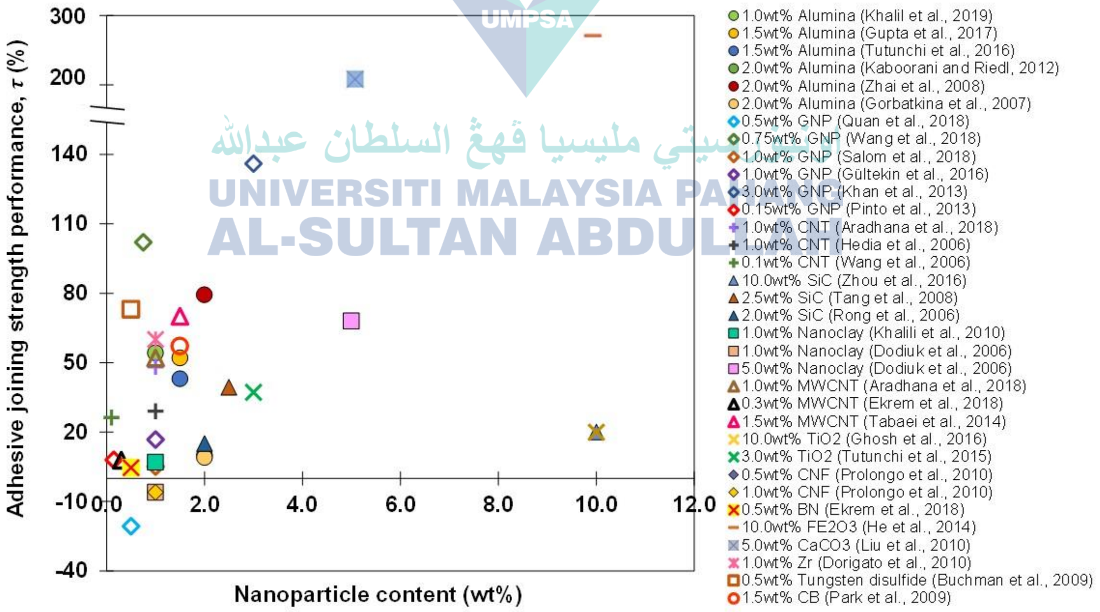

Figure 2.13 Adhesive joining strength performance with single nanoparticle

Table 2.7 Adhesive joining strength performance with single nanoparticle in single lap joint specimens

Nanofiller	**Nanoparticle content (wt%)**	**Adhesive**	**Adherend**	**Fracture mode**	**Strength performance (%)**	**Reference**
Alumina	1.0	Epoxy	AA1100	Cohesive and adhesive	+54.2	(Khalil et al., 2019)
	1.5		Aluminium alloy	N/A	+52.0	(Gupta et al., 2017)
	2.0		Steel		+10.0	(Kaboorani and Riedl, 2012)
					+79.3	(Zhai et al., 2008)
					+9.0	(Gorbatkina et al., 2007)
	1.5	Acrylic	Steel-composite		+30.0	(Tutunchi et al., 2016)
TiO_2	3.0		Carbon steel		+37.2	(Tutunchi et al., 2015b)
	10.0	Epoxy	Mild steel		+20.0	(Ghosh et al., 2016)
GNP	0.5		A109 steel		-20.7	(Quan et al., 2018)
	0.75		Stainless steel		+102	(Wang et al., 2018)
	1.0		AA2024-T3		+5.1	(Salom et al., 2018)
					+16.8	(Gültekin et al., 2016)
	0.15	PVA	Beech veneer	Cohesive	+49.0	(Pinto et al., 2013)
	3.0		Wood	N/A	+136.0	(Khan et al., 2013)

Table 2.7 Continued

Nanofiller	Nanoparticle content (wt%)	Adhesive	Adherend	Fracture mode	Strength performance (%)	Reference
CNT	1.0	PVA	Aluminium	N/A	+32.5	(Aradhana et al., 2018)
	0.1	Epoxy	Glass		+32.5%	
	1.0		White iron		+26.3	(Wang et al., 2006)
SiC	2.0		Composite		+29.0	(Hedia et al., 2006)
	2.5				+15.1	(Rong et al., 2006)
	10.0		Stainless steel		+39.4	(Tang et al., 2008)
Zr	1.0		Composite		+20.0	(H. Zhou et al., 2016)
MWCNT			White iron		+60.0	(Dorigato et al., 2010)
	1.5		Aluminium		+29.0	(Hedia et al., 2006)
	0.5		AA2024-T3		+70.0	(Tabaei et al., 2014)
Tungsten Disulphide	0.5				+7.9	(Ekrem et al., 2018)
Nanoclay	1.0				-6.0	(Buchman et al., 2009)
	0.5				+73.0	(Dodiuk et al., 2006)
	5.0				-22.6	

Table 2.7 Continued

Nanofiller	Nanoparticle content (wt%)	Adhesive	Adherend	Fracture mode	Strength performance (%)	Reference
CB	1.5	Epoxy	Glass	Interfacial and cohesive	+57.1	(Park et al., 2009)
CNF	0.5		Carbon Fibre	Cohesive	-6.0	(Prolongo et al., 2010)
	1.5				+5.0	
Boron Nitride (BN)	0.3		AA2024-T3	N/A	+11.5	(Ekrem et al., 2018)
Fe_2O_3	10.0	EVA	Iron		+276.0	(He et al., 2014)
$CaCO_3$	5.0	Soy protein	plywood		+209.0	(Liu et al., 2010)

‘(+)’: Increment of adhesive joining strength performance with single nanoparticle, ‘(-)’: Decrement of adhesive joining strength performance with single nanoparticle

2.7.3.2 Hybrid nano reinforcement

2.7.3.2.1 The usage of hybrid nano reinforcement in bulk specimens

The concept of introducing hybrid nanofillers into the epoxy matrix to create synergistic enhancements and multifunctional features has garnered significant attention (Ahmad et al., 2020; Zhang et al., 2020; Kesavulu and Mohanty, 2020). In recent years, several researchers have focused on hybrid nano-reinforcement in polymer adhesives. Nanocomposite manufacturing approaches involve adding two or more distinctly different morphologies (Ahmad et al., 2020), compositions (Kesavulu and Mohanty, 2020), and/or intrinsic properties of nanoparticles to the polymer matrix. In this section, the literature focuses solely on the effect of including hybrid nano-reinforcement in bulk adhesive specimens for their strength performance. The performance of hybrid nano-adhesives was evaluated based on a comparison with their pristine counterparts.

According Zhang et al. (2019), the incorporation of hybrid nano reinforcement of 2.0 wt% CNT/CB exhibited an improvement in strength performance of up to 10.58% compared to pristine adhesive at a 1:3 weight ratio combinations. The addition of hybrid nanoparticles into polymer adhesive significantly improved interfacial strength by reducing agglomeration (Zhang et al., 2019). The second nanoparticle acts as a spacer between the first nanoparticle and prevents aggregations in the polymer. Fu et al. (2019) reported that the addition of 0.5 wt% GO and SiO2 hybrid nano-reinforcement into polymer adhesive improved strength by up to 4.35% compared to pristine adhesive. This improvement is attributed to interfacial strength, where SiO2 acts as spacers to prevent GO from aggregating in the polymer. Yang et al. (2011) found that the addition of hybrid 1.0 wt% multi-graphene platelets (MGPs) and multi-walled carbon nanotubes (MWCNTs) into the polymer matrix significantly increased mechanical performance by up to 35.4% compared to pristine adhesive at a 1:9 weight ratio combination. Both MGPs and MWCNTs are embedded in the polymer matrix, which is held tightly by the polymer matrix due to the covalent bond between the polymer epoxy group and amine groups on the MWCNTs. Furthermore, the MWCNTs are aligned along the MGP surface through Van der Waals forces between graphene-based structures. The flexible MWCNTs can act as chelating arms to improve adhesion between the 3D MGP/ MWCNT hybrid nanofillers and the polymer matrix (Yang et al., 2011).

The introduction of a hybrid nanofiller consisting of multi-graphene platelets (MGP) and multi-walled carbon nanotubes (MWCNT) increases the amount of contact area. This larger contact area within the hybrid nanofiller leads to a reduction in interfacial resistance between nanofillers (Yu et al., 2008). Monfared et al. (2018) observed that the use of non-functionalized MWCNTs results in the precipitation of MWCNTs at higher weight percentages, leading to lower stability of carbon nanotubes in the polymer matrix. However, the addition of hybrid MWCNTs and silica demonstrated good dispersion within the polymer matrix. The effective dispersion of hybrid MWCNTs and silica can improve the interfacial adhesion between nanoparticles and the polymer matrix in bulk specimens, consequently improving tensile properties. Yue et al. (2014) utilised 0.1 wt% CNTs/GNP with various weight ratio combinations (e.g., 8:2, 6:4, 4:6, and 2:8) as experimental parameters. The results showed that the best hybrid ratio was at 8:2, significantly increasing bulk strength by up to 37.0% compared to pristine adhesive. The strategy of using hybrid nano-reinforcement with different geometric shapes proved to be an effective way to achieve better mechanical, electrical and thermal properties in composite materials (Yue et al., 2014). The geometric shapes and weight ratio combinations of fillers in the mixture are important factors governing the reinforcing capabilities of polymer nanocomposites. The dispersion of hybrid CNT/GNP led to higher complex viscosity at low loading of nanofiller, and the small amount of GNP acted as a dispersing agent, resulting in improved CNT dispersion. Min et al. (2018) investigated 1.0 wt% GO/CNTs with various weight ratio combinations (e.g., 1:1, 1:3, 1:6, 1:9, 3:1, 6:1, and 9:1) and demonstrated enhanced bulk strength up to 25.10% compared to pristine adhesive at the best 3:1 hybrid ratio combination. The three-dimensional structure of GO/CNTs hybrids greatly alleviated aggregation in the polymer matrix, making the interaction between GO/CNTs hybrid and polymer matrix more even as well as reducing stress concentration. Osman et al. (2021) dispersed 1.0 wt% alumina/reduced graphene oxide (RGO) with various weight ratio combinations (e.g., 10:0, 8:2, 6:4, 5:5, 4:6, 2:8, and 0:10) into epoxy adhesive and demonstrated an enhancement of bulk strength up to 24.6% at the best ratio of 4:6 hybrid alumina/RGO. As the proportion of alumina in the hybrid ratio increases, more particles adhere to the graphene surface, resulting in fewer aggregates and a more uniform dispersion of RGO sheets. These auxiliary particles (alumina) not only significantly reduce the aggregations of RGO sheets, but they also limit crack propagation into large cracks. It is worth noting that the nano-size nature of alumina is very small compared to the lateral size of graphene sheets, enabling alumina to easily settle on the large surface of graphene sheets. Furthermore, the mechanical strength of the epoxy-based hybrid nanocomposites is dramatically enhanced compared to either of the single nanocomposites. In brief, there is an optimum weight ratio combination of nano-reinforcement to enhance the mechanical performance of bulk specimens, where a precise formulation of the hybrid nano-reinforcement appears to be a key factor to avoid a dramatic increase in viscosity due to higher aspect ratio and larger surface area within the polymer matrix, subsequently reducing bulk strength performance (Jojibabu et al., 2020).

Ensuring the stable dispersion of hybrid nano-reinforcement in the polymer matrix is crucial to achieve optimal performance in bulk nano-adhesives. For example, carbon-based nano-reinforcements (e.g., CNTs) with smooth nonreactive surfaces exhibit poor interfacial adhesion. The tubular structure of CNTs leads to spontaneous entanglement and aggregation, limiting their reinforcing effectiveness and potentially degrading the mechanical properties of the nano-adhesive (Jia et al., 2013). An effective approach to mitigate the strong molecular inter-atomic forces between CNTs is through chemical modification of the nanofiller. Chemical functionalization of the surface of CNTs strengthens interfacial adhesion and positively impacts the dispersion stability of CNTs (Jia et al., 2013). A traditional method of modifying CNTs involves chemical oxidation, wherein specific oxygen-containing functional groups are grafted onto the sidewalls of the CNT.

Figure 2.14 presents various results for adhesive strength performance. Table 2.8 summarises the results of hybrid nano-adhesive strength performance. These nano-adhesive strength performances are based on various types of adhesives, weight contents, weight ratio combinations and nanoparticles (e.g., alumina, GNP, SiC, MWCNT, etc.). From Figure 2.13, it is evident that the trend of strength performance in nano-adhesives can either be enhanced or deteriorated. Based on literature studies, the inclusion of hybrid nanoparticles into polymer adhesive was typically done with nanoparticle content below 2.0 wt% to minimise possible agglomeration and high viscosity (Osman et al., 2021 (Tutunchi et al., 2015b). In conclusion, there are mainly two mechanisms of mechanical strengthening in hybrid nanocomposites. The first involves the chemical interaction of functional groups of the polymer and nanoparticle, resulting in a strong covalent bond. The second mechanism is the reduction of agglomeration due to the second particle acting as a dispersant or spacer, leading to increased interfacial interaction and adhesion. The increased interfacial interaction and adhesion cause an expansion of the contact area and uniform stress transfer, resulting in higher mechanical strength. The mechanisms involved depend on several factors, including the combined effects of nanoparticle type, geometry and orientation.

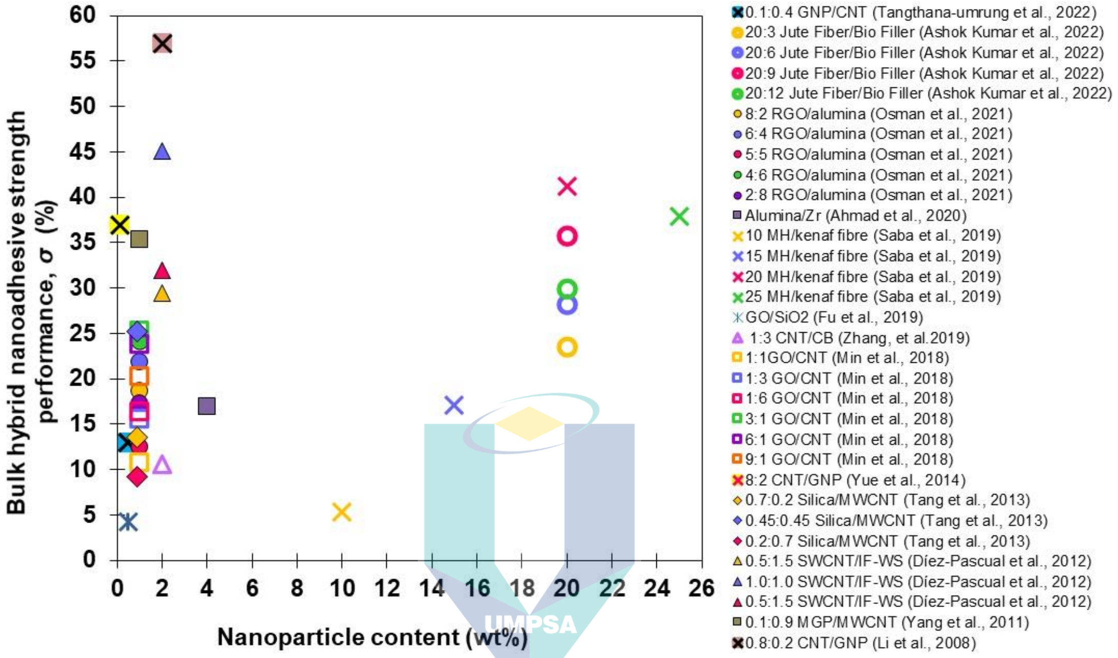

Figure 2.14 Bulk nanoadhesive strength performance with hybrid nanoparticle

Table 2.8 Bulk nanoadhesive strength performance with hybrid nanoparticle

Hybrid nanofiller	**Nanoparticle content (wt%)**	**Weight ratio**	**Adhesive**	**Strength performance (%)**	**Mechanism**	**Remarks**	**Reference**
RGO/ Alumina	1.0	8:2	Epoxy	+17.8	Intercalation	N/A	(Osman et al., 2021)
		6:4		+22.6			
		5:5		+12.6			
		4:6		+24.6			
		2:8		+17.6			
MH/Kenaf	10.0	N/A		+5.4	Enhanced interfacial interaction between nanofiller and polymer		(Saba et al., 2019)
	15.0			+17.1			
	20.0			+41.3			
	25.0			+37.9			
MGP/ MWCNT	1.0	1:9		+35.4	Chelating arm	Functionalized MWCNT	(Yang et al., 2011)
				+14.5		N/A	
Alumina/ Zr	4.0	N/A		+17.0	Uniform dispersion of nanofiller		(Ahmad et al., 2020)
GO/SiO_2	0.5			+4.35	Act as spacer		(Fu et al., 2019)
CNT/CB	2.0	1:3		+10.58			(Zhang et al., 2019)

Table 2.8 Continued

Hybrid nanofiller	Nanoparticle content (wt%)	Weight ratio	Adhesive	Strength performance (%)	Mechanism	Remark	Reference
GNP/CNT	0.5	1:4	Epoxy	+13.0	N/A	N/A	(Tangthana-umrung et al., 2022)
	2.0	1:1		+57.0	Crack tip pinning and bifurcation		(Li et al., 2008)
Jute fibre/ Bio filler	20.0	20:3		+23.5	N/A		(Ashok Kumar et al., 2022)
		20:6		+28.2			
		20:9		+35.7			
		20:12		+29.9			
SWCNT/ IF-WS	2.0	1:3		+29.4	Homogeneous dispersion		(Díez-Pascual et al., 2012)
CNT/GNP	0.1	8:2		+37.0			(Yue et al., 2014)
GO/CNT	1.0	1:1	Polyimide	+10.8			(Min et al., 2018)
		1:3		+15.6			
		1:6		+16.5			
		1:9		+22.5			
		3:1		+25.4			
		6:1		+23.9			

Table 2.8 Continued

Hybrid nanofiller	**Nanoparticle content (wt%)**	**Weight ratio**	**Adhesive**	**Strength performance (%)**	**Mechanism**	**Remark**	**Reference**
GO/CNT	1.0	9:1	Polyimide	+20.4	Homogeneous dispersion	N/A	(Min et al., 2018)

‘(+)’: Increment of bulk hybrid nano adhesive strength, ‘(-)’: Decrement of bulk hybrid nano adhesive strength

2.7.3.2.2 The usage of hybrid nano reinforcement in adhesive joining

The addition of hybrid nanoparticles to polymer adhesives primarily aims to improve the strength and toughness of joined materials. According to Yue et al. (2014), combining different shapes and small amounts of nano-reinforcement can enhance joining strength. For instance, as indicated by Kumar et al. (2019), the combination of carbon fillers with various morphologies (1D carbon nanotubes - CNT, carbon fibers - CF, 2D graphite nanoplatelets - GNP) influences the microstructure of composites, leading to a more homogeneous dispersion of fillers in the epoxy matrix. Yue et al. (2014) further emphasised that the dispersion of 1D carbon nanotubes (CNT) and 2D graphene improves the hybrid system by intercalation between 1D and 2D, leading to the formation of a 3D filler network that enhances mechanical and electrical properties. Meanwhile, the addition of ceramic nanoparticles as a secondary filler into polymer adhesive such as low-cost nano-alumina is well-known for its excellent mechanical properties, high thermal stability, superb electrical insulation properties and high surface area (Osman et al., 2021). The inclusion of ceramic nanoparticles in the graphene-epoxy solution can result in more attachment of ceramics to the GNP surface, reducing the aggregation of GNP and providing uniform dispersion.

Razavi et al. (2018a) demonstrated that the inclusion of SiC and MWCNT hybrid nanofiller into epoxy adhesive enhanced the shear strength of aluminium/epoxy composite joints. Specifically, the addition of 0.8 wt% SiC/MWCNT hybrid nano adhesive at a 1:1 weight ratio combination showed an improvement in joining strength of up to 28.3% compared to joining specimens with unmodified epoxy. The increased shear strength with the addition of hybrid SiC and MWCNT corresponded to plastic deformation around microcracks and a uniform distribution of nanofillers. Jojibabu et al. (2020) demonstrated that the dispersion of 0.5 wt% hybrid OZ-CNT and Styrene-Butadiene-Methyl methacrylate (SBM) into epoxy adhesive at a 10:3 resulted in an improvement in shear strength of up to 112.0% compared to unmodified epoxy. This improvement was attributed to the abundant functional groups on the OZ-CNT, providing good interfacial adhesion between the nanofiller and epoxy polymer. Subramanian et al. (2016) reported that the inclusion of 0.5 wt% polydopamine (PDA) /MWCNT hybrid led to an improvement in shear strength of up to 28.3% compared to pristine adhesive at a

1:0.5 weight ratio combination. This improvement was attributed to better interaction between the nanoparticle and the aluminium substrate surface, forming the stronger adhesive bond and resulting in a remarkable improvement in joining strength. May et al. (2010) demonstrated that the inclusion of 0.7 wt% MWCNT and alumina into sol gel epoxy adhesive improved shear strength by up to 58.3% compared to pristine epoxy. The polymer matrix and alumina-based sol-gel played a major role in providing a three-dimensional network within the adhesive. The presence of alumina in the adhesive prevented the phase separation within the matrix. Moreover, the addition of nano alumina as a secondary nanofiller affected the cure kinetic due to the catalytic effect of hydroxyl groups on the particles. Changes in the adhesive structure when adding nano alumina indicated a high degree of miscibility and cross linking, enhancing the structure of the adhesive and thus increasing shear strength.

However, the high loading amount of nanoparticle promoted agglomeration and imposed local stress concentrations in the adhesive layer. This led to rapid damage progress in the adhesive layer and reduced the shear strength and toughness of the adhesive joint (Razavi et al., 2018). According to Kumar et al. (2019), the inclusion of 30.0 wt% expanded graphite (EG) and silver flakes (AG) hybrid nanofiller into epoxy adhesive resulted in a decrease in shear strength of up to 38.27% at a 3:7 weight ratio combination compared to joining specimens with unmodified epoxy. The reduction in shear strength of the hybrid nano adhesive joint was attributed to the generation of extra voids and porosities and lower crosslinking density at a high level of loading during preparation. Moreover, the reduction in shear strength may be attributed to the different phase stress accumulated points of silver flakes, which aid in crack propagation (Kumar et al., 2019).

Figure 2.15 shows various results for adhesive strength performance. Table 2.9 summarises the results of the hybrid nano adhesive joining strength performance. These nano adhesive joining strengths were based on various types of nanofillers, adhesives, joining methods, fracture modes, nanoparticle content and weight ratio combinations. Based on these literatures, it can be interpreted that hybrid nano reinforcement can improve the nanofiller dispersion inside the polymer matrix by reducing possible agglomerations of nanofiller via the intercalation mechanism, which has been proven to enhance the joining performance.

It is worth mentioning that the best joining performances will be achieved at the optimum weight ratio combination of the hybrid nanofillers. However, the results outcome will vary depending on several factors such as the interfacial interactions of the hybrid nanofillers or the condition of the specimen itself. For example, the existing voids/porosities on the specimens, lower crosslinking density due to nanofiller presence, and formation of different phases of stress concentrations that aid crack propagation may greatly impact the joining performances (Kumar et al., 2019). The selection of suitable nanofiller combinations also needs to be considered before planning the investigation to achieve the best-desired outcome. Based on Figure 2.15, it is noted that a low concentration of nanoparticle content, which is below 2.0 wt%, is recommended to reduce possible agglomeration and viscosity.

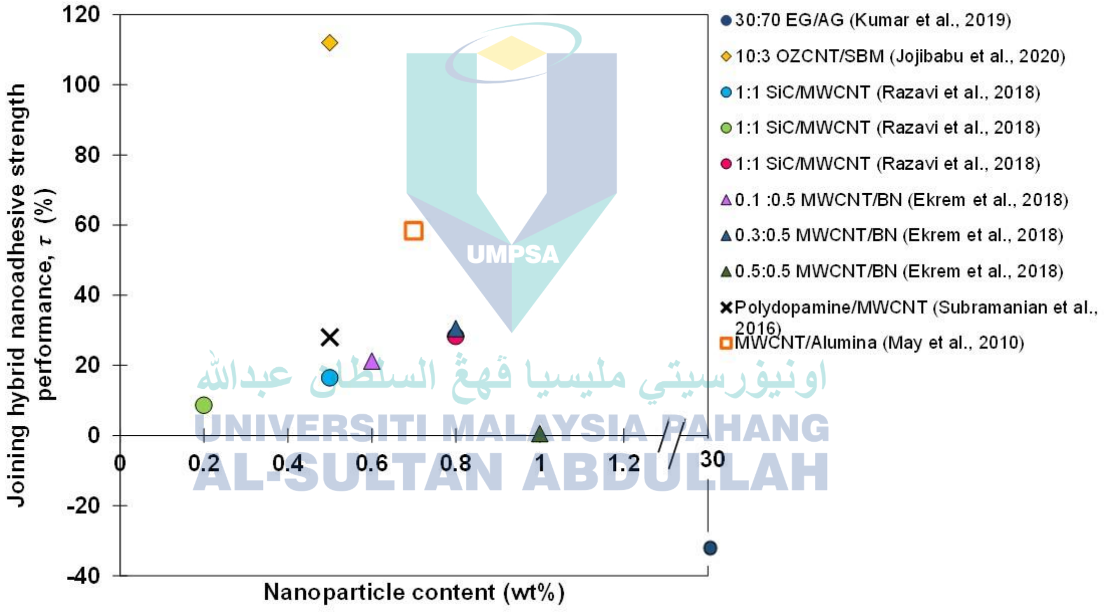

Figure 2.15 Adhesive joining strength performance with hybrid nanoadhesive

Table 2.9 Hybrid nano adhesive joining strength

Hybrid nanofiller	Nanoparticle content (wt%)	Weight ratio	Adherend	Adhesive	Strength performance (%)	Mechanism	Reference
OZCNT/ SBM	0.5	10:3	AA7075	Epoxy	+112.0	Good interfacial adhesion	(Jojibabu et al., 2020)
SiC/ MWCNT	0.2	1:1	AA7075-T6		+8.6	Plastic deformation around micro cracks and uniform distribution of nanofiller	Razavi et al. (2018a)
	0.5				+16.4		
	0.8				+28.3		
Polydopamine/ MWCNT	0.5	1:0.5	AA2024		+28.0	Better interaction between nanofiller and substrate	(Subramanian et al., 2016)
MWCNT/ Alumina	0.7	N/A	AA2024-T3		+58.3	Providing the 3D network within the adhesive	(May et al., 2010)
EG/AG	30.0	3:7	Aluminium		-38.3	Generation of extra void and porosities and lower crosslinking density	(Kumar et al., 2019)
MWCNT/BN	0.6	0.1:0.5	AA2024-T3		+21.2	Crack tip deflection and bifurcation, bridging, pull-out, fiber cracking	(Ekrem et al., 2018)
	0.8	0.3:0.5			+30.5		
	1.0	0.5:0.5			+0.6		

'(+)': Increment of hybrid nano adhesive joining strength, '(-)': Decrement of hybrid nano adhesive joining strength

2.8 Wetting characteristic of nano reinforced adhesive

Wetting behaviour is crucial in evaluating joining characteristics since it is used to measure the surface energy of both the solid surface and the adhesive (Kang et al., 2017) as shown in Figure 2.16. The higher the surface energy between the solid surface and the adhesive, the better the wetting behaviour and the stronger the bond will be. Conversely, lower surface energy can result in weaker bonding and decreased joining performance (Prakash and Prasanth, 2021). Figure 2.17 illustrates the relationship between contact angle and nanofiller concentration. This figure demonstrates two regions, which are hydrophilic and hydrophobic. According to the figure, the inclusion of nanofiller has mostly reduced the contact angle, indicating that the wetting behaviour of the adhesive is hydrophilic towards the substrate. However, in some cases, an increase in nanoparticle content (e.g., alumina and TiO_2) has resulted in the nano adhesive becoming more hydrophobic. Yet, further increments in nanofiller content have reversed the originally hydrophobic adhesive to become more hydrophilic as illustrated in Figure 2.18.

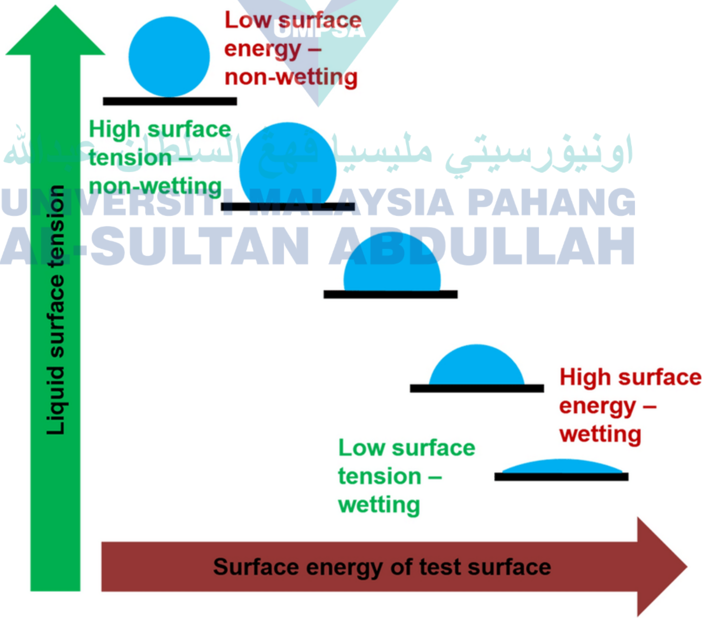

Figure 2.16 Influence of surface energy and surface tension in wettability alteration

Source : Jothi Prakash and Prasanth (2021)

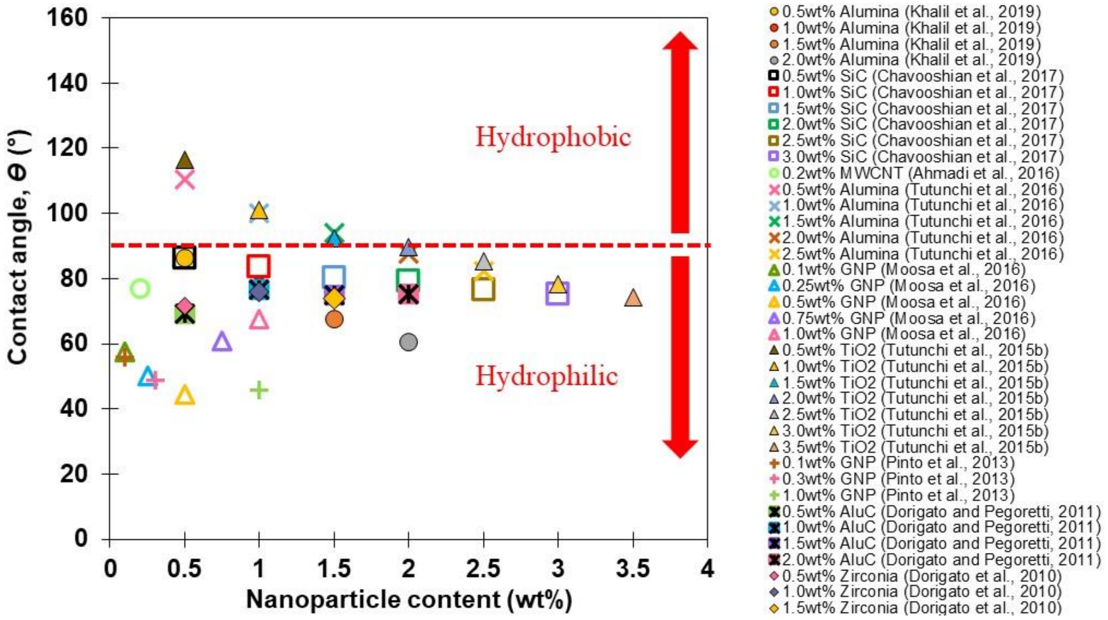

Figure 2.17 Contact angle of nanoadhesive

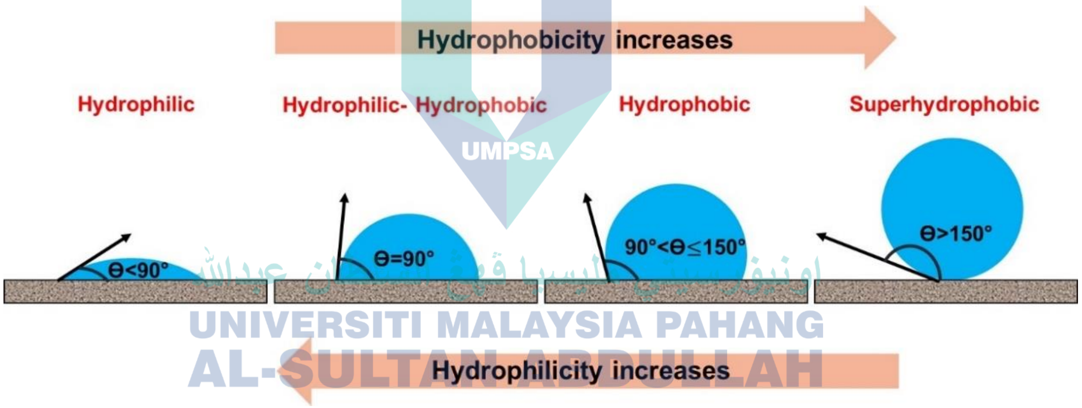

Figure 2.18 Contact angle as function of wetting behaviour
Source : Doshi et al., (2018)

Due to the differing surface and interface free energy of nanoparticles and their higher surface free energies, the inclusion of nanofillers into the polymer matrix improves wetting ability and produces a stronger bond. Khalil et al. (2019) evaluated both the contact angle and spread area of the nano adhesive. The contact angle demonstrated a decrement, while the spread area of the nano-reinforced adhesive demonstrated an increment with the increase in alumina content (0.0-2.0 wt%). This is attributed to the differing surface and interface free energy of nanoparticles and their higher surface free energy. As a result, the nano adhesive demonstrates a greater wetting tendency, transitioning towards a more hydrophilic nature, thereby enhancing wettability and leading to the formation of a stronger bond. Meanwhile, Dorigato and Pegoretti (2011) investigated the equilibrium contact angle of calcined alumina (AluC) reinforced adhesive. The incorporation of calcined alumina enhanced wettability between the adhesive and substrate, favourably impacting joining performance. This was evident when comparing the equilibrium contact angle of the nano-reinforced adhesive to the pristine adhesive. Additionally, Dorigato et al. (2010) studied the effect of adding Zirconia nanoparticles (Zr) into epoxy adhesive on wetting behaviour. Zirconia nanoparticles significantly reduced the equilibrium contact angle values due to the nanoscale size of the nanofiller, providing better interfacial wettability between the adhesive and substrate, which improved bonding efficiency.

On the other hand, Pinto et al. (2013) observed that the equilibrium water contact angle with poly(vinyl)acetate (PVA) film is around 43°. Meanwhile, it increased to roughly 56° with the addition of 0.1 wt% GNP, representing an increase of 30.23% compared to the unmodified adhesive. The presence of GNP partially exposed at the surface generates hydrophobic sites, justifying the increase in hydrophobicity of the PVA film (Pinto et al., 2013). In general, improving interfacial adhesion necessitates sufficient wettability between polyethylene fibre and matrix. Increasing the surface energy of the solid or decreasing the surface energy of a liquid could be used to produce satisfactory wetting. By adding nanofiller to the matrix, the surface energy of the resin may be reduced. According to Ahmadi et al. (2016), pristine epoxy had an equilibrium contact angle of roughly 56°, and the addition of 0.2 wt% MWCNT increased the contact angle to 76.9°, representing an increment of 37.32% compared to the pristine adhesive. The addition of MWCNT to epoxy adhesive significantly increased the contact angle and the hydrophobic property of epoxy resin. Meanwhile, Moosa et al. (2016) recorded that the equilibrium contact angle of pristine epoxy is 43.5° and the addition of 1.0 wt% GNP showed a contact angle of 67.5°, representing an improvement of 55.17% compared to the pristine adhesive. Graphene is generally hydrophobic in nature and epoxy is hydrophilic (43.5°). The increase in contact angle (reduction in wettability) of GNPs/epoxy composite is due to the molecular-level dispersion of the graphene sheets in the epoxy matrix and the strong hydrogen bonding between graphene and the epoxy matrix. These strong H-bonding interactions occur between oxygen-containing groups such as hydroxyls and carboxyl groups of the graphene sheets and the hydroxyl groups of the epoxy chains (Moosa et al., 2016).

The inclusion of the nanofiller enhances the interfacial interaction between the nanofiller, polymer and substrate by providing more surface area for the polymer adhesive to interact with the substrate, leading to an increase in the contact angle. This improvement in wetting behaviour contributes to enhanced bonding strength, thus playing a crucial role in increasing the shear and tensile strength of the joints. The relationship between shear strength and wetting behaviour (contact angle) is depicted in Figure 2.19, illustrating hydrophobic and hydrophilic regions. As observed in the figure, there are two ranges within the hydrophilic zones. The highest shear strength occurs at contact angles ranging from 70° to 90°, while the lowest shear strength occurs at contact angles ranging from 60° to 70°. Data are limited in hydrophobic zones. The increase in shear strength in a hydrophobic zone is inversely related to the contact angle, with smaller contact angles producing the largest shear strengths. Meanwhile, the addition of nanofiller leads to poor wetting due to increased hydrophobicity, especially for carbon-based nanofillers (e.g., GNP and MWCNT) as shown in Figure 2.19. The poor wetting ability is also attributed to the strong hydrogen (H) bond between GNP and the polymer matrix. Table 2.10 shows the wetting behaviour and strength performance of nano adhesive.

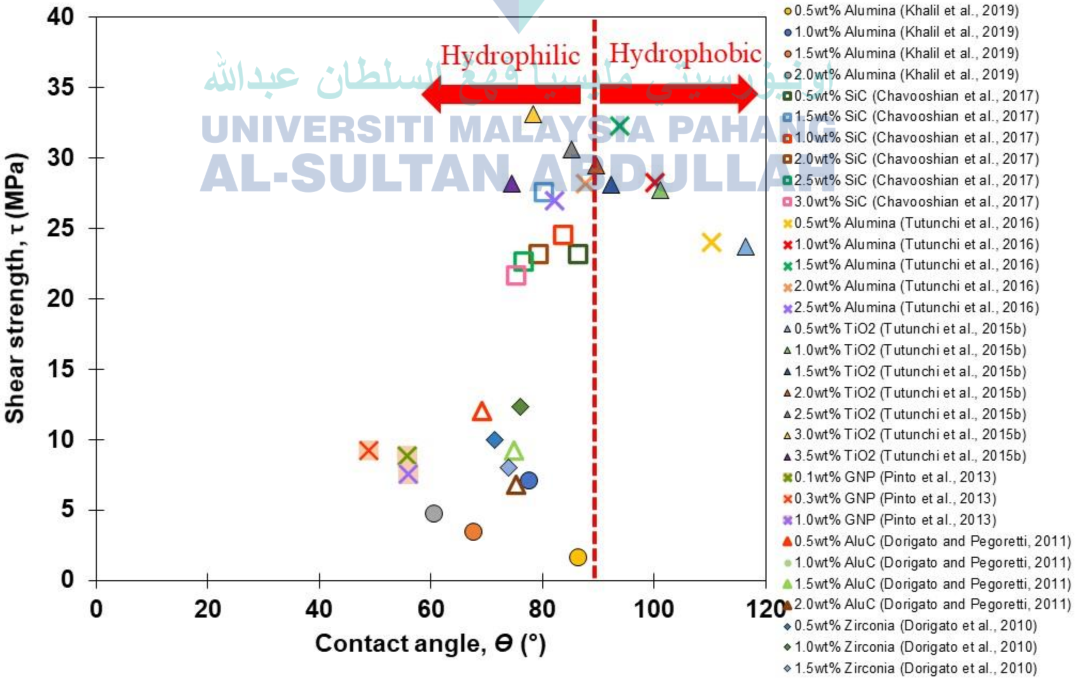

Figure 2.19 Relation between shear strength and contact angle

Table 2.10 Wetting behaviour and strength performance of nanoadhesive

Nanofiller	**Nanoparticle content (wt%)**	**Adhesive**	**Contact angle** $\boldsymbol{\theta}$ **(°)**	**Shear strength** $\boldsymbol{\tau}$ **(MPa)**	**Reference**
CNT	0.5	Silane	34.7 ± 4.1	N/A	(Khan et al., 2018)
GNP	0.1	PVA	55.8 ± 3.3	8.83 ± 0.4	(Pinto et al., 2013)
	0.3		48.8 ± 1.5	9.24 ± 0.2	
	1.0		45.6 ± 2.0	7.53 ± 0.4	
	0.1	Epoxy	57.5	N/A	(Moosa et al., 2016)
	0.25		50.0		
	0.5		44.5		
	0.75		61.0		
	1.0		67.5		
Zr	0.5		71.5 ± 5.3	10.0 ± 1.5	(Dorigato et al., 2010)
	1.0		76.0 ± 6.7	12.3 ± 1.4	
	1.5		74.0 ± 5.1	8.0 ± 1.0	
AluC	0.5		69.1	12.0 ± 1.1	(Andrea Dorigato and Pegoretti, 2011)
	1.0		76.5	12.3 ±1.4	
	1.5		74.8	9.2 ± 1.4	
	2.0		75.2	6.8 ± 0.6	

Table 2.10 Continued

Nanofiller	Nanoparticle content (wt%)	Adhesive	Contact angle Θ (°)	Shear strength τ (MPa)	Reference
MWCNT	0.25	Epoxy	37.3	N/A	(Ahmadi et al., 2016)
Alumina	0.5		86.3	1.6 ± 4.1	(Khalil et al., 2019)
	1.0		77.4	7.1± 1.1	
	1.5		67.6	3.5 ± 2.1	
	2.0		60.6	4.7 ± 2.1	
	0.5	Acrylic	110.0	24.0	(Tutunchi et al., 2016)
	1.0		100.2	28.2	
	1.5		92.9	32.3	
	2.0		87.6	28.2	
	2.5		82.2	26.9	
TiO_2	0.5		116.4 ± 4.1	23.7 ± 0.3	(Tutunchi et al., 2015b)
	1.0		101.0 ± 5.1	27.7 ± 0.5	
	1.5		92.2 ± 2.2	28.1 ± 0.9	
	2.0		89.6 ± 3.4	29.4 ± 0.8	
	2.5		85.2 ± 3.9	30.6 ± 0.5	
	3.0		78.3± 1.7	33.1 ± 1.2	
	3.5		74.4 ± 3.13	28.2 ± 1.1	

Table 2.10 Continued

Nanofiller	**Nanoparticle content (wt%)**	**Adhesive**	**Contact angle ϴ (°)**	**Shear Strength τ (MPa)**	**Reference**
SiC	0.5	Epoxy	86.3	23.2	(Chavooshian et al., 2017)
	1.0		83.7	24.5	
	1.5		80.2	27.6	
	2.0		79.2	23.1	
	2.5		76.5	22.7	
	3.0		75.3	21.6	

2.9 Fracture behaviour of joining specimen

Based on the literature findings, some of the research paper provided the fracture behaviour of the joining specimen for single phase nano reinforcement as stated in Table 2.7 in section 2.7.3.1.2. Meanwhile, for hybrid phase nano reinforcement, there has not been yet reported. In general, cohesive and adhesive failures represent two typical types of failures in adhesive joints. Adhesive failure (AF) occurs when the adhesive layer remains on one surface due to an interface bonding failure, while cohesive failure happens when the adhesive layer remains on both surfaces after the fracture as shown in Figure 2.20. Adhesive failure (AF) is often related to insufficient adhesion interaction between the adhesive and adherends (Kong and Khalil, 2022). Cohesive failure (CF) in the substrate generally indicates that the adherend fails before the adhesive, implying that sufficient strength in the adhesive has been achieved. An increased CF mode region signifies robust interfacial adhesion between adherends and nanofillers. This suggests that a greater amount of energy is necessary to compromise the joining strength, leading to an enhancement in bonding strength (Khalil et al., 2019).

Figure 2.20 Re-illustration of failure mode in adhesive joining specimen
Source: Poulis et al., (2022)

2.10 Pearson’s correlation analysis

Essentially, Pearson’s correlation matrix and heatmap was used to interpret the relation and the dependence between various variable. Correlation coefficient is a statistical measure of the linear relationship between two variables. Correlation coefficients, which are denoted by R (Ratner, 2009), indicate the strength of linear or straight-line relationships between variables. Its values range from -1 to 1. where -1 indicates a perfect negative or inverse correlation, 1 shows a perfect positive or direct relationship, and 0 indicates no linear relationship. Correlation coefficients are useful for determining the strength and direction of relationships between variables. To discover potential correlations between variables and assess their strength, correlation heatmaps can be employed for visualising likely connections (Wanatasanappan et al., 2023). Both the correlation matrix and correlation heatmap are useful tools for evaluating the quality of correlations within a dataset as shown in Figure 2.21. The degree of correlation between two sets of numerical data can be graphically represented using a method called a correlation heatmap. These plots are utilised to identify correlated variables and assess the quality of the correlation. A correlation plot often includes multiple variables, with each variable represented by a column. Each row in this table signifies the relationship between two variables. Positive values indicate a favourable correlation, while negative values indicate an unfavourable relationship.

Numerous theoretical and experimental endeavours have been undertaken to comprehensively characterize the physical and mechanical properties of nano reinforced adhesive. Often, the complexity arises from the multitude of influencing parameters, including the specific type of nanoparticle, polymer, adherend, nanoparticle content, and weight ratio combination. therefore, in current work, Pearsons correlation matrix and heatmaps were used to establish the complex correlation between Alumina/GNP hybrid nano reinforcement towards various properties in adhesive joining specimens.

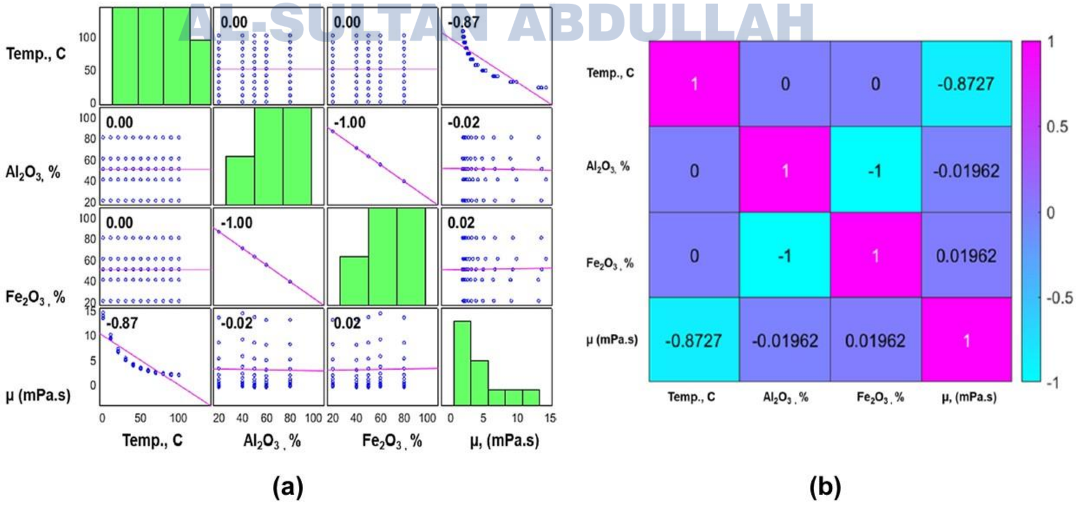

Figure 2.21 Example of (a) correlation matrix and (b) heatmap
Source : Wanatasanappan et al., (2023)

2.11 Summary of literature findings

As a summary, based on Table 2.11, the strengthening mechanisms involved in single-phase nano reinforcement for bulk specimens include efficient stress transfer, crack deviation, and network formation due to improvement in dispersion. Efficient stress transfer between nanoparticles and the polymer matrix plays an important role in improving the mechanical properties of nano adhesive. The local stress can be easily transferred onto the tougher particle, resulting in larger plastic deformation when the nanoparticles come into intimate contact with the polymer matrix, thus increasing the strength performance of the nano adhesive (Kaboorani and Riedl, 2012). The nanoparticles are able to twist and tilt the crack directions, hence increasing the strength of the nano adhesive (Osman et al.,2021).

Similarly, for single-phase nano reinforcement for joining specimens, the strengthening mechanisms involved are efficient stress transfer between nanoparticles and adherend surface, mechanical interlocking as well as interfacial wetting and chemical compatibility. The presence of small amounts of nanofillers enhances the interfacial adhesion properties of the nano adhesive-adherend because the tiny dimensions of nanofillers allow them to penetrate into any small voids on the adherend surface, thus enhancing joint strength through mechanical interlocking (Yadollahi et al., 2015). Efficient stress transfer between nanofiller and polymer plays an important role in improving adhesion strength. The local stress can be easily transferred onto the joined particles, leading to a larger local plastic deformation of the matrix when the particle comes into close contact with the polymer. The introduction of nanoparticles leads to better interfacial wettability and chemical compatibility between the adhesive and the substrate with a positive contribution to the shear resistance of the joints.

For hybrid phase nano reinforcement for bulk specimens, the strengthening mechanisms involve improved dispersion and the formation of a strong covalent bond. The addition of hybrid nanoparticles into polymer adhesive significantly improves interfacial strength by reducing agglomeration (Zhang et al., 2019). The second nanoparticle acts as a spacer between the first nanoparticle and prevents aggregations in the polymer. Moreover, the inclusion of hybrid nano-reinforcement into the polymer matrix provides the formation of a strong covalent bond between polymer groups and amine groups (Yang et al., 2011).

Similarly, for hybrid phase nano-reinforcement in joining specimens, the strengthening mechanisms involved include homogeneous dispersion, 3D filler network formation, abundance of functional groups, mechanical interlocking, catalytic effect and a high degree of miscibility. The addition of hybrid nano-reinforcement leads to more homogeneous filler dispersion. Moreover, the inclusion of hybrid nanofillers can lead to the formation of 3D network within the polymer matrix, resulting in better mechanical properties. The interaction between nanoparticles and adherend surface forms stronger adhesive bonding, leading to an improvement in joining strength. Furthermore, the secondary filler may affect to the kinetic cure due to the catalytic effect of hydroxyl groups, and changes in adhesive structure indicate a high degree of miscibility and cross-linking, which increases the joining strength.

Although studies have indicated that hybrid nano-reinforcement can improve the strength of adhesive joining, there is limited data available on this topic. Furthermore, the effects of concentration and weight ratio combinations of hybrid nano-reinforcement have not been extensively studied in detail in the literature. It appears that the addition of nanoparticles at certain concentrations has managed to improve the strength of adhesive joining to some extent. Below a certain concentration, the number of nanoparticles is not sufficient to induce a mechanical interlocking effect, resulting in no appreciable improvement in joining strength (Kaboorani and Riedl, 2012; Tutunchi et al., 2015a). On the other hand, above a certain concentration, the number of nanoparticles exceeds the number of available pores/voids, causing an inability of excess nanoparticles to fill the voids or pores on the adherend surface. As a result, the polymer is forced to be in a "strained" state, causing the specimen to debone easily (Yadollahi et al., 2015). Moreover, as discussed before, due to Van Der Waals force, excessive addition of nanoparticle tends to cause agglomeration, which may result in stress concentration and a subsequent reduction in joining strength.

Furthermore, it is also noticed that in most works in the literature, the effective nano-reinforcement content in polymeric adhesive for strength improvement has been reported to be up 2.0 wt%, where above this concentration, nanoparticles tend to agglomerate due to Van der Waals force (Jojibabu et al., 2020b). For this reason, in this current work, the addition of nanoparticles is made in the range up to 2.0 wt% to minimise the agglomeration effect that can cause a detrimental effect on the strength of adhesive joining. From literatures discussed in section 2.7.3.2 it is also noticed that for both bulk and adhesive joining specimens, it is unclear that how the weight ratio combination for different hybrid nano adhesives affects the strength of adhesive joining. This may be due to the combination of various type of nanoparticles, each with a unique geometry and chemical composition, resulting in different strengthening mechanisms when incorporated into polymeric adhesives. Specific to adhesive joining specimens, the very limited data available has also made it difficult to analyse the dependence of joining strength on the weight ratio combination in hybrid nanoparticles. Therefore, this study aimed to investigate the effect of weight ratio combination for Alumina/GNP hybrid nanoparticle, which was set to 0:10, 7:3, 5:5, 3:7 and 10:0.

In conclusion, the introduction of nanoparticles can lead to better interfacial wettability and chemical compatibility between the adhesive and the substrate, directly contributing to improved shear resistance of the joints. Literature suggests a lack of correspondence between wetting characteristics and joining, with the mechanism not well understood (Refer to Figure 2.19 and Table 2.11). Therefore, research on the effect of nanofiller inclusion on mechanical and physical properties is becoming a necessity for a more in-depth understanding.

Table 2.11 Strengthening mechanisms in nanomodified adhesives

Reinforcement	**Specimens**	**Strengthening mechanism**	**Remarks**	**Reference**
Single phase nano reinforcement	Bulk	Efficient stress transfer within polymer matrix	Silica carbide	(Guo et al., 2017)
		Crack deviation by nanoparticle	Alumina nanoparticle	(Osman et al., 2021)
		Network formation by good nanoparticle dispersion	Carbon nanotube	(Kaboorani and Riedl, 2012)
	Joining specimens	Efficient stress transfer between adhesive and adherend surface	N/A	(Yadollahi et al., 2015)
		Mechanical interlocking		(Kaboorani and Riedl, 2012; Tutunchi et al., 2015a)
		Interfacial wetting and chemical compatibility	Alumina nanoparticle	(Tutunchi et al. 2016)

Table 2.11 Continued

Reinforcement	**Specimens**	**Strengthening mechanism**	**Remarks**	**Reference**
Hybrid nano reinforcement	Bulk	Improved dispersion stability of nanoparticle in polymer	MWCNT/SiC	(Moghimi Monfared et al., 2018)
		Formation of strong covalent bond due to chemical interaction of functional group	MGP/MWCNT	(Yang et al., 2011)
	Joining specimens	Homogeneous filler dispersion	Different geometric shape of nanoparticle CNT/GNP	(Kumar et al., 2019)
		Formation of 3-D filler network	Different morphology of 1D and 2D nanoparticle	(Yue et al., 2014)
		Abundance of functional group leads to good interfacial adhesion	Functionalized CNT / SBM	(Jojibabu et al., 2020)
		Enhanced interfacial interaction between nanoparticle and substrate (mechanical interlocking)	PDA / MWCNT	(Subramanian et al., 2016)
		Catalytic effect of hydroxyl group and high degree of miscibility and cross linking	MWCNT / Alumina	(May et al., 2010)

CHAPTER 3

METHODOLOGY

3.1 Introduction

This chapter outlined the methodology in this research. It provided a comprehensive overview and detailed explanation of the project flow, encompassing specimen preparation, surface treatment, hybrid nano adhesive preparation, wetting behaviour analysis, tensile properties assessment, fracture behaviour evaluation and microstructural characterization through FE-SEM observation. The specification, characteristics, parameters of the materials would be presented in tabular form. Each table entry would be accompanied by a detailed description to facilitate a comprehensive understanding of the material properties under investigation.

Figure 3.1 shows the methodology flowchart for this study. Previous relevant research articles and pre-tests were pivotal in guiding the parameters for the experimental work. In this study, alumina nanoparticles and graphene nanoplatelets (GNP) would serve as nanofillers, with a specific Alumina/GNP hybrid nanoparticle content (0.0, 0.5, 1.0, 1.5 and 2.0 wt%) and weight ratio combination (0:10, 7:3, 5:5, 3:7 and 10:0). The dispersion of alumina and GNP into epoxy adhesive would create hybrid nano adhesives used in various types of specimens, including dog bone and single lap joint configurations. The aluminium alloy 7075-T6 adherends underwent surface treatment (abrasive blasting) before being subjected to wetting characteristic evaluation and single lap joint specimen preparation. For the wetting characteristic evaluation, a simple experimental setup was utilised. Validation of single lap joint specimens is crucial to ensure a uniform bond line thickness and complete coverage of the overlap region by the hybrid nano adhesive before proceeding to tensile testing. Various tests were conducted to comprehend the wetting behaviour, mechanical properties and microstructural characterisation of Alumina/GNP hybrid nano-reinforced adhesive. Lastly, the analysis and summary of these results would be presented and discussed in Chapter 4.

3.2 Methodology flow chart

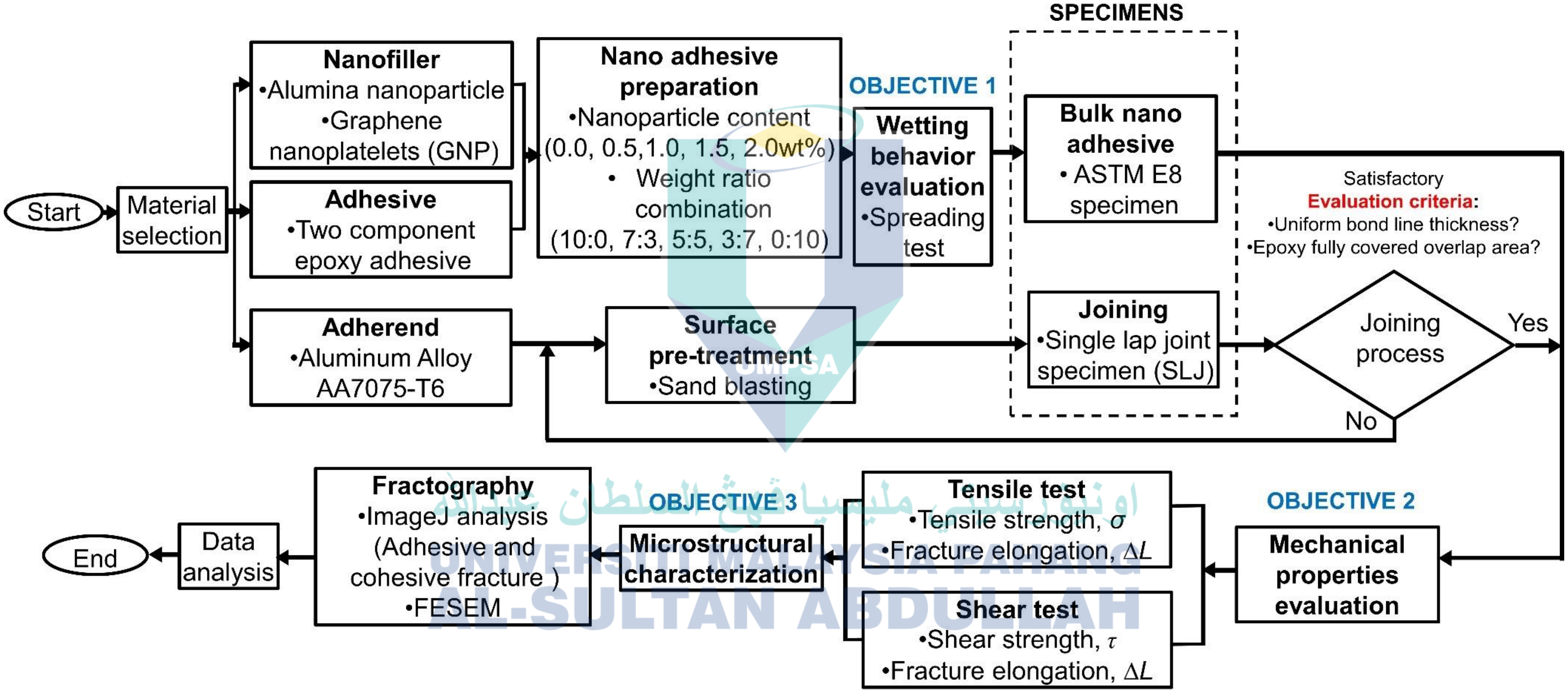

Figure 3.1 Methdology flow chart

3.3 Specimen preparation

The adherend used in this experiment was an Aluminium alloy 7075-T6 with a thickness of 2 mm. Aluminium alloy sheets were cut into the desired dimensions of 40 mm x 40 mm for physical properties analysis (Figure 3.2) and followed ASTM D1002 for joining specimens (Figure 3.3) using an LVD MVS-C 31/6 shear cutting machine as shown in Figure 3.4. A hole with an 8.0 mm diameter was drilled at one end of the adherend (grip area) to accommodate the customized slotted jig. At least 10 sets of specimens were utilised for every concentration and weight ratio combination.

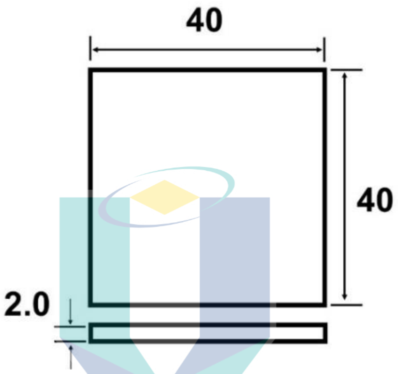

Figure 3.2 Dimension adherend in mm

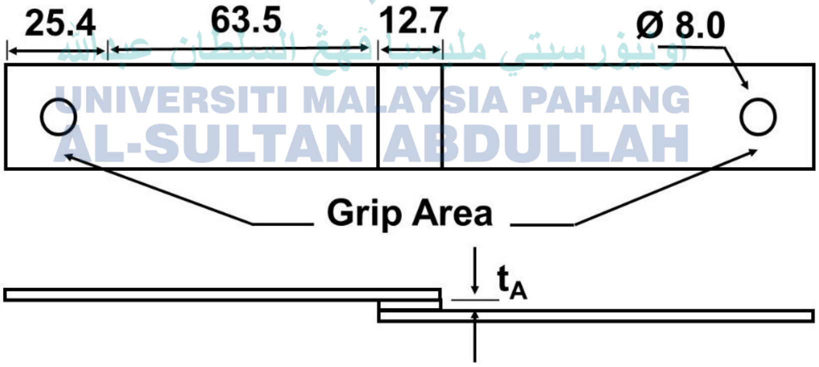

Figure 3.3 Schematic of lap configuration (according to ASTM D1002 specification) All dimensions are in mm

Figure 3.4 Shear cutting machine (LVD MVSC 31/6)

3.4 Surface treatment

To achieve optimal adhesion results between the substrate and adhesive, substrate surface preparation was a mandatory stage. For the pre-treatment process, the adherend surface of aluminium alloy 7075-T6 was wiped using Kim wipes (KIMTECH Science 34155A Kim wipes) and ethanol to remove existing contaminants such as identification markings from drawings or paint, dust, lubricants, and others. Subsequently, the adherend surface underwent a treatment process using abrasive blasting equipment (PanBlastTM, Woodlands, Singapore) as shown in Figure 3.5.

Figure 3.5 Abrasive blasting machine

The adherend was placed with a trajectory angle of 90° from the h=150 mm between the nozzle and the surface of the adherend, and it was subjected to a 621 kPa propelling stream of abrasive blasting with brown aluminium oxide powder grits#80, with an average particle size of 0.65 nm for 60s as shown in Figure 3.6. Table 3.1 shows the parameters used for abrasive blasting. Figure 3.7 displays the magnification of the aluminium oxide powder grits#80 under an optical microscope used for the blasting process. To eliminate debris residue, dry blown compressed air was used and the adherend was degreased in ethanol for 480 s using a Digital ultrasonic cleaning machine (GT Sonic VGT-2000, Guandong, China) as shown in Figure 3.8. Table 3.2 provides details on the degreasing process.

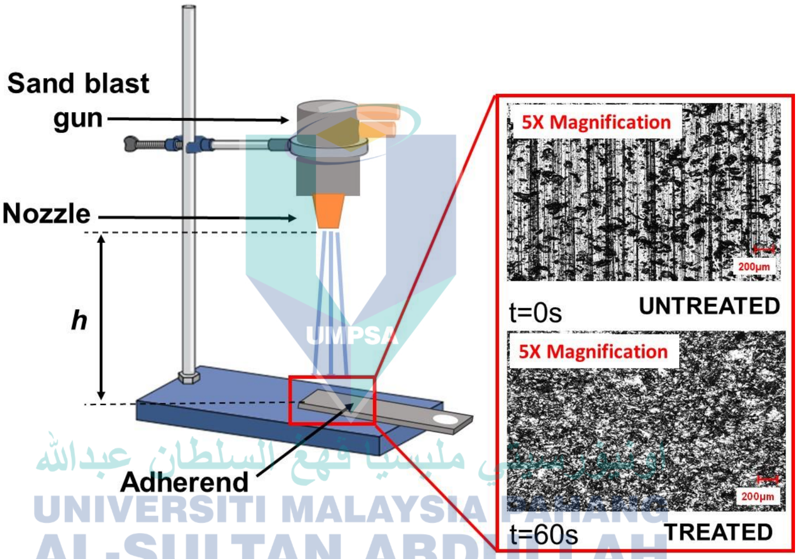

Figure 3.6 Schematic diagram for abrasive blasting

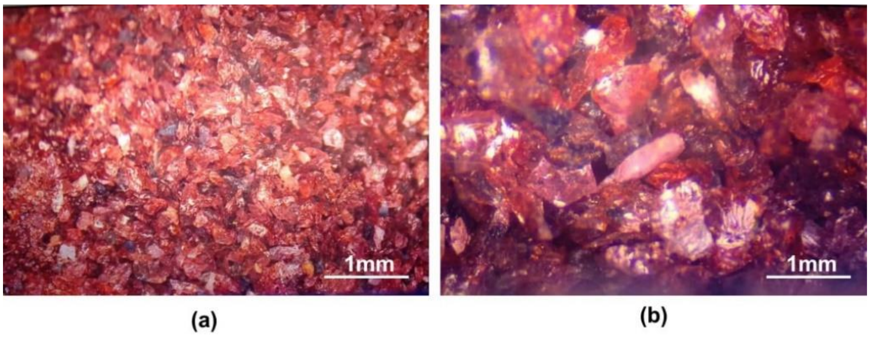

Figure 3.7 Microstructure of brown aluminium oxide powder under optical microscope with (a) 1x and (b) 4x magnification

Table 3.1 Parameter for abrasive blasting process

Specification	**Parameter**
Blasting distance, *h*	150 mm
Blasting angle, *Θ*	90 °
Blasting Time, *t*	60 s
Blasting pressure, *p*	621 kPa
Blasting powder	Brown aluminium oxide (#80)

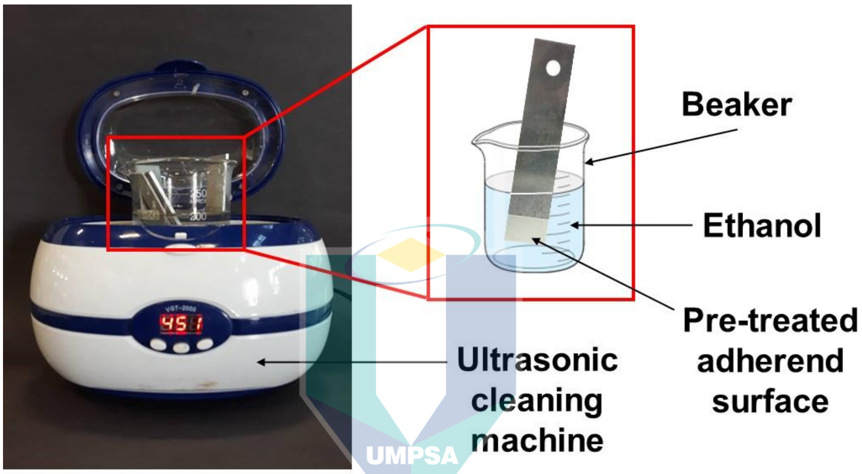

Figure 3.8 Digital ultrasonic cleaning machine

Table 3.2 Parameter for ultrasonic cleaning process

Specification	**Parameter**
Type of solvent cleaning	Ethanol
Time, *t*	480 s

3.5 Surface roughness

After the abrasive blasting process, the surface roughness of the adherends was determined using the surface roughness machine (MarSurf PS1, Mahr GMBH, Göttigen, Germany) as shown in the Figure 3.9. Surface roughness (Ra) determination was performed on both the untreated and treated surface adherends. The length of the measurement was set to 17.50 mm. Measurements were taken at random points on the adherend surfaces. For each specimen, the measurement was conducted five times and the obtained values were averaged.

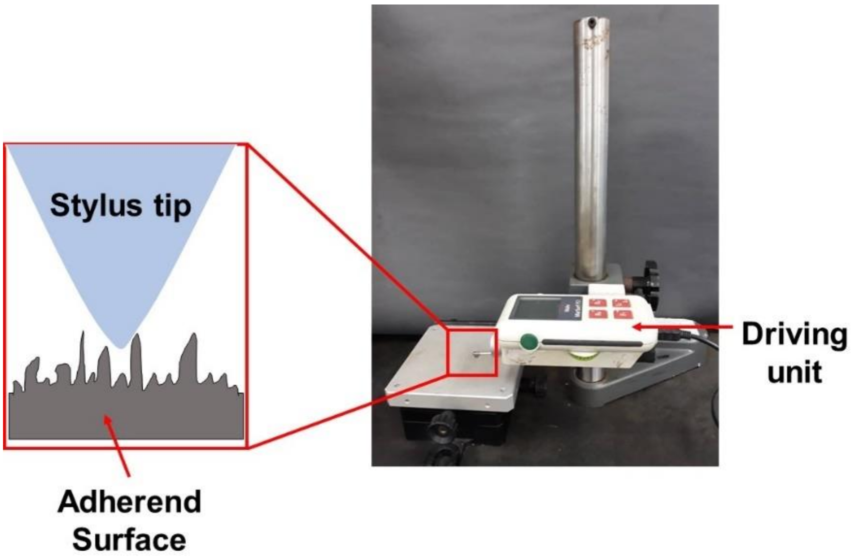

Figure 3.9 Surface roughness machine machine

3.6 Preparation of nano adhesive

The epoxy used for this experiment was Pioneer All-Purpose Epoxy Adhesive supplied by Republic Chemical Industries Inc, Quezon City, Philippines as shown in Figure 3.10. It consists of two parts: part A for the epoxy and part B for the hardener. Tables 3.3 and 3.4 show the properties of two-part components of the epoxy adhesive used in this experiment (epoxy A and epoxy B). Table 3.5 shows the parameters used to prepare the Alumina/GNP hybrid nano adhesive. As discussed in Chapter 2, Section 2.7.3.1 and 2.7.3.2, the nanoparticle content was set (0.0, 0.5, 1.0, 1.5 and 2.0 wt%) to minimize the risk of agglomeration (Osman et al., 2021) and high viscosity (Tutunchi et al., 2015b). In the previous discussion in section 2.11, the challenges arising from the limited and inconsistent data available on the impact of hybrid nanoparticles on joining performance were highlighted. This lack of data complicates the analysis of how joining performance depends on the weight ratio combination in hybrid nano adhesive. To address this issue, the current study focuses on establishing specific weight ratio combinations for the Alumina/GNP hybrid nano reinforcement, which include (0:10, 7:3, 5:5, 3:7, and 10:0).

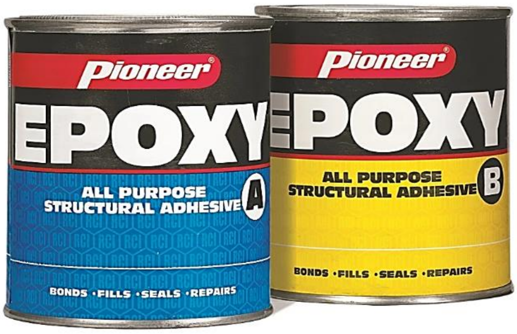

Figure 3.10 Epoxy adhesive (ALL PURPOSE STRUCTURAL ADHESIVE)

Table 3.3 Properties for Epoxy part A

Characteristic	**Properties**
Appearance (colour and physical state)	Pink, Paste
Relative density	1.90
Flash point	247 °C
Flammability	330 °C
Viscosity	1,500,000 cps

Refer Appendix A

Table 3.4 Properties for Epoxy part B

Characteristic	**Properties**
Appearance (colour and physical state)	Beige, Paste
Solubility	Immiscible
Relative density	1.47
Flammability	258 °C
Viscosity	745,000 cps

Refer Appendix B

Alumina/GNP hybrid nano adhesive was prepared under ambient conditions, at room temperature (25°C) and pressure. In order to achieve the performance demanded by the manufacturer, it was necessary to follow all the specified requirements, such as the recommended mixing ratio, which was 1:1. The preparation of Alumina/GNP hybrid nano adhesive was done in several stages as shown in Figure 3.11. It is expected that the staged mixing of nanoparticles under varying mixing intensities to gradually disperse them and decrease agglomeration (McGlasson et al., 2019). In specific, step 1 includes Ethanol (99.5% absolute C_2H_5OH supplied by EMC^2 Technology, Selangor, Malaysia) with a 1:10 weight ratio was added to the beakers containing alumina and GNP. The mixture of alumina and GNP with ethanol was performed in separate beakers using a magnetic stirrer (INTLAB, Shenzhen, Guangdong, China) for 10 minutes at 1000 rpm at room temperature. Afterward, the alumina solution and GNP solution were combined in one beaker using a magnetic stirrer for an additional 10 minutes at 1000 rpm at room temperature until both solutions were well dispersed, and no visible colour difference appeared as shown in step 2. Subsequently, epoxy Part A was added to the alumina-GNP solution and stirred continuously using a magnetic stirrer until all the hybrid nanoparticle/ethanol solutions were fully mixed with epoxy Part A. The usage of ethanol as dispersant can temporarily reduce adhesive's viscosity and facilitating nanoparticle dispersion during mixing. The ethanol was then removed later. The stirring process continued at 3000 rpm until all the ethanol fully evaporated as shown in step 3. The stirring process was monitored at intervals of 10 minutes to obtain the weight difference of the solution. The ethanol was removed from the solution by intermittent monitoring of the solution weight every 10 minutes, Specifically, the alumina/GNP nano adhesive solution containing ethanol solvent was placed on a high-precision analytical balance. The weight of the solution was recorded initially and then at 10-minute intervals during the ethanol removal process. As the ethanol evaporates from the open container, the total solution weight decreases over time. By tracking the weight change every 10 minutes, the rate of ethanol evaporation can be assessed as shown in Figure 3.12. Once the weight loss levels off, this indicates that most of the excess ethanol has been removed, leaving primarily the nanoparticles dispersed in the resin. The intermittent 10 minutes weight measurements allow for careful monitoring of the ethanol evaporation rate and determining the optimal endpoint for solvent removal. The total time needed can vary based on factors like the amount of ethanol, temperature, and air flow. Systematic weight tracking ensures reproducible solvent removal and prevents over-drying of the nano adhesive solution. Using solvents has been widely accepted as the simplest method to dispersed nanoparticle (J. Wei et al., 2015). Lastly, step 4 showed that the hybrid nanoparticle solution was mechanically mixed with hardener part B by using a mechanical stirring for about 1 minute until no visible colour was observed.

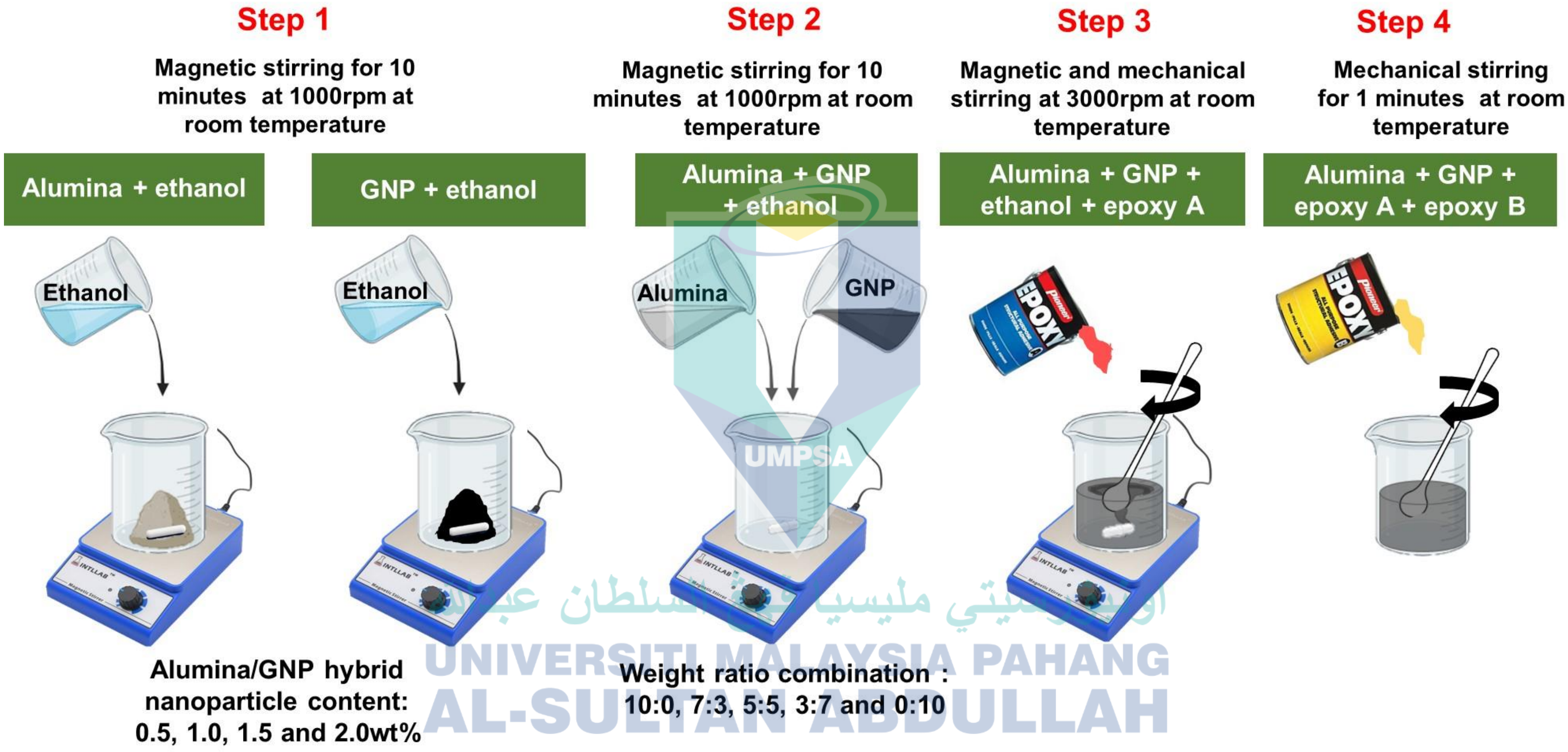

Figure 3.11 Schematic diagram for preparation of Alumina/GNP hybrid nano adhesive

Table 3.5 Parameter use for preparation of Alumina/GNP hybrid nano adhesive

Specification	**Ratio**	**Mixing method**	**Time**
Epoxy A: Epoxy B	1:1(100g)	-	-
Step 1 and 2	1 (Nanofiller): 10 (Ethanol) (0, 0.5,1.0, 1.5, 2.0wt.%) (0:10,3:7,5:5, 7:3,10:0)	Magnetic Stirring	10 min
Step 3	Epoxy A (50g)	Mechanical+ Magnetic Stirring	Until ethanol fully evaporated
Step 4	Epoxy B (50g)	Mechanical Stirring	1 min

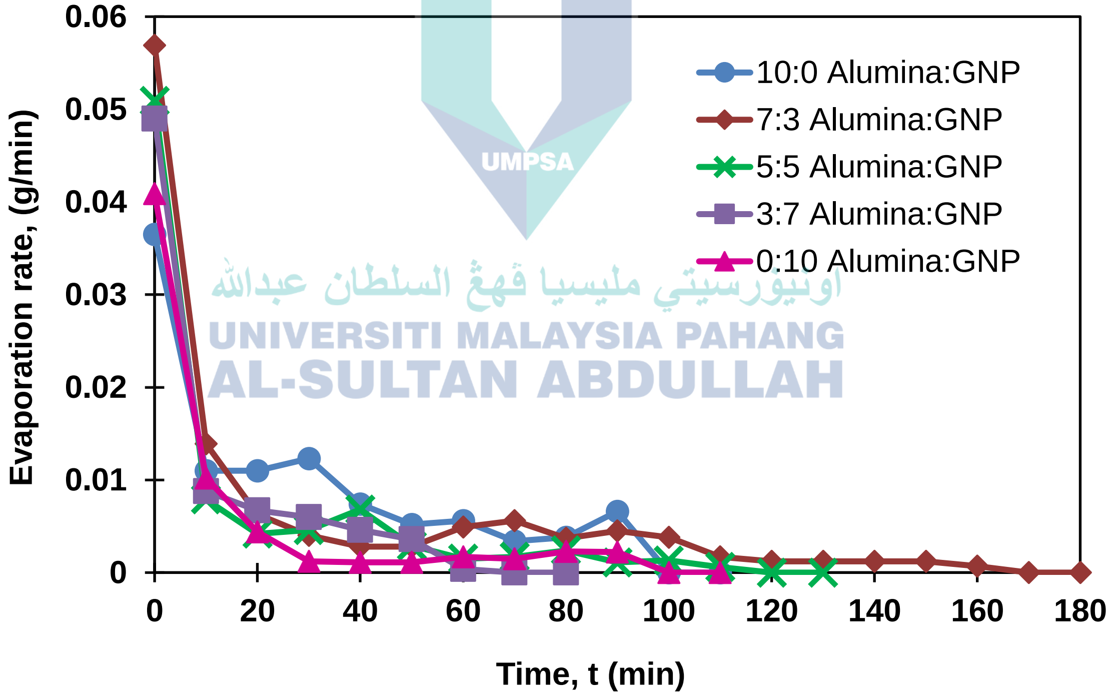

Figure 3.12 Evaporation rate of ethanol in Alumina/GNP/epoxy (Step 3)

3.7 Joining process

Two pieces of aluminium plates were assembled by using a customised fixture as shown in Figure 3.13. Table 3.6 shows the parameters used for curing single lap joint specimens. A 1.0ml drop of Alumina/GNP hybrid nano adhesive was applied to the pre-treated adherend surface using a syringe. The curing time was extended from the technical data sheet recommendation (i.e., 8 hours) for two reasons. First, to ensure complete curing of the materials, and second, due to practical concerns when scheduling laboratory operations. During the curing process, pressure was applied to the bonding area using a 1.0 kg weight to obtain a consistent adhesive layer and ensure that the hybrid nano-adhesive fully spread over the adherend surfaces. The pressure applied during the bonding process enhanced the surface wetting ability of the adhesive and affects the adhesive thickness. The main purpose of using this jig was to control the thickness of the adhesive (Alies and Khalil, 2022; Kong and Khalil, 2022). All specimens were measured to have an adhesive thickness, t_A of approximately 0.86 mm ± 0.02 mm.

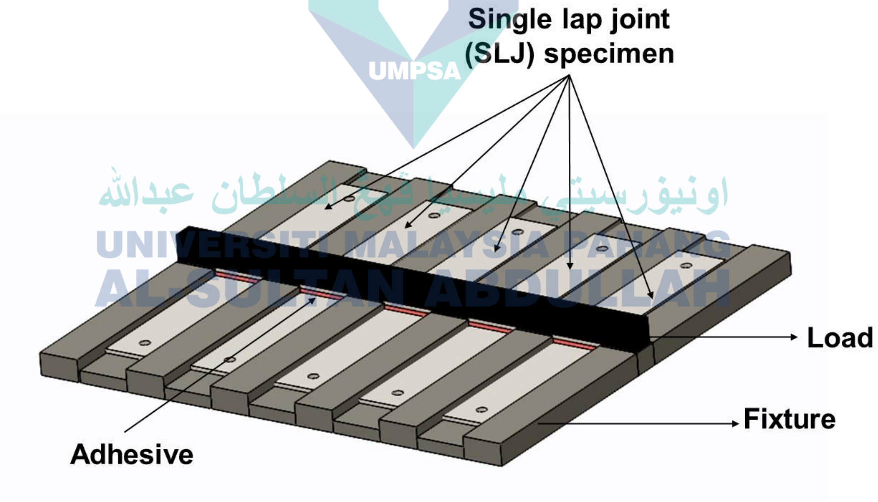

Figure 3.13 Schematic of fixture for curing single lap joint specimens

Table 3.6 Parameter use for curing process

Specification	Parameter
Overlap area, A	12.7 mm x 25.7 mm
Adhesive thickness, t_A	0.86 mm ± 0.02 mm
Curing time, t	24 h
Load weight	1.0 kg

3.8 Bulk adhesive specimen preparation

The bulk specimen was prepared into dog bond shape according to ASTM E8 standards as shown in Figure 3.14. An industrial silicone mold, which was as shown in Figure 3.15, was employed for specimen preparation. It is important to note that the application of a release agent (BUEHLER Release agent) is crucial to facilitate easy detachment/removal from the silicone mold. At least 10 specimens for each Alumina/GNP hybrid nanoparticle content and weight ratio combination were prepared to ensure the reliability of the results.

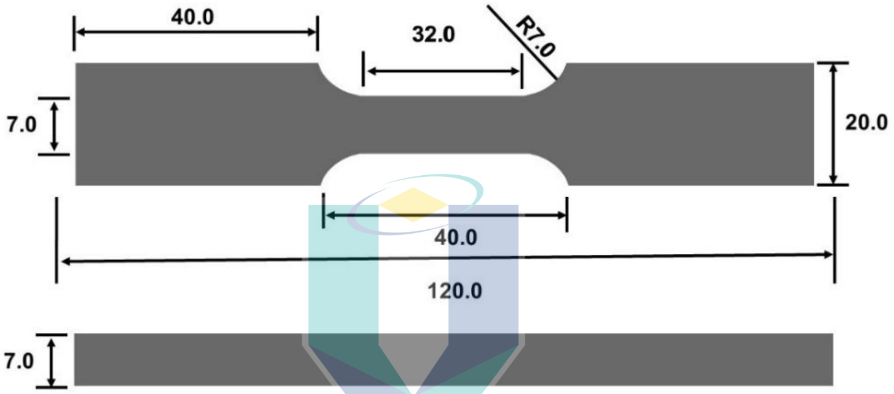

Figure 3.14 Geometry and dimension of bulk adhesive sample in mm (ASTM-E8)

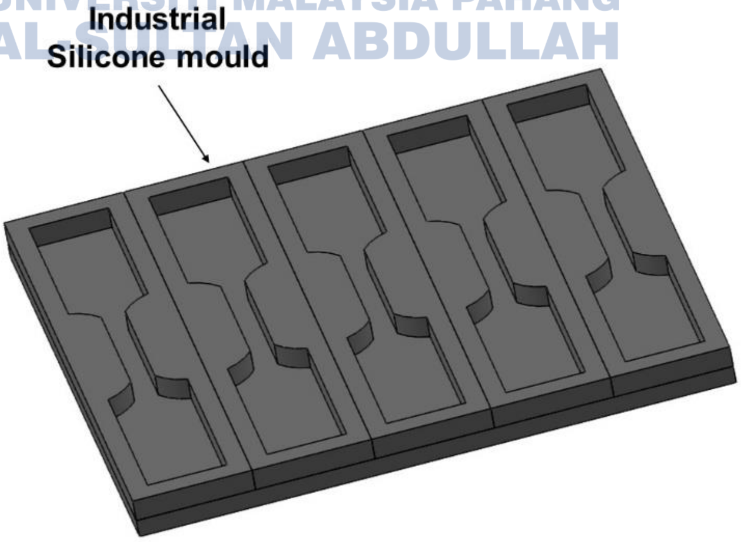

Figure 3.15 Industrial silicone mould designed following the ASTM E8 standard

3.9 Wetting properties

The spreadability test involved calculating the area of the epoxy mixture that had spread after a 3-minute drop onto the aluminum plate as illustrated in Figure 3.16. A 1.0 mL drop of epoxy mixture was dispensed using a clear syringe as shown in step 1 (Figure 3.16 (a)). A top-view photo of the epoxy droplet was taken with a smartphone equipped with a macro lens for better clarity. After the 5-minute droplet period, another photo was taken as shown in Step 2 (Figure 3.16 (b)). Subsequently, the photos were uploaded to a computer and analysed using an open-source pixel counting image processing software called ImageJ. Table 3.7 indicates the parameter used for wettability test.

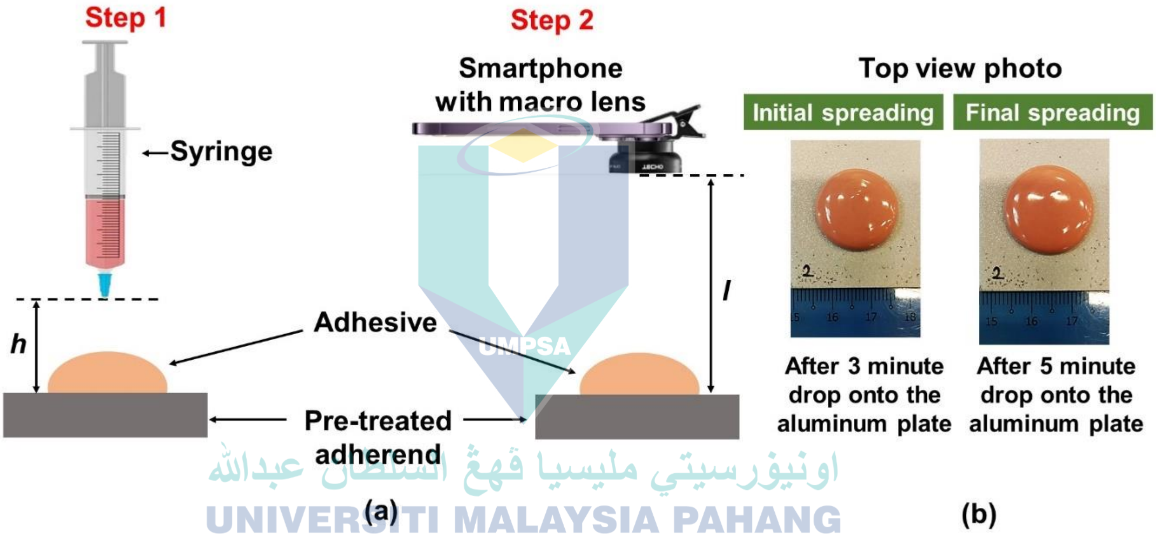

Figure 3.16 Schematic diagram of spread ability evaluation (a) Spread ability configuration and (b) Image taken using smartphone attached with macro lens

Table 3.7 Parameter for wettability test

Specification	**Parameter**
Volume drop, *v*	1.0 ml
Drop height, *h*	0.5 mm
Lens height, *l*	20.0 mm

3.10 Mechanical properties

The Alumina/GNP hybrid nano adhesive for bulk specimens (ASTM E8 specimens) and adhesive joining specimens (SLJ specimens) underwent testing using the Universal Instron tensile machine (INSTRON 3300 series, Norwood, MA, USA) at room temperature. The tensile test machine was configured with a force rate of 2.5 MPa/min and a crosshead rate of 1.0 Nm/min for bulk specimens, and 1.3 Nm/min for single lap joint specimens. Additional 0.8 mm diameter holes were drilled in the grip region to accommodate the geometry of the customized slotted jigs with 1 degree of freedom (1DOF, 1 translational) along the X-X axis. It is important to note that the use of customised slotted jigs aimed to reduce stress concentration and misalignment in the specimen. Figure 3.17 illustrates the configuration of the tensile shear testing. Table 3.8 provides the tensile test parameters.

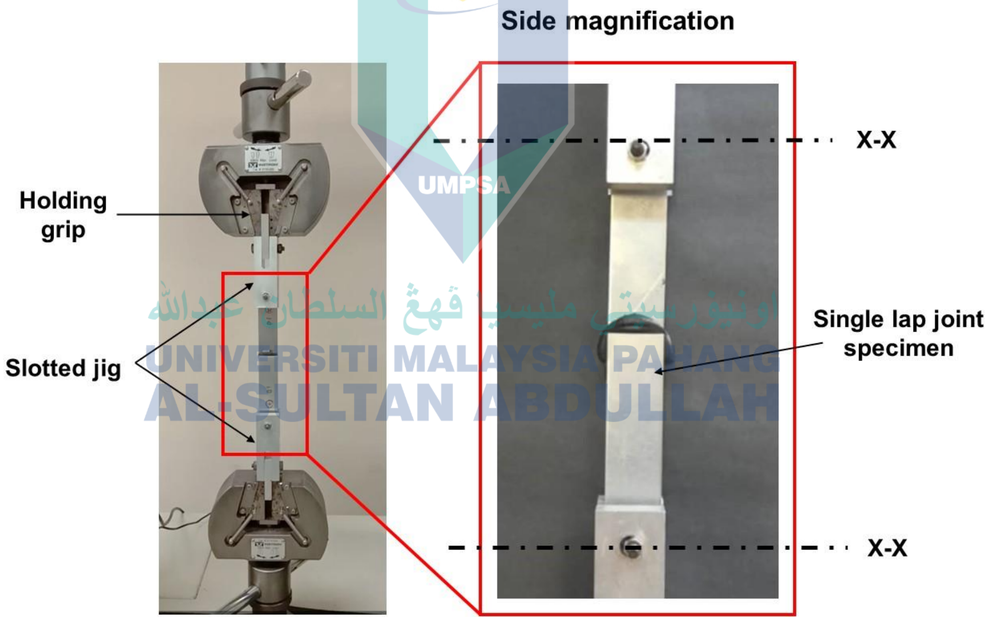

Figure 3.17 Tensile test machine

Table 3.8 Tensile test parameter

Specification	Parameter
Crosshead rate (ASTM E8 specimen)	1.0 Nm/min
Crosshead rate (single lap joint specimen)	1.3 Nm/min
Force rate	2.5 MPa/min

3.11 Fracture behaviour

The aluminium alloy joints subjected to tensile shear testing were examined for the type of fracture mode. The fractured joints were laid out on a flat surface and pictures of the fractured overlapping areas were taken. These images were then be observed to determine the type of fracture mode present. The fracture modes for each Alumina/GNP hybrid nanoparticle content and weight ratio combination were documented. Subsequently, the images were processed using an open-source pixel counting program called ImageJ. The software calculated the area of epoxy coverage on both sides of the adherends. Figure 3.18 (a) show fracture image of the joining specimen and Figure 3.18 (b) show fracture image of joining specimen after the brightness and saturation colour adjustment were made by ensuring the epoxy coverage was distinctly marked in yellow for cohesive fracture mode.

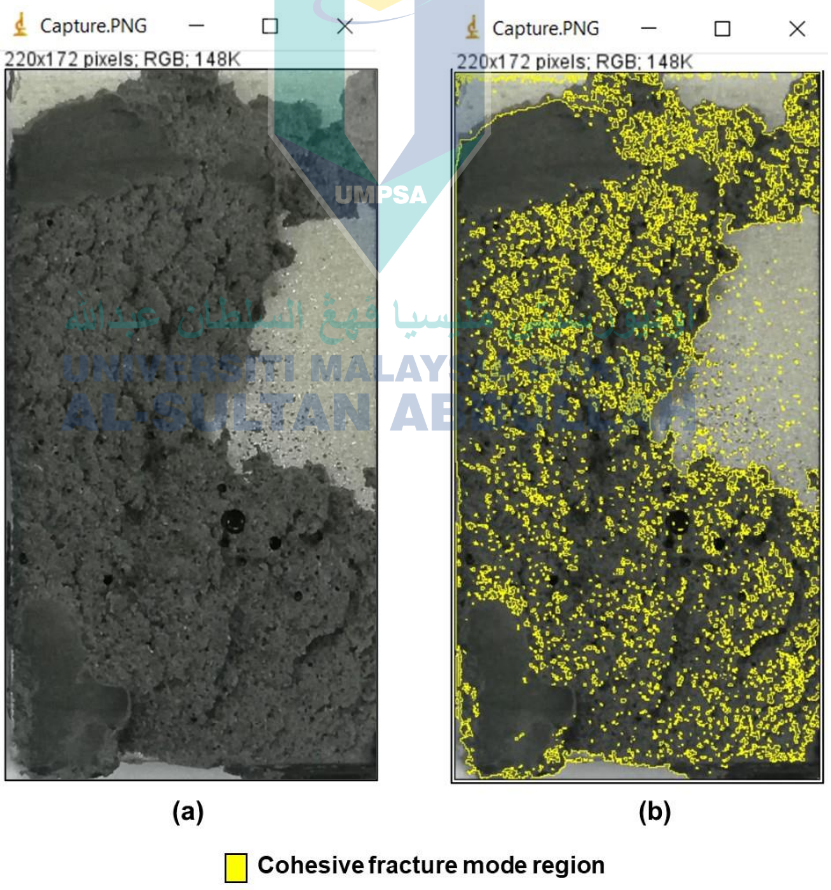

Figure 3.18 Type of fracture mode distinguish by ImageJ software (a) Fracture image of joining specimen and (b) Fracture image of joining specimen after the brightness and saturation colour adjustment

3.12 Microstructural analysis

The microstructural analysis of the fracture behaviour of Alumina/GNP hybrid nano adhesive utilized a field emission scanning electron microscope (FE-SEM). The fractured samples from bulk specimens were cut to a maximum dimension of 30 mm x 30 mm x 30 mm to fit within the FE-SEM machine (JSM-7800F, JEOL Ltd., Akishima, Tokyo, Japan) as depicted in Figure 3.19. The microstructural investigation was conducted at a high voltage of 10 kV and the samples had to be coated to enhance electron signal reception. This method offers detailed topographical information about the fractured surface, ranging from magnifications of 250x to 100,000x.

Figure 3.19 Field Emission Scanning Electron Microscope (FE-SEM) machine

CHAPTER 4

RESULTS AND DISCUSSION

4.1 Introduction

On the scope of this work, this chapter discussed the results and analysis. Each result was explained and discussed accordingly, including wetting behaviour studies, tensile properties (ASTM E8 specimen), shear properties (SLJ specimen) and fracture behaviour analysis (ImageJ and FE-SEM). The discussion also included parametric analysis using a correlation matrix and correlation heatmap.

4.2 Nanoparticles

In the present work, commercially available Alumina nanoparticles and GNP supplied by Sigma Aldrich (St, Louis,Mi USA) were used as the hybrid nano reinforcement particles. Figure 4.1 illustrates the morphology of Alumina nanoparticle and GNP. Alumina nanoparticles exhibit a spherical shape with a particle size of 13 nm and an average surface area of 85m^2 as received. Meanwhile, GNP has a random flake-like morphology with the presence of agglomeration. The lateral dimension was observed to be about 1~2 µm, which matched the specifications provided by the manufacturer (<2 µm).

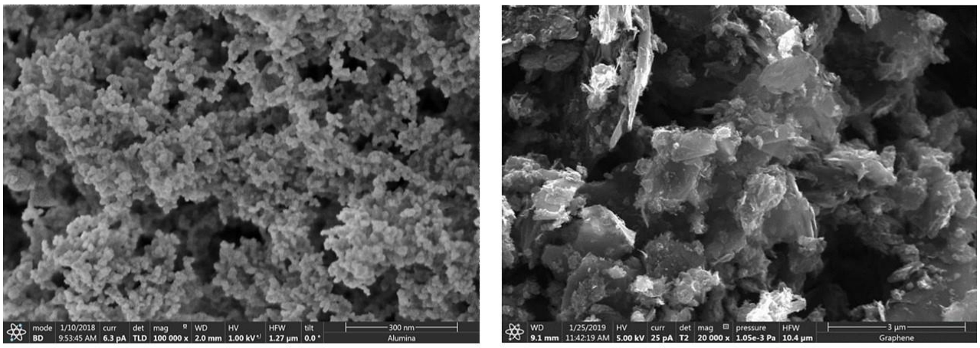

(a) (b)

Figure 4.1 The morphology of as-received (a) Alumina nanoparticle and (b) GNP

4.3 Morphology and profilometer of adherend surface

As mentioned in section 3.4, abrasive blasting was chosen as the surface treatment for the AA7075-T6 adherend. Figure 4.2 shows the morphology of the untreated adherend and treated adherend under an optical microscope. Based on the morphology images, it could be observed that the untreated adherend had a relatively smooth surface with some corrugated patterns, while the treated adherend had a rougher surface with the existence of dimples and holes.

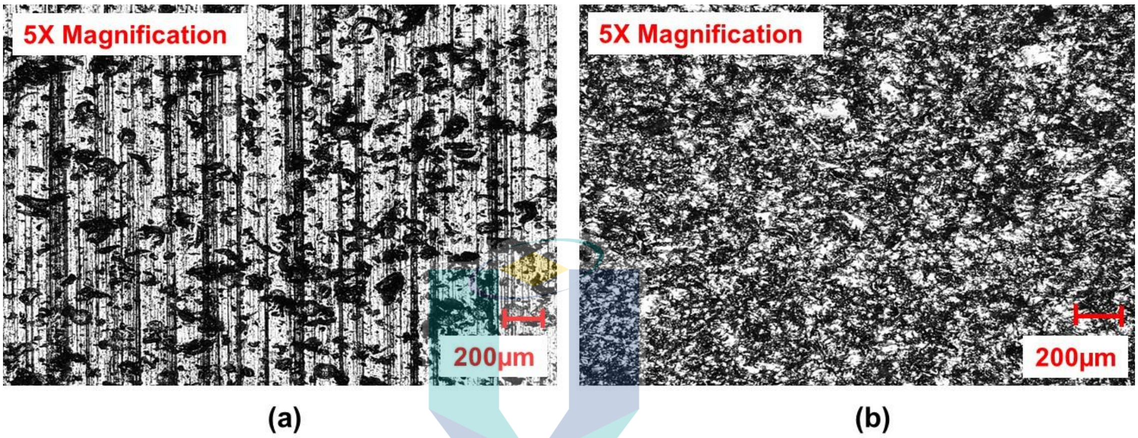

Figure 4.2 Morphology of (a) untreated adherend and (b) treated adherend under optical microscope

Figure 4.3 represents profilometer surface roughness of the untreated and treated adherend respectively. Ra represent the average value of surface roughness, measuring the average distance between peaks and valley as well as the deviation from the mean line on the entire surface within the sampling line (Georgakopoulos-Soares et al., 2023). A higher Ra value indicates higher roughness. There was a distinct difference in the surface profile roughness of the adherend surface. The Ra value of the adherend increased after surface treatment was conducted. The average Ra value for the untreated surface was 0.31 µm ± 0.03 µm, while the average Ra value of the treated adherend was 2.51 µm ± 0.19 µm. It is worth noting that the main purpose of adherend surface treatment was to remove existing contaminants and, at the same time, to create a textured surface to allow for optimum/sufficient adhesion between the adhesive and substrate. This is expected for the nano adhesive to flow into these gaps to provide better adhesion by mechanical interlocking (Molitor et al., 2001), which was previously discussed in Section 2.7.2.

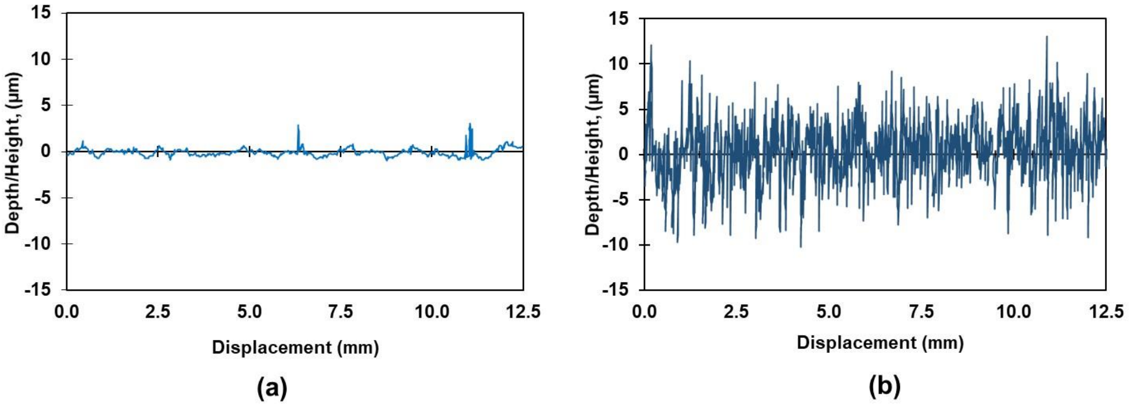

Figure 4.3 Profilometer of (a) untreated adherend and (b) treated adherend with its respective roughness average (Ra) value

4.4 Wetting behaviour

This section discussed the effect of Alumina/GNP hybrid nano reinforcement on the wettability of adhesive joining at various Alumina/GNP hybrid nanoparticle content and weight ratio combinations. The discussion also included parametric analysis by using a correlation matrix and a correlation heatmap.

Due to some limitations, in current setup, the contact angle could not be measured precisely. However, the spread area does give the similar indicator as contact angle does. Spread area is one of the common parameters for determining the wetting behaviour of hybrid nano adhesive where smaller contact angle and/or larger spread area represent the larger wetting behaviour (Alies and Khalil, 2022). For ease comprehension, the illustration of wetting behaviour with common parameter (Spread area and contact angle) are shown in Figure 4.4.

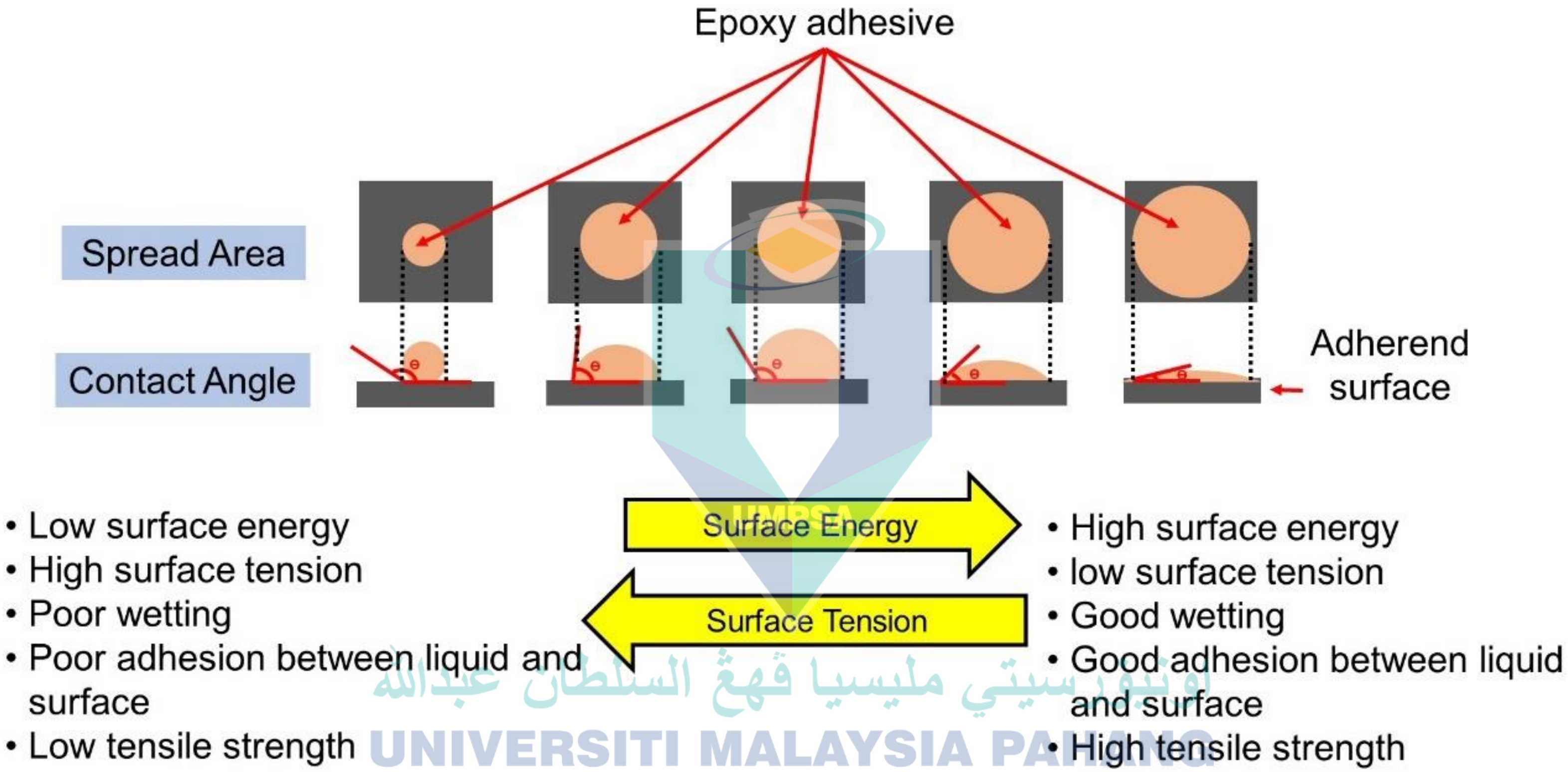

Figure 4.4 Re-illustration of wetting behaviour of adhesive

Source : Alies and Khalil (2022)

4.4.1 Effect of Alumina/GNP hybrid nano reinforcement to the spread area

Figure 4.5 shows the representative spread area of Alumina/GNP hybrid nano adhesive at various hybrid nanoparticle content and weight ratio combinations. Additionally, Table 4.1 provides a summary of the spread area for alumina/GNP hybrid nano adhesive at various hybrid nanoparticle content and weight ratio combinations.

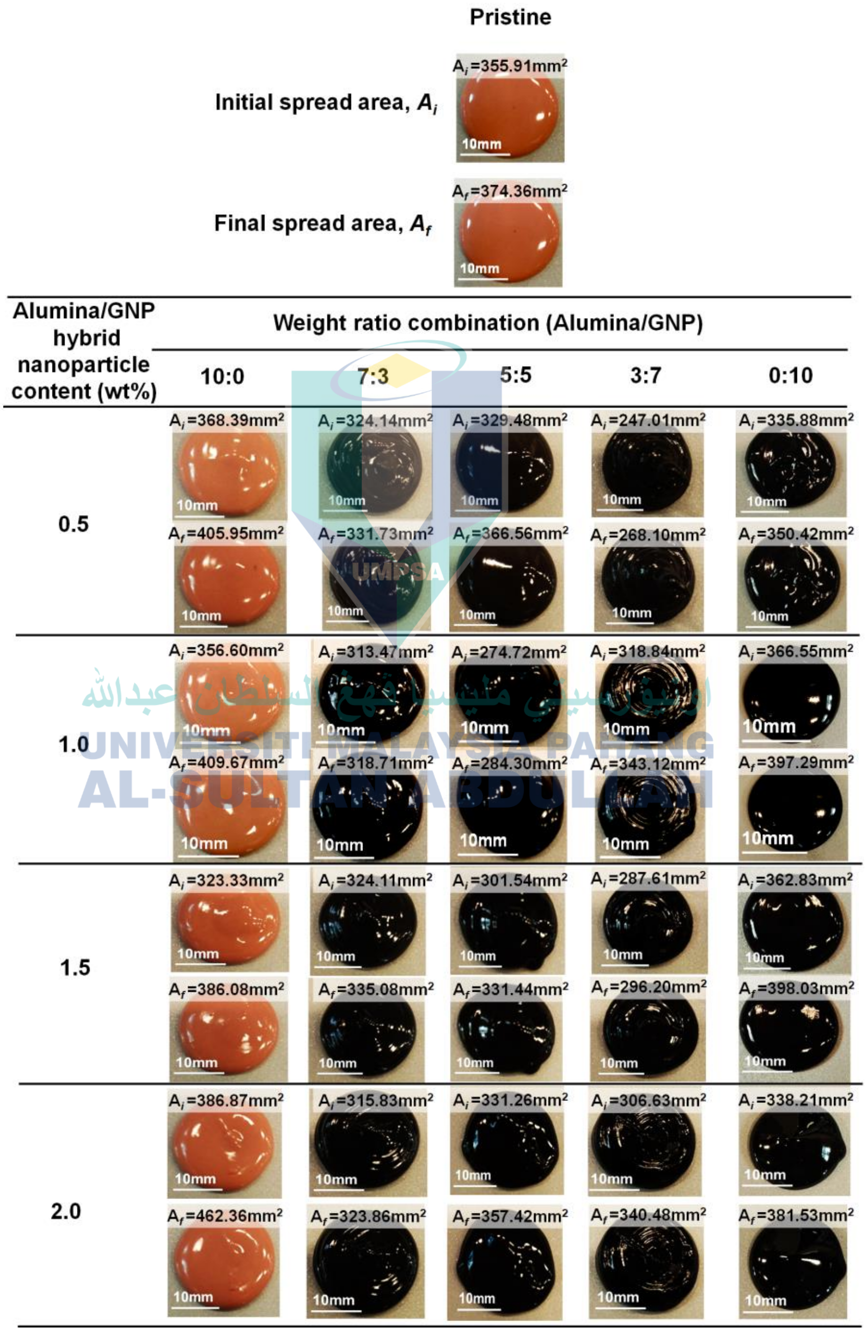

Figure 4.5 Representative spread area of Alumina/GNP hybrid nano adhesive at various hybrid nanoparticle content and weight ratio combinations

Table 4.1 Summary of spread area for Alumina/GNP hybrid nano adhesive at various hybrid nanoparticle content and various weight ratio combinations

Alumina/GNP hybrid nanoparticle content (wt%)	**Weight ratio combination (Alumina:GNP)**	**Spread area, *A* (mm^2)**
Pristine	-	18.45 ± 1.49
0.5	10:0	41.57 ± 6.31
	7:3	7.59 ± 0.66
	5:5	37.08 ± 2.52
	3:7	21.08 ± 3.07
	0:10	14.55 ± 0.82
1.0	10:0	53.07 ± 3.49
	7:3	5.24 ± 0.66
	5:5	9.58 ± 0.84
	3:7	24.28 ± 1.39
	0:10	30.37 ± 4.62
1.5	10:0	62.73 ± 5.01
	7:3	10.97 ± 2.14
	5:5	29.90 ± 3.40
	3:7	8.59 ± 0.89
	0:10	35.20 ± 5.66
2.0	10:0	75.48 ± 3.10
	7:3	8.03 ± 2.12
	5:5	26.16 ± 2.05
	3:7	33.84 ± 4.55
	0:10	43.31 ± 6.84

Figure 4.6 shows the spread area of Alumina/GNP hybrid nano adhesive at various hybrid nanoparticle contents for different weight ratio combinations, specifically (a) 10:0, (b) 7:3, (c) 5:5, (d) 3:7 and (e) 0:10. In Figure 4.6 (a), when compared to the pristine adhesive at the 10:0 weight ratio combination (i.e., Single alumina weight ratio), the addition of 0.5-2.0 wt% Alumina/GNP hybrid nano reinforcement resulted in an increment in spread area up to 125.31% ± 323.49%, 187.65% ±134.23%, 240.0% ± 236.24% and 309.12% ± 108.05%, respectively. As for spread area in Figure 4.6 (b), it could be seen that Alumina/GNP hybrid nano adhesive at the 7:3 weight ratio combination exhibited a decrement in spread area of 58.84% ± 55.70%, 71.58% ± 55.70%, 40.57% ± 43.62% and 56.50% ± 42.28%, respectively compared to the pristine adhesive. In Figure 4.6 (c), the addition of Alumina/GNP hybrid nano reinforcement at the 5:5 weight ratio combination had shown improvement in spread area by 100.96% ± 69.13%, 62.08% ± 128.19%, and 41.78% ± 37.58%, respectively compared to the pristine adhesive counterpart at 0.5, 1.5 and 2.0 wt%. However, at 1.0 wt% of Alumina/GNP hybrid nano adhesive, a decrement in spread area was recorded, with a reduction of 48.06% ± 43.62% compared to the pristine adhesive counterpart. From Figure 4.6 (d), when compared to the pristine adhesive, the addition of 0.5, 1.0 and 2.0 wt% of Alumina/GNP hybrid nano adhesives at the 3:7 weight ratio combination resulted in an increment in spread area by 14.28% ± 106.04%, 31.61% ± 6.71% and 83.44% ± 205.37%, respectively. Meanwhile, a decrement in spread area up to 53.43% ± 40.27% was recorded for 1.5 wt% of Alumina/GNP hybrid nano reinforcement. In Figure 4.6 (e), when compared to the pristine adhesive at the 0:10 weight ratio combination (i.e., Single GNP weight ratio), the addition of 0.5 wt% Alumina/GNP hybrid nano reinforcement resulted in a decrement in spread area by 21.16% ± 44.97%. Meanwhile, the addition of single GNP nano reinforcement at 1.0, 1.5 and 2.0 wt% recorded an improvement in spread area by 64.63% ± 210.07%, 90.81% ± 279.87% and 134.76% ± 359.06%, respectively compared to the pristine adhesive counterparts.

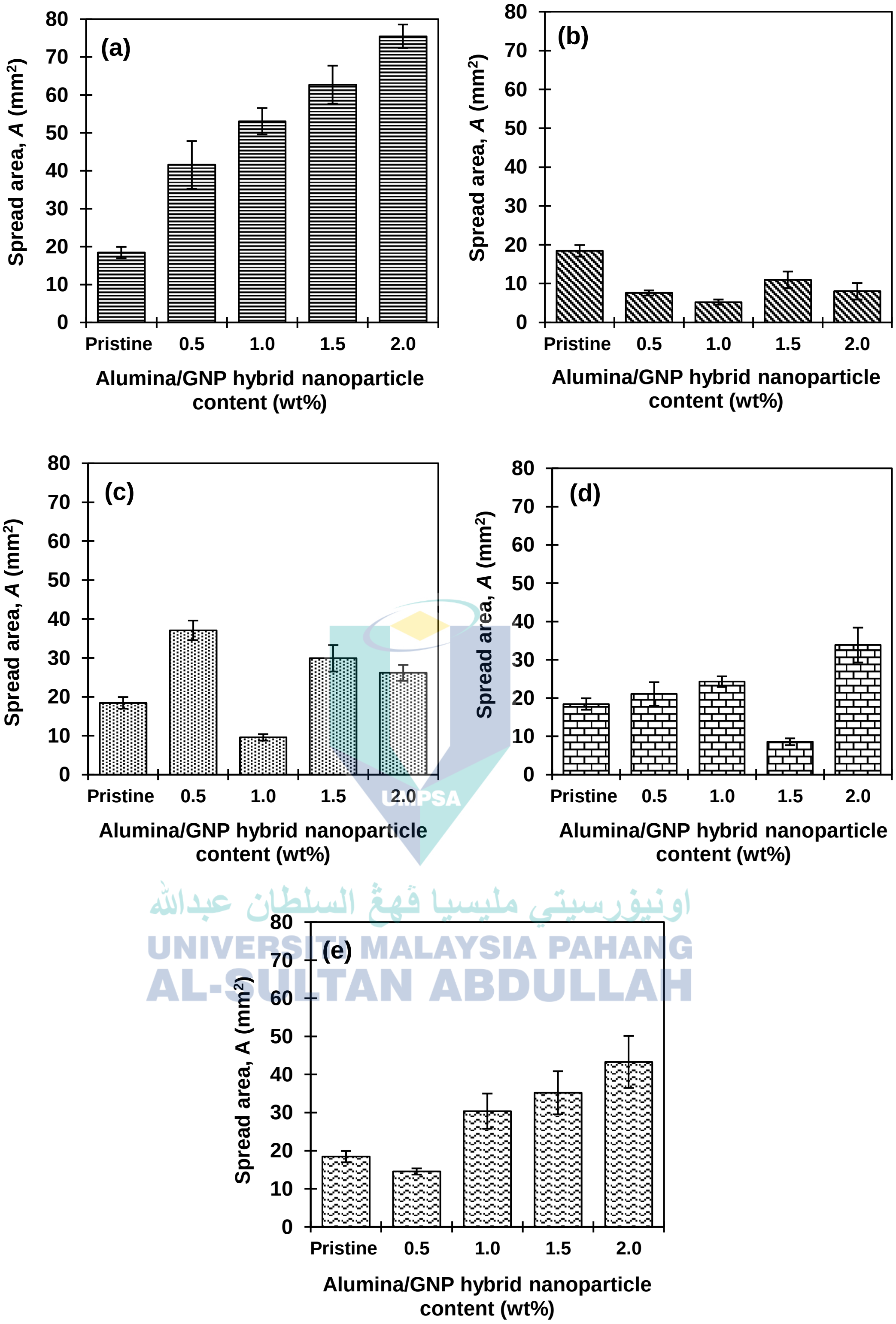

Figure 4.6 Spread area of Alumina/GNP hybrid nano adhesive at various hybrid nanoparticle content in (a) 10:0, (b) 7:3, (c) 5:5, (d) 3:7 and (e) 0:10 weight ratio combinations

Figure 4.7 illustrates the spread area of Alumina/GNP hybrid nano adhesive at various weight ratio combinations for different hybrid nanoparticle contents, specifically (a) 0.5 wt%, (b) 1.0 wt%, (c) 1.5 wt%, and (d) 2.0 wt%. In Figure 4.7 (a), a comparison with the pristine adhesive showed that at the 10:0, 5:5, and 3:7 weight ratio combinations, the addition of 0.5 wt% Alumina/GNP hybrid nanoparticle content resulted in an increase in spread area by125.31% ± 323.49%, 100.96% ± 69.13% and 14.28% ± 106.04%, respectively. Meanwhile, at the 7:3 and 0:10 weight ratio combinations of Alumina/GNP hybrid nanoparticle content, there was a decrement in spread area up to 58.84% ± 55.70% and 21.16% ± 44.97%, respectively when compared to the spread area of pristine adhesive counterparts. In Figure 4.7 (b), a comparison with the pristine adhesive revealed that at the 10:0, 3:7, and 0:10 weight ratio combinations, the addition of 1.0 wt% Alumina/GNP hybrid nanoparticle content led to an increase in spread area by 187.65% ± 134.23%, 31.61% ± 6.71% and 64.63% ± 210.07%, respectively. Meanwhile, at the 7:3 and 5:5 weight ratio combinations of Alumina/GNP hybrid nano reinforcement, there was a decrement in spread area up to 71.58% ± 55.70% and 48.06% ± 43.62%, respectively when compared to the spread area of pristine adhesive counterparts. In Figure 4.7 (c), when compared to pristine adhesive counterparts at 10:0, 5:5, and 0:10 weight ratio combinations, the addition of 1.5 wt% Alumina/GNP hybrid nanoparticle content resulted in an increment in spread area up to 240.0% ± 236.24%, 62.05% ± 128.19, and 90.81% ± 279.87%, respectively. Meanwhile, at the 7:3 and 3:7 weight ratio combinations of Alumina/GNP hybrid nano reinforcement, there was a decrement in spread area up to 40.57% ± 43.62% and 53.43% ± 40.27%, respectively when compared to the spread area of pristine adhesive counterparts. As for Figure 4.7 (d), when compared to pristine adhesive at 10:0, 5:5, 3:7 and 0:10 weight ratio combinations, the addition of 2.0 wt% Alumina/GNP hybrid nanoparticle content resulted in an increment in spread area up to 309.12% ± 108.05%, 41.78% ± 37.58%, 83.44% ± 205.37% and 134.76% ± 359.06%, respectively. Meanwhile, at the 7:3 weight ratio combination of Alumina/GNP hybrid nano reinforcement, there was a decrement in spread area up to 56.50% ± 42.28% when compared to pristine adhesive counterparts. To further investigate quantitatively and in more detail, heatmap analysis and Pearson’s correlation for the effect of varying nanoparticle content and weight ratio combinations of Alumina/GNP hybrid nano adhesives have been extensively discussed in Section 4.4.2.

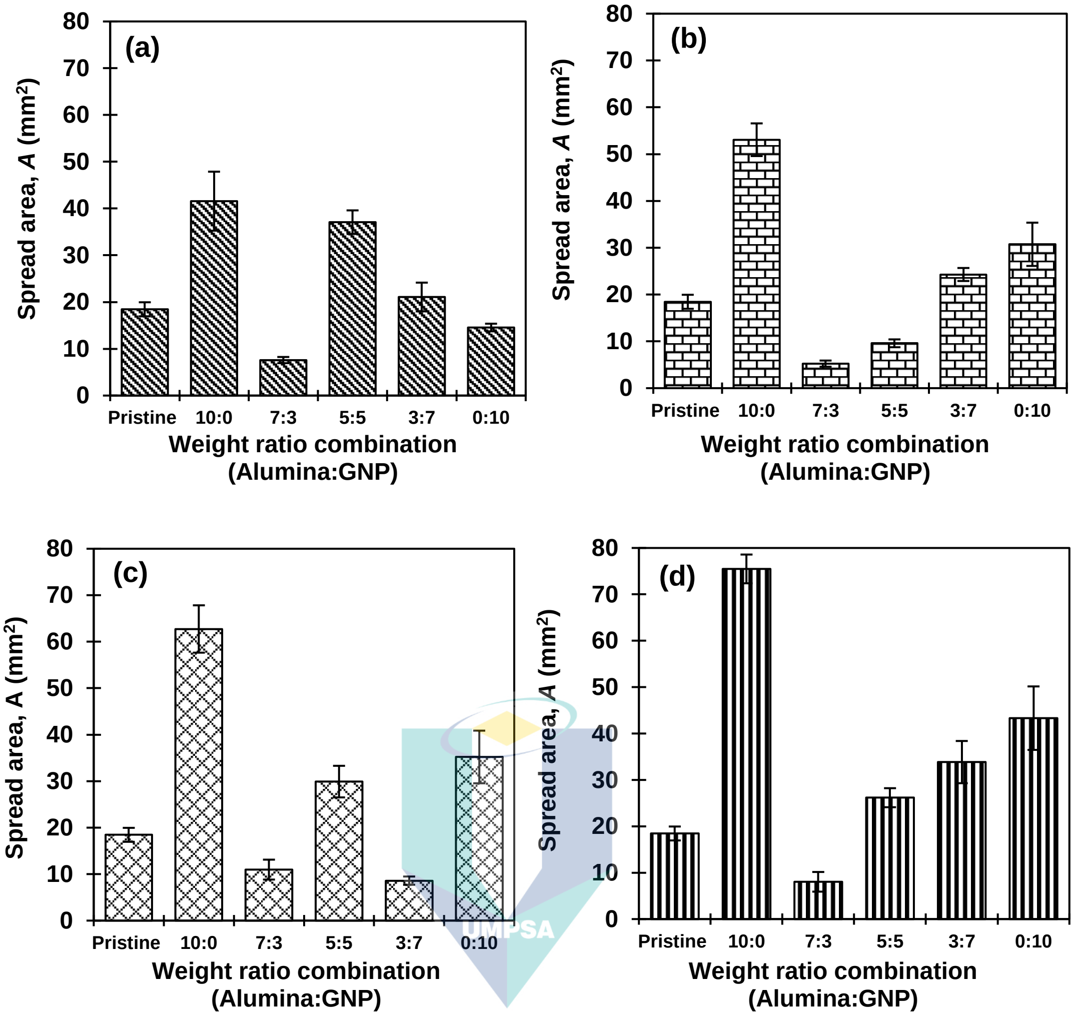

Figure 4.7 Spread area of Alumina/GNP hybrid nano adhesive at various weight ratio combination in (a) 0.5 wt%, (b) 1.0 wt%, (c) 1.5 wt%, and (d) 2.0 wt% hybrid nanoparticle content

4.4.2 Pearson correlation and Heatmap analysis for wetting behaviour in Alumina/GNP hybrid nano adhesive

Figures 4.8 to 4.11 depict the correlation matrix and correlation heatmap for the spread area in Alumina/GNP hybrid nano adhesive. In the correlation heatmap, colour coding represents the correlation between two variables, with red shades indicating a positive correlation (R > 0) and green shades indicating a negative correlation (R < 0). From these figures, it is evident that, irrespective of the Alumina/GNP hybrid nanoparticle content, the combination of alumina nanoparticle weight ratio and spread area exhibited a positive relationship at 0.5-2.0 wt% with R-values of 0.47, 0.25, 0.42 and 0.28, respectively. This implied that the alumina nanoparticle weight ratio was directly proportional to the spread area of Alumina/GNP hybrid nano adhesive. One possible mechanism for this observation was the higher surface free energy of the nanoparticle, which might have contributed to an improvement in surface interface energy, resulting in a hydrophilic nature and subsequent enhancement in wetting behaviour (Khalil et al., 2019). Furthermore, the presence of alumina nanoparticle enlarged the area of interaction between the alumina and polymer matrix, thus enhancing the adhesion strength per interaction area (Zhai et al., 2008).

On the contrary, it was noteworthy that the GNP weight ratio and spread area exhibited a negative relationship at 0.5-2.0 wt% with R-values of -0.47, -0.25, -0.42 and -0.28, respectively. This suggested that the GNP weight ratio was inversely proportional to the spread area of the Alumina/GNP hybrid nano adhesive. This inverse correlation might be attributed to a robust interaction between GNP and the polymer matrix, resulting in a significant increase in viscosity (Dong et al., 2021). In addition, the reduction in the spread area of Alumina/GNP hybrid nano adhesives could be linked to the molecular-level dispersion of GNPs in the polymer matrix and the formation of strong hydrogen bonds between GNPs and the polymer matrix. The presence of strong hydrogen bonding interactions between oxygen-containing groups such as hydroxyls and carboxyl's in GNP and the hydroxyls in epoxy chains might be responsible for these strong hydrogen bonding interactions (Moosa et al., 2016).

In summary, irrespective of the Alumina/GNP hybrid nanoparticle content, the inclusion of alumina nanoparticle at every weight ratio combination indicated improved wetting behaviour, resulting in improved spreading. Conversely, the inclusion of GNP at every weight ratio combination indicated reduced wetting behaviour as shown in Figure 4.12. For easy comprehension, the overall summary findings of the wetting behaviour (i.e., spread area) for Alumina/GNP hybrid nano adhesive are shown in Figure 4.13.

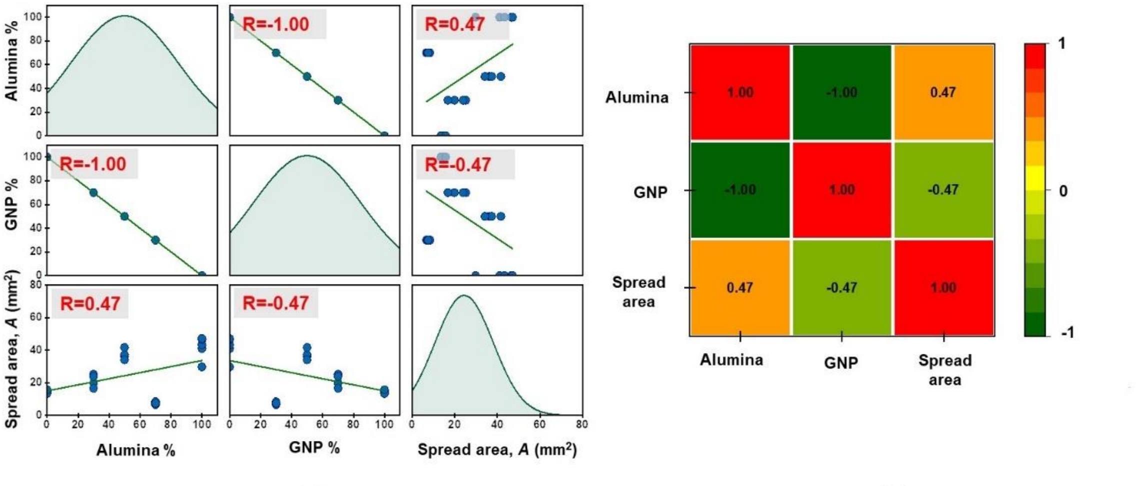

(a) (b)

Figure 4.8 (a) Correlation matrix and (b) correlation heatmap presenting the significance of Alumina/GNP hybrid nano reinforcement to spread area of nano adhesive at 0.5 wt% hybrid nanoparticle content

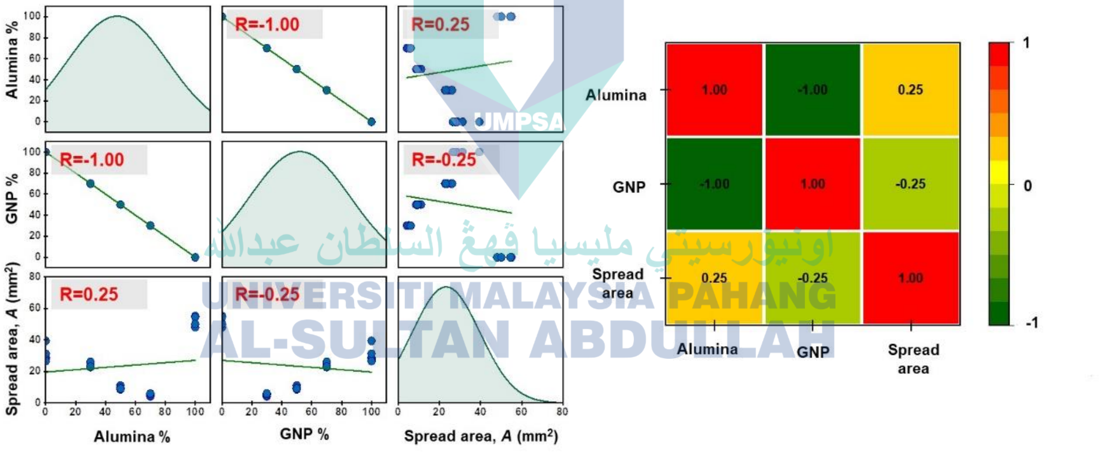

(a) (b)

Figure 4.9 (a) Correlation matrix and (b) correlation heatmap presenting the significance of Alumina/GNP hybrid nano reinforcement to spread area of nano adhesive at 1.0 wt% hybrid nanoparticle content

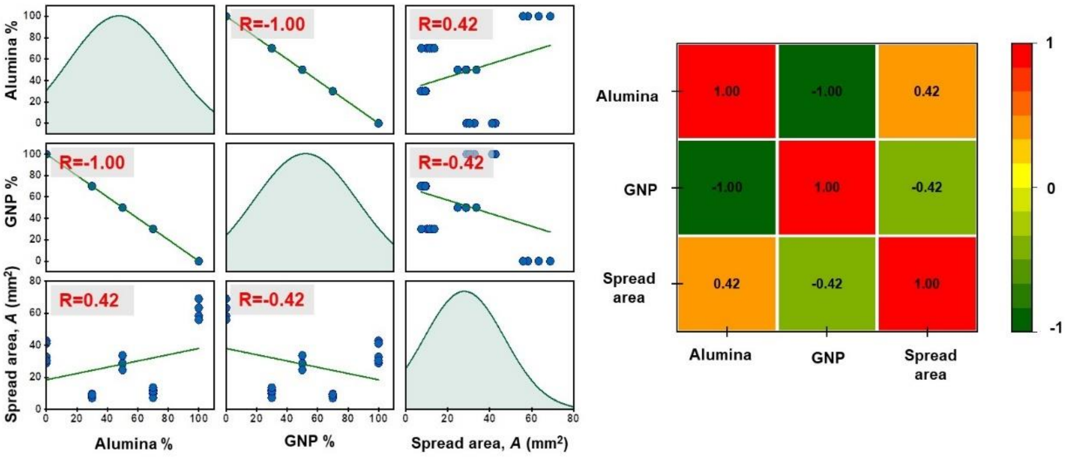

(a) (b)

Figure 4.10 (a) Correlation matrix and (b) correlation heatmap presenting the significance of Alumina/GNP hybrid nano reinforcement to spread area of nano adhesive at 1.5 wt% hybrid nanoparticle content

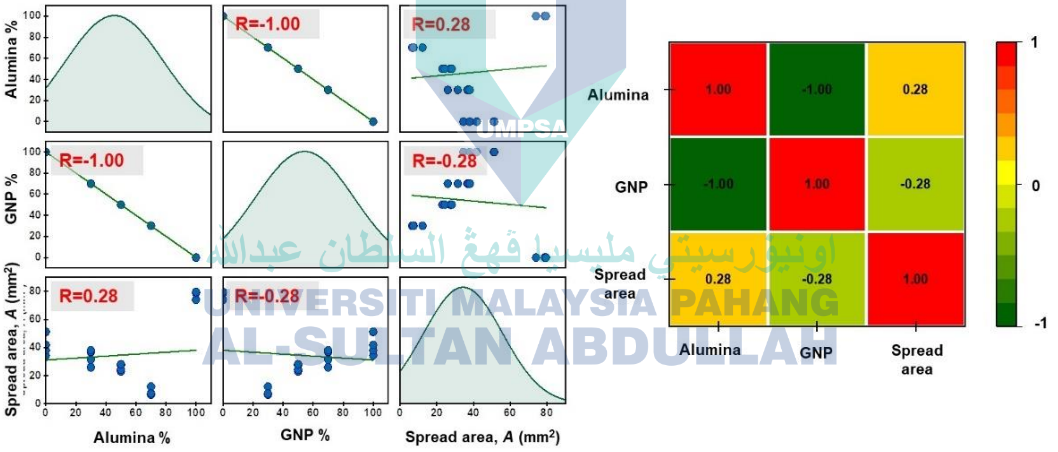

(a) (b)

Figure 4.11 (a) Correlation matrix and (b) correlation heatmap presenting the significance of Alumina/GNP hybrid nano reinforcement to spread area of nano adhesive at 2.0 wt% hybrid nanoparticle content

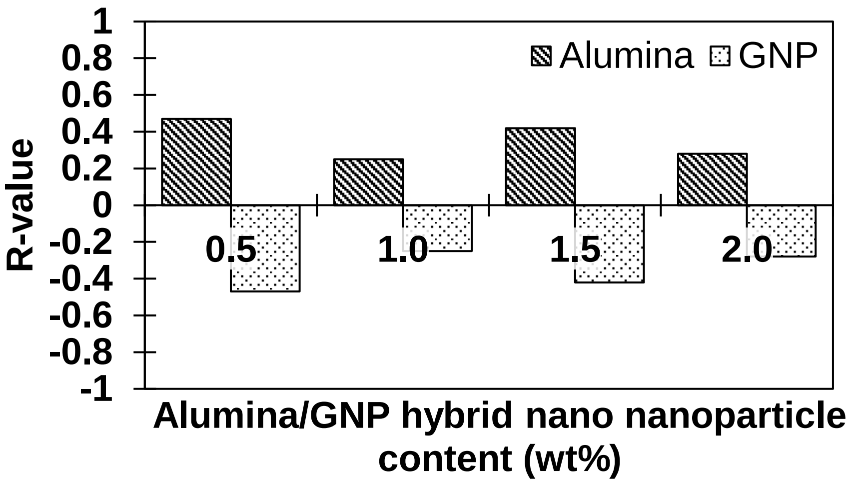

Figure 4.12 The dependence of R value to the Alumina/GNP hybrid nano particle content for spread area

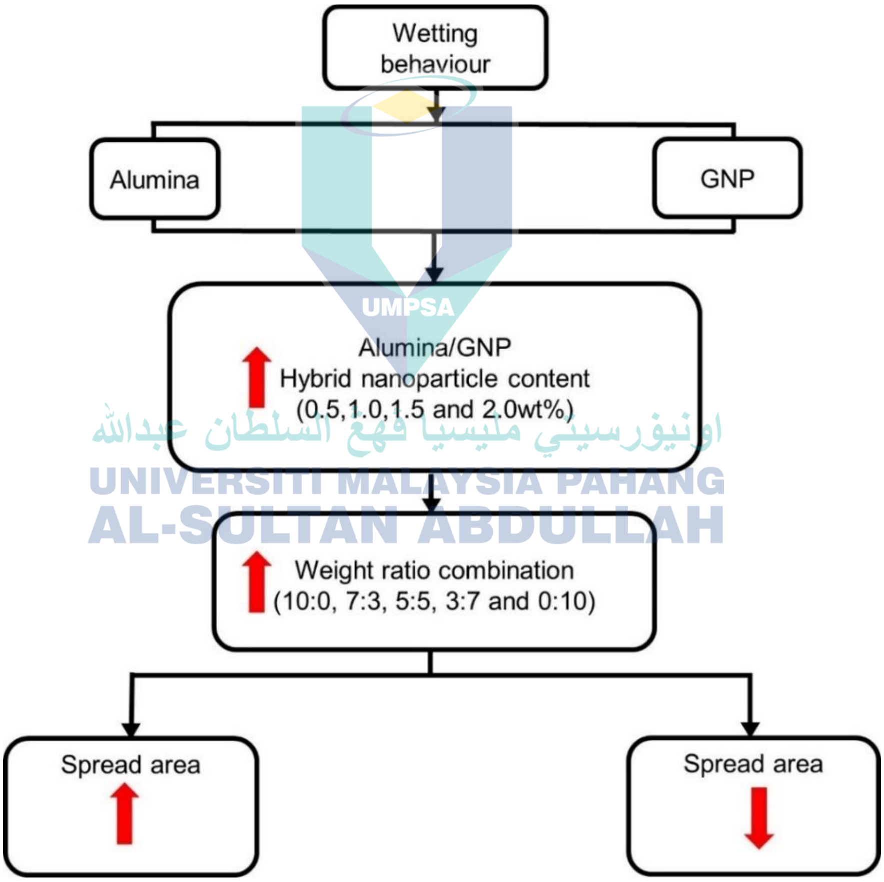

Figure 4.13 Graphical summary on the effect of hybrid nanoreinforcement to the wetting behaviour for epoxy adhesive

4.5 Mechanical properties result (ASTM E8 Specimen)

This section explored the effect of Alumina/GNP hybrid nano reinforcement on the mechanical properties of ASTM E8 specimen across various hybrid nanoparticle contents and weight ratio combinations. The discussion also included a parametric analysis by using correlation matrices and correlation heatmaps.

4.5.1 Representative tensile strength and fracture elongation of tensile specimens

Figure 4.14 show the representative stress and elongation of bulk Alumina/GNP hybrid nano adhesive at various weight ratio combinations for (a) 0.5 wt%, (b) 1.0 wt%, (c) 1.5 wt% and (d) 2.0 wt% hybrid nanoparticle content. The detailed results of tensile strength and fracture elongation are shown in Table 4.2.

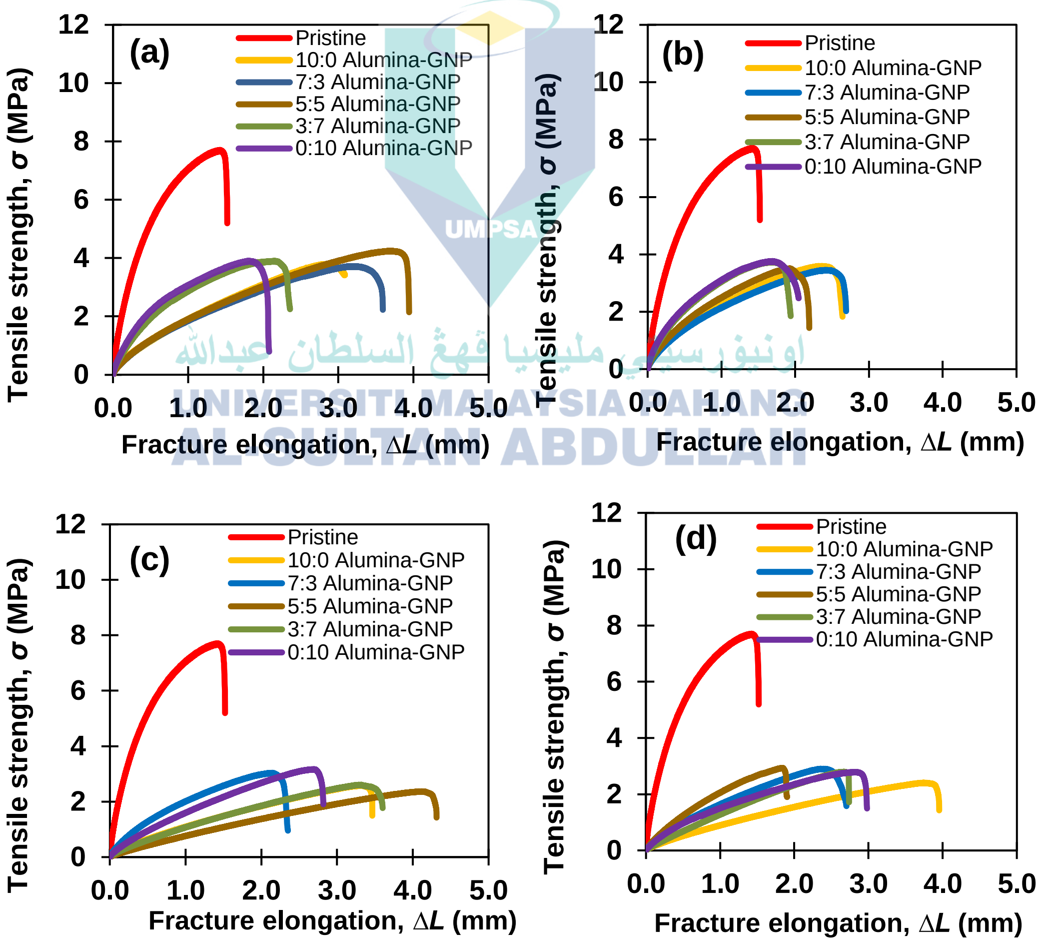

Figure 4.14 Representative stress elongation curve of bulk Alumina/GNP hybrid nano adhesive at various weight ratio combinations for (a) 0.5 wt%, (b) 1.0 wt%, (c) 1.5 wt% and (d) 2.0 wt% hybrid nanoparticle content

Table 4.2 Summary of tensile strength and fracture elongation for ASTM E8 specimen at various hybrid nanoparticle content and various weight ratio combinations of Alumina/GNP hybrid nanoreinforcement

Alumina/GNP hybrid nanoparticle content (wt%)	**Weight ratio combination (Alumina: GNP)**	**Tensile strength, *σ* (MPa)**	**Fracture elongation, Δ*L* (mm)**
Pristine	-	8.17 ± 1.34	1.82 ± 0.75
0.5	10:0	3.88 ± 0.28	3.25 ± 0.32
	7:3	3.47 ± 0.39	4.03 ± 0.53
	5:5	4.23 ± 0.74	3.25 ± 0.42
	3:7	3.59 ± 0.52	2.55 ± 0.49
	0:10	3.87 ± 0.48	2.07 ± 0.40
1.0	10:0	3.76 ± 0.23	2.57 ± 0.40
	7:3	3.52 ± 0.06	2.39 ± 0.57
	5:5	3.54 ± 0.42	2.47 ± 0.28
	3:7	3.63 ± 0.28	2.06 ± 0.20
	0:10	3.77 ± 0.12	2.24 ± 0.46
1.5	10:0	2.35 ± 0.09	2.88 ± 0.00
	7:3	2.88 ± 0.33	2.54 ± 0.28
	5:5	2.38 ± 0.41	4.20 ± 0.60
	3:7	2.80 ± 0.36	3.30 ± 0.56
	0:10	3.16 ± 0.24	2.76 ± 0.24
2.0	10:0	2.57 ± 0.14	3.89 ± 0.63
	7:3	2.49 ± 0.41	2.90 ± 0.50
	5:5	2.52 ± 0.29	2.20 ± 0.66
	3:7	3.09 ± 0.37	2.76 ± 0.33
	0:10	2.61 ± 0.39	2.99 ± 0.39

4.5.2 Effect of Alumina/GNP hybrid nano reinforcement to the tensile properties of ASTM E8 specimen

Figure 4.15 presents the tensile strength of ASTM E8 specimens with various hybrid nanoparticle contents of Alumina/GNP hybrid nano reinforcement in different weight ratio combinations: (a) 10:0, (b) 7:3, (c) 5:5, (d) 3:7, and (e) 0:10. In Figure 4.15 (a), at the 10:0 weight ratio combination (i.e., single alumina weight ratio), the addition of 0.5-2.0 wt% Alumina/GNP hybrid nanoparticle content resulted in a decrement of tensile strength by 52.51% ± 79.10%, 53.98% ± 82.84%, 71.24% ± 93.28% and 68.58% ± 89.55%, respectively compared to the pristine adhesive. Similarly, in Figure 4.15 (b), at the 7:3 weight ratio combination, the addition of 0.5-2.0 wt% Alumina/GNP hybrid nanoparticle content led to a decrease in tensile strength by 57.53% ± 70.90%, 53.98% ± 95.52%, 64.75% ± 75.37% and 69.52% ± 75.37%, respectively compared to the pristine adhesive. For the 5:5 weight ratio combination, (Figure 4.15 (c)), the addition of 0.5-2.0 wt% Alumina/GNP hybrid nanoparticle content resulted in a reduction of tensile strength by 48.23% ± 44.78%, 56.67% ± 68.66%, 70.87% ± 69.40% and 69.16% ± 78.36%, respectively compared to pristine adhesive. At the 3:7 weight ratio combination (Figure 4.15 (d)), the addition of 0.5-2.0wt% Alumina/GNP hybrid nanoparticle content into epoxy adhesive demonstrated a decrease in tensile strength compared to the pristine adhesive, with values of 61.69% ± 23.13%, 55.57% ± 79.10%, 65.73% ± 73.13% and 62.18% ± 72.39%, respectively. Finally, in Figure 4.15 (e), at the 0:10 weight ratio combination (i.e., single GNP weight ratio), the addition of 0.5-2.0 wt% Alumina/GNP hybrid nanoparticle content resulted in a decrease in tensile strength by 52.63% ± 64.18%, 53.86% ± 91.04%, 61.32% ± 82.09% and 68.05% ± 68.05%, respectively compared to the pristine adhesive.

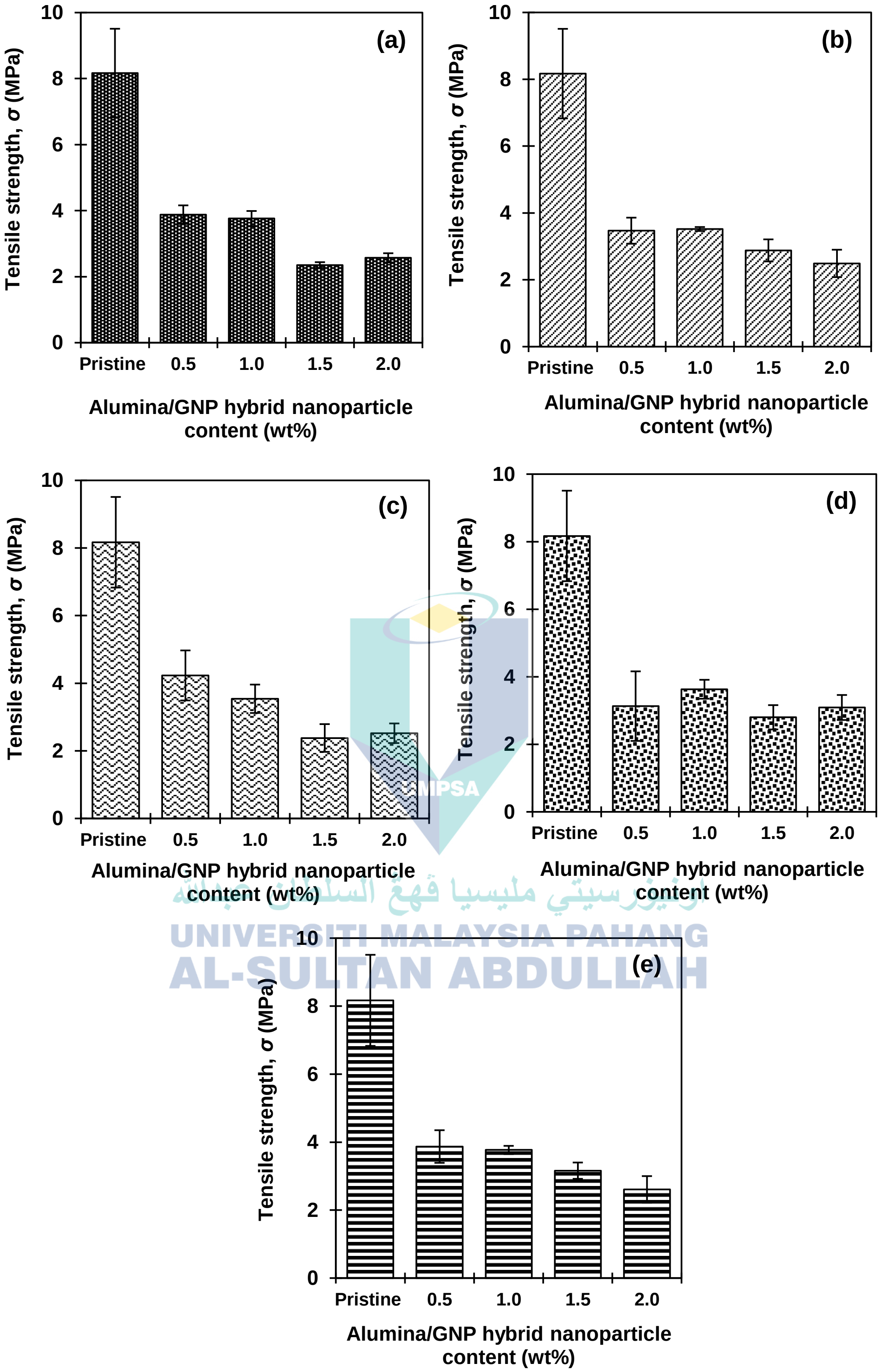

Figure 4.15 Tensile strength for ASTM E8 specimens at various hybrid nanoparticle content of Alumina/GNP hybrid nano reinforcement in (a) 10:0, (b) 7:3, (c) 5:5, (d) 3:7, and (e) 0:10 weight ratio combinations

Figure 4.16 illustrates the tensile strength of ASTM E8 specimens at various weight ratio combinations of Alumina/GNP hybrid nano reinforcement for different hybrid nanoparticle contents: (a) 0.5 wt%, (b) 1.0 wt%, (c) 1.5 wt% and (d) 2.0 wt%. Regardless of the weight ratio combination and Alumina/GNP hybrid nanoparticle content, specimens with Alumina/GNP hybrid nano reinforcement consistently exhibited lower tensile strength compared to their pristine adhesive counterparts. In Figure 4.16 (a), irrespective of Alumina/GNP hybrid nanoparticle content, the addition of Alumina/GNP hybrid nano reinforcement at weight ratio combinations (10:0, 7:3, 5:5, 3:7, and 0:10) resulted in a decrement of tensile strength by 52.51% ± 79.10%, 57.53% ± 70.90%, 48.23% ± 44.78%, 61.69% ± 23.13% and 52.63% ± 64.18%, respectively compared to pristine counterparts In Figure 4.16 (b), regardless of Alumina/GNP hybrid nanoparticle content, the addition of Alumina/GNP hybrid nano reinforcement at 10:0, 7:3, 5:5, 3:7 and 0:10 weight ratio combinations resulted in a decrement of tensile strength by 53.98% ± 82.84%, 56.92% ± 95.52%, 56.67% ± 68.66%, 55.57% ± 79.10% and 53.86% ± 91.04%, respectively as compared to pristine counterparts. In Figure 4.16 (c), regardless of Alumina/GNP hybrid nanoparticle content, the addition of Alumina/GNP hybrid nano reinforcement at 10:0, 7:3, 5:5, 3:7 and 0:10 weight ratio combinations resulted in a decrement of tensile strength by 71.24% ± 93.28%, 64.75% ± 75.37%, 70.87% ± 69.40%, 65.73% ± 73.13% and 61.32% ± 82.09%, respectively compared to pristine counterparts. From Figure 4.16 (d), regardless of Alumina/GNP hybrid nanoparticle content, the addition of Alumina/GNP hybrid nano reinforcement at 10:0, 7:3, 5:5, 3:7 and 0:10 weight ratio combinations resulted in a decrement of tensile strength by 68.54% ± 89.55%, 69.16% ± 69.40%, 69.16% ± 78.36%, 62.18% ± 72.39% and 68.05% ± 70.90%, respectively compared to pristine counterparts.

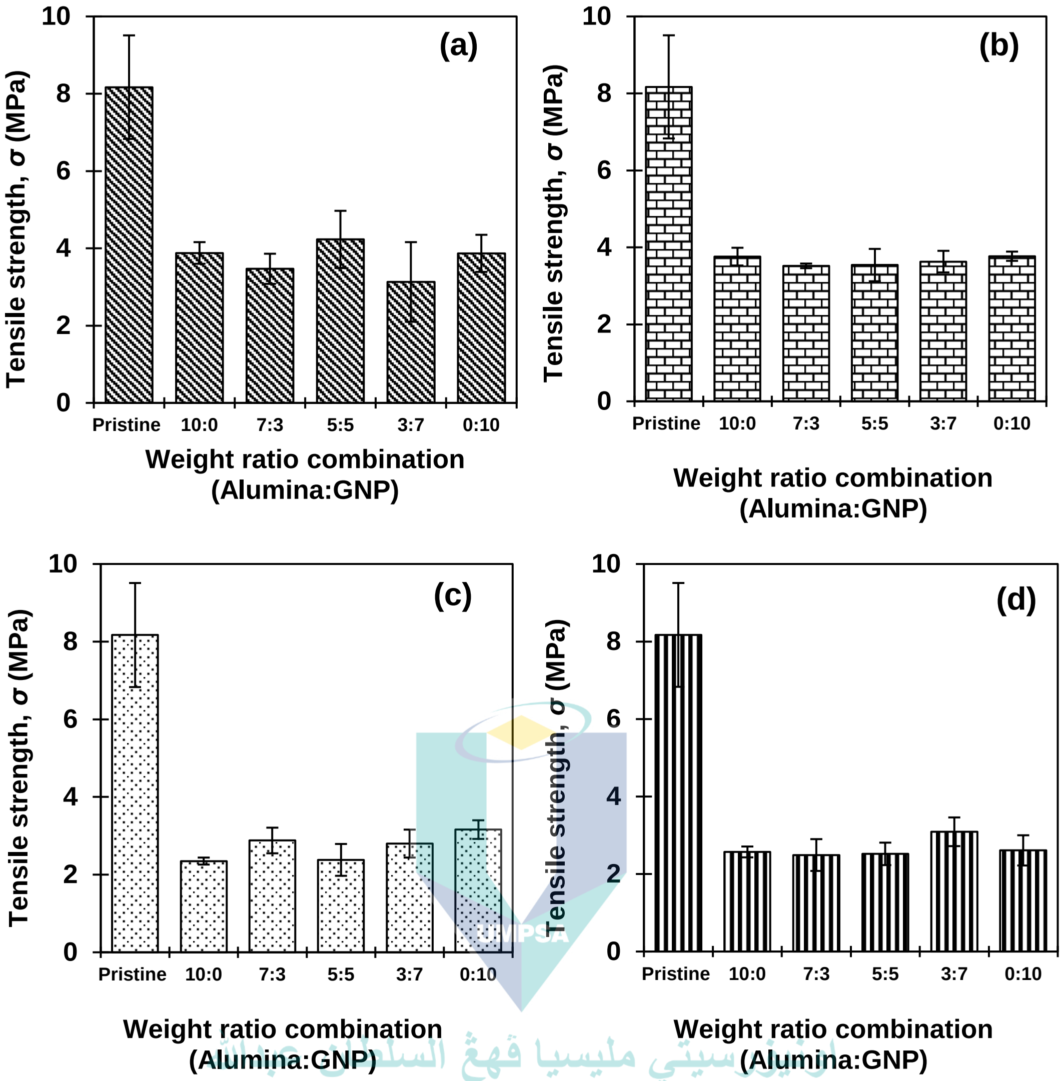

Figure 4.16 Tensile strength for ASTM E8 specimens at various weight ratio combinations of Alumina/GNP hybrid nano reinforcement in (a) 0.5 wt%, (b) 1.0 wt%, (c) 1.5 wt%, and (d) 2.0 wt% hybrid nanoparticle content

Figure 4.17 shows the fracture elongation for ASTM E8 specimens with various Alumina/GNP hybrid nanoparticle contents in the Alumina/GNP hybrid nano reinforcement at different weight ratio combinations: (a) 10:0, (b) 7:3, (c) 5:5, (d) 3:7, and (e) 0:10. In Figure 4.17 (a), compared to the pristine adhesive, Alumina/GNP hybrid nano reinforcement specimens at the 10:0 weight ratio combination showed an increase in the average value of fracture elongation when 0.5-2.0 wt% Alumina/GNP hybrid nanoparticle content was added, ranging from 78.57% ± 57.33% to 113.74% ± 16.00%. Conversely, in Figure 4.17 (b), all Alumina/GNP hybrid nanoparticle contents at the 7:3 weight ratio combination exhibited an increase in the average value for fracture elongation compared to the pristine adhesive, with increments of 121.43% ± 29.33%, 31.32% ± 24.00%, 39.56% ± 62.67% and 59.34% ± 33.33%, respectively. Additionally, in Figure 4.17 (c), at all hybrid nanoparticle contents (i.e., 0.5-2.0 wt%) of Alumina/GNP hybrid nano reinforcement at the 5:5 weight ratio combination, higher average values for fracture elongation were observed, with increments of 78.57% ± 44.00%, 35.71% ± 62.67%, 130.77% ± 20.00% and 20.88% ± 12.00%, respectively compared to the pristine adhesive. Within the range of 0.5-2.0wt% Alumina/GNP hybrid nanoparticle content, a fluctuation in the fracture elongation trend was observed. In Figure 4.17 (d), Alumina/GNP hybrid nano reinforcement specimens at the 3:7 weight ratio combination showed an increase in the average value for fracture elongation compared to the pristine adhesive when 0.5-2.0 wt% Alumina/GNP hybrid nanoparticle content was added. The increments ranged from 40.11% ± 34.67% to 51.65% ± 56.00%. Similar to the trend observed in Figure 4.17 (c), there was a fluctuation in the fracture elongation trend within the 0.5-2.0wt% Alumina/GNP hybrid nanoparticle content. Additionally, Figure 4.17 (e) reveals an enhancement in the average value for fracture elongation compared to the pristine adhesive, with increments of 13.74% ± 46.67%, 23.08% ± 38.67%, 51.65% ± 68.00% and 64.29% ± 48.00%, respectively. The fracture elongation trend was slightly increasing.

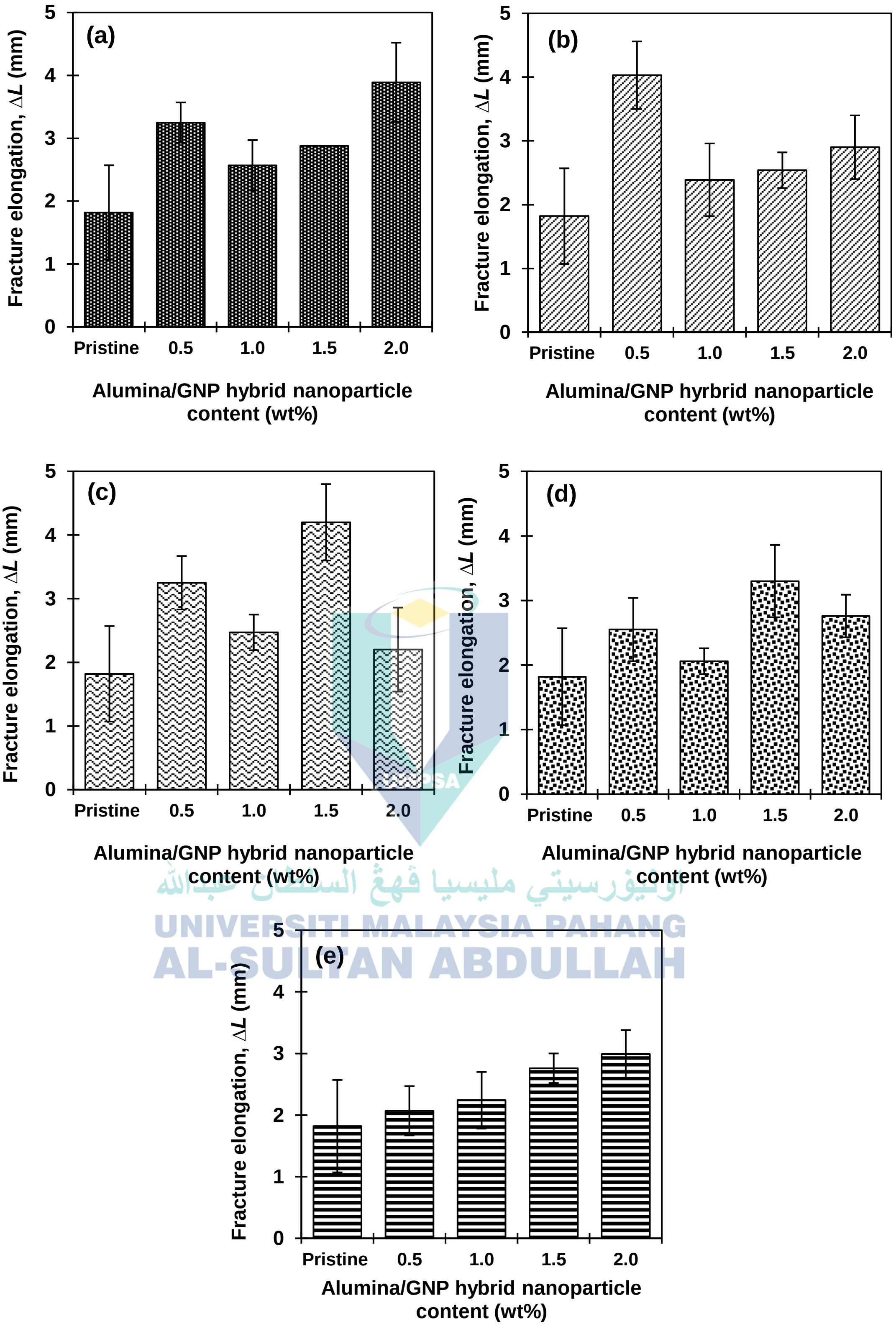

Figure 4.17 Fracture elongation for ASTM E8 specimens at various hybrid nanoparticle content of Alumina/GNP hybrid nano reinforcement (a) 10:0, (b) 7:3, (c) 5:5, (d) 3:7, and (e) 0:10 weight ratio combinations

Figure 4.18 presents the fracture elongation for ASTM E8 specimens at different weight ratio combinations of Alumina/GNP hybrid nano reinforcement: (a) 0.5 wt%, (b) 1.0 wt%, (c) 1.5 wt%, and (d) 2.0 wt% hybrid nanoparticle content. Observations from Figure 4.18 indicated that specimens with Alumina/GNP hybrid nano reinforcement content demonstrated higher average values for fracture elongation across all weight ratio combinations (10:0, 7:3, 5:5, 3:7, and 0:10) compared to the pristine adhesive. In Figure 4.18 (a), it was evident that the average value for fracture elongation gradually increased when adding 0.5 wt% Alumina/GNP hybrid nanoparticle content at 10:0, 7:3, 5:5, 3:7 and 0:10 weight ratio combinations. The increments ranged from 78.58% ± 57.33% to 13.74% ± 46.67% compared to the pristine adhesive. In Figure 4.18 (b), the addition of 1.0 wt% Alumina/GNP hybrid nanoparticle content at different weight ratio combinations resulted in an increment in the average value for fracture elongation, ranging from 41.21% ± 46.67% to 23.08% ± 38.67% compared to the pristine adhesive. In Figure 4.18 (c), a comparison to the pristine adhesive revealed that for Alumina/GNP hybrid nano reinforcement specimens at 10:0, 7:3, 5:5, 3:7 and 0:10 weight ratio combinations, the addition of 1.5 wt% Alumina/GNP hybrid nanoparticle content resulted in an increase in the average value for fracture elongation. The increments were notable, reaching 58.24% ± 100.00%, 39.56% ± 62.67%, 130.77% ± 20.00%, 81.32% ± 25.33% and 51.56% ± 68.00%, respectively. In Figure 4.18 (d), a comparison with the pristine adhesive highlighted the positive impact of adding 2.0 wt% Alumina/GNP hybrid nanoparticle content on fracture elongation in Alumina/GNP hybrid nano reinforcement specimens at 10:0, 7:3, 5:5, 3:7, and 0:10 weight ratio combinations. The average values witnessed substantial increments, reaching 113.74% ± 16.00%, 59.34% ± 33.33%, 20.88% ± 12.00%, 51.65% ± 56.00% and 64.29% ± 48.00%, respectively.

Based on these results, it has been observed that the mechanical properties of ASTM E8 specimens are lower than the standard range of 7 ~ 40.0 MPa in the industry (Wei et al., 2024). Several factors can be attributed to this, such as the presence of voids and pores, agglomeration of nanoparticles, and other factors that have been discussed in detail in Section 4.5.3. Accordingly, several recommendations have been given to address this issue in section 5.3.

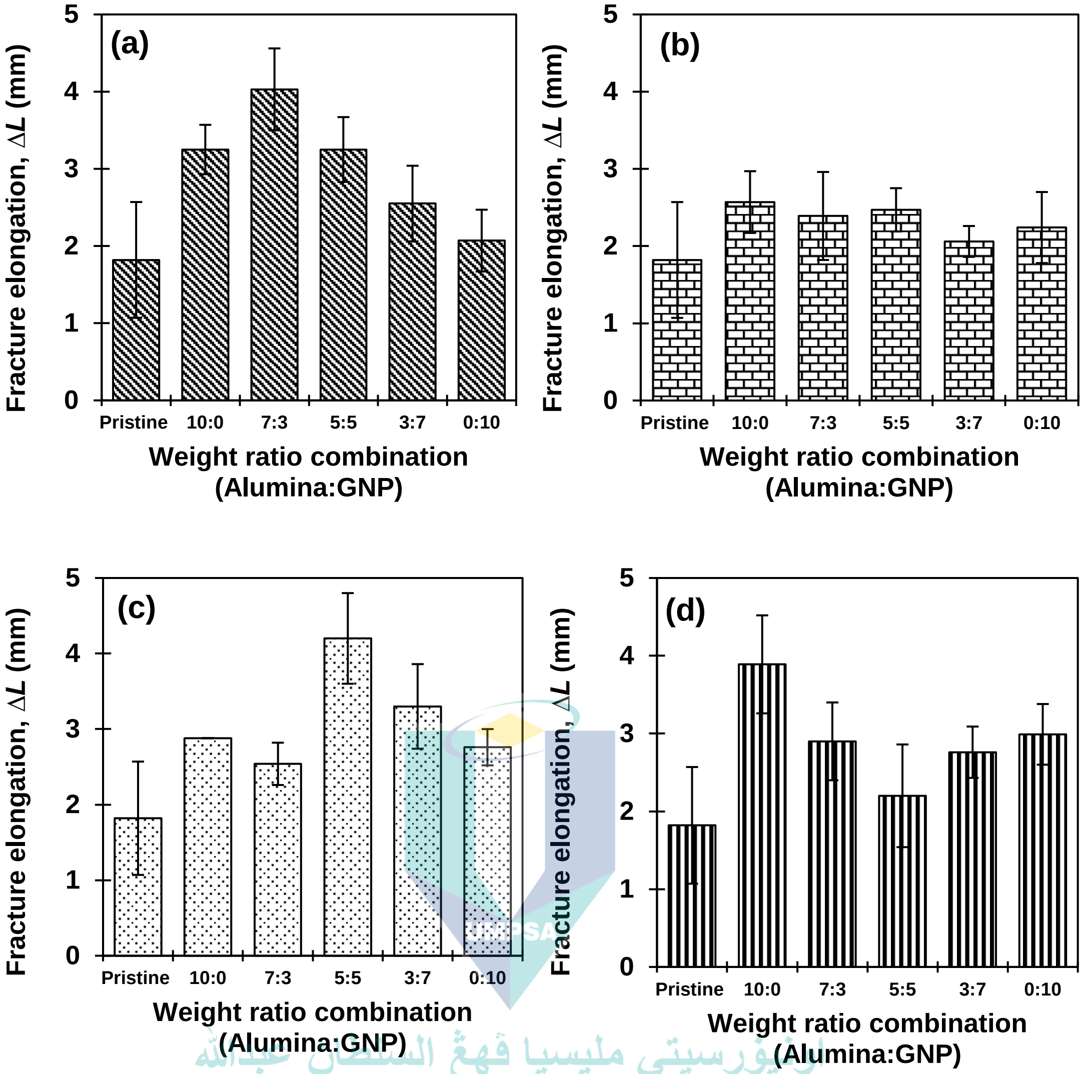

Figure 4.18 Fracture elongation for ASTM E8 specimens at various weight ratio combination of Alumina/GNP hybrid nano reinforcement in (a) 0.5 wt%, (b) 1.0 wt%, (c) 1.5 wt%, and (d) 2.0 wt% hybrid nanoparticle content

4.5.3 Fracture behaviour analysis ASTM E8 specimen

To assess the fracture behaviour of Alumina/GNP hybrid nano adhesive specimens, images of the fractured surfaces were captured using a camera for all hybrid nanoparticle contents and weight ratio combinations of Alumina/GNP hybrid nano reinforcement. Additionally, microstructural analysis was conducted using FE-SEM on specific specimens exhibiting distinct tensile characteristics.

Figure 4.19 shows representative images of the fractured surface of Alumina/GNP hybrid nano adhesive at 0.5-2.0 wt% with various weight ratio combinations (i.e., 10:0, 7:3, 5:5, 3:7 and 0:10). Voids and pores were highlighted with red-coloured arrows. The presence of these voids/pores could be attributed to factors such as air entrapment during the preparation of the hybrid nano adhesive and gas formation due to chemical reactions during the curing process. Since no further degassing process was implemented in this study, air bubbles remained in the epoxy adhesive. Figure 4.19 revealed that specimens with Alumina/GNP hybrid nanoparticles exhibited a rougher fractured surface compared to the pristine adhesive counterpart. The relatively smoother fractured specimen in pristine adhesive might indicate its brittle nature and weak resistance to crack initiation and propagation (Tang et al., 2013). On the other hand, the rougher morphology in specimens with Alumina/GNP hybrid nanoparticles might be attributed to crack path deviation and propagation. This observation suggested that more energy was required during fracture, leading to a higher fracture elongation of the bulk adhesive (Osman et al., 2021).

Figure 4.20 illustrates the fracture surface of the ASTM E8 specimen at 1.5wt% hybrid nanoparticle content and 10:0 Alumina/GNP hybrid nano reinforcement weight ratio. In Figure 4.20 (a), the presence of void/pores was clearly evident, aligning well with the camera observations in Figure 4.19. These voids/pores within the epoxy matrix led to a reduction in tensile strength, reaching 71.24% ± 93.28% compared to the pristine adhesive (8.17 MPa ± 1.34 MPa). The existence of voids/pores in the epoxy matrix facilitated easier crack propagation, increased the fracture path and dissipated energy, resulting in lower tensile strength as discussed in Section 2.7.3.1 and supported by Figure 4.20 (b). Meanwhile, the addition of 1.5wt% Alumina/GNP hybrid nanoparticle content at the 10:0 weight ratio combination exhibited a relative deterioration in tensile strength (Refer Figure 4.15 (a) and 4.16 (c)) compared to the pristine adhesive counterpart, indicating potential agglomeration of Alumina nanoparticles in the epoxy matrix. Figure 4.20 (c) revealed the presence of nano-sized particles (~25 nm) on the fracture surface, specifically alumina nanoparticles. Some agglomeration of Alumina nanoparticles was also observable in the FE-SEM image presented in Figure 4.20 (d). As previously discussed, the agglomeration of nanofiller weakened the interfacial bonding between the nanofiller and the epoxy matrix due to strong Van Der Waals interactions (Kesavulu and Mohanty, 2020). This agglomeration created stress concentrations, thus facilitating the easy initiation of cracks and resulting in lower tensile strength as observed in the ASTM E8 specimens of the current work. In relation to the ductility of the specific specimen with 1.5 wt% and 10:0 Alumina/GNP weight ratio combination as discussed in Section 4.5.2 (Refer to Figure 4.17 (a) and 4.18 (c)), the fracture elongation of this sample showed an increment of up to 78.57% ± 57.33% compared to the pristine adhesive (1.82 mm ± 0.75 mm). The enhanced fracture elongation of the sample suggested that the presence of microparticles in the epoxy adhesive contributed to its improved ductility. This observation was substantiated by the particle breakage and pull-out mechanism depicted in Figure 4.20 (e and f), further fortifying the resistance to crack initiation and propagation. The higher energy required to fracture these specimens could be attributed to particle breakage, underscoring the efficacy of micron-particles in enhancing adhesive performance. The existence of micron particle sized (approx. size <100µm) might be Calcium carbonate ($CaCO_3$) that were pre-mixed with the epoxy adhesive during the production of the adhesive (Refer in Appendix B) and they appeared to be homogeneously distributed inside the epoxy matrix. It is worth noting that, the use of $CaCO_3$ in polymer formulations is a cost-effective way to enhance various mechanical properties, such as stiffness, impact strength, and thermal stability, while also providing the ability to adjust density and improve surface finish, making it a versatile additive in the polymer industry (Khalil et al., 2024; Martin-Martinez, 2002). The pull-out mechanism of micron sized particles was particularly advantageous for enhancing the ductility of the epoxy adhesive as it allowed for greater deformation and stretching before failure occurs. Essentially, the pull-out mechanism of micron-particle occurred in the epoxy adhesive when the stress exceeded the interfacial strength, partially pulling the filler out from the matrix and resulting in increased fracture elongation due to the higher energy required to break the specimen (Tang et al., 2013). In summary, Figure 4.21 provides an overview of the possible mechanisms present in the epoxy at 1.5 wt% in 10:0 Alumina/GNP hybrid nano adhesive which is influenced by various factors.

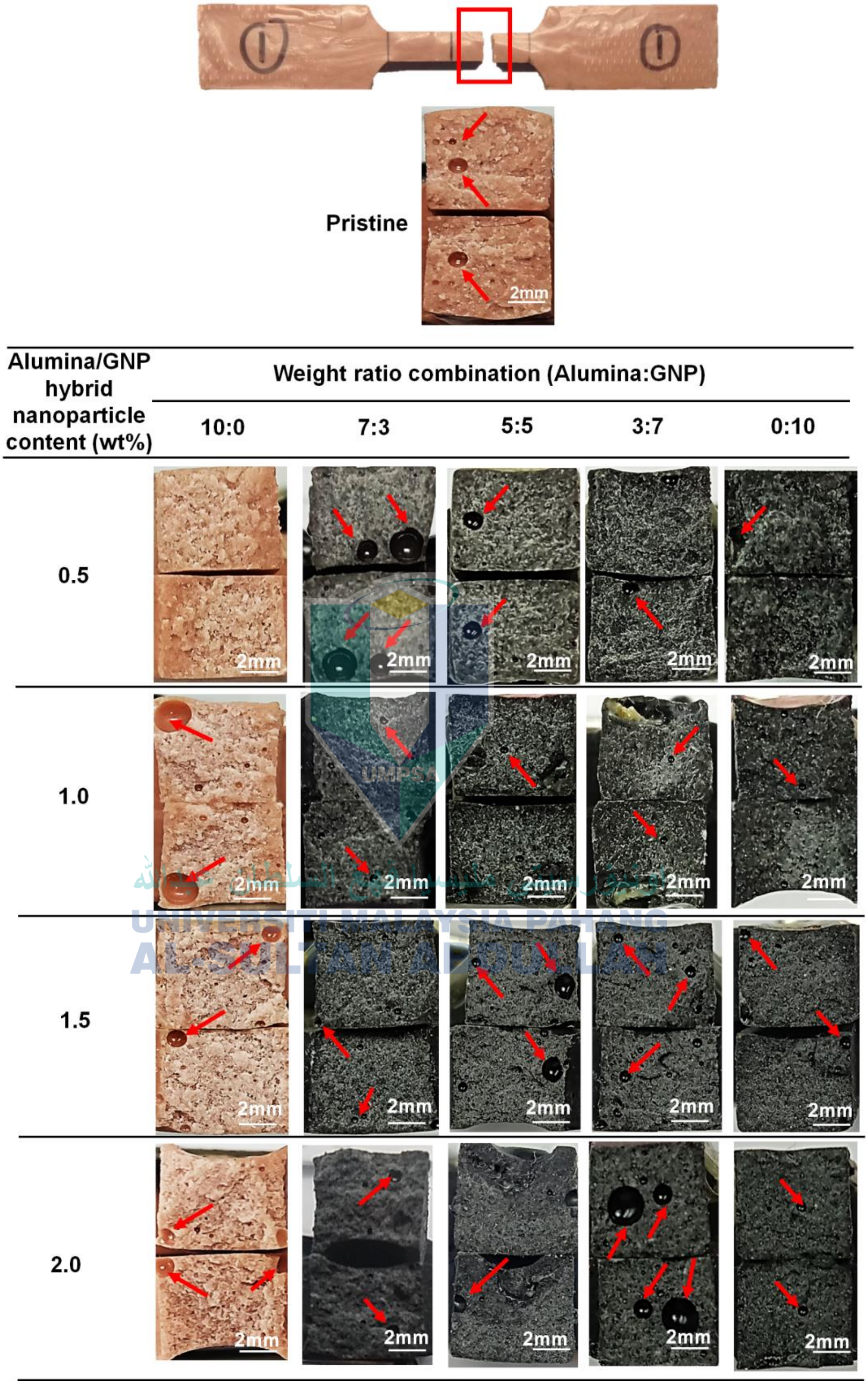

Figure 4.19 Representative images of fractured surface in ASTM E8 specimens at various hybrid nanoparticle content and weight ratio combinations (Red arrows represent void/pores)

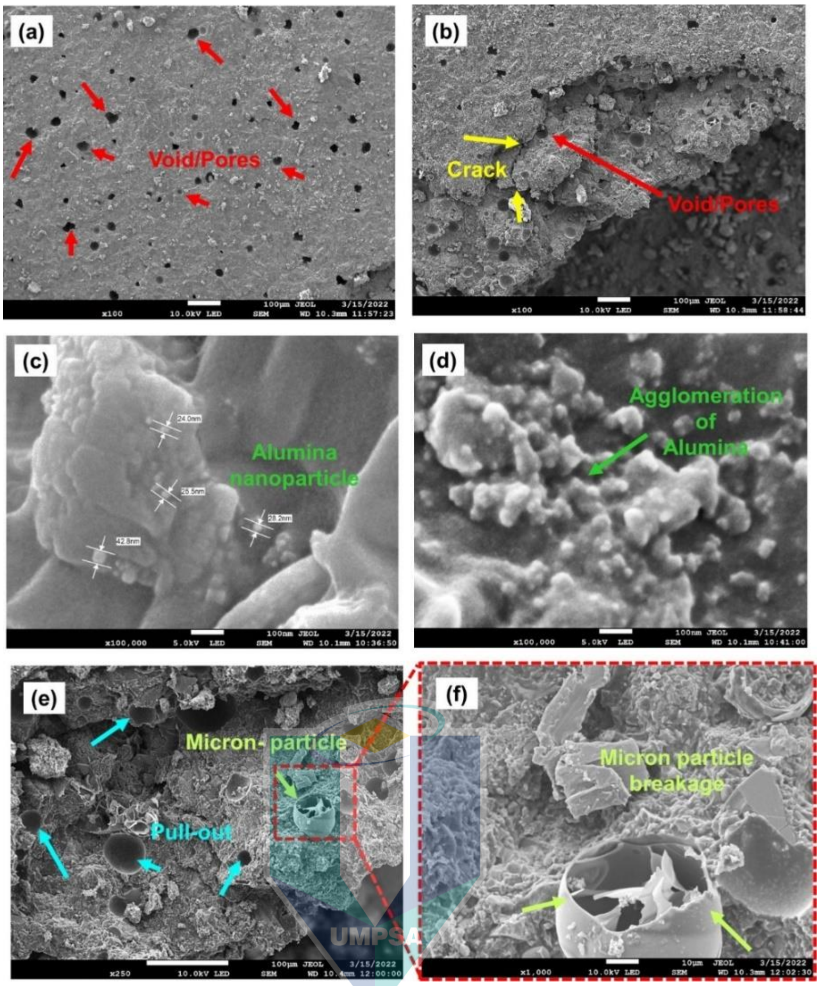

Figure 4.20 FE-SEM image for ASTM E8 specimens at 1.5 wt% hybrid nanoparticle content and 10:0 weight ratio combination (a and b) existence of voids/pores, (c) dispersion of alumina nanoparticle in epoxy matrix, (d) agglomeration of nanoparticle in epoxy matrix, and (e and f) pull-out and micro particle breakage

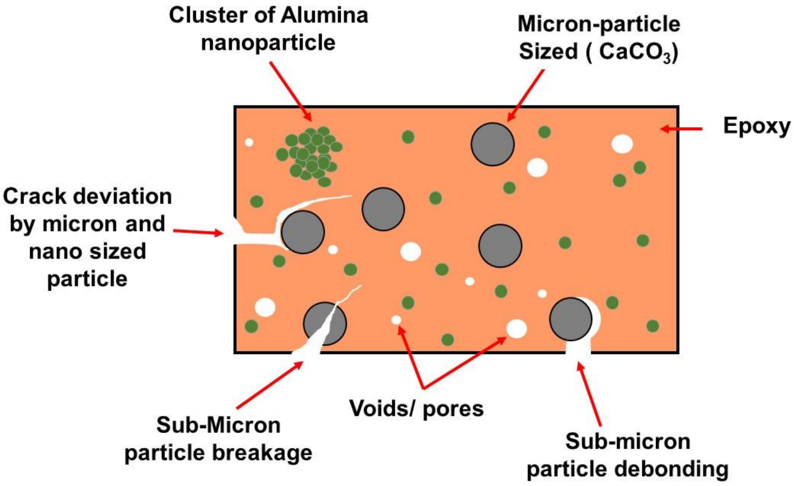

Figure 4.21 Schematic representation of various mechanism in Alumina/GNP hybrid nano adhesive at 1.5 wt% in 10:0 weight ratio combination

Meanwhile, Figure 4.22 depicts the fracture surface of the ASTM E8 specimen with a 1.0 wt% Alumina/GNP hybrid nanoparticle content at a 7:3 weight ratio combination. In the context of the current study, as previously discussed in Section 4.5.2 (Refer to Figure 4.15 (b) and 4.16 (b)), this specimen exhibited a decrement in tensile strength of up to 53.98% ± 95.52% when compared to the pristine adhesive, which was primarily attributed to the agglomeration of nanofillers. The FE-SEM images in Figure 4.22 (a, b, c, d, and e) revealed observable agglomeration of nanoparticles on the fracture surface. As discussed in Section 2.7.3.1, nanofillers have a tendency to agglomerate in the epoxy matrix due to strong Van der Waals interactions, especially given their nanosized nature. This agglomeration could affect the tensile performance by introducing local stress concentration, thereby facilitating crack initiation and propagation within the polymer matrix (Kesavulu and Mohanty, 2020).

Nevertheless, in terms of fracture elongation, this specimen demonstrated an improvement of up to 31.32% ± 24.00% compared to the pristine adhesive counterpart (Refer to Figures 4.17 (b) and 4.18 (b). The enhanced fracture elongation could be attributed to the altered crack path and the formation of a corrugated pattern inside the polymer matrix. The FE-SEM image in Figure 4.22 (f) clearly showed that the distinctive crack path and the formation of a corrugated pattern on the fractured specimen. As reported by Dorigato and Pegoretti (2011), the formation of a corrugated fracture surface is a result of the presence of nanofillers in the epoxy matrix. A more corrugated pattern indicates a higher amount of energy needed to break the specimens (Tutunchi et al., 2015a). The presence of a corrugated pattern on the fracture surface of the ASTM E8 specimen allowed for greater deformation and stretching before failure occurred, which was attributed to the increased energy required to break the specimen. In addition, the particle breakage and pull-out mechanism observed on the fracture surface of this specimen contribute to the enhancement in ductility as depicted in Figure 4.22 (g and h). In summary, Figure 4.23 provides an overview of the possible mechanisms present in the epoxy at 1.0 wt% in 7:3 Alumina/GNP hybrid nano adhesive, which is influenced by various factors.

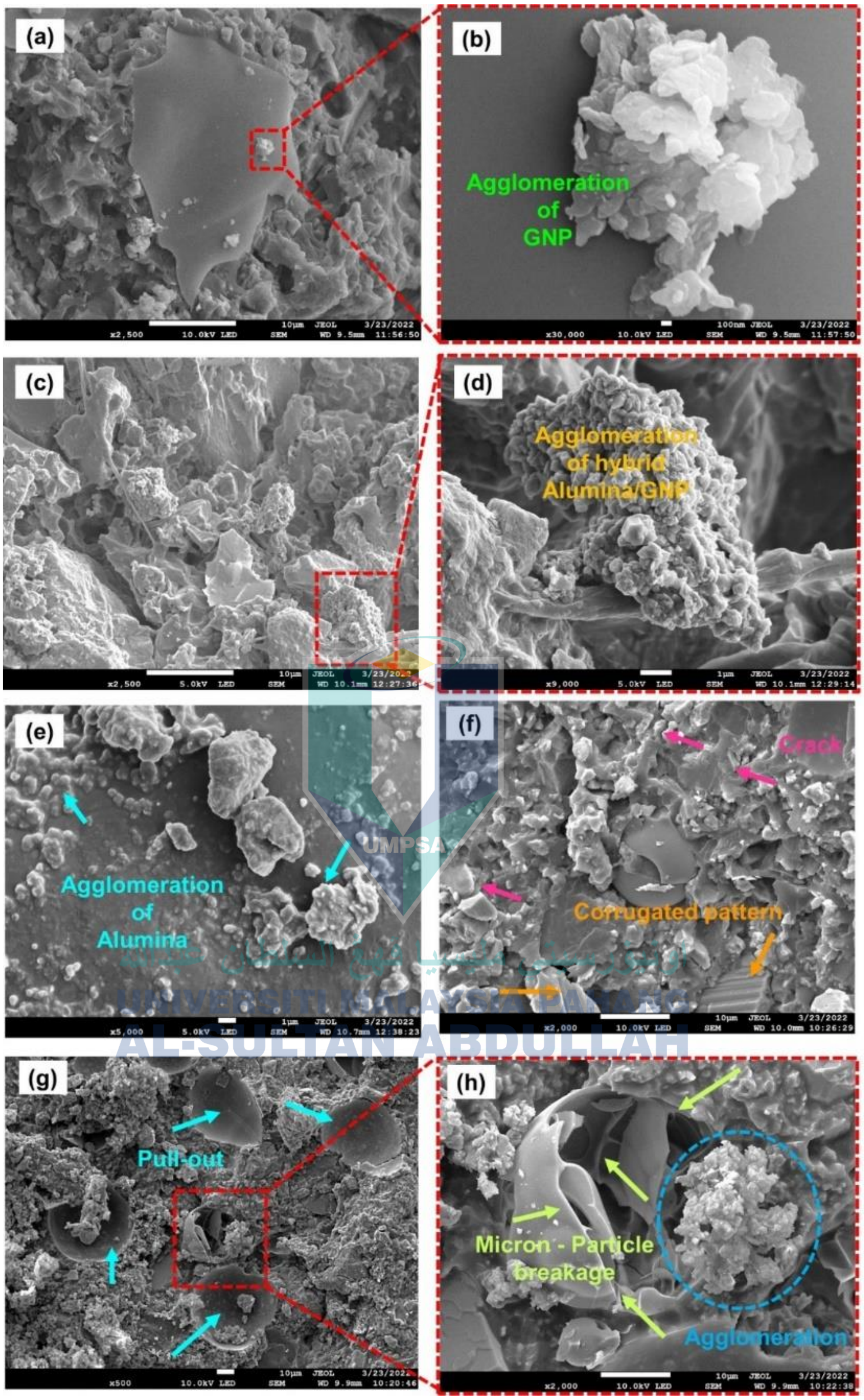

Figure 4.22 FESEM image for 1.0 wt% Alumina/GNP hybrid nanoadhesive at 7:3 weight ratio combination (a and b) Agglomeration of GNP (c and d) Agglomeration of hybrid Alumina/GNP (e) Agglomeration of alumina (f) the presence of crack and corrugated pattern, (g) pull-out (h) micron sized particle breakage

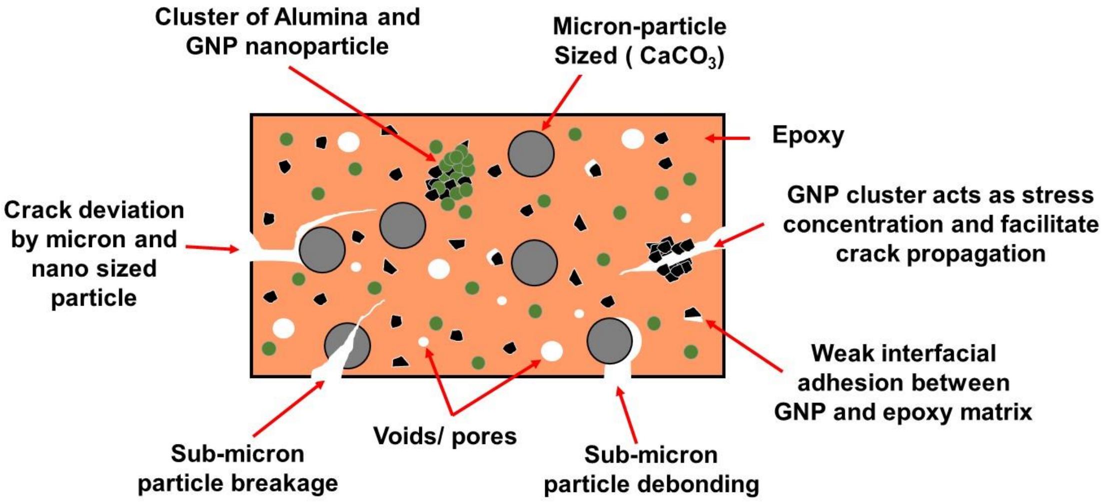

Figure 4.23 Schematic representation of various mechanism in Alumina/GNP hybrid nano adhesive at 1.0 wt% in 7:3 weight ratio combination

Meanwhile, Figure 4.24 represents the ASTM E8 specimen with 2.0 wt% Alumina/GNP hybrid nano reinforcement at 0:10 weight ratio combination. In alignment with the findings discussed in Section 4.5.2 (Refer Figure 4.15 (e) and 4.16 (d)), this specific specimen exhibited a reduction in tensile strength, decreasing by 68.05% ± 70.90% compared to the pristine adhesive counterpart. Similar to previous specimens such as the 1.5 wt% of Alumina/GNP hybrid nano reinforcement at 10:0 weight ratio combination and 1.0 wt% of Alumina/GNP hybrid nano reinforcement at 7:3 weight ratio combination, agglomeration of GNP and crack path propagation could be observed, contributing to the lower tensile strength as evident in Figure 4.24 (a). Nevertheless, the presence of micro-sized particles contributed to an improvement in fracture elongation, increasing by 64.29% ± 48.00% compared to the pristine adhesive counterpart (Refer Figure 4.17 (e) and 4.18 (d)). This improvement could be attributed to particle breakage. The FE-SEM images in Figure 4.24 (b and c) revealed the presence of pull-out and microparticle breakage, enhancing the ductility of this specimen in the epoxy adhesive. It is noteworthy that all the ASTM E8 specimens, regardless of the weight concentrations and weight ratio combinations, consist of macro-sized particles. Therefore, the effects stemming from this filler might be consistent across all specimens. In summary, Figure 4.25 provides an overview of the possible mechanisms present in the epoxy at 2.0 wt% in 0:10 Alumina/GNP hybrid nano adhesive, which is influenced by various factors.

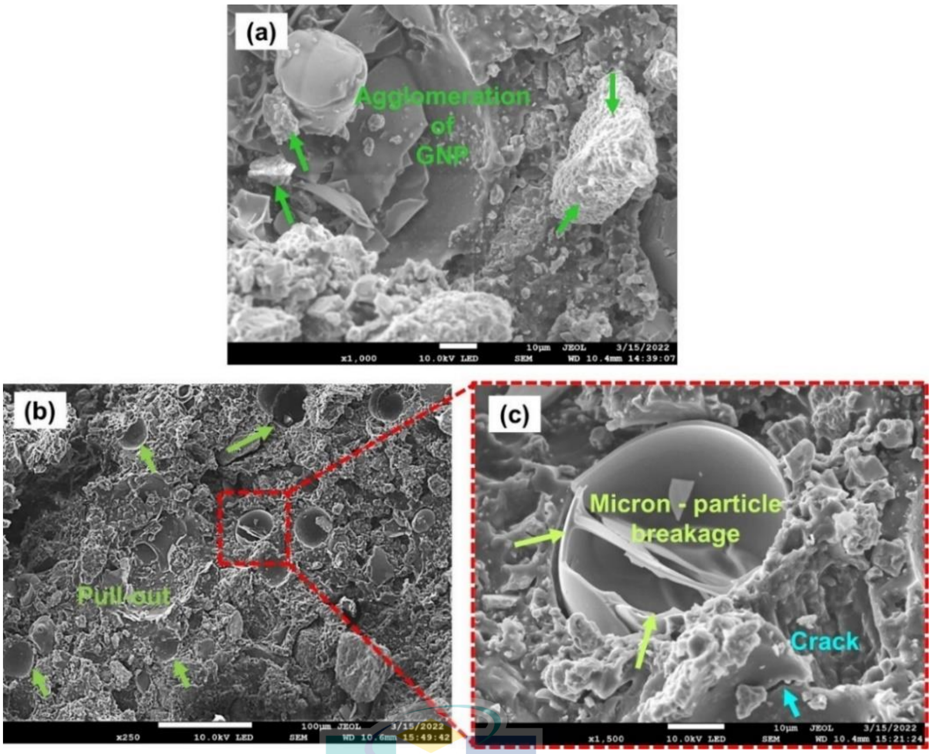

Figure 4.24 FESEM optical image for 2.0 wt% Alumina/GNP hybrid nano adhesive at 0:10 weight ratio combination (a) Agglomeration of GNP, and (b and c) Micro particle breakage and crack deviation propagation

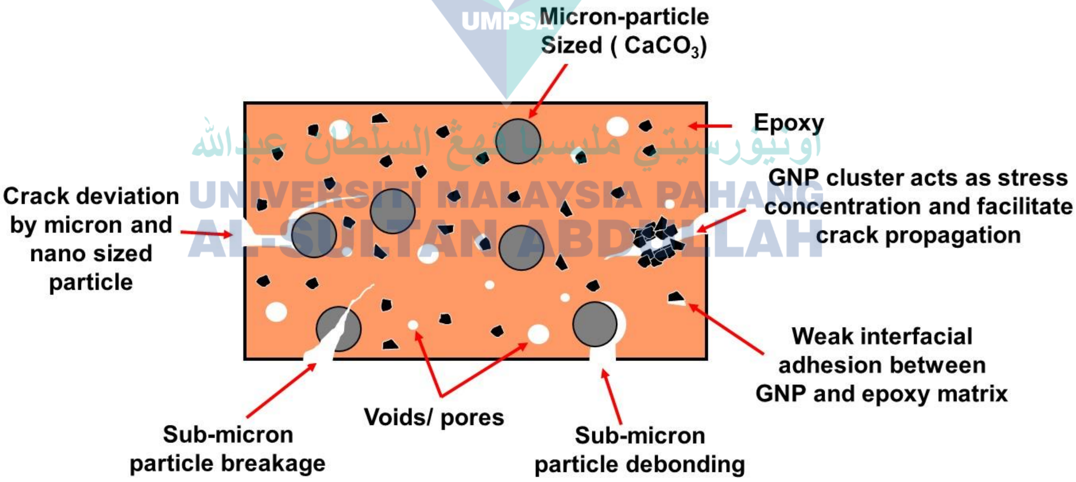

Figure 4.25 Schematic representation of various mechanism in Alumina/GNP hybrid nano adhesive at 2.0 wt% in 0:10 weight ratio combination

4.5.4 Pearson correlation and heatmap analysis for tensile properties of ASTM E8 specimen in Alumina/GNP hybrid nano adhesive

In these Figures 4.26 to 4.29, it could be seen that, regardless of Alumina/GNP hybrid nano particle content, the alumina nanoparticle weight ratio and tensile strength demonstrated a negative correlation at 0.5-2.0 wt% with R-values of -0.03, -0.03, -0.52 and -0.21, respectively. A possible mechanism for this observation was that the presence agglomeration of alumina nanoparticle weakened the interfacial bonding between the nanofiller and epoxy matrix as proven in Figure 4.20 (d) and Figure 4.22 (e). Due to the high concentration of nanofillers, alumina nanoparticles adhered to each other due to strong Van Der Waals interactions (Kesavulu and Mohanty, 2019). The failure crack could pass through the agglomeration of nanoparticles as the nanoparticles had contact with each other but did not have bonding (Gupta et al., 2017). Furthermore, at high loading of alumina nanoparticles, a non-uniform distribution of alumina within the epoxy matrix took place due to the increase in viscosity, which could be the reasons for the decrease in tensile strength (Gupta et al., 2017). Conversely, it could also be observed that there was no correlation between GNP weight ratio and tensile strength at 0.5 and 1.0 wt% with R-values of 0.03 and 0.03, respectively. As for 1.5 and 2.0 wt% of GNP weight ratio, a positive relation was observed with a correlation (R-value) of 0.52 and 0.21, respectively. This implied that the higher surface-to-volume ratio of GNP resulted in the improvement of interfacial bonding between the epoxy matrix and GNP, facilitating the load transfer mechanism (Kong et al., 2021).

On the other hand, from this figure (Refer Figures 4.26 to 4.29), it was also noted that at 0.5, 1.0 and 2.0 wt%, alumina nanoparticle weight ratio and fracture elongation demonstrated a positive relation with R-values of 0.65, 0.33 and 0.38 respectively. Meanwhile, at 1.5 wt% Alumina/GNP hybrid nanoparticle content, alumina nanoparticle weight ratio demonstrated a negative relation with R-value of -0.08. A possible mechanism for this observation was that the nanocomposite having alumina nanoparticles could facilitate crack deflection (Gupta et al., 2017). Furthermore, the agglomeration of nanofiller that weakened the interfacial bonding between the nanofiller and epoxy matrix could act as a stress concentration and the crack could easily initiate, resulting in lower tensile properties.

Meanwhile, from the figures (Refer Figures 4.26 to 4.29), it was noted that at 0.5, 1.0 and 2.0 wt%, GNP weight ratio and fracture elongation demonstrated a negative relation with R-values of -0.65, -0.33 and -0.38, respectively. At 1.5 wt% Alumina/GNP hybrid nanoparticle content, GNP weight ratio demonstrated a positive relation with R-value of 0.08. A possible mechanism for this observation was the presence agglomeration of GNP, making the weak interfacial adhesion between the nanofiller and epoxy matrix (Salom et al., 2018), resulting in stress concentration that caused crack initiation and propagation (Kong et al., 2021). The agglomeration of GNP was proven with the FE-SEM images in Figures 4.22 (a and b) and Figure 4.24 (a).

As a summary, in ASTM E8 specimens with Alumina/GNP hybrid nano reinforcement, the weight ratio of Alumina and GNP demonstrated distinct effects on tensile strength. Regardless of Alumina/GNP hybrid nanoparticle content, an increase in Alumina nanoparticle weight ratio resulted in a decrement in tensile strength. Meanwhile, at lower hybrid nanoparticle content (i.e., 0.5 and 1.0 wt%), the increase in GNP weight ratio combination did not affect the tensile strength. However, at higher hybrid nanoparticle content (i.e., 1.5 and 2.0 wt%), a higher GNP weight ratio improved tensile strength (Refer to Figure 4.30 (a)). Regarding fracture elongation, an increase in alumina nanoparticle weight ratio resulted in increased fracture elongation. Meanwhile, regardless of Alumina/GNP hybrid nanoparticle content, an increase in GNP weight ratio resulted in decreased fracture elongation, except for Alumina/GNP hybrid nanoparticle content at 1.5 wt%, where the fracture elongation was not affected (Refer to Figure 4.30 (b)). For ease of comprehension, the overall summary findings of the tensile properties (i.e., tensile strength and fracture elongation) for ASTM E8 specimen are shown in Figure 4.31.

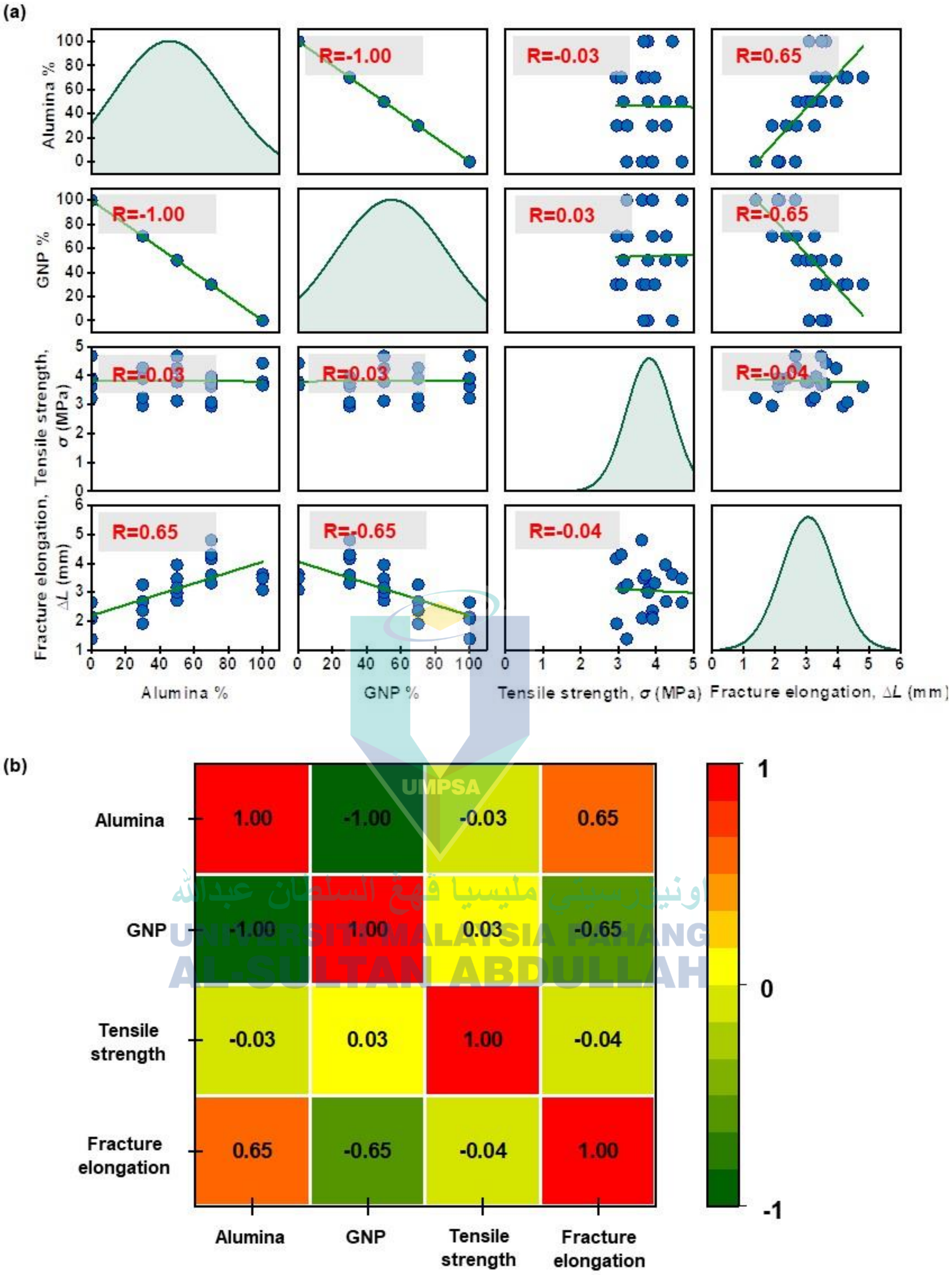

	Alumina	GNP	Tensile strength	Fracture elongation
Alumina	1.00	-1.00	-0.03	0.65
GNP	-1.00	1.00	0.03	-0.65
Tensile strength	-0.03	0.03	1.00	-0.04
Fracture elongation	0.65	-0.65	-0.04	1.00

Figure 4.26 (a) Correlation matrix and (b) correlation heatmap presenting the significance of Alumina/GNP hybrid nano reinforcement to tensile properties in ASTM E8 specimen at 0.5 wt% hybrid nanoparticle content

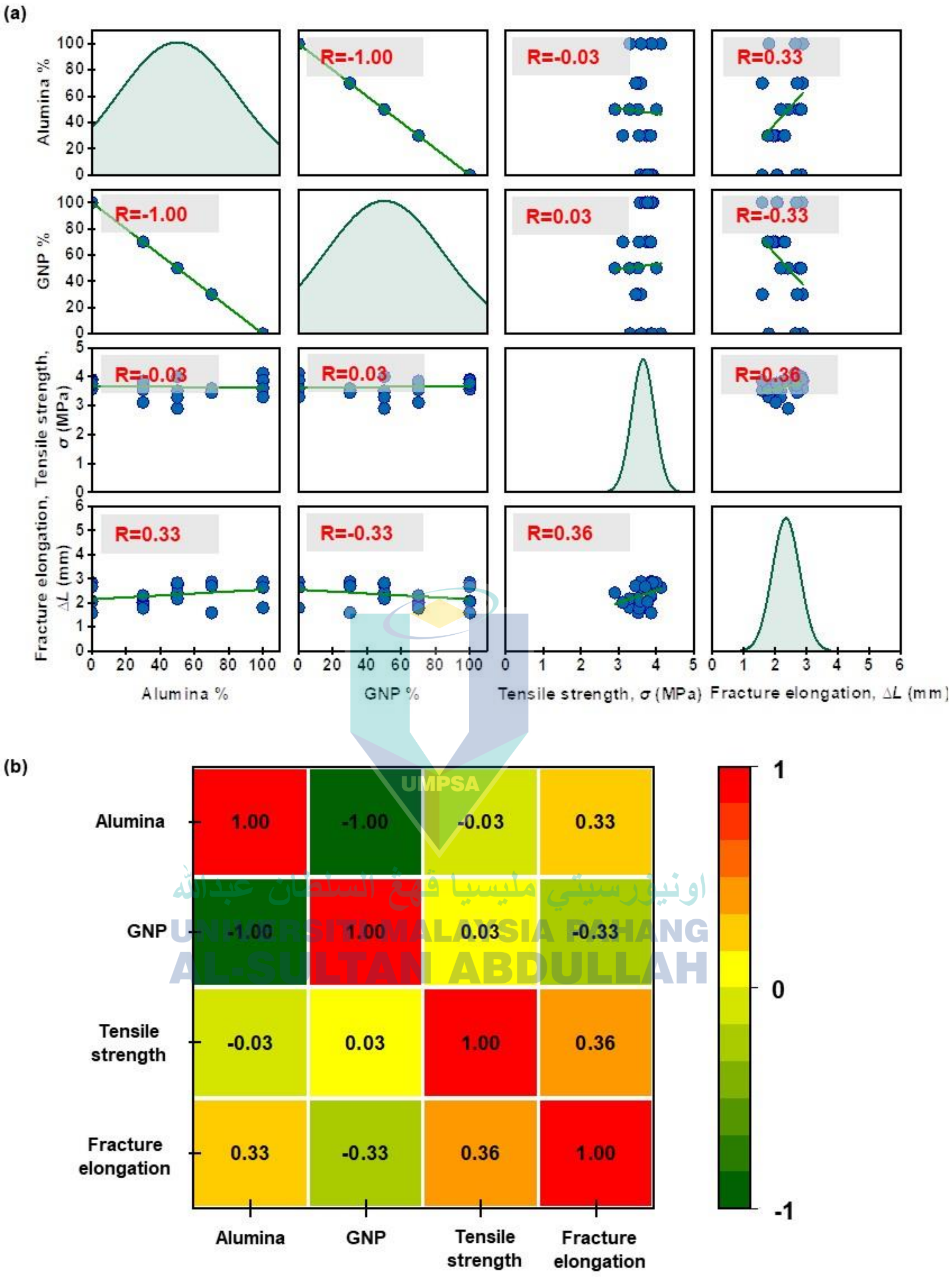

Figure 4.27 (a) Correlation matrix and (b) correlation heatmap presenting the significance of Alumina/GNP hybrid nano reinforcement to tensile properties in ASTM E8 specimen at 1.0 wt% hybrid nanoparticle content

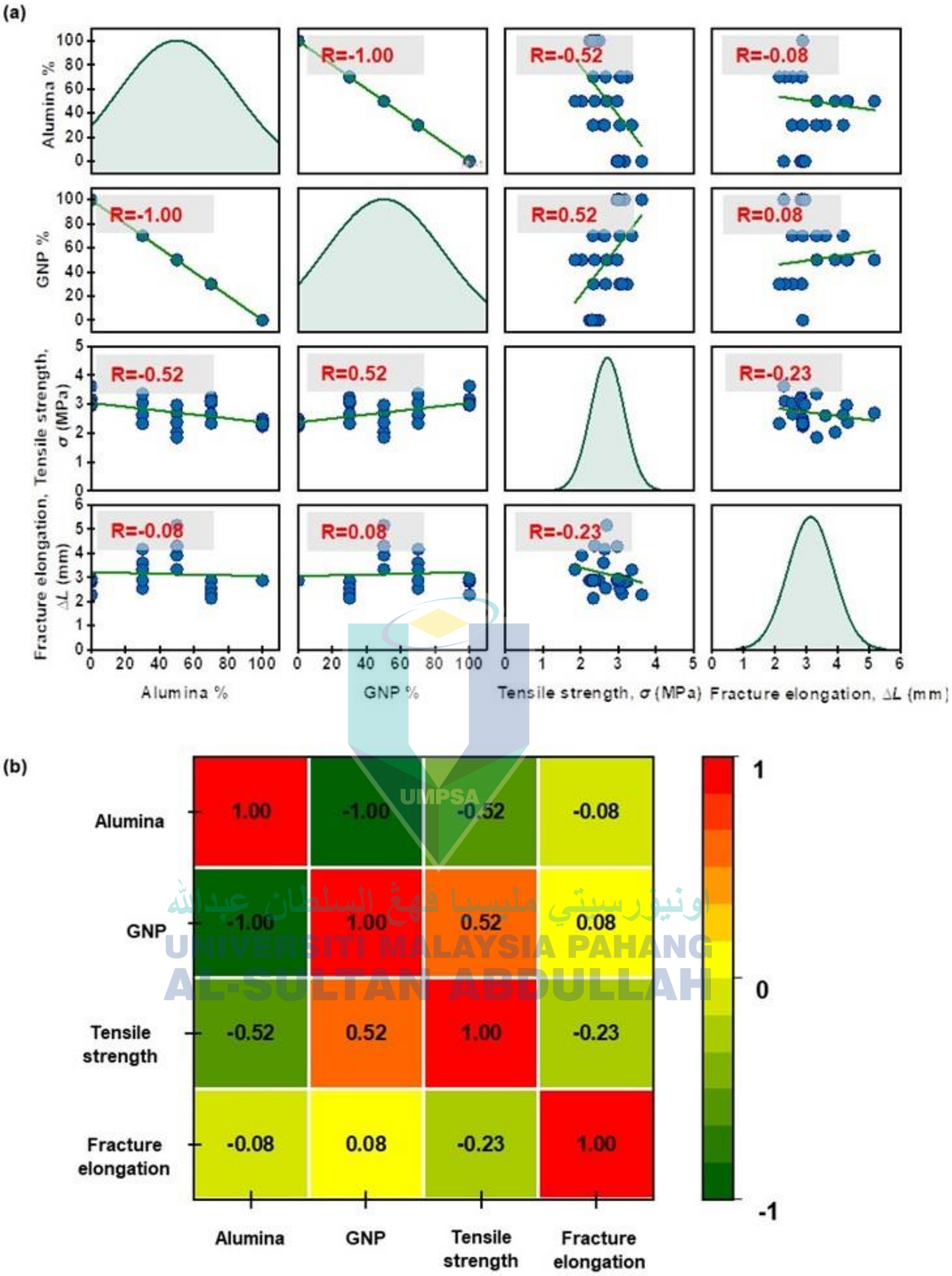

Figure 4.28 (a) Correlation matrix and (b) correlation heatmap presenting the significance of Alumina/GNP hybrid nano reinforcement to tensile properties in ASTM E8 specimen at 1.5 wt% hybrid nanoparticle content

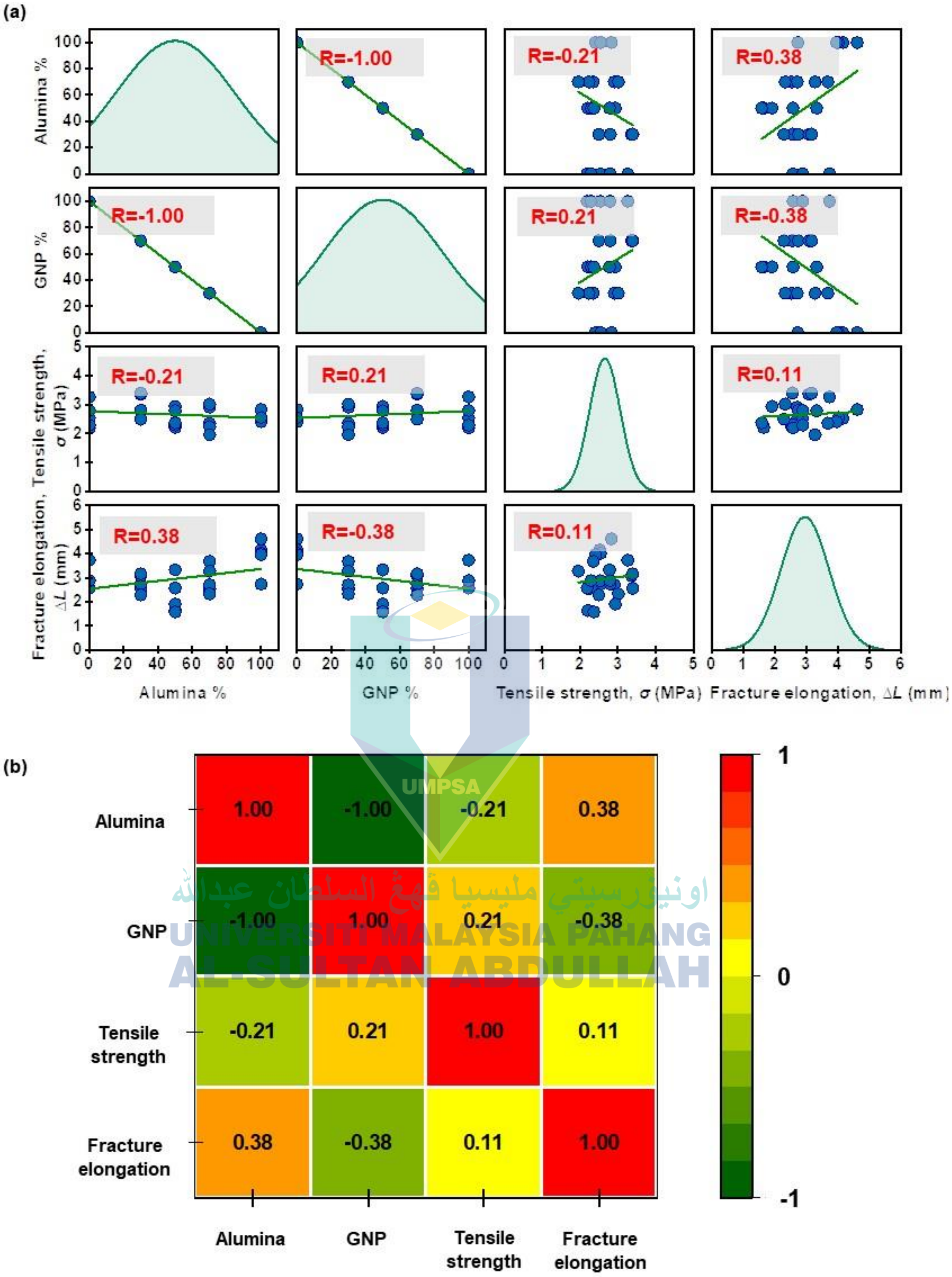

	Alumina	GNP	Tensile strength	Fracture elongation
Alumina	1.00	-1.00	-0.21	0.38
GNP	-1.00	1.00	0.21	-0.38
Tensile strength	-0.21	0.21	1.00	0.11
Fracture elongation	0.38	-0.38	0.11	1.00

Figure 4.29 (a) Correlation matrix and (b) correlation heatmap presenting the significance of Alumina/GNP hybrid nano reinforcement to tensile properties in ASTM E8 specimen at 2.0 wt% hybrid nanoparticle content

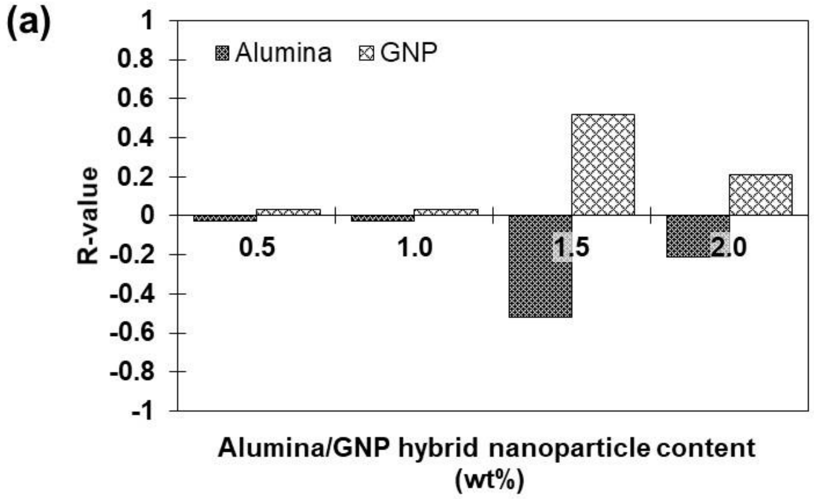

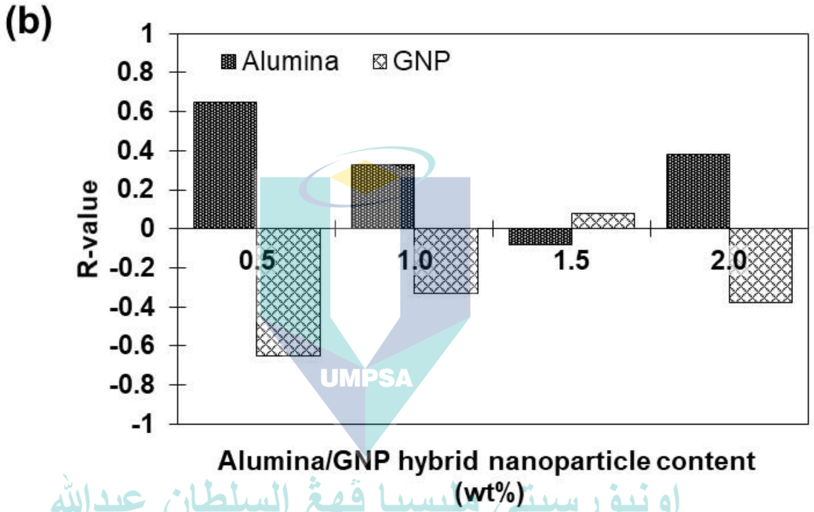

Figure 4.30 The dependence of R value to the Alumina/GNP hybrid nanoparticle content for (a) tensile strength and (b) fracture elongation of ASTM E8 specimens

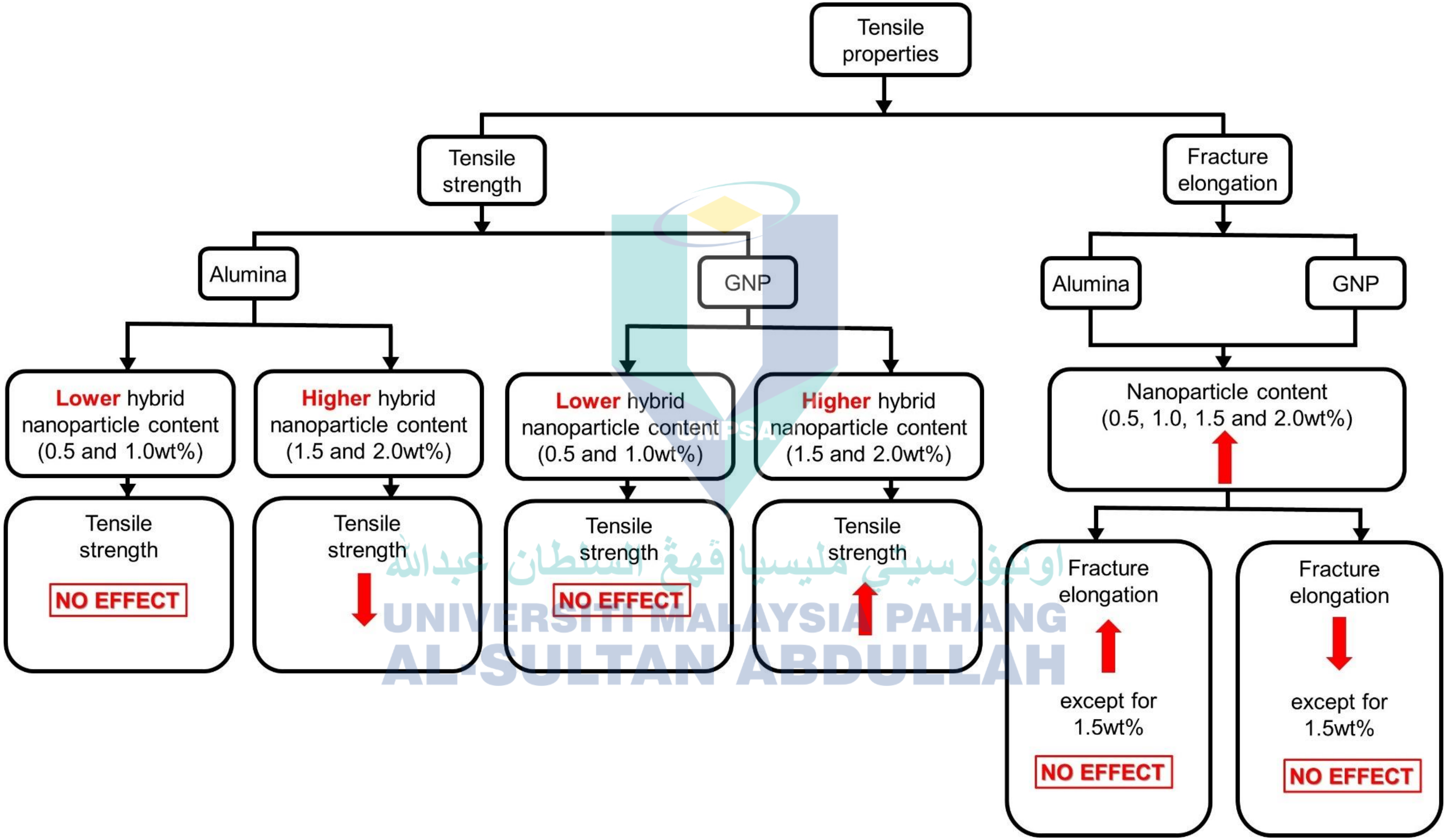

Figure 4.31 Graphical summary on the effect of hybrid nanoreinforcement to the tensile properties in ASTM E8 specimens

4.6 Mechanical properties result (Single lap joint specimen)

This section discussed the effect of Alumina/GNP hybrid nano reinforcement on the tensile properties of the joining specimens at various hybrid nanoparticle contents and weight ratio combinations. The discussion also included a parametric analysis by using correlation matrices and correlation heatmaps.

4.6.1 Representative of shear strength and fracture elongation of SLJ specimen

Figure 4.32 shows the representative shear strength and elongation of SLJ specimens with Alumina/GNP hybrid nano adhesive at various weight ratio combinations for (a) 0.5 wt%, (b) 1.0 wt%, (c) 1.5 wt% and (d) 2.0 wt% hybrid nanoparticle content. The detailed results of shear strength and fracture elongation are shown in Table 4.3.

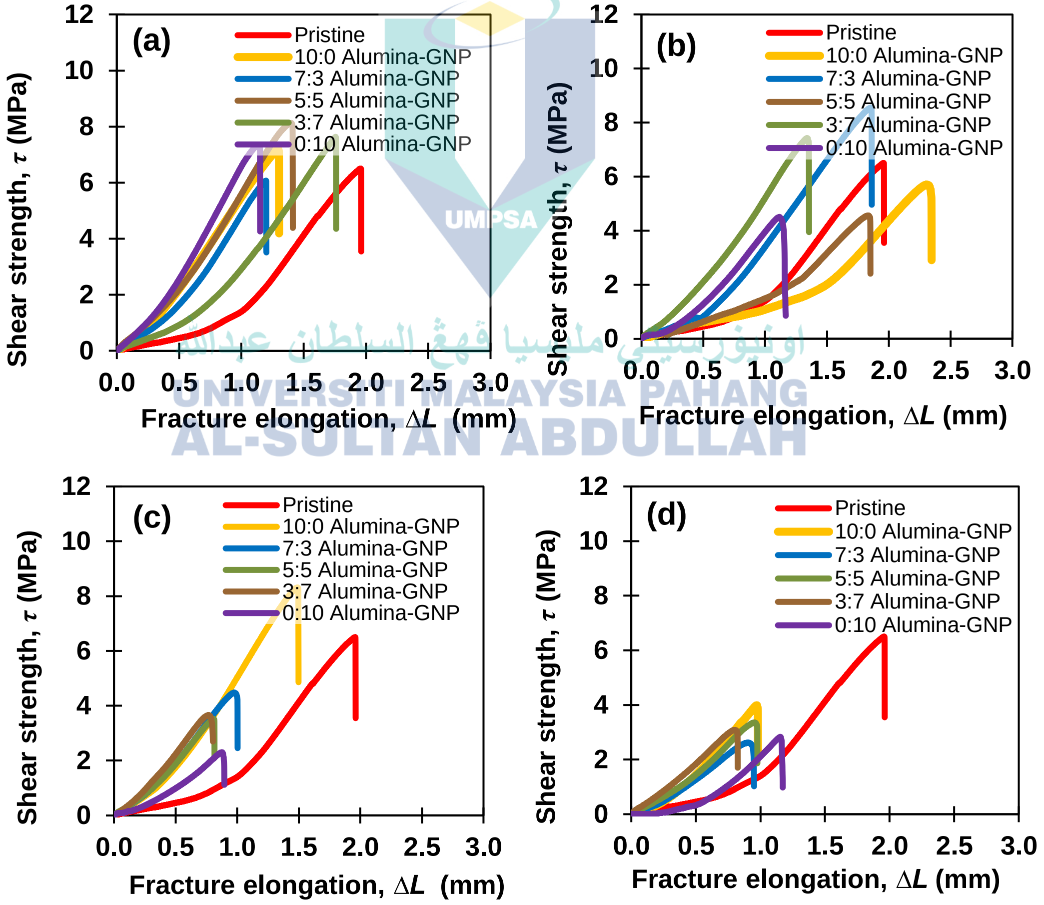

Figure 4.32 Representative stress and elongation of hybrid Alumina/GNP hybrid nano adhesive of SLJ specimen at various weight ratio combinations for (a) 0.5 wt%, (b) 1.0 wt%, (c) 1.5 wt%, and (d) 2.0 wt% hybrid nanoparticle content

Table 4.3 Summary of shear strength and fracture elongation for SLJ specimen at various hybrid nanoparticle content and various weight ratio combinations of Alumina/GNP hybrid nanoreinforcement

Alumina/GNP hybrid Nanoparticle content (wt%)	**Weight ratio combination (Alumina:GNP)**	**Shear strength, τ (MPa)**	**Fracture elongation, ΔL (mm)**
Pristine	-	6.94 ± 0.41	1.33 ± 0.34
0.5	10:0	6.88 ± 0.42	1.22 ± 0.19
	7:3	7.12 ± 0.61	1.38 ± 0.14
	5:5	7.62 ± 0.97	1.45 ± 0.16
	3:7	7.11 ± 0.53	1.38 ± 0.20
	0:10	6.82 ± 0.61	1.16 ± 0.12
1.0	10:0	5.76 ± 0.31	3.00 ± 0.59
	7:3	9.82 ± 0.89	2.50 ± 0.93
	5:5	4.53 ± 0.14	1.35 ± 0.36
	3:7	6.64 ± 0.78	1.46 ± 0.19
	0:10	4.56 ± 0.25	1.19 ± 0.05
1.5	10:0	7.99 ± 0.82	1.47 ± 0.11
	7:3	4.45 ± 0.28	1.05 ± 0.06
	5:5	3.64 ± 0.29	0.77 ± 0.04
	3:7	3.49 ± 0.45	0.95 ± 0.13
	0:10	2.36 ± 0.05	0.79 ± 0.07
2.0	10:0	4.01 ± 0.34	0.99 ± 0.13
	7:3	2.56 ± 0.28	1.20 ± 0.28
	5:5	3.10 ± 0.43	0.89 ± 0.11
	3:7	3.29 ± 0.42	1.07 ± 0.35
	0:10	2.85 ± 0.08	1.04 ± 0.23

4.6.2 Effect of Alumina/GNP hybrid nano reinforcement to the shear properties of joining specimens

Figure 4.33 shows the shear strength for SLJ specimens with various hybrid nanoparticle contents of Alumina/GNP hybrid nano reinforcement at different weight ratio combinations: (a) 10:0, (b) 7:3, (c) 5:5, (d) 3:7, and (e) 0:10. In Figure 4.33 (a), the 10:0 weight ratio combination of Alumina/GNP hybrid nano reinforcement demonstrated the highest shear strength at 1.5 wt% with an increase of 15.13% ± 82.93% compared to the pristine adhesive. However, the addition of 0.5 wt%, 1.0 wt%, and 2.0 wt% hybrid nanoparticle content resulted in significant decreases in shear strength by 0.86% ± 2.44%, 17.0% ± 24.39% and 42.36% ± 17.07% respectively compared to the pristine adhesive. For Figure 4.33 (b), in the 7:3 weight ratio combination, the inclusion of Alumina/GNP hybrid nano reinforcement at 1.0wt% yielded the highest shear strength, showing an increase of 41.50% ± 117.07% compared to the pristine adhesive. However, further inclusions of hybrid Alumina/GNP nano reinforcement at 0.5 wt%, 1.5 wt%, and 2.0 wt% resulted in decrease in shear strength by 2.59% ± 48.78%, 15.13% ± 82.93% and 63.11% ± 31.71%, respectively compared to the pristine adhesive. In the case of 5:5 weight ratio combination (Figure 4.33 (c)), the 0.5 wt% of Alumina/GNP hybrid nano reinforcement recorded the highest shear strength compared to the pristine adhesive, with a decrease of 9.80% ± 136.59%. However, further additions of 1.0 wt%, 1.5 wt%, and 2.0 wt% resulted in decrease in shear strength by 34.73% ± 65.85%, 47.55% ± 29.27%, and 55.33% ± 4.88%, respectively. A gradual decrease in shear strength was observed from 1.0 wt% to 2.0 wt% Alumina/GNP hybrid nano reinforcement. For the specimens at 3:7 weight ratio combination (Figure 4.33 (d)) at 0.5 wt% Alumina/GNP hybrid nano reinforcement, there was an increase in shear strength compared to the pristine adhesive, with an increment of 2.45% ± 29.27%. However, further inclusions up to 2.0 wt% Alumina/GNP hybrid nanoparticle content resulted in decrease in shear strength by 4.32% ± 90.24%, 49.71% ± 4.88% and 52.59% ± 2.44%, respectively. A steady decreasing trend in shear strength was observed from 1.0 wt% to 2.0 wt%. In Figure 4.32 (e), the addition of single GNP nano reinforcement (0:10 weight ratio combination) into the epoxy adhesive resulted in a decrease in tensile strength by 1.73% ± 48.78%, 34.29% ± 39.02%, 65.99% ± 90.24% and 58.93% ± 80.49%, respectively compared to the pristine adhesive.

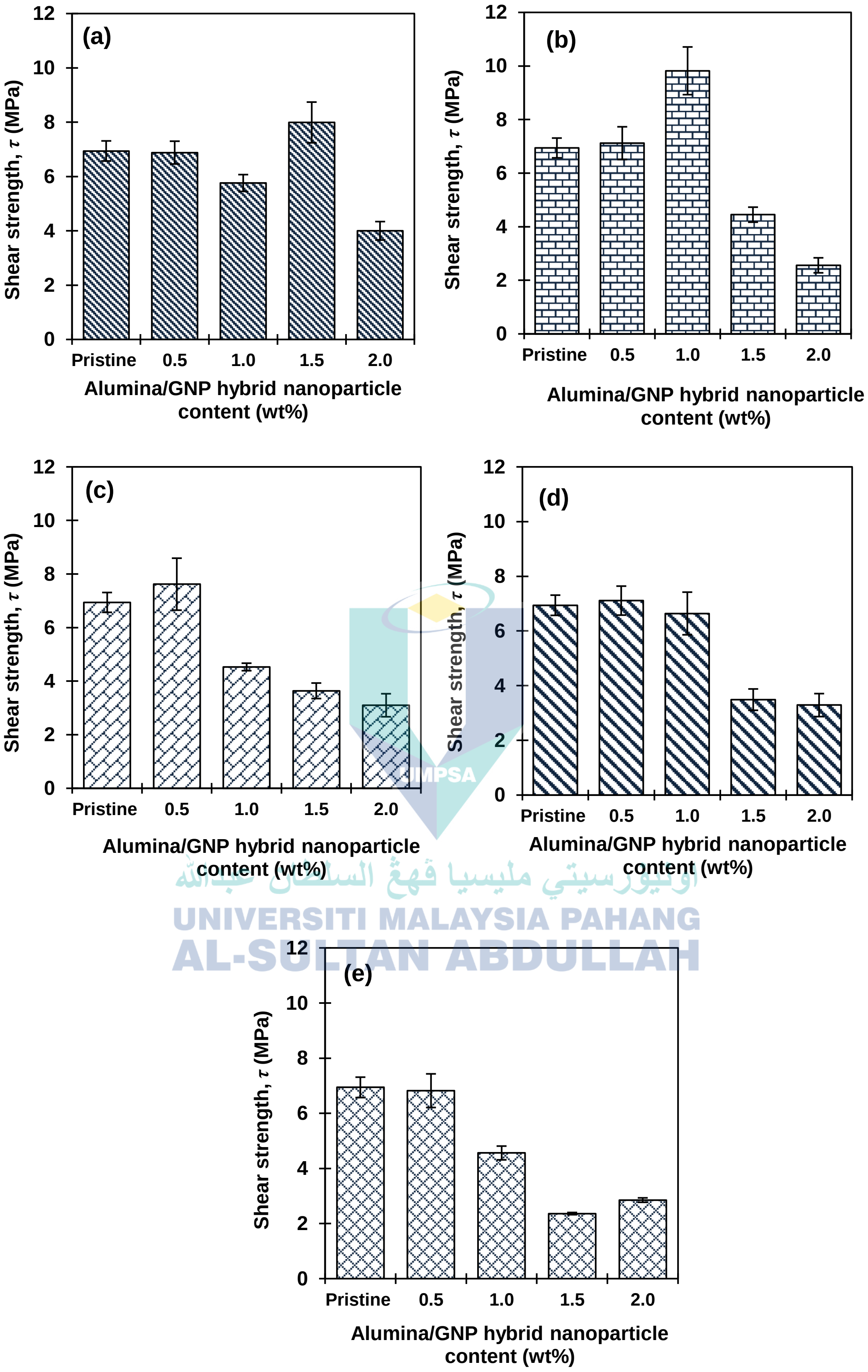

Figure 4.33 Shear strength for SLJ specimens at various hybrid nanoparticle content of Alumina/GNP hybrid nano reinforcement in (a) 10:0, (b) 7:3, (c) 5:5, (d) 3:7, and (e) 0:10 weight ratio combinations

Figure 4.34 shows the shear strength for SLJ specimens at various weight ratio combinations of Alumina/GNP hybrid nano reinforcements at different hybrid nanoparticle contents: (a) 0.5 wt%, (b) 1.0 wt%, (c) 1.5 wt% and (d) 2.0 wt%. In Figure 4.34 (a), when compared to the pristine adhesive at 10:0 and 0:10 weight ratio combinations, the addition of 0.5wt% Alumina/GNP hybrid nano reinforcement resulted in a decrease in shear strength by 0.86% ± 2.44% and 1.73% ± 48.78% respectively. Meanwhile, at 7:3, 5:5 and 3:7 weight ratio combinations of Alumina/GNP hybrid nano reinforcement, there was a decrease in shear strength by 2.59% ± 48.78%, 9.80% ± 136.59% and 2.45% ± 29.27%, respectively when compared to pristine adhesive counterparts. For Figure 4.34 (b), in the 7:3 weight ratio combination, the addition of 1.0 wt% Alumina/GNP hybrid nanoparticle content resulted in an increase in shear strength by 41.50% ± 117.07% compared to the pristine adhesive. Meanwhile, at the 10:0, 5:5, 3:7 and 0:10 weight ratio combinations of Alumina/GNP hybrid nano-reinforcement, there was a decrement in shear strength of up to 17.0% ± 24.39%, 34.73% ± 65.85%, 4.32% ± 90.24% and 34.29% ± 39.02% respectively when compared to pristine adhesive counterparts. As for Figure 4.34 (c), in comparison to pristine adhesive at the 10:0 weight ratio combination, the addition of 1.5 wt% Alumina/GNP hybrid nanoparticle content resulted in an increment in shear strength of up to 15.13% ± 82.93%. Meanwhile, at the 7:3, 5:5, 3:7 and 0:10 weight ratio combinations of Alumina/GNP hybrid nano-reinforcement, there was a decrement in shear strength of up to 35.88% ± 31.71%, 47.55% ± 29.27%, 49.71% ± 4.88% and 65.99% ± 90.24% respectively when compared to pristine adhesive counterparts. In Figure 4.34 (d), in comparison to pristine adhesive at all weight ratio combinations, the addition of 2.0 wt% Alumina/GNP hybrid nanoparticle content resulted in a decrement in shear strength of up to 42.36% ± 17.07%, 63.11% ± 31.71%, 55.33% ± 4.88%, 52.59% ± 2.44% and 58.93% ± 80.49%, respectively.

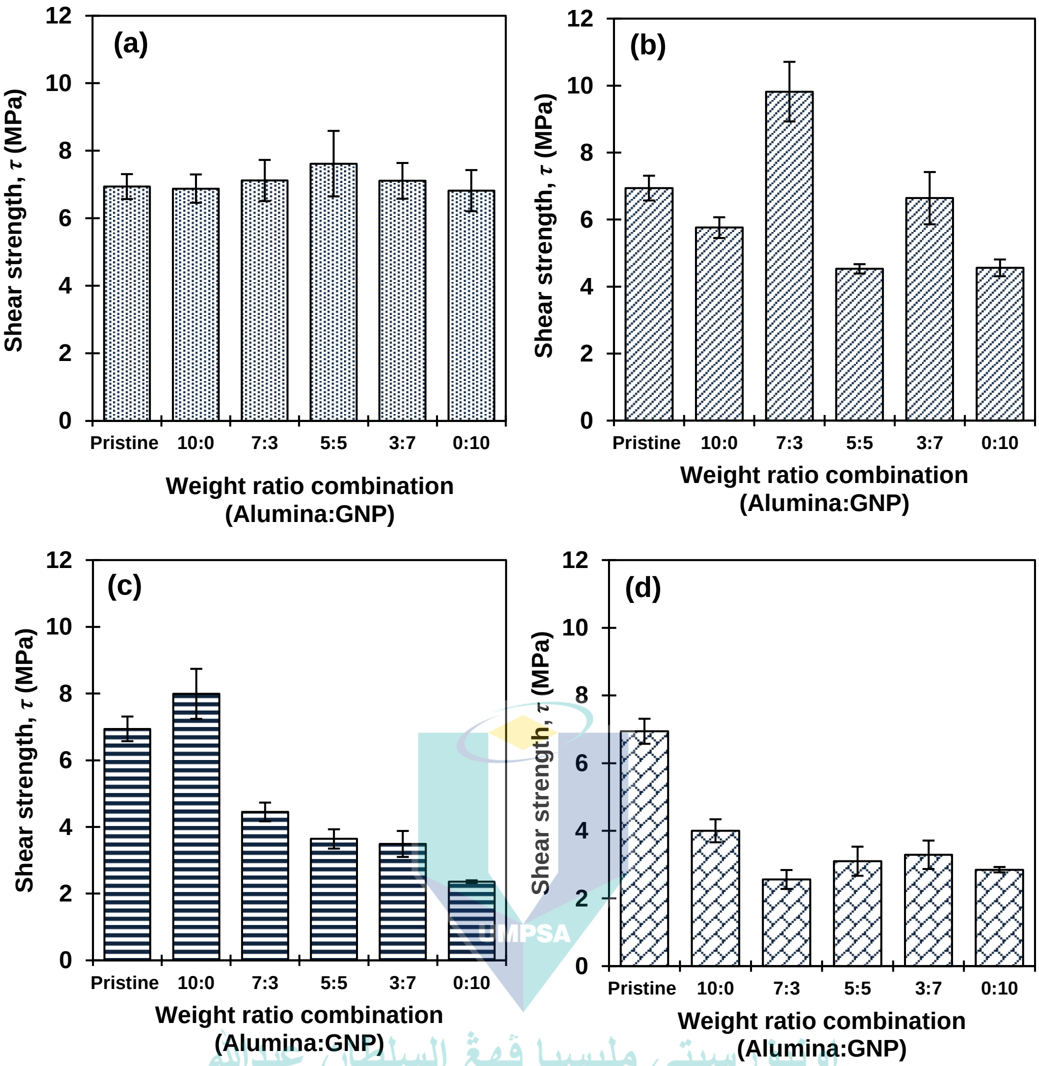

Figure 4.34 Shear strength for SLJ specimens at various weight ratio combination of Alumina/GNP hybrid nano reinforcement in (a) 0.5 wt%, (b) 1.0 wt%, (c) 1.5 wt%, and (d) 2.0 wt% hybrid nanoparticle content

Figure 4.35 shows the fracture elongation for SLJ specimens at various hybrid nanoparticle contents of Alumina/GNP hybrid nano-reinforcement in (a) 10:0, (b) 7:3, (c) 5:5, (d) 3:7, and (e) 0:10 weight ratio combinations. From Figure 4.35 (a), when compared to the pristine adhesive counterpart for Alumina/GNP hybrid nano-reinforcement specimens at a 10:0 weight ratio combination, the addition of 1.0 wt% Alumina/GNP hybrid nanoparticle content resulted in the highest average value for fracture elongation up to 125.56% ± 73.53%, while the addition of 0.5 and 2.0 wt% Alumina/GNP hybrid nanoparticle content resulted in a decrement of the average value for fracture elongation up to 8.27% ± 44.12% and 25.56% ± 61.67%, respectively.

Meanwhile, at 1.5 wt%, the average value for fracture elongation resulted in an increment of up to 10.53% ± 67.65% when compared to the pristine adhesive counterpart. As for fracture elongation (Figure 4.35 (b)), Alumina/GNP hybrid nano reinforcement specimens at 7:3 weight ratio combination, the addition of 1.0 wt% Alumina/GNP hybrid nanoparticle content resulted in an increment in the highest average value for fracture elongation, with 87.97% ± 173.53%. At 0.5 wt% of Alumina/GNP hybrid nanoparticle content, there was a significant improvement in the average value for fracture elongation, with 3.76% ± 58.82%. Further inclusion of Alumina/GNP hybrid nano-reinforcement at the 7:3 weight ratio combination at 1.5 and 2.0 wt% resulted in a decrement in the average value for fracture elongation, with 21.05% ± 82.35% and 9.77% ± 17.65% respectively. When compared to the pristine adhesive counterpart for fracture elongation (Figure 4.35 (c)) at 5:5 weight ratio combination of Alumina/GNP hybrid nano reinforcement specimens, there was a recorded increment in the average value for fracture elongation up to 9.02% ± 52.94% at 0.5 wt%, while the average value for fracture elongation at 1.0 wt% was recorded with a slightly improvement at 1.50% ± 5.88%. It resulted in a decrement of 42.11% ± 88.24% and 33.08% ± 67.65% for 1.5 and 2.0 wt% Alumina/GNP hybrid nanoparticle content respectively. From 1.5-2.0 wt% of Alumina/GNP hybrid nanoparticle content, there was a gradual decrease in the average value for the fracture elongation trend. As for fracture elongation (Figure 4.35 (d)) at 3:7 weight ratio combination of Alumina/GNP hybrid nano-reinforcement, the average value for fracture elongation was recorded with a slightly significant improvement of 3.76% ± 41.18% at 0.5 wt% when compared to the pristine adhesive, while the average value for fracture elongation at 1.0 wt% recorded the highest improvement of up to 9.77% ± 44.12%. It resulted in a decrement of 28.57% ± 61.76% and 19.55% ± 2.94% for 1.5 and 2.0 wt%, respectively. From 1.5-2.0 wt% of Alumina/GNP hybrid nanoparticle content, there was a gradual decrease in the fracture elongation trend. Meanwhile, fracture elongation of the 0:10 weight ratio combination of Alumina/GNP hybrid nano-reinforcement specimens (Figure 4.35 (e)) resulted in a slightly significant decrement in the average value for fracture elongation when compared to the pristine adhesive, with 12.78% ± 64.71%, 10.53% ± 85.29%, 40.60% ± 79.41% and 21.80% ± 32.35%, respectively.

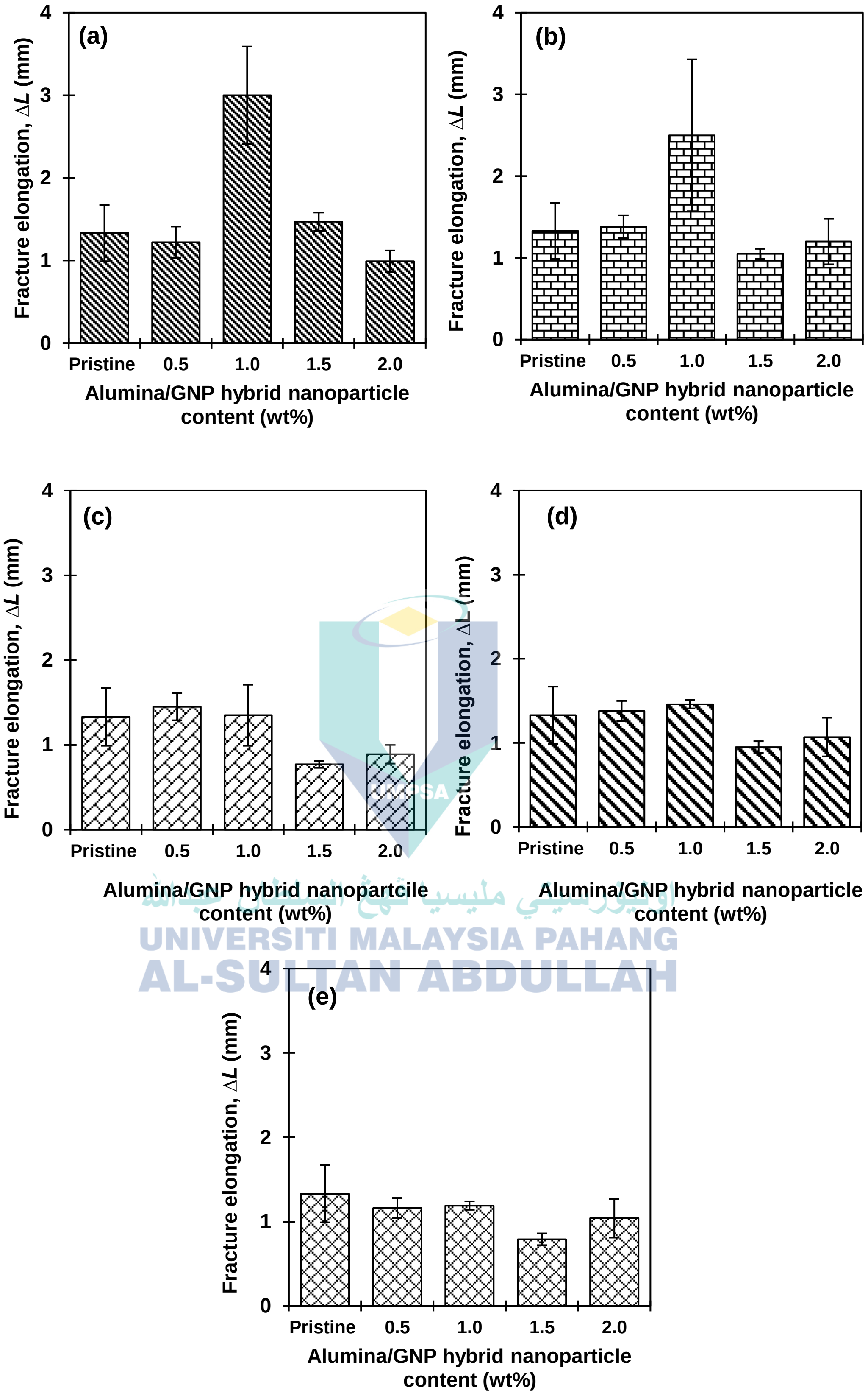

Figure 4.35 Fracture elongation for SLJ specimens at various hybrid nanoparticle content of Alumina/GNP hybrid nano reinforcement in (a) 10:0, (b) 7:3, (c) 5:5, (d) 3:7, and (e) 0:10 weight ratio combinations

Figure 4.36 shows the fracture elongation for SLJ specimens at various weight ratio combinations of Alumina/GNP hybrid nano-reinforcement in (a) 0.5 wt%, (b) 1.0 wt%, (c) 1.5 wt%, and (d) 2.0 wt% hybrid nanoparticle content. From Figure 4.36 (a), it clearly showed that the average value for fracture elongation of 0.5wt% Alumina/GNP hybrid nano-reinforcement specimens at various weight ratio combinations. When compared to the pristine adhesive, the addition of single alumina nano-reinforcement (i.e., 10:0 weight ratio combination) and single GNP nano-reinforcement (i.e., 0:10 weight ratio combination) exhibited a significant decrement in the average value for fracture elongation up to 8.27% ± 44.12% and 12.78% ± 64.71%, respectively. Meanwhile, at 7:3, 5:5 and 3:7 weight ratio combinations of Alumina/GNP hybrid nano-reinforcement, there was a relatively significant improvement of 3.76% ± 58.82%, 9.02% ± 52.94% and 3.76% ± 41.18%, respectively when compared to the pristine adhesive. As for fracture elongation (Figure 4.36 (b)), the average value for fracture elongation of 1.0wt% Alumina/GNP hybrid nano-reinforcement specimens at various weight ratio combinations demonstrated an increment when compared to the pristine adhesive. Specifically, at 10:0, 7:3, 5:5 and 3:7 weight ratio combinations of Alumina/GNP hybrid nano-reinforcement, there was an increase of up to 125.56% ± 73.53%, 87.97% ± 173.53%, 1.50% ± 5.88% and 9.77% ± 44.12%, respectively. Meanwhile, the addition of a single GNP nano-reinforcement (i.e., 0:10 weight ratio combination) showed a decrement of 10.53% ± 85.29% in the average value for fracture elongation compared to the pristine adhesive counterparts. As for fracture elongation (Figure 4.36 (c)), it also showed the average value for the fracture elongation of the epoxy nanocomposite at 1.5 wt%. The addition of a single alumina nano-reinforcement (i.e., 10:0 weight ratio combination) showed an increment of 10.53% ± 67.65% compared to the pristine adhesive. In contrast, the 7:3, 5:5, 3:7 and 0:10 weight ratio combinations of Alumina/GNP hybrid nano-reinforcement showed a significant decrement in the average value for fracture elongation, reaching up to 21.05% ± 82.35%, 42.11% ± 88.24%, 28.57% ± 61.76% and 40.60% ± 79.41%, respectively. As for fracture elongation (Figure 4.36 (d)), when compared to the pristine adhesive, the average values for fracture elongation of 2.0 wt% Alumina/GNP hybrid nano-reinforcement specimens at all weight ratio combinations showed a decrement of up to 25.56% ± 67.76%, 9.77% ± 17.65%, 33.08% ± 67.65%, 19.55% ± 2.94% and 21.80% ± 32.35%, respectively.

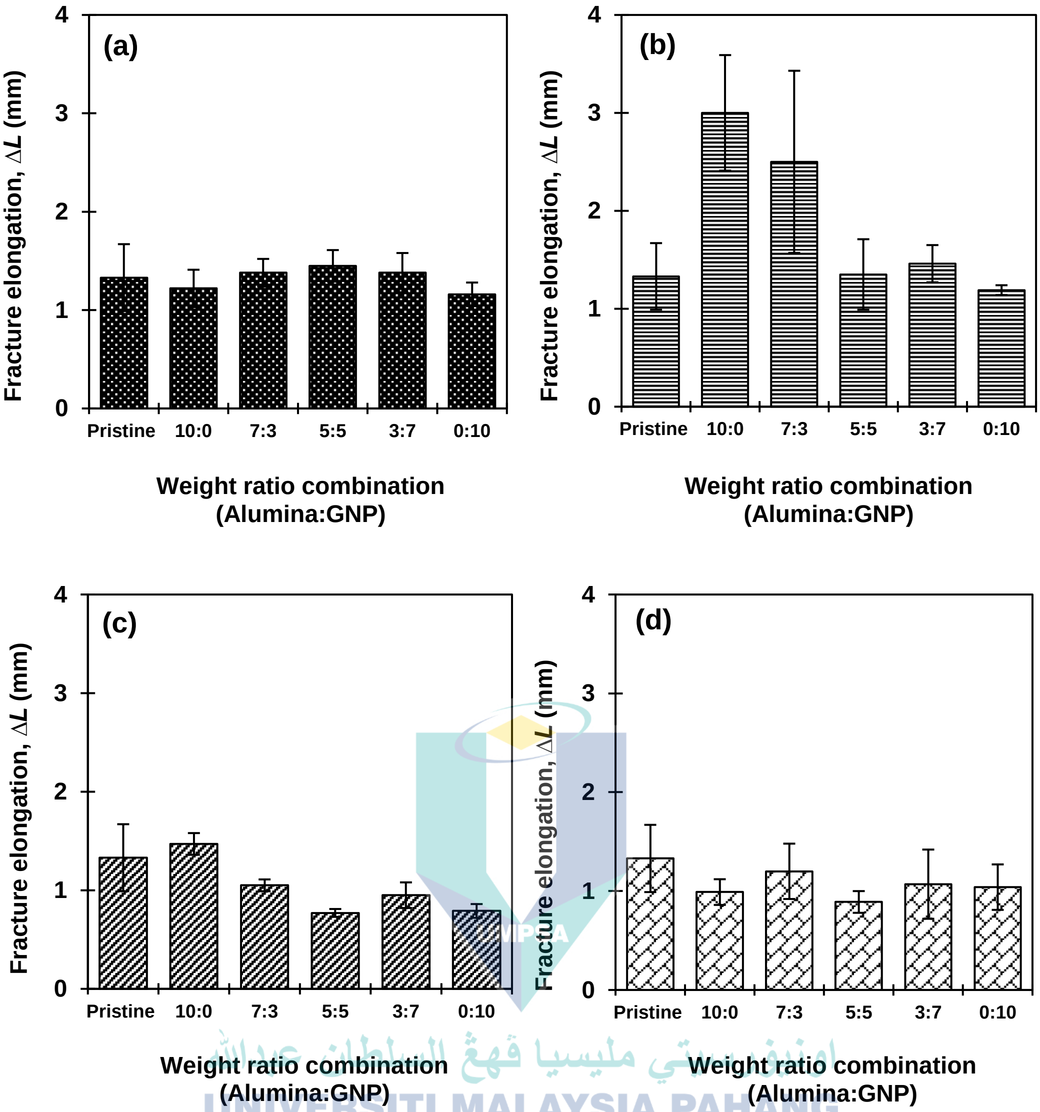

Figure 4.36 Fracture elongation for SLJ specimens at various weight ratio combination of Alumina/GNP hybrid nano reinforcement in (a) 0.5 wt%, (b) 1.0 wt%, (c) 1.5 wt%, and (d) 2.0 wt% hybrid nanoparticle content

4.6.3 Fracture behaviour analysis (Single lap joint specimen)

The fracture behaviour of ASTM D1002 joining specimens subjected to various hybrid nanoparticle contents and weight ratio combinations of Alumina/GNP hybrid nano-reinforcement is illustrated in Figure 4.37, where representative images of fractured specimens can be observed. The detailed results of the fractured regions are shown in Table 4.4. From the figure, it was apparent that the fractured specimens demonstrated either adhesive failure, cohesive failure or a combination of both modes. The red-coloured regions indicated the cohesively fractured regime in the specimens. To evaluate the failure modes in the fractured specimens, open-source software ImageJ was used by altering the colour threshold of the fractured specimen's image. The failure mode ratios for each specimen were calculated by dividing the surface area of each failure mode via the overlap surface area. All fractured specimens exhibited the existence of several fracture modes, namely adhesive fracture mode (AF), cohesive fracture mode (CF) or a combination of both modes. Generally, the cohesive failure mode (CF) was considered preferable.

Figures 4.38 and 4.39 depict the adhesive fractured region as a function of various hybrid nanoparticle content and weight ratio combinations of Alumina/GNP hybrid nano-reinforcement. Meanwhile, Figures 4.40 and 4.41 show the cohesive fractured region as a function of various hybrid nanoparticle contents and weight ratio combinations of Alumina/GNP hybrid nano-reinforcement. An increased CF mode region signifies robust interfacial adhesion between adherends and nanofillers. This suggests that a greater amount of energy is necessary to compromise the joining strength, leading to an enhancement in bonding strength (Khalil et al., 2019). The reinforcement of Alumina/GNP and the pre-treated adherend surface, where roughness is added onto the adherend surface, is expected to increase the CF percentage through mechanical interlocking, possibly enhancing the joining strength (Kong and Khalil, 2022; Tutunchi et al., 2016). Studies conducted by Ahmadi-Moghadam et al. (2015) and Ahmadi (2019) reported that factors contributing to increased CF include crack bridging, nanoparticle breakage and crack deviation.

Figure 4.42 and Figure 4.43 depict the relationship between fracture behaviour (i.e., Adhesive, AF and cohesive fracture, CF) and the shear strength of the joining specimen. The correlation between shear strength and adhesive fracture (AF) and cohesive fracture (CF) is not immediately evident. However, based on the trendline, subtle relationships emerged. Specifically, shear strength slightly increased with a rise in AF%, while it slightly decreased with an increase in CF%. As mentioned previously, in most cases, shear strength is directly proportional to CF, indicating that the material has reached its maximum strength (Khalil et al., 2019). Conversely, a higher AF mode region usually indicates insufficient adhesion (Kong et al., 2021). The CF mode region is commonly used in various applications due to its tendency for sufficient adhesion, which is determined by the bulk properties of the adhesive. These variations in the relationship might be attributed to several factors such as dispersion stability influenced by the high viscosity of epoxy adhesive at higher nanoparticle content (Park et al., 2009) as discussed earlier. Therefore, a detailed analysis through correlation matrices and heatmaps were applied in Section 4.6.4 to further investigate the relationship of these two elements concerning the content of each hybrid nanoparticle.

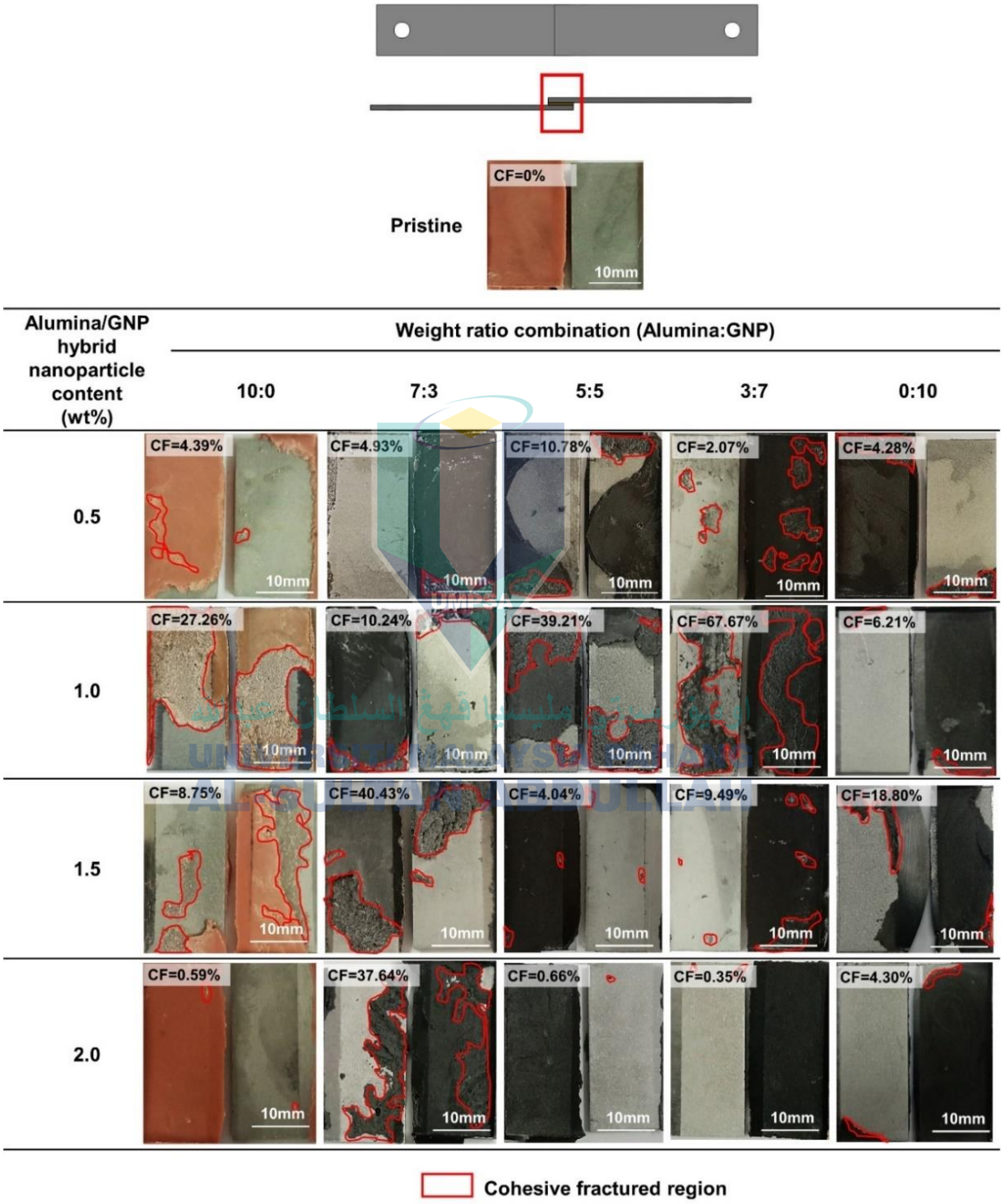

Figure 4.37 Representative images of fractured surface in single lap joint specimens at various hybrid nanoparticle content and various weight ratio combinations (Red-coloured line represented CF region)

Table 4.4 Summary of adhesive and cohesive fracture of single lap joint specimens

	Alumina/GNP hybrid nanoparticle content (wt%)	**Weight ratio combination (Alumina: GNP)**					
		-	**10:0**	**7:3**	**5:5**	**3:7**	**0:10**
Adhesive fracture, *AF* (%)	Pristine	100.0 ± 0.0	-	-	-	-	-
	0.5	-	95.61 ± 1.83	95.07 ± 3.70	89.22 ± 7.42	97.93 ± 2.45	95.72 ± 4.30
	1.0	-	72.74 ± 28.06	89.76 ± 3.84	60.79 ± 22.14	32.33 ± 34.89	93.79 ± 2.45
	1.5	-	91.25 ± 11.53	59.57 ± 24.41	95.95 ± 4.28	90.51 ± 13.48	81.20 ± 40.31
	2.0	-	99.41 ± 0.16	62.36 ± 14.67	99.34 ± 0.21	99.65 ± 0.30	95.70 ± 6.73
Cohesive fracture, *CF* (%)	Pristine	0.00 ± 0.00	-	-	-	-	-
	0.5	-	4.39 ± 1.83	4.93 ± 3.38	10.78 ± 7.42	2.07 ± 2.24	4.28 ± 4.30
	1.0	-	27.26 ± 28.06	10.24 ± 3.84	39.21 ± 22.14	67.67 ± 34.89	6.21 ± 2.45
	1.5	-	8.75 ± 11.53	40.43 ± 24.41	4.04 ± 4.28	9.49 ± 13.48	18.80 ± 40.31
	2.0	-	0.59 ± 0.16	37.64 ± 14.67	0.66 ± 0.21	0.35 ± 0.30	4.30 ± 6.73

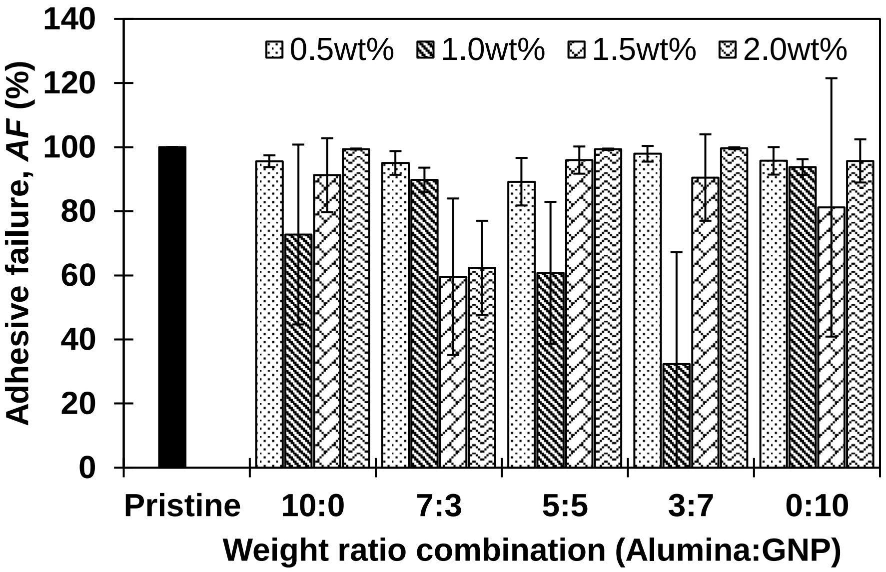

Figure 4.38 Adhesive fracture region as function of Alumina/GNP hybrid nanoreinforcement weight ratio combination at various hybrid nanoparticle content in SLJ specimen

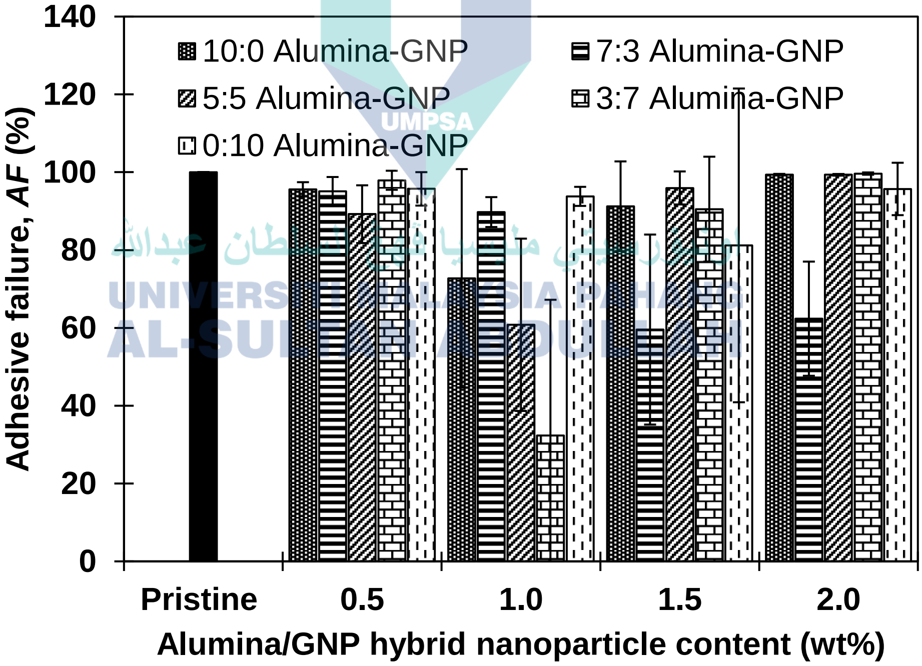

Figure 4.39 Adhesive fracture region as function of Alumina/GNP hybrid nanoreinforcement content at various weight ratio combination in SLJ specimen

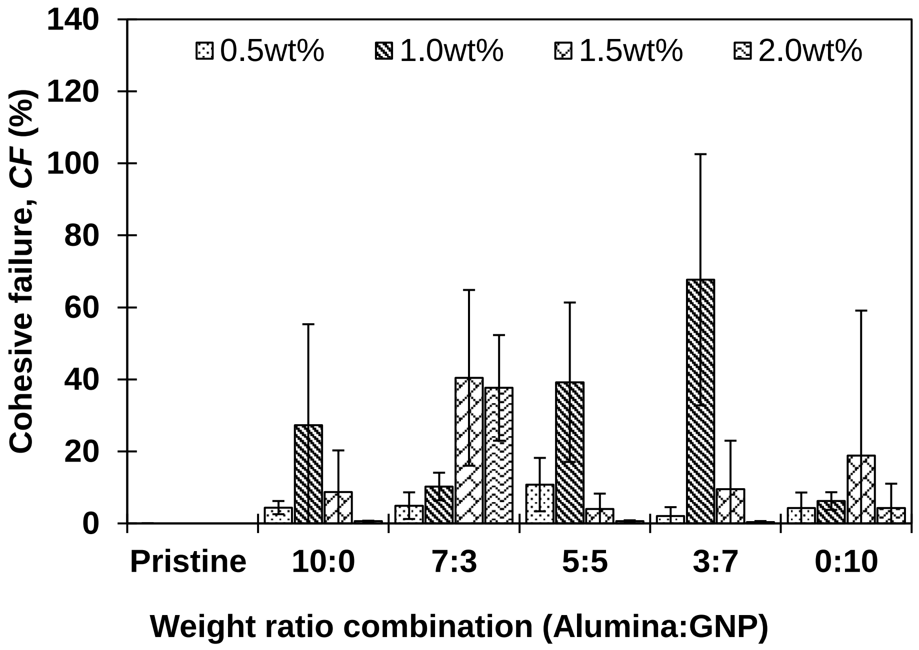

Figure 4.40 Cohesive fracture region as function of Alumina/GNP hybrid nanoreinforcement weight ratio combination at various hybrid nanoparticle content in SLJ specimen

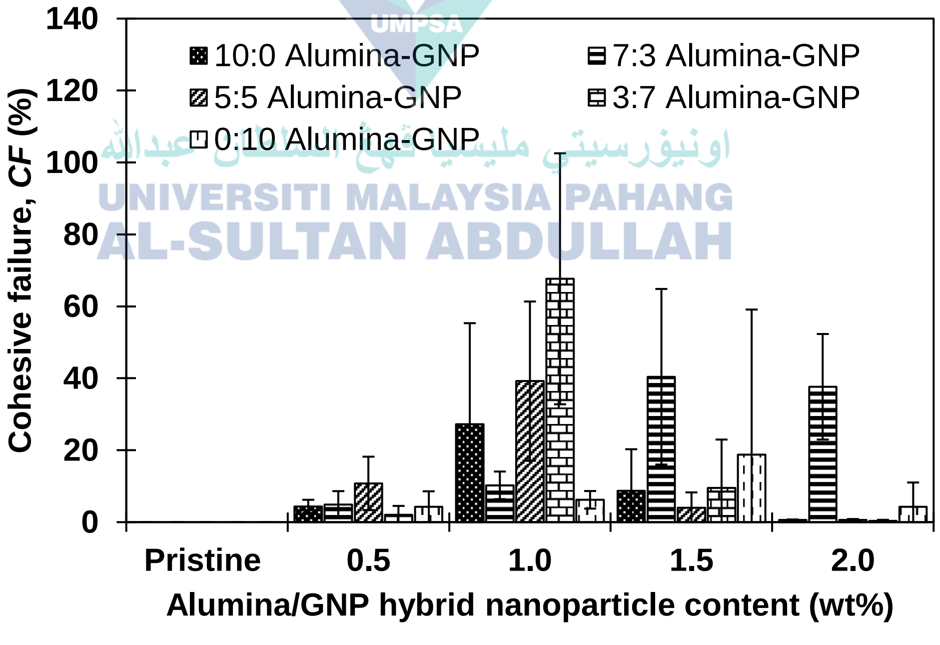

Figure 4.41 Cohesive fracture region as function of Alumina/GNP hybrid nanoreinforcement content at various weight ratio combination in SLJ specimen

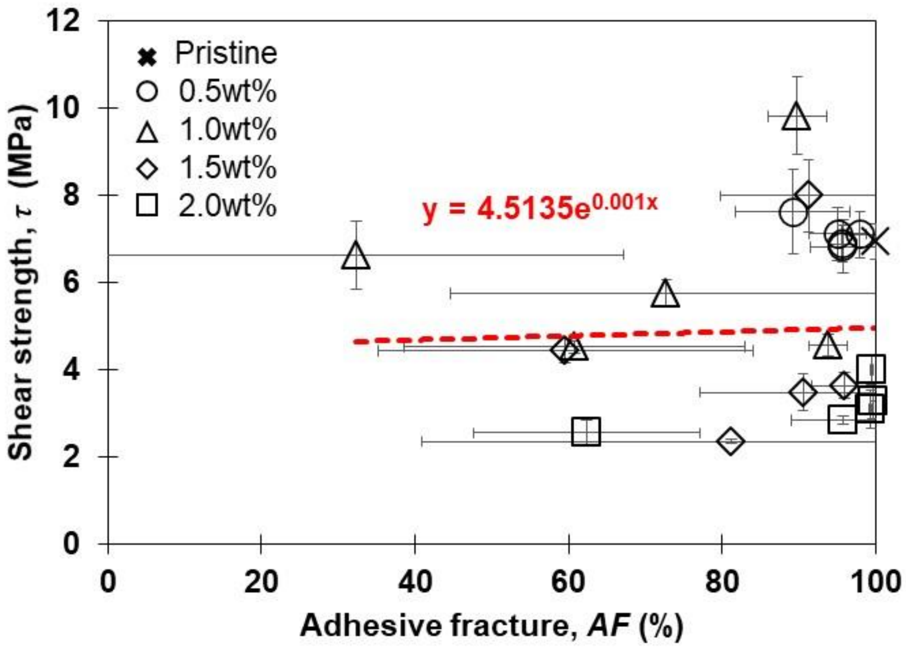

Figure 4.42 Relation between shear strength and adhesive fracture mode in SLJ specimens

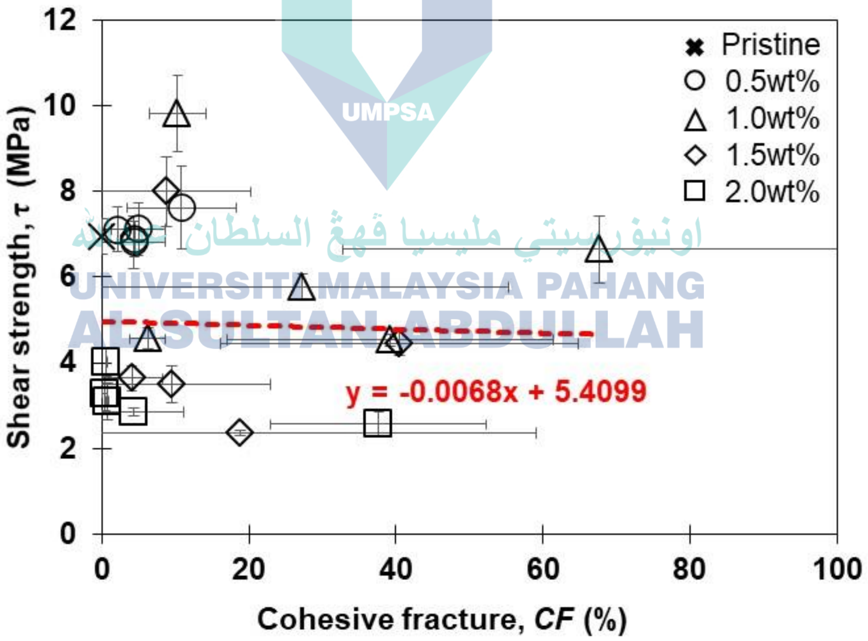

Figure 4.43 Relation between shear strength and cohesive fracture mode in SLJ specimens

4.6.4 Pearson correlation and heatmap analysis for shear properties of SLJ specimen in Alumina/GNP hybrid nano adhesive

4.6.4.1 Correlation between hybrid nano reinforcement and shear properties

Figure 4.44 to Figure 4.47 show the correlation matrix and correlation heatmap for shear properties and fracture behaviour with Alumina/GNP hybrid nano adhesive. The figures delved into the correlation between hybrid nano-reinforcement (i.e., alumina nanoparticle weight ratio and GNP weight ratio) and shear properties (i.e., shear strength and fracture elongation).

From these figures (Refer Figure 4.44 to 4.47), it was evident that, regardless of Alumina/GNP hybrid nano-reinforcement content, alumina nanoparticle weight ratio and shear strength demonstrated a positive relationship at 1.0-2.0 wt%, with R-values of 0.36, 0.89 and 0.43, respectively. Notably, at 0.5 wt%, there was no discernible impact on the shear strength of the joining specimen as reflected by an R-value of -0.03. Incorporating Alumina nanoparticles into the epoxy adhesive is likely to enhance the surface-to-volume ratio of alumina. This increase in the quantity of interfacial region is expected to improve stress distribution and transfer, ultimately contributing to higher bonding performance. They could be further emphasised by the mechanical interlocking between the nanofiller and adherend surface (Khalil et al., 2019). Furthermore, the presence of small amounts of alumina nanoparticle due to tiny dimensions might penetrate into any small voids on the adherend surface, thus enhancing the joint strength through mechanical interlocking (Yadollahi et al., 2015).

On the other hand, from these figures also (Refer Figure 4.44 to 4.47), it was noted that the GNP weight ratio and shear strength at 1.0-2.0 wt% demonstrated a negative relation with R-values of -0.36, -0.89 and -0.43, respectively. However, at 0.5 wt%, there was no discernible impact on the shear strength of the joining specimen, with an R-value of 0.03. These negative R-values indicated that, regardless of Alumina/GNP hybrid nanoparticle content, the shear strength decreased with an increasing GNP weight ratio. This decrease may be attributed to the agglomeration of GNP, causing a reduction in shear strength (Salom et al., 2018). Additionally, a weak GNP-polymer matrix interface might contribute to the reduction in shear strength of the joining specimen (Rider et al., 2020).

Meanwhile, from these figures (Refer Figure 4.44 to 4.47), it was also noted that at 1.0 and 1.5 wt%, the alumina nanoparticle weight ratio and fracture elongation demonstrated a positive relation with R-values of 0.73 and 0.78, respectively. However, at 0.5 and 2.0 wt%, there was no discernible impact on the fracture elongation of the joining specimen, with R-values of 0.09 and 0.00, respectively. These observations might be attributed to the stress within the polymeric matrix. Local stress can be more easily transferred onto the tougher particle, resulting in the matrix appearing amenable to a larger local plastic deformation. Therefore, a higher composite strength is achieved when the particles are in intimate contact with the polymer matrix (Kaboorani and Riedl, 2012). Furthermore, these alumina particles not only significantly reduce but also limit the propagation of cracks into larger cracks (Osman et al., 2021).

On the other hand, from these figures (Refer Figure 4.44 to 4.47), it was noted that at 1.0 and 1.5 wt%, the GNP weight ratio and fracture elongation demonstrated a negative relation with R-values of -0.73 and -0.78, respectively. However, at 0.5 and 2.0 wt%, there was no discernible impact on the fracture elongation of the joining specimen, with R-values of -0.09 and 0.00, respectively. These negative R-value indicated that, regardless of Alumina/GNP hybrid nanoparticle content, the fracture elongation decreased with an increasing GNP weight ratio. This observation may be attributed to the aggregation of GNP and the resultant stress concentration, leading to crack initiation and propagation (Kong et al., 2021).

In summary, the Alumina/GNP hybrid nanoparticle content showed that increasing the alumina nanoparticle weight ratio at every weight ratio combination (10:0, 7:3, 5:5, 3:7 and 0:10) indicated an increase in shear strength, except for 0.5 wt% which did not affect the shear strength of the joining specimen. Conversely, regardless of Alumina/GNP hybrid nanoparticle content, the inclusion of GNP weight ratio at every weight ratio combination indicated a decrease in shear strength, except for 0.5 wt% which did not affect the shear strength of the joining specimen as shown in Figure 4.48 (a).

Meanwhile, for fracture elongation, increasing the alumina nanoparticle weight ratio at every weight ratio combination (10:0, 7:3, 5:5, 3:7 and 0:10) in Alumina/GNP hybrid nanoparticle content indicated an increase in fracture elongation, except for 0.5 and 2.0 wt% which did not affect the fracture elongation of the joining specimen. Conversely, regardless of Alumina/GNP hybrid nanoparticle content, the inclusion of GNP weight ratio at every weight ratio combination indicated a decrease in fracture elongation, except for 0.5 and 2.0 wt% which did not affect the fracture elongation of the joining specimen as shown in Figure 4.48 (b). For ease of comprehension, the overall summary findings of the shear properties (i.e., tensile strength and fracture elongation) for joining the specimen are shown in Figure 4.49.

4.6.4.2 Correlation between hybrid nano reinforcement and fracture behaviour

Figure 4.44 to Figure 4.47 shows the correlation matrices and correlation heatmaps for hybrid nanoparticle content and fracture behaviour with Alumina/GNP hybrid nano adhesive joining specimen. The figures illustrate the correlation between hybrid nano-reinforcement (i.e., Alumina nanoparticle and GNP weight ratio) and fracture behaviour (i.e., Adhesive fracture, AF, and Cohesive fracture, CF).

From these figures (Refer Figure 4.44 to 4.47), it could be seen that alumina nanoparticle weight ratio and adhesive fracture at 0.5-2.0 wt% demonstrated a negative relation with R-values of -0.07, -0.26, -0.04 and -0.20, respectively. Meanwhile, it was also noted that alumina nanoparticle weight ratio and cohesive fracture at 0.5-2.0 wt% demonstrated a positive relation with R-values of 0.07, 0.26, 0.04 and 0.20, respectively. This observation might be attributed to the increase in the number of points of interaction between epoxy and alumina nanoparticles in the adhesive joint. Alumina nanoparticles fill any microscopic void or gap present on the adherend surface. Extensive contact regions between the alumina nanoparticles and adhesive enhanced the mechanical interlocking (Gupta et al., 2021). Furthermore, alumina nanoparticles are evenly distributed within the matrix, leaving a rough surface. This is one of the possible reasons for a higher cohesive fracture mode (CF) (Osman et al., 2021). The formation of a larger CF mode region involves greater adhesive toughness to maintain the stability of the joining specimens (Ahmadi, 2019).

On the other hand, based on these figures (Refer Figure 4.44 to 4.47), it could be seen that the GNP weight ratio and adhesive fracture at 0.5-2.0 wt% demonstrated a positive relationship with R-values of 0.07, 0.26, 0.04, and 0.20, respectively. Meanwhile, it was also noted that the GNP weight ratio and cohesive fracture at 0.5-2.0 wt% demonstrated a negative relationship with R-values of -0.07, -0.26, -0.04, and -0.20, respectively. A possible mechanism for this observation might be attributed to the weak interfacial interaction between GNP and the substrate, which was often related to the lower energy required to induce debonding/separation in the joining adherends, resulting in lower bonding strength (Kong et al., 2021).

In summary, the Single-Lap Joint (SLJ) specimens with Alumina/GNP hybrid nano-reinforcement exhibited distinct effects on fracture behaviour. Regardless of the Alumina/GNP hybrid nanoparticle content (0.5, 1.0, 1.5 and 2.0 wt%), an increase in the Alumina nanoparticle weight ratio demonstrated a decrease in Adhesive Fracture (AF) and an increase in Cohesive Fracture (CF) mode region as depicted in Figure 4.50 (a) and (b). For clarity, the overall summary findings of the fracture behaviour (i.e., Adhesive Fracture, AF, and Cohesive Fracture, CF) for the joining specimens are presented in Figure 4.51.

4.6.4.3 Correlation between shear properties and fracture behaviour

Figure 4.44 to Figure 4.47 shows the correlation matrices and correlation heatmaps for hybrid nanoparticle content and fracture behaviour with Alumina/GNP hybrid nano adhesive. The figures illustrate the correlation between shear properties (i.e., shear strength and fracture elongation) and fracture behaviour (i.e., Adhesive fracture and cohesive fracture). From these figures, it could be seen that at 0.5 wt%, there was negative relation on the shear strength of the joining specimen and adhesive fracture, with an R-value of -0.31. These might be attributed to several factors such as dispersion stability influenced by the high viscosity of epoxy adhesive (Park et al., 2009) as previously mentioned in section 4.6.3. However, at 1.0, 1.5 and 2.0 wt%, there was the positive relation between shear strength and adhesive fracture with R-value of 0.19, 0.13, and 0.53, respectively. A possible mechanism for this observation might be due to the sufficient adhesion between adhesive and adherend surface (Kong et al., 2021).

On the other hand, from these figures (Refer Figure 4.44 to 4.47), it was noted that the fracture elongation and adhesive fracture at 0.5, 1.0 and 2.0 wt% demonstrated a negative relation with R-values of -0.31, -0.19 and -0.42, respectively. This observation might be attributed adhesive achieving insufficient adhesion to the adherend surface (Kong et al., 2021). However, at 1.5 wt% there was no discernible impact on fracture elongation of the joining specimen and adhesive fracture, with an R-value of 0.05. At 1.5 wt%, the content of nanoparticle might be just sufficient to offer minimal reinforcement without appreciably causing a significant increment of strength.

Meanwhile, from these figures (Refer Figure 4.44 to 4.47), it was also noted that at 0.5 wt%, there was positive relation on the shear strength of the joining specimen and cohesive fracture, with R-value of 0.31. This observation might be attributed to the higher energy is required to debonding/separation the joining specimen, leading to an enhancement in bonding strength (Khalil et al., 2019). Additionally, the sufficient adherend surface roughness, is expected to increase the CF percentage through mechanical interlocking, possibly enhancing the joining strength (Kong and Khalil, 2022; Tutunchi et al., 2016). However, at 1.0, 1.5, and 2.0 wt%, the shear strength and cohesive fracture demonstrated a negative relation with R-values of -0.19, -0.13 and -0.53, respectively. A possible mechanism might be associated with several factors which include dispersion stability of nanofiller in the epoxy matrix combined with chemical interaction between nanofiller and substrate (Alies and Khalil, 2022).

On the other hand, from these figures (Refer Figure 4.44 to 4.47), it was noted that the fracture elongation and cohesive fracture at 0.5, 1.0, and 2.0 wt% demonstrated a positive relation between fracture elongation and cohesive fracture with R-values of 0.31, 0.19 and 0.42, respectively. This observation might attributed to the increment in CF mode region in Alumina/GNP hybrid nano adhesive probably caused by sufficient interaction between nano adhesive and adherend substrate (Kong et al., 2021; Tiwari et al., 2020). A sufficient mechanical interlocking mechanism may have promoted robust adhesion. This is achieve by increasing interfacial contact area and providing mechanical anchorage sites for the adhesive to grip onto (van Dam et al., 2020) as previously discussed in section 4.6.3. However, at 1.5 wt% there was no discernible impact on the fracture elongation of the joining specimen and cohesive fracture, with an R-value of -0.05. This observation might be attributed to the addition of GNP had weakened the bulk nano adhesive properties, causing failure of the joining to occur at lower forces.

In summary, the shear properties (i.e., shear strength) shows positive relation with adhesive fracture for 1.0, 1.5 and 2.0 wt% except for lower nanoparticle content (0.5 wt%). Meanwhile, the shear properties (i.e., fracture elongation) demonstrate the negative relation to the adhesive fracture for 0.5, 1.0 and 2.0 wt% except for 1.5 wt% as shown in Figure 4.52 (a). The shear strength indicates the negative relation to the cohesive fracture for 1.0, 1.5, and 2.0 wt% except for lower nanoparticle content. Meanwhile, relation between fracture elongation and cohesive fracture for 0.5, 1.0, and 2.0 wt% demonstrate positive relation with cohesive fracture except for 1.5 wt% as shown in Figure 4.52 (b). For ease of comprehension, the overall summary findings of the shear properties (i.e., tensile strength and fracture elongation) and fracture behaviour (i.e., adhesive fracture and cohesive fracture) for joining the specimen are shown in Figure 4.53.

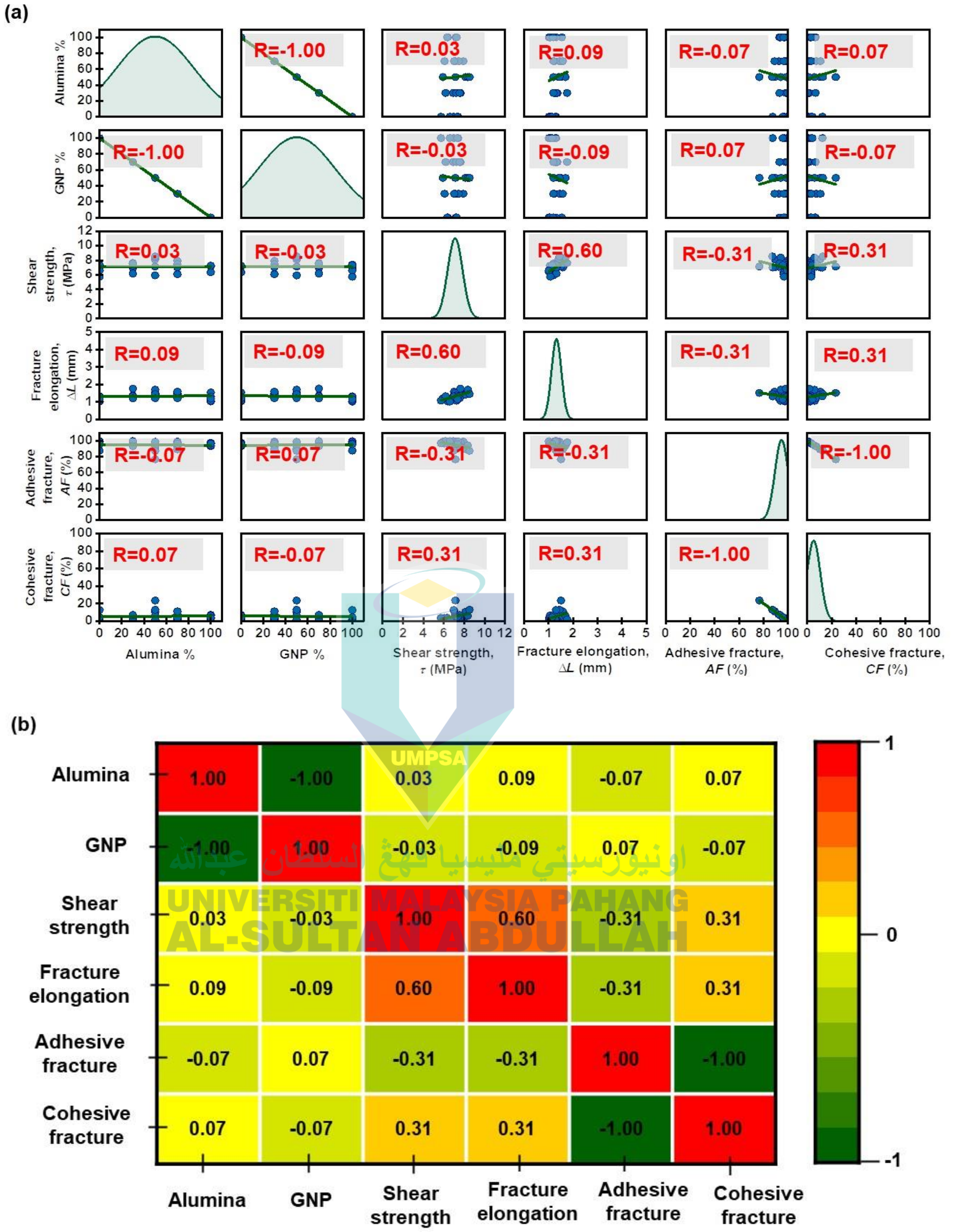

	Alumina	GNP	Shear strength	Fracture elongation	Adhesive fracture	Cohesive fracture
Alumina	1.00	-1.00	0.03	0.09	-0.07	0.07
GNP	-1.00	1.00	-0.03	-0.09	0.07	-0.07
Shear strength	0.03	-0.03	1.00	0.60	-0.31	0.31
Fracture elongation	0.09	-0.09	0.60	1.00	-0.31	0.31
Adhesive fracture	-0.07	0.07	-0.31	-0.31	1.00	-1.00
Cohesive fracture	0.07	-0.07	0.31	0.31	-1.00	1.00

Figure 4.44 (a) Correlation matrix and (b) correlation heatmap presenting the significance of Alumina/GNP hybrid nano reinforcement to shear properties in SLJ specimen at 0.5 wt% hybrid nanoparticle content

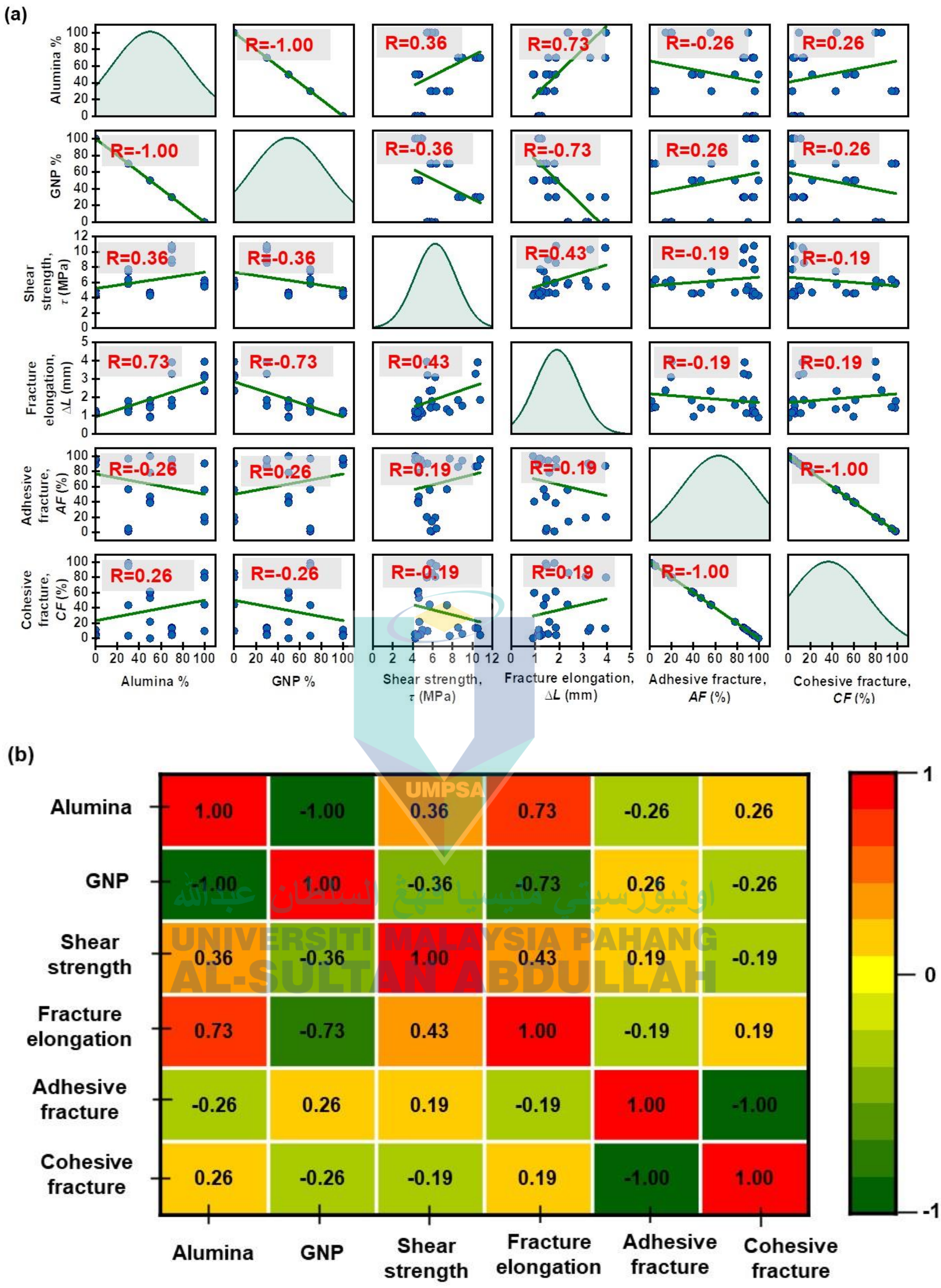

	Alumina	GNP	Shear strength	Fracture elongation	Adhesive fracture	Cohesive fracture
Alumina	1.00	-1.00	0.36	0.73	-0.26	0.26
GNP	-1.00	1.00	-0.36	-0.73	0.26	-0.26
Shear strength	0.36	-0.36	1.00	0.43	0.19	-0.19
Fracture elongation	0.73	-0.73	0.43	1.00	-0.19	0.19
Adhesive fracture	-0.26	0.26	0.19	-0.19	1.00	-1.00
Cohesive fracture	0.26	-0.26	-0.19	0.19	-1.00	1.00

Figure 4.45 (a) Correlation matrix and (b) correlation heatmap presenting the significance of Alumina/GNP hybrid nano reinforcement to shear properties in SLJ specimen at 1.0 wt% hybrid nanoparticle content

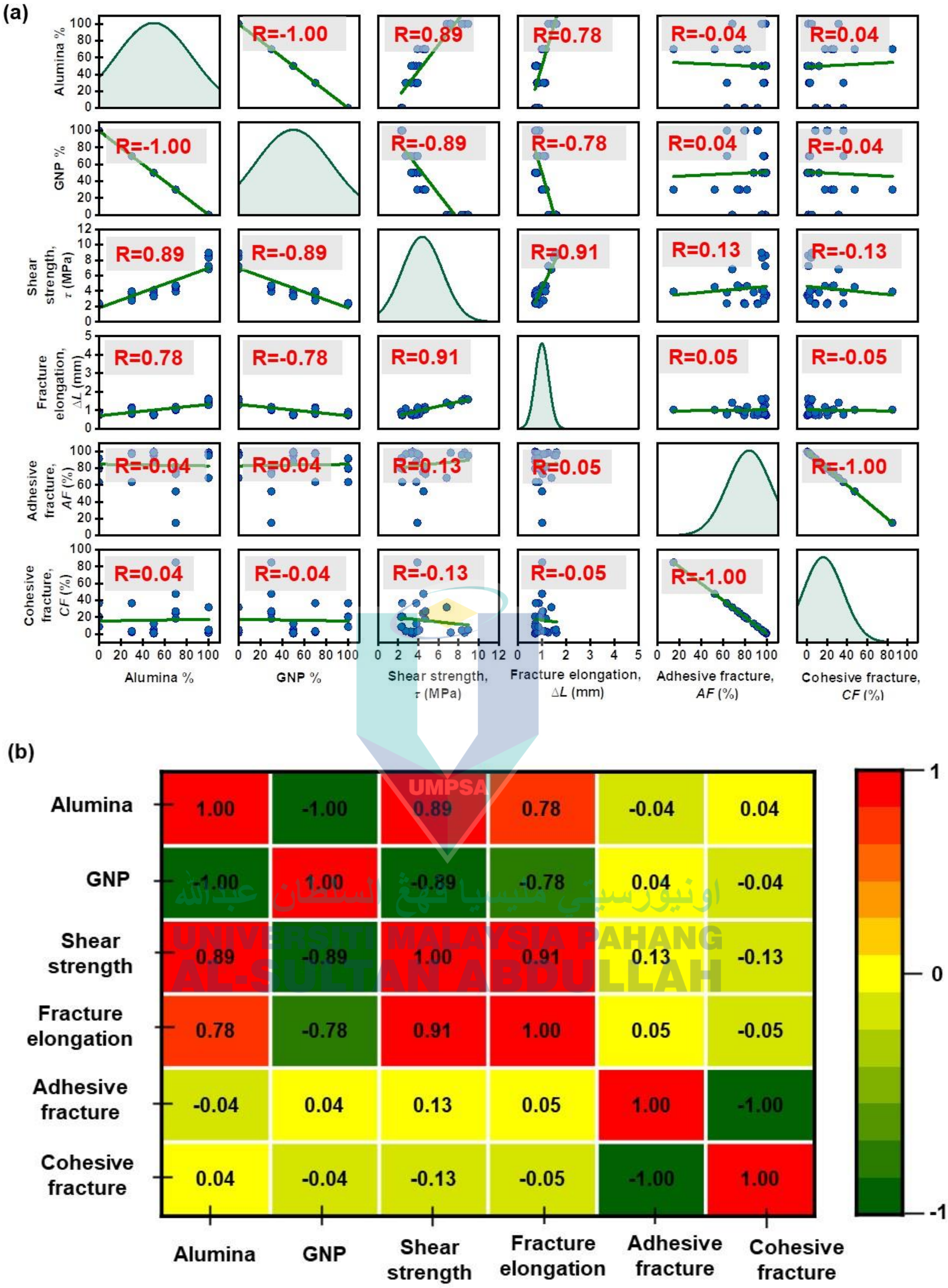

	Alumina	GNP	Shear strength	Fracture elongation	Adhesive fracture	Cohesive fracture
Alumina	1.00	-1.00	0.89	0.78	-0.04	0.04
GNP	-1.00	1.00	-0.89	-0.78	0.04	-0.04
Shear strength	0.89	-0.89	1.00	0.91	0.13	-0.13
Fracture elongation	0.78	-0.78	0.91	1.00	0.05	-0.05
Adhesive fracture	-0.04	0.04	0.13	0.05	1.00	-1.00
Cohesive fracture	0.04	-0.04	-0.13	-0.05	-1.00	1.00

Figure 4.46 (a) Correlation matrix and (b) correlation heatmap presenting the significance of Alumina/GNP hybrid nano reinforcement to shear properties in SLJ specimen at 1.5 wt% hybrid nanoparticle content

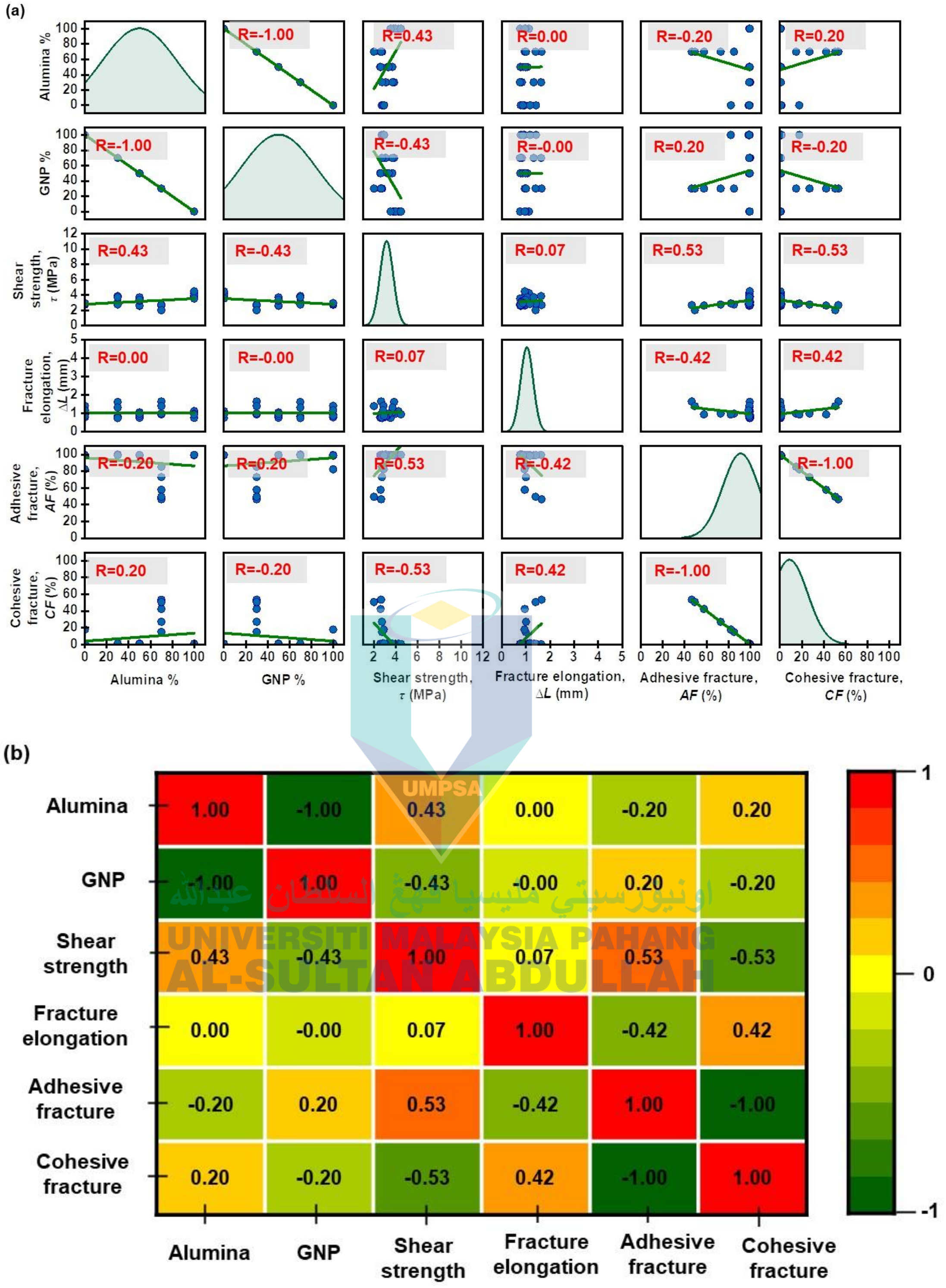

	Alumina	GNP	Shear strength	Fracture elongation	Adhesive fracture	Cohesive fracture
Alumina	1.00	-1.00	0.43	0.00	-0.20	0.20
GNP	-1.00	1.00	-0.43	-0.00	0.20	-0.20
Shear strength	0.43	-0.43	1.00	0.07	0.53	-0.53
Fracture elongation	0.00	-0.00	0.07	1.00	-0.42	0.42
Adhesive fracture	-0.20	0.20	0.53	-0.42	1.00	-1.00
Cohesive fracture	0.20	-0.20	-0.53	0.42	-1.00	1.00

Figure 4.47 (a) Correlation matrix and (b) correlation heatmap presenting the significance of Alumina/GNP hybrid nano reinforcement to shear properties in SLJ specimen at 2.0 wt% hybrid nanoparticle content

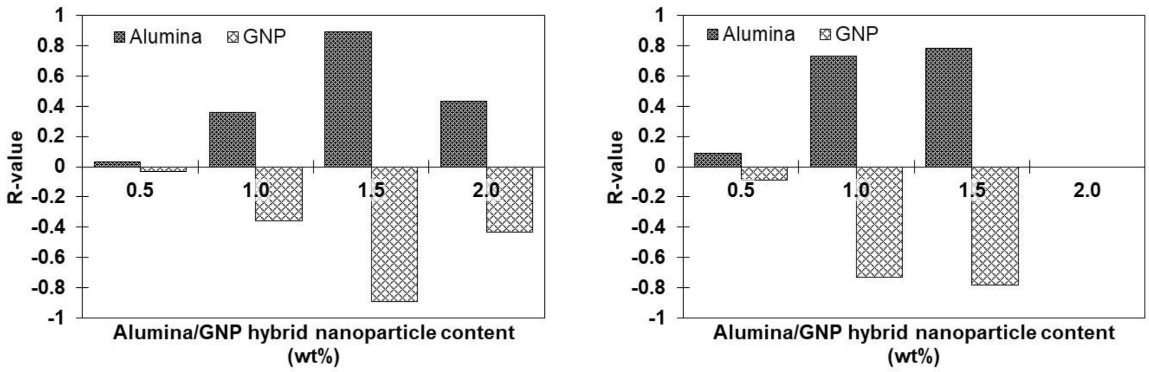

(a)

(b)

Figure 4.48 The dependence of R value to the Alumina/GNP hybrid nano particle content for (a) shear strength and (b) fracture elongation in SLJ specimens

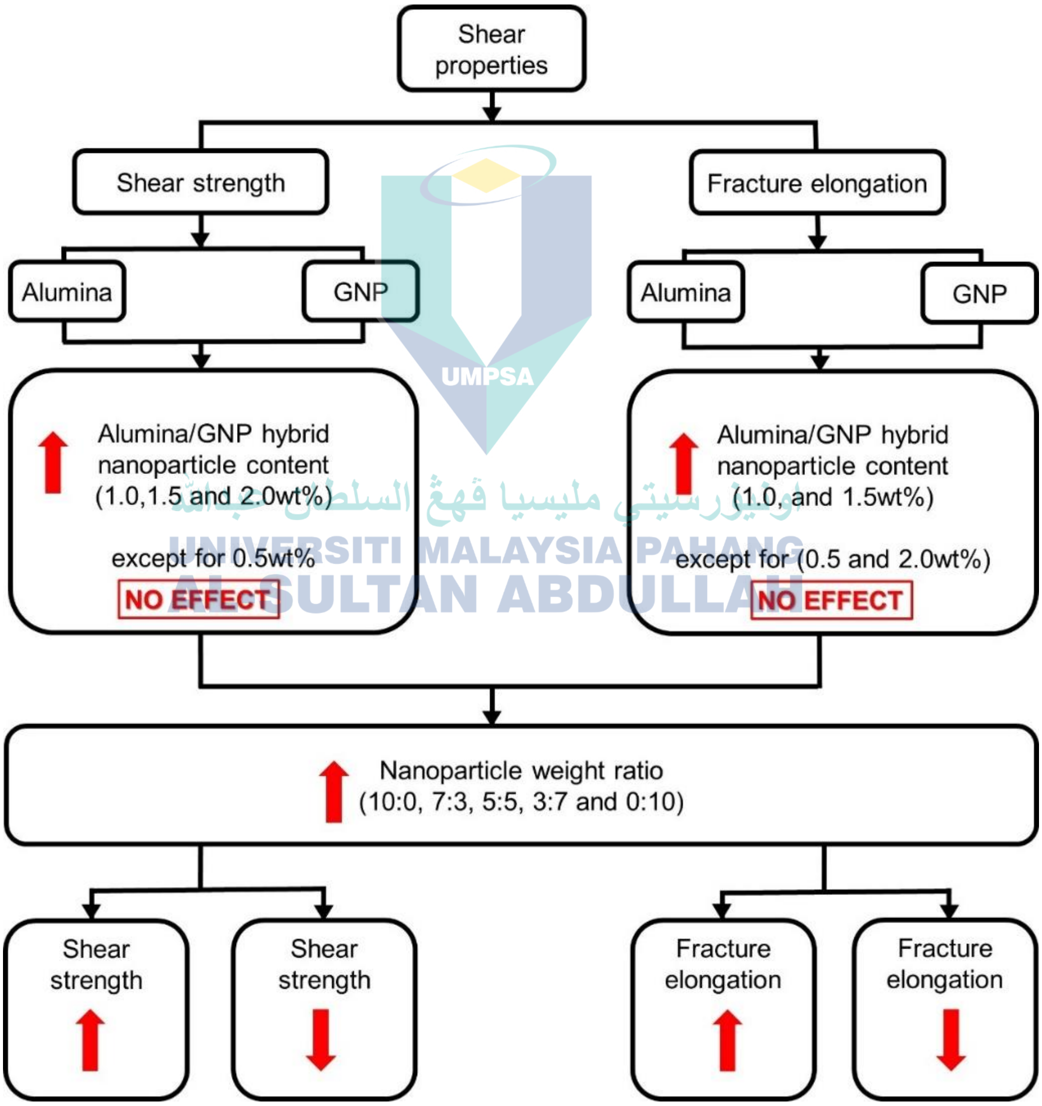

Figure 4.49 Graphical summary on the effect of hybrid nanoreinforcement to the shear properties in SLJ specimens

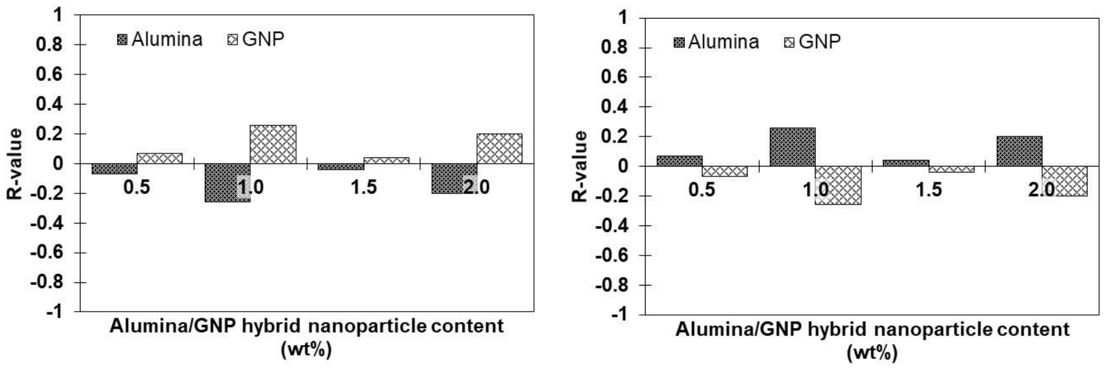

(a)

(b)

Figure 4.50 The dependence of R value to the Alumina/GNP hybrid nanoparticle content for (a) adhesive fracture and (b) cohesive fracture

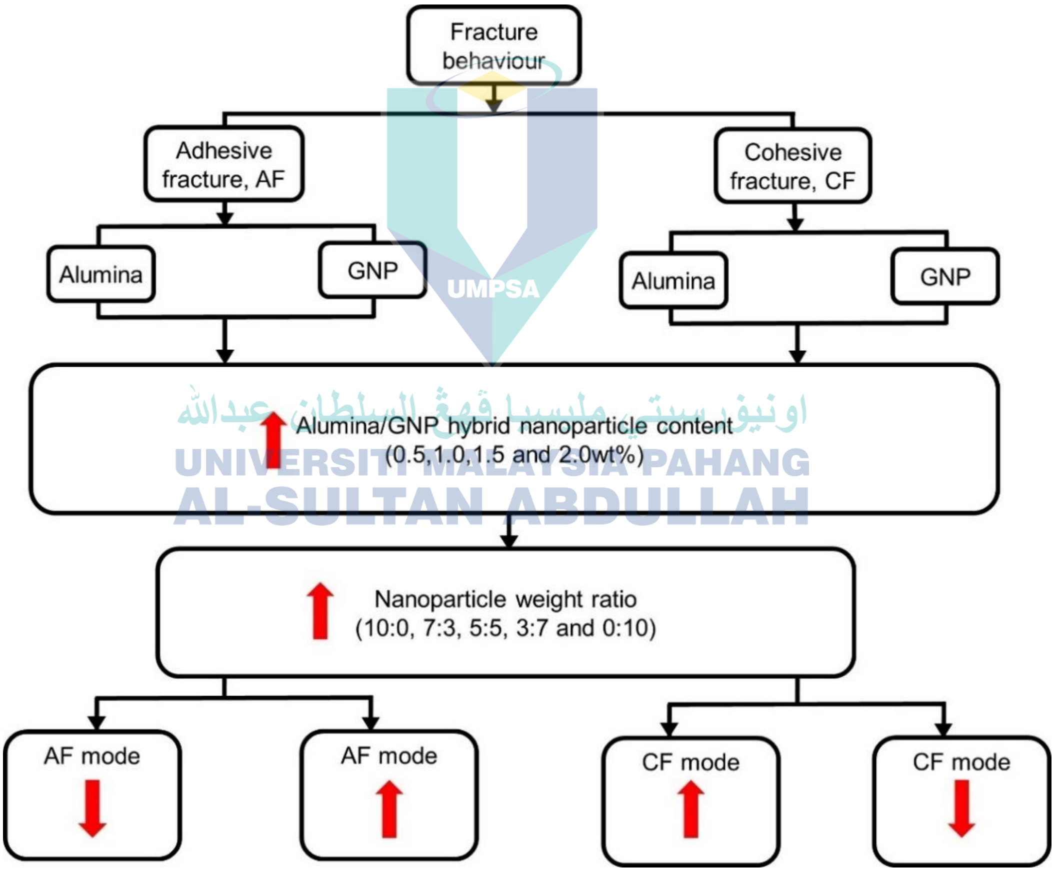

Figure 4.51 Graphical summary on the effect of hybrid nanoreinforcement to the fracture behaviour in SLJ specimens

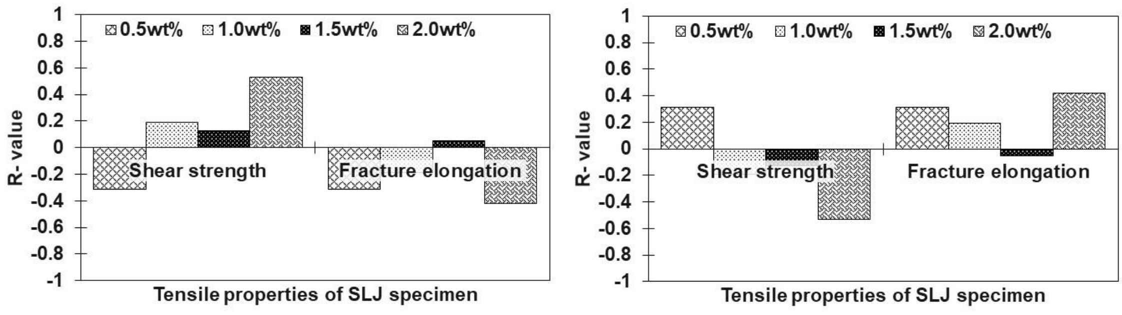

(a)

(b)

Figure 4.52 The dependence of R value to the tensile properties of SLJ specimen for (a) adhesive fracture and (b) cohesive fracture

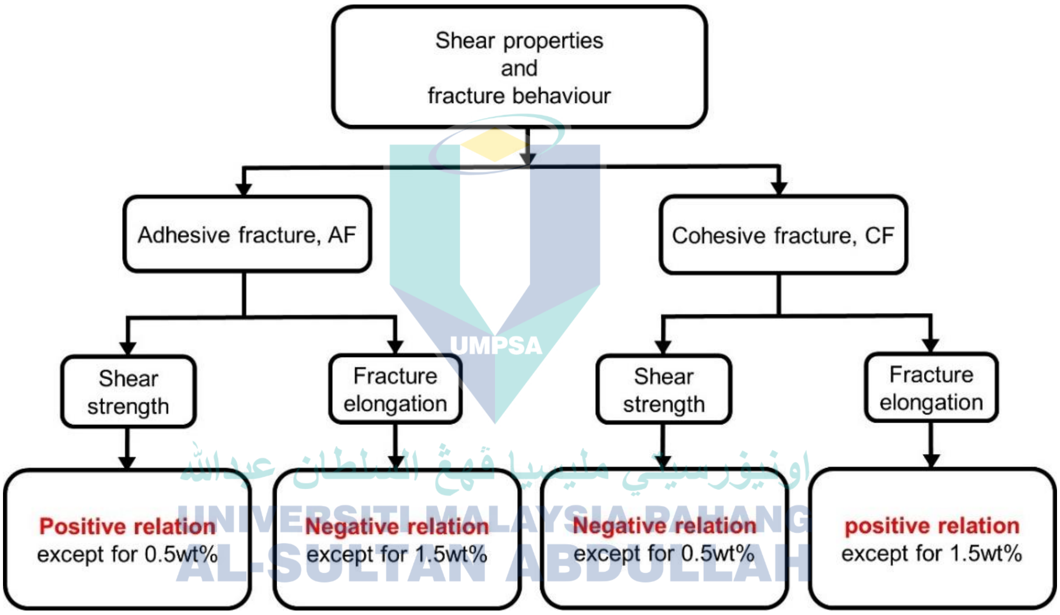

Figure 4.53 Graphical summary on the dependence of shear properties and fracture behaviour in single lap joining specimen

4.6.5 Pearson correlation and heatmap analysis for wetting behaviour and shear properties of SLJ specimen in Alumina/GNP hybrid nano adhesive

Figure 4.54 illustrates the relationship between the spread area and shear strength of joining specimens. According to the trend lines, subtle negative relations were observed between the spread area and shear strength, indicating a slight decrease in shear strength with an increasing spread area. As mentioned earlier, in most cases, shear strength is typically directly proportional to the spread area because appropriate wetting is crucial for allowing sufficient spreading of the adhesive onto the adherend. Furthermore, adequate wetting of the adhesive generally resulted in a more uniform bond line thickness (better spreading) and facilitated the interaction between the adhesive and adherend surfaces, thereby increasing the contact area between them. This improved wetting contributed to enhanced bonding strength, playing a crucial role in improving mechanical properties (Ahmadi, 2019). However, in the current study, variations in these relationships might be attributed to several factors such as the high viscosity of the epoxy adhesive (Park et al., 2009), surface topography (including nano-scale pores, texture direction and roughness value) (Guo et al., 2021), and the type of surface preparation method used, which in turn affected the adhesion between the adhesive and substrate (Droździel-Jurkiewicz and Bieniaś, 2022). To determine the independent effects on spread area and shear strength, a comprehensive examination of each composition of Alumina and GNP nanoparticles was necessary. For this purpose, a precise assessment was conducted through the use of a correlation matrix and heatmap analysis.

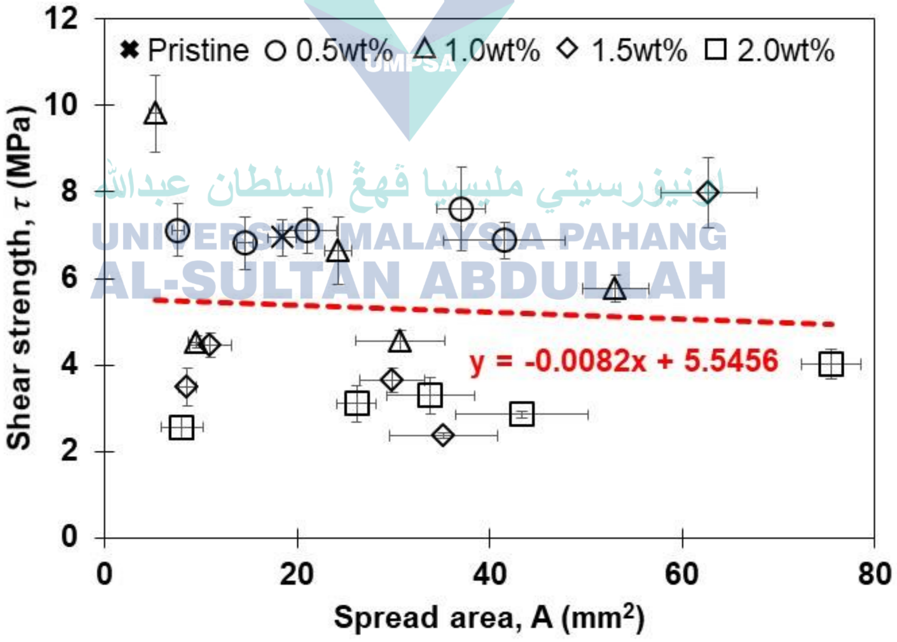

Figure 4.54 Relation between spread area and shear strength

Figures 4.55 to 4.58 depict the correlation matrix and correlation heatmap for the wetting behaviour and shear strength of joining specimens with Alumina/GNP hybrid nano adhesive. These figures specifically address the correlation between spread area and shear strength. Upon closer examination of these figures, it became evident that the Alumina/GNP hybrid nano adhesive at a lower hybrid nanoparticle content (0.5 wt%) demonstrated a weak relation with R-value of 0.16. However, at 1.0 wt% hybrid nanoparticle content, the spread area and shear strength exhibited a negative relation with R-value of -0.38. At the lower Alumina/GNP hybrid nanoparticle content, the limited number of nanoparticles might have limited the effectiveness of mechanical interlocking due to fewer interactions. Therefore, although the spread area was increasing, the share strength might not have been significantly affected.

On the other hand, at higher Alumina/GNP hybrid nanoparticle content (1.5 and 2.0 wt%), there was a positive relationship between shear strength and spread area with R-values of 0.62 and 0.71 respectively. The possible mechanism for this observation was the presence of nanoparticles significantly increased the wetting behaviour due to the nanoscale size of the nanofiller, providing better interfacial wettability between the adhesive and substrate, thus improving bonding efficiency (Dorigato et al., 2010). In addition, nanoparticles enlarged the area of interaction between the nanoparticle and the polymer matrix, enhancing the adhesion strength per interaction area (Zhai et al., 2008). The nano adhesive exhibited a higher wetting tendency, causing it to become more hydrophilic, which enhanced wettability and produced a stronger bond as previously discussed in Section 2.8.

In summary, at lower Alumina/GNP hybrid nanoparticle content (0.5 wt%), there was a weak relationship between shear strength and spread area. Conversely, at 1.0 wt% Alumina/GNP hybrid nanoparticle content, there was a negative relationship between shear strength and spread area. Meanwhile, at higher Alumina/GNP hybrid nanoparticle content (1.5 and 2.0 wt%), there was a positive relationship between shear strength and spread area (Refer Figure 4.59). For ease of comprehension, the overall summary findings of the shear properties (i.e., tensile strength and fracture elongation) for the joining specimen are shown in Figure 4.60.

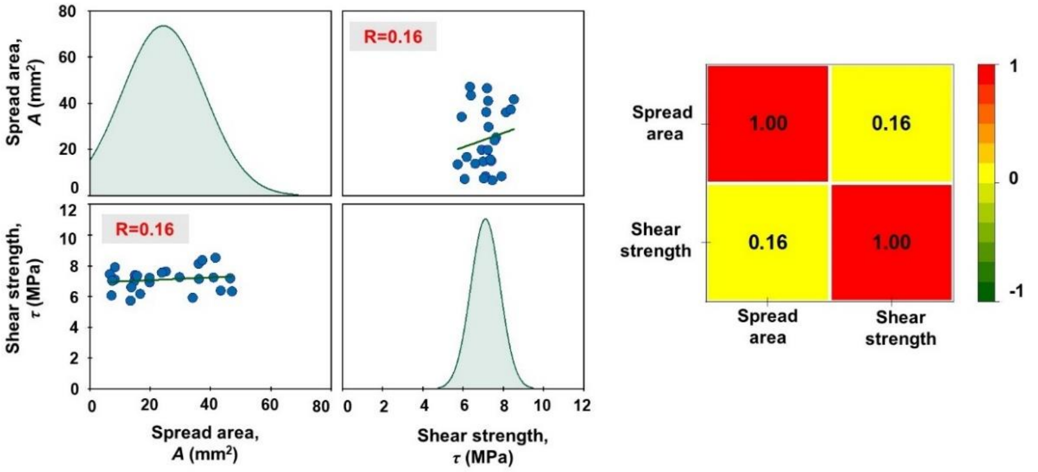

(a) (b)

Figure 4.55 (a) Correlation matrix and (b) correlation heatmap presenting the significance of Alumina/GNP hybrid nano reinforcement to wetting behaviour and shear properties in SLJ specimen at 0.5 wt% hybrid nanoparticle content

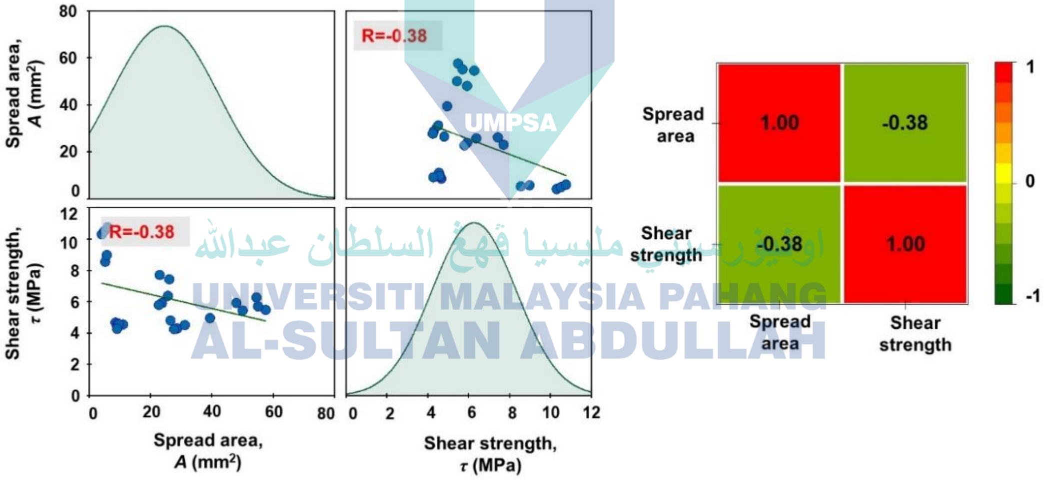

(a) (b)

Figure 4.56 (a) Correlation matrix and (b) correlation heatmap presenting the significance of Alumina/GNP hybrid nano reinforcement to wetting behaviour and shear properties in SLJ specimen at 1.0 wt% hybrid nanoparticle content

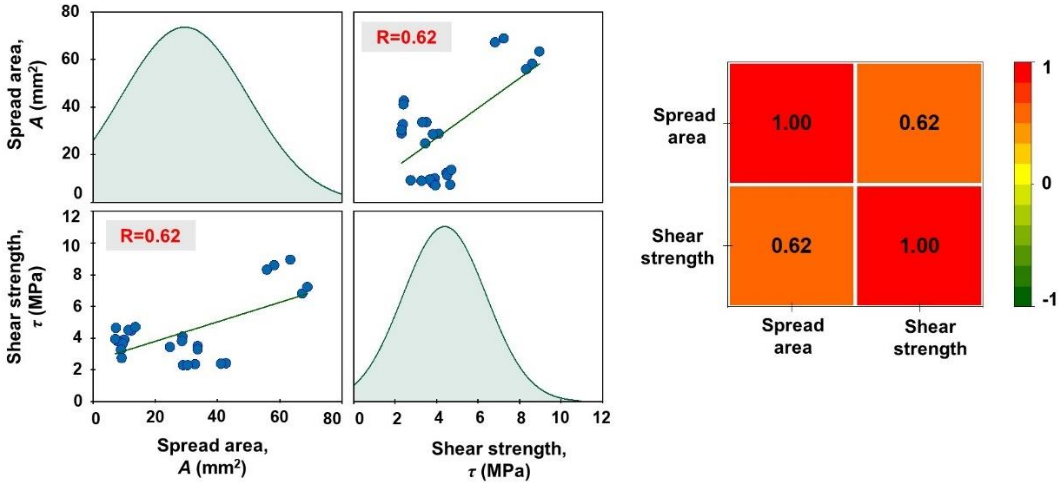

(a) (b)

Figure 4.57 (a) Correlation matrix and (b) correlation heatmap presenting the significance of Alumina/GNP hybrid nano reinforcement to wetting behaviour and shear properties in SLJ specimen at 1.5 wt% hybrid nanoparticle content

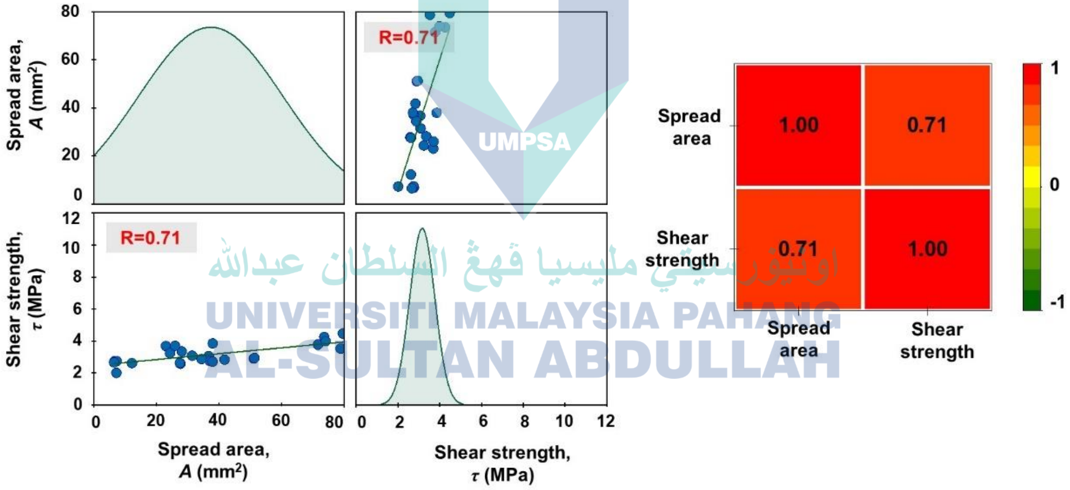

(a) (b)

Figure 4.58 (a) Correlation matrix and (b) correlation heatmap presenting the significance of Alumina/GNP hybrid nano reinforcement to wetting behaviour and shear properties in SLJ specimen at 2.0 wt% hybrid nanoparticle content

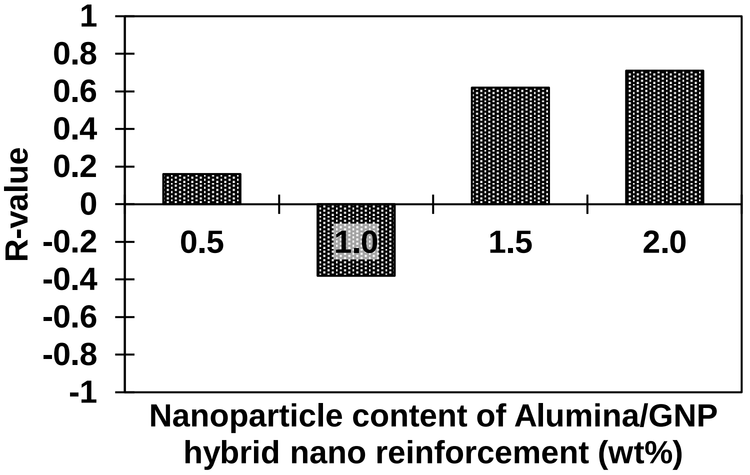

Figure 4.59 The dependence of R value to the Alumina/GNP hybrid nanoparticle content for spread area and shear strength

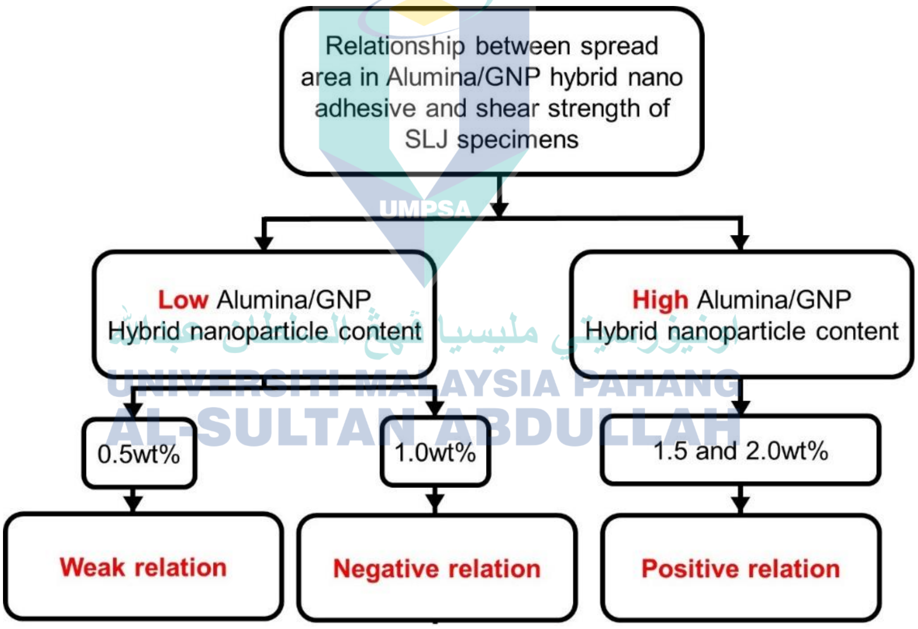

Figure 4.60 Graphical summary on the dependence of spread area in Alumina/GNP hybrid nanoadhesive with shear strength

CHAPTER 5

CONCLUSION AND RECOMMENDATION

5.1 Introduction

The effect of alumina nanoparticle and graphene nanoplatelets hybrid nano reinforcement on the wetting behaviour and mechanical properties of bulk and joining specimens was examined in this study. The following findings could be obtained from the use of Alumina/GNP hybrid nano adhesive at various hybrid nanoparticle contents (i.e., 0.5, 1.0, 1.5 and 2.0 wt%) with weight ratio combinations (i.e., 10:0, 7:3, 5:5, 3:7 and 0:10) in a two-component epoxy adhesive.

5.2 Conclusion

1. Regardless of Alumina/GNP hybrid nanoparticle content, the inclusion of alumina nanoparticle weight ratio at every weight ratio combination (10:0, 7:3, 5:5, 3:7 and 0:10 Alumina:GNP) indicated improved wetting behaviour (i.e., enhanced spreading), with the highest R-value observed at 0.5wt% (R=0.47). Conversely, the increase in GNP weight ratio indicated reduced wetting behaviour (i.e., reduced spreading), where the lowest R-value observed at 0.5wt% (R=-0.47).

2. In ASTM E8 specimen with Alumina/GNP hybrid nano reinforcement, the weight ratio of Alumina and GNP demonstrated distinct effects on tensile strength and fracture elongation. For tensile strength, regardless of Alumina/GNP hybrid nanoparticle content, an increase in Alumina nanoparticle weight ratio caused a decrease in tensile strength, with the lowest R-value observed at 1.5wt% (R=-0.52). Conversely, a higher GNP weight ratio improved tensile strength, with the highest R-value observed at 1.5wt% (R=0.52). (ii) As for fracture elongation, an increase in alumina nanoparticle weight ratio led to increased fracture elongation, with the highest R-value observed at 0.5wt% (R=0.65). Meanwhile, regardless of Alumina/GNP hybrid nanoparticle content, an

increase in GNP weight ratio led to decreased fracture elongation, with the lowest R-value observed at 0.5wt% (R=-0.65).

3. FE-SEM observations revealed various mechanisms, including nanoparticle agglomeration, particle pull-out, the presence of micro-sized particles and micro-particle breakage. These mechanisms contributed to a complex interplay of interactions affecting the tensile properties of ASTM E8 specimens. For instance, agglomeration of Alumina nanoparticles, GNP and Alumina/GNP hybrid nanoparticles, the existence void and pores affect the tensile strength. Meanwhile, particle debonding, crack deviation and corrugated pattern involve the increment in strength and ductility of the nanoadhesive. Additionally, increased the ductility is significant impacted by the present of microparticle, particle breakage.

4. In joining specimens, regardless of Alumina/GNP hybrid nanoparticle content, an increase in alumina nanoparticle weight ratio at every weight ratio combination (10:0, 7:3, 5:5, 3:7 and 0:10) resulted in higher shear strength and fracture elongation. The highest R-values were observed at 1.5 wt% (R=0.89 and R=0.78) for shear strength and fracture elongation respectively. Meanwhile, regardless of Alumina/GNP hybrid nanoparticle content, the inclusion of GNP weight ratio at every weight ratio combination led to a decrease in shear strength and fracture elongation, with the lowest R-values observed at 1.5 wt% (R=-0.89 and R=-0.78) respectively.

5. In the fracture behaviour of the joining specimen, optical microscope observations demonstrated instances of adhesive failure, cohesive failure or a combination of both modes. Firstly, an increase in Alumina nanoparticle weight ratio demonstrated a decrease in adhesive failure (AF), with the lowest R-value observed at 1.0wt% Alumina/GNP hybrid nanoparticle content (R=-0.26). Conversely, an increase in graphene weight ratio led to an increase in adhesive failure (AF), with the highest R-value observed at 1.0 wt% Alumina/GNP hybrid nanoparticle content (R=0.26). Secondly, an increase in Alumina nanoparticle weight ratio resulted in an increase in cohesive failure (CF), with the highest R-value observed at 1.0 wt% Alumina/GNP hybrid nanoparticle content (R=0.26). Conversely, an increase in graphene weight ratio

led to a decrease in cohesive failure (CF), with the lowest R-value observed at 1.0 wt% Alumina/GNP hybrid nanoparticle content (R=0.26).

6. At 0.5, 1.0, and 1.5 wt%, positive relation between shear strength and adhesive fracture was observed, with the highest R-value = 0.53. Meanwhile, at (0.5, 1.0, and 2.0 wt%), negative relation between fracture elongation and adhesive fracture was observed, with the lowest R-value = -0.42. Conversely, at 1.0, 1.5, and 2.0 wt%, negative relation between fracture elongation and cohesive fracture was observed, with the lowest R-value =-0.53. Meanwhile, at (0.5, 1.0, and 2.0 wt%), positive relation between fracture elongation and cohesive fracture was observed, with the highest R-value = 0.42.

7. At low Alumina/GNP hybrid nanoparticle content (0.5 and 1.0 wt%), a weak relation between shear strength and spread area was observed, with the lowest R-value observed at 1.0 wt% Alumina/GNP hybrid nanoparticle content (R=-0.38). Conversely, at higher Alumina/GNP hybrid nanoparticle content (1.5 and 2.0 wt%), a positive relation between shear strength and spread area was observed, reaching the highest R-value at 2.0 wt% Alumina/GNP hybrid nanoparticle content (R=0.71). Based on current research, a poor relationship between shear strength and wetting behaviour (Spread area) at low nanoparticle content may be caused by a restricted number of nanoparticles having a limited ability to mechanically interlock due to fewer contacts. Higher nanoparticle contents, on the other hand, increase the adhesion strength through an expanded region of contact between the nanoparticle and the polymer matrix.

8. The synergy between Alumina and GNP with excellent mechanical properties (shear strength and fracture elongation) at 1.0 wt% nanoparticle content and 7:3 weight ratio combination of Alumina/GNP hybrid nanoreinforcement was considered to be the best among the formulations tested.

5.3 Recommendation

There are some limitations encountered during the planning and investigation of the project. Therefore, several suggestions for improvement are proposed for future work.

1. For the preparation Alumina/GNP hybrid nano adhesive, it is recommended to use an ultrasonic homogenizer for the preparation of Alumina nanoparticles and GNP. This will provide a more stable nanoparticle distribution, minimising agglomerations of nanoparticles within the epoxy matrix

2. Using Automation or more controlled methods might enhance the precision instead of relies heavily to the manual operation like cutting and drilling that could introduce variability.

3. To improve the interfacial contact between GNP and the adhesive matrix, it is suggested to employ functionalized GNP instead of unfunctionalized GNP. This is expected to improve the reactivity of its functional groups towards the epoxy matrix.

4. To reduce voids or pores inside the ASTM E8 specimen that can be associated with factors such as air entrapment during the preparation of Alumina/GNP hybrid nano adhesive and gas generation during the curing process, it is essential to undergo a degassing process. This process involves using a vacuum pump or chamber to reduce the air bubbles in the epoxy adhesive before pouring the Alumina/GNP hybrid nano adhesive mixture into an industrial silicone mold.

5. For the study of wetting behaviour, it is recommended to use a sessile drop test setup instead of the current setup in order to achieve more accurate spread area and contact angle values.

6. To comprehensively understand the effects of Alumina/GNP hybrid nano reinforcement on wetting behaviour and mechanical properties, additional tests and result analyses can be conducted using techniques such as dynamic

mechanical analysis (DMA), dynamic viscosity, Fourier transform infrared spectroscopy (FTIR), X-ray powder dispersion (XRD) and energy dispersive X-ray (EDX).

7. To conduct a study on long-term stability and ageing studies for assessing adhesive stability and performance over time and evaluating the durability under real world environmental conditions like humidity and high/low temperature.

8. To conduct a benchmarking study Alumina/GNP adhesive against other nanoparticle reinforced adhesive and comparing the performance metrics like adhesion strength, toughness and thermal conductivity across different nano adhesive formulation and identify optimal combination of nanoparticle type and loadings for particular applications and adherend.

REFERENCES

Ahmad, I., Islam, M., Al Habis, N., & Parvez, S. (2020). Hot-pressed graphene nanoplatelets or/and zirconia reinforced hybrid alumina nanocomposites with improved toughness and mechanical characteristics. *Journal of Materials Science and Technology*, *40*, 135–145. https://doi.org/10.1016/j.jmst.2019.08.048

Ahmadi, M., Zabihi, O., Masoomi, M., & Naebe, M. (2016). Synergistic effect of MWCNTs functionalization on interfacial and mechanical properties of multi-scale UHMWPE fibre reinforced epoxy composites. *Composites Science and Technology*, *134,* 1–11. https://doi.org/10.1016/j.compscitech.2016.07.026

Ahmadi, Z. (2019). Nanostructured epoxy adhesives: A review. *Progress in Organic Coatings*, *135*, 449–453. https://doi.org/10.1016/j.porgcoat.2019.06.028

Alies, M. S. I., & Khalil, N. Z. (2022). Effect of alumina/graphene hybrid nano reinforcement to the adhesion and mechanical properties of adhesively bonded aluminum alloy with epoxy. *Materials Today: Proceedings*, *51*, 1437–1443. https://doi.org/10.1016/j.matpr.2021.12.087

Aradhana, R., Mohanty, S., & Nayak, S. K. (2018). High performance epoxy nanocomposite adhesive: Effect of nanofillers on adhesive strength, curing and degradation kinetics. *International Journal of Adhesion and Adhesives*, *84*, 238–249. https://doi.org/10.1016/j.ijadhadh.2018.03.013

Ashok Kumar, B., Saminathan, R., Tharwan, M., Vigneshwaran, M., Sekhar Babu, P., Ram, S., & Manoj Kumar, P. (2022). Study on the mechanical properties of a hybrid polymer composite using egg shell powder based bio-filler. *Materials Today: Proceedings*, *xxxx*, 10–14. https://doi.org/10.1016/j.matpr.2022.07.114

Aslan, A., Salur, E., Düzcükoğlu, H., Sinan Şahin, Ö., & Ekrem, M. (2021). The effects of harsh aging environments on the properties of neat and MWCNT reinforced epoxy resins. *Construction and Building Materials*, *272*. https://doi.org/10.1016/j.conbuildmat.2020.121929

Balos, S., Marques, A. C., Mocanu, A., Tomi, N. Z., Stammen, E., Lundevall, A., Abrahami, S. T., Günther, R., Kok, J. M. M. De, & Freitas, S. T. De. (2020). *Review on Adhesives and Surface Treatments for Structural Applications : Recent Developments on Sustainability and Implementation for Metal and Composite Substrates*. https://doi.org/10.3390/ma13245590

Barbosa, N. G. C., Campilho, R. D. S. G., Silva, F. J. G. D., & Moreira, R. D. F. (2018). Comparison of different adhesively-bonded joint configurations for mechanical structures. *Procedia Manufacturing*, *17*, 721–728. https://doi.org/10.1016/j.promfg.2018.10.122

Buchman, A., Dodiuk-Kenig, H., Dotan, A., Tenne, R., & Kenig, S. (2009). Toughening of Epoxy Adhesives by Nanoparticles. *Journal of Adhesion Science and Technology*, *23*(5), 753–768. https://doi.org/10.1163/156856108X379209

Çakır, M. V. (2023). The synergistic effect of hybrid nano-silica and GNP additives on the flexural strength and toughening mechanisms of adhesively bonded joints. *International Journal of Adhesion and Adhesives*, *122*(January 2023), 103333. https://doi.org/10.1016/j.ijadhadh.2023.103333

Campilho, R. D. S. G., Pinto, A. M. G., Banea, M. D., Silva, R. F., & Da Silva, L. F. M. (2011). Strength improvement of adhesively-bonded joints using a reverse-bent geometry. *Journal of Adhesion Science and Technology*, *25*(18), 2351–2368. https://doi.org/10.1163/016942411X580081

Carbas, R. J. C., Dantas, M. A., Marques, E. A. S., & da Silva, L. F. M. (2021). Effect of the adhesive thickness on butt adhesive joints under torsional loads. *Journal of Advanced Joining Processes*, *3*(December 2020), 100061. https://doi.org/10.1016/j.jajp.2021.100061

Carolan, D., He, S., & Taylor, A. C. (2023). 8 - Advances in toughening strategies for structural adhesives. In *Advances in Structural Adhesive Bonding* (2nd ed.). Elsevier Ltd. https://doi.org/10.1016/B978-0-323-91214-3.00024-7

Chang, B., Shi, Y., & Dong, S. (2000). Studies on a computational model and the stress field characteristics of weld-bonded joints for a car body steel sheet. *Journal of Materials Processing Technology*, *100*(1), 171–178. https://doi.org/10.1016/S0924-0136(99)00472-0

Chavooshian, M., Kamali, R., Tutunchi, A., & Kianvash, A. (2017). Effect of silicon carbide nanoparticles on the adhesion strength of steel–epoxy composite joints bonded with acrylic adhesives. *Journal of Adhesion Science and Technology*, *31*(4), 345–357. https://doi.org/10.1080/01694243.2016.1215015

Da Silva, Lucas Filipe Martins, & Öchsner, A. (2008). Modeling of adhesively bonded joints. In *Modeling of Adhesively Bonded Joints*. https://doi.org/10.1007/978-3-540-79056-3

Dahmen, V., Redmann, A. J., Austermann, J., Quintanilla, A. L., Mecham, S. J., & Osswald, T. A. (2020). Fabrication of hybrid composite T-joints by co-curing with 3D printed dual cure epoxy. *Composites Part B: Engineering*, *183*, 107728. https://doi.org/https://doi.org/10.1016/j.compositesb.2019.107728

Deng, S., Zhang, J., Ye, L., & Wu, J. (2008). Toughening epoxies with halloysite nanotubes. *Polymer*, *49*(23), 5119–5127. https://doi.org/10.1016/j.polymer.2008.09.027

Díez-Pascual, A. M., Naffakh, M., Marco, C., & Ellis, G. (2012). Mechanical and electrical properties of carbon nanotube/poly(phenylene sulphide) composites incorporating polyetherimide and inorganic fullerene-like nanoparticles. *Composites Part A: Applied Science and Manufacturing*, *43*(4), 603–612. https://doi.org/10.1016/j.compositesa.2011.12.026

Dilger, K. (2010). Selecting the right joint design and fabrication techniques. *Advances in Structural Adhesive Bonding*, 295–315. https://doi.org/10.1533/9781845698058.3.295

Dilger, Klaus. (2021). Automobiles. In *Adhesive Bonding: Science, Technology and Applications*. https://doi.org/10.1016/B978-0-12-819954-1.00018-6

Djebbar, N., Boutabout, B., Hadj, B. R., & Oudad, W. (2022). Effect of spew adhesive and beveling substrate geometrical shape on stresses in a bonded single lap joint. *Engineering Structures*, *256*(January), 114049. https://doi.org/10.1016/j.engstruct.2022.114049

Dodiuk, H., Belinski, I., Dotan, A., & Kenig, S. (2006). Polyurethane adhesives containing functionalized nanoclays. *Journal of Adhesion Science and Technology*, *20*(12), 1345–1355. https://doi.org/10.1163/156856106778456573

Dong, L., Li, Y., Huang, M., Hu, X., Qu, Z., & Lu, Y. (2022). Effect of anodizing surface morphology on the adhesion performance of 6061 aluminum alloy. *International Journal of Adhesion and Adhesives*, *113*(November 2021), 103065. https://doi.org/10.1016/j.ijadhadh.2021.103065

Dorigato, A., Pegoretti, A., Bondioli, F., & Messori, M. (2010). Improving epoxy adhesives with zirconia nanoparticles. *Composite Interfaces*, *17*(9), 873–892. https://doi.org/10.1163/092764410X539253

Dorigato, A, Pegoretti, A., Bondioli, F., & Messori, M. (2010). Improving Epoxy Adhesives with Zirconia Nanoparticles. *Composite Interfaces*, *17*(9), 873–892. https://doi.org/10.1163/092764410X539253

Dorigato, Andrea, & Pegoretti, A. (2011). The role of alumina nanoparticles in epoxy adhesives. *Journal of Nanoparticle Research*, *13*(6), 2429–2441. https://doi.org/10.1007/s11051-010-0130-0

Doshi, B., Sillanpää, M., & Kalliola, S. (2018). A review of bio-based materials for oil spill treatment. *Water Research*, *135*(February), 262–277. https://doi.org/10.1016/j.watres.2018.02.034

Duncan, B. (2010). Developments in testing adhesive joints. *Advances in Structural Adhesive Bonding*, 389–436. https://doi.org/10.1533/9781845698058.3.389

Eayal Awwad, K. Y., Yousif, B. F., Fallahnezhad, K., Saleh, K., & Zeng, X. (2021). Influence of graphene nanoplatelets on mechanical properties and adhesive wear performance of epoxy-based composites. *Friction*, *9*(4), 856–875. https://doi.org/10.1007/s40544-020-0453-5

Ebnesajjad, S. (2014). Material Surface Preparation Techniques. In *Surface Treatment of Materials for Adhesive Bonding*. https://doi.org/10.1016/b978-0-323-26435-8.00006-x

Ekrem, M., Şahin, Ö. S., Karabulut, S. E., & Avcı, A. (2018). Thermal stability and adhesive strength of boron nitride nano platelets and carbon nano tube modified adhesives. *Journal of Composite Materials*, *52*(11), 1557–1565. https://doi.org/10.1177/0021998317726147

Faria, D., Abreu, C. S., Buciumeanu, M., Dourado, N., Carvalho, O., Silva, F. S., & Miranda, G. (2018). Ti6Al4V laser surface preparation and functionalization using hydroxyapatite for biomedical applications. *Journal of Biomedical Materials Research - Part B Applied Biomaterials*, *106*(4), 1534–1545. https://doi.org/10.1002/jbm.b.33964

Fu, J., Zhang, M., Jin, L., Liu, L., Li, N., Shang, L., Li, M., Xiao, L., & Ao, Y. (2019). Enhancing interfacial properties of carbon fibers reinforced epoxy composites via Layer-by-Layer self assembly GO/SiO 2 multilayers films on carbon fibers surface. *Applied Surface Science*, *470*(August 2018), 543–554. https://doi.org/10.1016/j.apsusc.2018.11.168

Ghosh, P. K., Kumar, K., Preeti, P., Rajoria, M., & Misra, N. (2016). Superior dissimilar adhesive joint of mild steel and aluminium using UDM processed epoxy based TiO2 nano-filler composite adhesive. *Composites Part B: Engineering*, *99*, 224–234. https://doi.org/10.1016/j.compositesb.2016.06.014

Gorbatkina, Y. A., Ivanova-Mumzhieva, V. G., & Ul'Yanova, T. M. (2007). Adhesiveness of an epoxy oligomer filled with aluminum oxide powders. *Polymer Science - Series C*, *49*(2), 131–134. https://doi.org/10.1134/S1811238207020063

Gude, M. R., Prolongo, S. G., & Uren, A. (2013). *International Journal of Adhesion & Adhesives Hygrothermal ageing of adhesive joints with nanoreinforced adhesives and different surface treatments of carbon fibre / epoxy substrates*. *40*, 179–187. https://doi.org/10.1016/j.ijadhadh.2012.09.005

Gültekin, K., Akpinar, S., Gürses, A., Eroglu, Z., Cam, S., Akbulut, H., Keskin, Z., & Ozel, A. (2016). The effects of graphene nanostructure reinforcement on the adhesive method and the graphene reinforcement ratio on the failure load in adhesively bonded joints. *Composites Part B: Engineering*, *98*, 362–369. https://doi.org/https://doi.org/10.1016/j.compositesb.2016.05.039

Guo, Q., Zhu, P., Li, G., Wen, J., Wang, T., Lu, D. (Daniel), Sun, R., & Wong, C. (2017). Study on the effects of interfacial interaction on the rheological and thermal performance of silica nanoparticles reinforced epoxy nanocomposites. *Composites Part B: Engineering*, *116*, 388–397. https://doi.org/10.1016/j.compositesb.2016.10.081

Gupta, S. K., Shukla, D. K., & Bharti, A. (2017). Effect of alumina nanoparticles on shear strength of epoxy adhesive: Experimental and finite element analysis. *2017 International Conference on Advances in Mechanical, Industrial, Automation and Management Systems (AMIAMS)*, 307–313. https://doi.org/10.1109/AMIAMS.2017.8069230

Hart-Smith, J. (2021). Aerospace industry applications of adhesive bonding. In *Adhesive Bonding: Science, Technology and Applications* (2nd ed.). Elsevier Ltd. https://doi.org/10.1016/B978-0-12-819954-1.00001-0

He, X. R., Zhang, R., Chen, Q., Rong, Y. Q., & Yang, Z. Q. (2014). Different surface functionalized nano-Fe3O4 particles for EVA composite adhesives. *International Journal of Adhesion and Adhesives*, *50*(April), 128–135. https://doi.org/10.1016/j.ijadhadh.2014.01.023

Hedia, H. S., Allie, L., Ganguli, S., & Aglan, H. (2006). The influence of nanoadhesives on the tensile properties and Mode-I fracture toughness of bonded joints. *Engineering Fracture Mechanics*, *73*(13), 1826–1832. https://doi.org/10.1016/j.engfracmech.2006.02.013

Hentinen, M. (2021). Boats and marine. In *Adhesive Bonding: Science, Technology and Applications* (2nd ed.). Elsevier Ltd. https://doi.org/10.1016/B978-0-12-819954-1.00005-8

Heshmati, M., Haghani, R., & Al-Emrani, M. (2016). Effects of moisture on the long-term performance of adhesively bonded FRP/steel joints used in bridges. *Composites Part B: Engineering*, *92*, 447–462. https://doi.org/10.1016/j.compositesb.2016.02.021

Hu, Y., Yuan, B., Cheng, F., & Hu, X. (2019). NaOH etching and resin pre-coating treatments for stronger adhesive bonding between CFRP and aluminium alloy. *Composites Part B: Engineering*, *178*(May), 107478. https://doi.org/10.1016/j.compositesb.2019.107478

Jojibabu, P., Zhang, Y. X., & Prusty, B. G. (2020). A review of research advances in epoxy-based nanocomposites as adhesive materials. *International Journal of Adhesion and Adhesives*, *96*(October 2019), 102454. https://doi.org/10.1016/j.ijadhadh.2019.102454

Jojibabu, P., Zhang, Y. X., Rider, A. N., & Wang, J. (2020). Mechanical performance of adhesive joints using high-performance nanocomposite adhesive material with carbon nanotube and triblock copolymer hybrids. *Composites Part B: Engineering*, *186*(January), 107813. https://doi.org/10.1016/j.compositesb.2020.107813

Jothi Prakash, C. G., & Prasanth, R. (2021). Approaches to design a surface with tunable wettability: a review on surface properties. *Journal of Materials Science*, *56*(1), 108–135. https://doi.org/10.1007/s10853-020-05116-1

Jucienė, M., & Dobilaitė, V. (2021). Impact of climatic effects and various surfaces on the tack of adhesive tapes for building & construction. *Journal of Building Engineering*, *42*(March). https://doi.org/10.1016/j.jobe.2021.102825

Kaboorani, A., & Riedl, B. (2012). Nano-aluminum oxide as a reinforcing material for thermoplastic adhesives. *Journal of Industrial and Engineering Chemistry*, *18*(3), 1076–1081. https://doi.org/10.1016/j.jiec.2011.12.001

Kesavulu, A., & Mohanty, A. (2020). Tribological characterization of graphene nanoplatelets/alumina particles filled epoxy hybrid nanocomposites. *Journal of Applied Polymer Science*, *137*(46), 1–12. https://doi.org/10.1002/app.49518

Khalil, N. Z., Johanne, M. F., & Ishak, M. (2019). Influence of Al2O3 nanoreinforcement on the adhesion and thermomechanical properties for epoxy adhesive. *Composites Part B: Engineering*, *172*(September 2018), 9–15. https://doi.org/10.1016/j.compositesb.2019.05.007

Khalil, N. Z., Kong, N., & Fricke, H. (2024). The influence of GNP on the mechanical and thermomechanical properties of epoxy adhesive: Pearson correlation matrix and heatmap application in data interpretation. *Polymer Composites*, *March*, 1–22. https://doi.org/10.1002/pc.28390

Khan, A. A., Al Kheraif, A. A., Syed, J., Divakar, D. D., & Matinlinna, J. P. (2018). Enhanced resin zirconia adhesion with carbon nanotubes-infused silanes: A pilot study. *Journal of Adhesion*, *94*(3), 167–180. https://doi.org/10.1080/00218464.2016.1242422

Khan, U., May, P., Porwal, H., Nawaz, K., & Coleman, J. N. (2013). Improved adhesive strength and toughness of polyvinyl acetate glue on addition of small quantities of graphene. *ACS Applied Materials and Interfaces*, *5*(4), 1423–1428. https://doi.org/10.1021/am302864f

Khoramishad, H., & Alizadeh, O. (2017). Effects of silicon carbide nanoparticles and multi-walled carbon nanotubes on water uptake and resultant mechanical properties degradation of polymer nanocomposites immersed in hot water. *Polymer Composites*, *39*. https://doi.org/10.1002/pc.24303

Kim, D. Y., Park, J. W., Lee, D. Y., & Seo, K. H. (2020). Correlation between the crosslink characteristics and mechanical properties of natural rubber compound via accelerators and reinforcement. *Polymers*, *12*(9), 1–14. https://doi.org/10.3390/polym12092020

Kong, N., & Khalil, N. Z. (2022). Water absorption mechanism and mechanical performance of adhesively joint aluminum alloy with GNP reinforced epoxy. *Materials Today: Proceedings*, *51*(2022), 1392–1398. https://doi.org/10.1016/j.matpr.2021.11.528

Kong, N., Khalil, N. Z., & Fricke, H. (2021). Moisture absorption behavior and adhesion properties of gnp/epoxy nanocomposite adhesives. *Polymers*, *13*(11), 1–17. https://doi.org/10.3390/polym13111850

Konstantakopoulou, M., & Kotsikos, G. (2016). Effect of MWCNT filled epoxy adhesives on the quality of adhesively bonded joints. *Plastics, Rubber and Composites*, *45*(4), 166–172. https://doi.org/10.1080/14658011.2016.1165788

Korayem, A. H., Tourani, N., Zakertabrizi, M., Sabziparvar, A. M., & Duan, W. H. (2017). A review of dispersion of nanoparticles in cementitious matrices : Nanoparticle geometry perspective. *Construction and Building Materials*, *153*, 346–357. https://doi.org/10.1016/j.conbuildmat.2017.06.164

Kumar, R., Mohanty, S., & Nayak, S. K. (2019). Study on epoxy resin based thermal adhesive composite incorporated with expanded graphite/silver flake hybrids. In *Materials Today Communications* (Vol. 20). Elsevier Ltd. https://doi.org/10.1016/j.mtcomm.2019.100561

Lang, T. P., & Mallick, P. K. (1998). Effect of spew geometry on stresses in single lap adhesive joints. *International Journal of Adhesion and Adhesives*, *18*(3), 167–177. https://doi.org/10.1016/S0143-7496(97)00056-0

Lempke, M. P. (2013). *A study of single lap joint*.

Li, J., Wong, P. S., & Kim, J. K. (2008). Hybrid nanocomposites containing carbon nanotubes and graphite nanoplatelets. *Materials Science and Engineering A*, *483–484*(1-2 C), 660–663. https://doi.org/10.1016/j.msea.2006.08.145

Li, M., Chen, P., Kong, B., Peng, T., Yao, Z., & Qiu, X. (2016). Influences of thickness ratios of flange and skin of composite T-joints on the reinforcement effect of Z-pin. *Composites Part B: Engineering*, *97*, 216–225. https://doi.org/10.1016/j.compositesb.2016.05.007

Liao, L., Huang, C., & Sawa, T. (2013). Effect of adhesive thickness, adhesive type and scarf angle on the mechanical properties of scarf adhesive joints. *International Journal of Solids and Structures*, *50*(25–26), 4333–4340. https://doi.org/10.1016/j.ijsolstr.2013.09.005

Liu, D., Chen, H., Chang, P. R., Wu, Q., Li, K., & Guan, L. (2010). Biomimetic soy protein nanocomposites with calcium carbonate crystalline arrays for use as wood adhesive. *Bioresource Technology*, *101*(15), 6235–6241. https://doi.org/10.1016/j.biortech.2010.02.107

Mansourian-Tabaei, M., Jafari, S. H., & Khonakdar, H. A. (2014). Lap shear strength and thermal stability of diglycidyl ether of bisphenol a/epoxy novolac adhesives with nanoreinforcing fillers. *Journal of Applied Polymer Science*, *131*(6). https://doi.org/https://doi.org/10.1002/app.40017

Martin-Martinez, J. (2002). *Rubber base adhesives* (pp. 573–675). https://doi.org/10.1016/B978-044451140-9/50013-5

May, M., Wang, H. M., & Akid, R. (2010). *International Journal of Adhesion & Adhesives Effects of the addition of inorganic nanoparticles on the adhesive strength of a hybrid sol – gel epoxy system*. *30*, 505–512. https://doi.org/10.1016/j.ijadhadh.2010.05.002

McGlasson, A., Rishi, K., Beaucage, G., Narayanan, V., Chauby, M., Mulderig, A., Kuppa, V. K., Ilavsky, J., & Rackaitis, M. (2019). The effects of staged mixing on the dispersion of reinforcing fillers in elastomer compounds. *Polymer*, *181*(May). https://doi.org/10.1016/j.polymer.2019.121765

Min, C., Liu, D., Shen, C., Zhang, Q., Song, H., Li, S., Shen, X., Zhu, M., & Zhang, K. (2018). Unique synergistic effects of graphene oxide and carbon nanotube hybrids on the tribological properties of polyimide nanocomposites. *Tribology International*, *117*, 217–224. https://doi.org/10.1016/j.triboint.2017.09.006

Miturska-Barańska, I., Rudawska, A., & Doluk, E. (2021). The influence of sandblasting process parameters of aerospace aluminium alloy sheets on adhesive joints strength. *Materials*, *14*(21). https://doi.org/10.3390/ma14216626

Moghimi Monfared, R., Ayatollahi, M. R., & Barbaz Isfahani, R. (2018). Synergistic effects of hybrid MWCNT/nanosilica on the tensile and tribological properties of woven carbon fabric epoxy composites. *Theoretical and Applied Fracture Mechanics*, *96*(April), 272–284. https://doi.org/10.1016/j.tafmec.2018.05.007

Moosa, A. A., Kubba, F., Raad, M., & Ramazani, A. (2016). Mechanical and Thermal Properties of Graphene Nanoplates and Functionalized Carbon-Nanotubes Hybrid Epoxy Nanocomposites. *American Journal of Materials Science*, *6*(5), 125–134. https://doi.org/10.5923/j.materials.20160605.02

Nassiet, V., Hassoune-Rhabbour, B., Tramis, O., & Petit, J. A. (2021). Electrical and electronics. In *Adhesive Bonding: Science, Technology and Applications*. https://doi.org/10.1016/B978-0-12-819954-1.00025-3

Osman, A., Elhakeem, A., Kaytbay, S., & Ahmed, A. (2021). Thermal, electrical and mechanical properties of graphene/nano-alumina/epoxy composites. *Materials Chemistry and Physics*, *257*(September 2020), 123809. https://doi.org/10.1016/j.matchemphys.2020.123809

Otorgust, G., Dodiuk, H., Kenig, S., & Tenne, R. (2017). Important insights into polyurethane nanocomposite-adhesives; a comparative study between INT-WS2 and CNT. *European Polymer Journal*, *89*, 281–300. https://doi.org/10.1016/j.eurpolymj.2017.02.027

Ouyang, X., & Chen, C. (2023). Research on the joining of aluminum alloy and high-strength steel by dieless clinched-adhesive processes. *Journal of Materials Research and Technology, 24,* 5526–5540. https://doi.org/10.1016/j.jmrt.2023.04.132

Park, S., Kim, B. C., & Lee, D. (2009). Tensile StrenPark, S., Kim, B. C., & Lee, D. (2009). Tensile Strength of Joints Bonded With a Nano-particle-Reinforced Adhesive. Journal of Adhesion Science and Technology, 23, 95–113. https://doi.org/10.1163/156856108X344063gth of Joints Bonded With a Na. *Journal of Adhesion Science and Technology*, *23*, 95–113. https://doi.org/10.1163/156856108X344063

Pinto, A. M., Martins, J., Moreira, J. A., Mendes, A. M., & Magalhães, F. D. (2013). Dispersion of graphene nanoplatelets in poly(vinyl acetate) latex and effect on adhesive bond strength. *Polymer International*, *62*(6), 928–935. https://doi.org/10.1002/pi.4379

Pocius, A. V. (2021). Introduction. *Adhesion and Adhesives Technology*, 1–16. https://doi.org/10.3139/9781569908501.001

Poulis, J. A., Mosleh, Y., Cansell, E., Cimino, D., Ploeger, R., René de la Rie, E., McGlinchey, C. W., & Seymour, K. (2022). Mechanical and physical characterization of natural and synthetic consolidants. *International Journal of Adhesion and Adhesives*, *117*(October), 103015. https://doi.org/10.1016/j.ijadhadh.2021.103015

Prolongo, S. G., Gude, M. R., & Ureña, A. (2010). Nanoreinforced adhesives. *Nanotechnology and Nanomaterials “Nanofibers*, 39–68.

Queval, J., Geslain, E., & Broussaud-laloue, P. (2024). *Joining thin galvanized low carbon steel sheet to AA6056-T4 by resistance spot welding and adhesive weld bounding*. *110*(September 2023), 70–81. https://doi.org/10.1016/j.jmapro.2023.12.049

Rathore, D. K., Singh, B. P., Mohanty, S. C., Prusty, R. K., & Ray, B. C. (2016). Temperature dependent reinforcement efficiency of carbon nanotube in polymer composite. *Composites Communications*, *1*, 29–32. https://doi.org/10.1016/j.coco.2016.08.002

Razavi, S. M. J., Esmaeili, E., Samari, M., & Razavi, S. M. R. (2018). Stress analysis on a non-flat zigzag interface bonded joint. *Journal of Adhesion*, *94*(3), 199–217. https://doi.org/10.1080/00218464.2016.1257942

Razavi, S. M. J. J., Ayatollahi, M. R., Nemati Giv, A., Khoramishad, H., Giv, A. N., Khoramishad, H., Nemati Giv, A., & Khoramishad, H. (2018). Single lap joints bonded with structural adhesives reinforced with a mixture of silica nanoparticles and multi walled carbon nanotubes. *International Journal of Adhesion and Adhesives*, *80*(October 2017), 76–86. https://doi.org/https://doi.org/10.1016/j.ijadhadh.2017.10.007

Rispler, A., Tong, L., Steven, G., & Wisnom, M. (2000). Shape optimisation of adhesive fillets. Int J Adhes Adhes 20:221. *International Journal of Adhesion and Adhesives*, *20*, 221–231. https://doi.org/10.1016/S0143-7496(99)00047-0

Rodríguez, R., Pérez, B., & Flórez, S. (2014). Effect of different nanoparticles on mechanical properties and curing behavior of thermoset polyurethane adhesives. *Journal of Adhesion*, *90*(10), 848–859. https://doi.org/10.1080/00218464.2014.893509

Rong, M. Z., Zhang, M. Q., & Ruan, W. H. (2006). *Surface modification of nanoscale fillers for improving properties of polymer nanocomposites : a review*. *22*(7), 787–796. https://doi.org/10.1179/174328406X101247

Saba, N., Alothman, O. Y., Almutairi, Z., & Jawaid, M. (2019). Magnesium hydroxide reinforced kenaf fibers/epoxy hybrid composites: Mechanical and thermomechanical properties. *Construction and Building Materials*, *201*(2019), 138–148. https://doi.org/10.1016/j.conbuildmat.2018.12.182

Saeed, M. B., & Zhan, M. S. (2007). Adhesive strength of nano-size particles filled thermoplastic polyimides. Part-I: Multi-walled carbon nano-tubes (MWNT)-polyimide composite films. *International Journal of Adhesion and Adhesives*, *27*(4), 306–318. https://doi.org/10.1016/j.ijadhadh.2006.06.001

Saleema, N., Sarkar, D. K., Paynter, R. W., Gallant, D., & Eskandarian, M. (2012). Applied Surface Science A simple surface treatment and characterization of AA 6061 aluminum alloy surface for adhesive bonding applications. *Applied Surface Science*, *261*, 742–748. https://doi.org/10.1016/j.apsusc.2012.08.091

Salom, C., Prolongo, M. G., Toribio, A., Martínez-Martínez, A. J., de Cárcer, I. A., & Prolongo, S. G. (2018). Mechanical properties and adhesive behavior of epoxy-graphene nanocomposites. *International Journal of Adhesion and Adhesives*, *84*, 119–125. https://doi.org/10.1016/j.ijadhadh.2017.12.004

Shadlou, S., Ahmadi-Moghadam, B., & Taheri, F. (2014). Nano-enhanced adhesives: A critical review. *Reviews of Adhesion and Adhesives*, *2*(3), 371–412. https://doi.org/10.7569/RAA.2014.097307

Shang, X., Marques, E. A. S., Machado, J. J. M., Carbas, R. J. C., Jiang, D., & Silva, L. F. M. (2019). Review on techniques to improve the strength of adhesive joints with composite adherends. *Composites Part B*, *177*(August), 107363.

https://doi.org/10.1016/j.compositesb.2019.107363

Shoja, R., & Reza, G. (2011). Laser Surface Treatments of Aluminum Alloys. *Recent Trends in Processing and Degradation of Aluminium Alloys*, *January*. https://doi.org/10.5772/18451

Silva, Lucas F M. (2011). Handbook of Adhesion Technology. In *Handbook of Adhesion Technology*. https://doi.org/10.1007/978-3-642-01169-6

Subramanian, A. S., Tey, J. N., Zhang, L., Ng, B. H., Roy, S., Wei, J., & Hu, X. M. (2016). Synergistic bond strengthening in epoxy adhesives using polydopamine/MWCNT hybrids. *Polymer*, *82*, 285–294. https://doi.org/10.1016/j.polymer.2015.11.031

Sydor, M., Mirski, R., Stuper-Szablewska, K., & Rogoziński, T. (2021). Efficiency of machine sanding of wood. *Applied Sciences (Switzerland)*, *11*(6), 1–12. https://doi.org/10.3390/app11062860

Tang, L. C., Wan, Y. J., Peng, K., Pei, Y. B., Wu, L. Bin, Chen, L. M., Shu, L. J., Jiang, J. X., & Lai, G. Q. (2013). Fracture toughness and electrical conductivity of epoxy composites filled with carbon nanotubes and spherical particles. *Composites Part A: Applied Science and Manufacturing*, *45*, 95–101. https://doi.org/10.1016/j.compositesa.2012.09.012

Tang, S., Zou, P., Xiong, H., & Tang, H. (2008). Effect of nano-SiO2 on the performance of starch/polyvinyl alcohol blend films. *Carbohydrate Polymers*, *72*(3), 521–526. https://doi.org/10.1016/j.carbpol.2007.09.019

Tangthana-umrung, K., Zhang, X., & Gresil, M. (2022). Synergistic toughening on hybrid epoxy nanocomposites by introducing engineering thermoplastic and carbon-based nanomaterials. *Polymer*, *245*(March), 124703. https://doi.org/10.1016/j.polymer.2022.124703

Taylor, A. C. (2011). *55 Adhesives with Nanoparticles*. https://doi.org/10.1007/978-3-642-01169-6

Tiwari, S. K., Sahoo, S., Wang, N., & Huczko, A. (2020). Graphene research and their outputs: Status and prospect. *Journal of Science: Advanced Materials and Devices*, *5*(1), 10–29. https://doi.org/10.1016/j.jsamd.2020.01.006

Tutunchi, A., Kamali, R., & Kianvash, A. (2015a). Adhesive strength of steel–epoxy composite joints bonded with structural acrylic adhesives filled with silica nanoparticles. *Journal of Adhesion Science and Technology*, *29*(3), 195–206. https://doi.org/10.1080/01694243.2014.981469

Tutunchi, A., Kamali, R., & Kianvash, A. (2015b). Steel-Epoxy Composite Joints Bonded with Nano- TiO 2 Reinforced Structural Acrylic Adhesive Steel-Epoxy Composite Joints Bonded. *GADH*, *91*(9), 663–676. https://doi.org/10.1080/00218464.2014.961187

Tutunchi, A., Kamali, R., & Kianvash, A. (2016). Effect of Al2O3 nanoparticles on the steel-glass/epoxy composite joint bonded by a two-component structural acrylic adhesive. *Soft Materials*, *14*(1), 1–8. https://doi.org/10.1080/1539445X.2014.1003269

V. Natu, A., R. Sharma, A., & R. Anekar, N. (2019). Variation of Adhesive Strength in Single Lap Joint (SLJ) with Surface Irregularities. *American Journal of Mechanical Engineering*, *7*(2), 61–67. https://doi.org/10.12691/ajme-7-2-2

Vallée, T., & Albiez, M. (2021). Building and construction steel and aluminium. In *Adhesive Bonding: Science, Technology and Applications*. https://doi.org/10.1016/B978-0-12-819954-1.00019-8

van Dam, J. P. B., Abrahami, S. T., Yilmaz, A., Gonzalez-Garcia, Y., Terryn, H., & Mol, J. M. C. (2020). Effect of surface roughness and chemistry on the adhesion and durability of a steel-epoxy adhesive interface. *International Journal of Adhesion and Adhesives*, *96*(October 2019), 102450. https://doi.org/10.1016/j.ijadhadh.2019.102450

Wagih, A., Hashem, M., & Lubineau, G. (2022). Simultaneous strengthening and toughening of composite T-joints by microstructuring the adhesive bondline. *Composites Part A: Applied Science and Manufacturing*, *162*, 107134. https://doi.org/https://doi.org/10.1016/j.compositesa.2022.107134

Wan, H., Min, J., Lin, J., Carlson, B. E., & Maddela, S. (2021). Effect of laser spot overlap ratio on surface characteristics and adhesive bonding strength of an Al alloy processed by nanosecond pulsed laser. *Journal of Manufacturing Processes*, *62*(January), 555–565. https://doi.org/10.1016/j.jmapro.2020.12.055

Wang, T., Lei, C., Dalton, A., Creton, C., Lin, yi, Fernando, K., Sun, Y.-P., Manea, M., Asua, J. M., & Keddie, J. (2006). Waterborne, Nanocomposite Pressure-Sensitive Adhesives with High Tack Energy, Optical Transparency, and Electrical Conductivity. *Advanced Materials*, *18*, 2730–2734. https://doi.org/10.1002/adma.200601335

Wang, Z., Jia, Z., Feng, X., & Zou, Y. (2018). Graphene nanoplatelets/epoxy composites with excellent shear properties for construction adhesives. *Composites Part B: Engineering*, *152*, 311–315. https://doi.org/10.1016/j.compositesb.2018.08.113

Wei, J., Atif, R., Vo, T., & Inam, F. (2015). Graphene Nanoplatelets in Epoxy System: Dispersion, Reaggregation, and Mechanical Properties of Nanocomposites. *Journal of Nanomaterials*, *2015*. https://doi.org/10.1155/2015/561742

Wei, Y., Jin, X., Luo, Q., Li, Q., & Sun, G. (2024). Jo ur na l P re r f. *Composites Part B*, 111225. https://doi.org/10.1016/j.compositesb.2024.111225

Yadav, S. K., & Cho, J. W. (2013). Functionalized graphene nanoplatelets for enhanced mechanical and thermal properties of polyurethane nanocomposites. *Applied Surface Science*, *266*, 360–367. https://doi.org/10.1016/j.apsusc.201

Yadollahi, M., Barkhordari, S., Gholamali, I., & Farhoudian, S. (2015). Effect of nanofillers on adhesion strength of steel joints bonded with acrylic adhesives. In *Science and Technology of Welding and Joining* (Vol. 20, Issue 5, pp. 443–450). https://doi.org/10.1179/1362171815Y.0000000037

Yang, S. Y., Lin, W. N., Huang, Y. L., Tien, H. W., Wang, J. Y., Ma, C. C. M., Li, S. M., & Wang, Y. S. (2011). Synergetic effects of graphene platelets and carbon nanotubes on the mechanical and thermal properties of epoxy composites. *Carbon*, *49*(3), 793–803. https://doi.org/10.1016/j.carbon.2010.10.014

Yang, Y. (2015). *Stress Analysis and Failure Prediction of Adhesively Bonded Single-lap Laminates Joints Subjected to the Tensile Loading*. *9*(11), 19–28. https://doi.org/10.14257/ijsh.2015.9.11.03

Yue, L., Pircheraghi, G., Monemian, S. A., & Manas-Zloczower, I. (2014). Epoxy composites with carbon nanotubes and graphene nanoplatelets – Dispersion and synergy effects. *Carbon*, *78*, 268–278. https://doi.org/10.1016/j.carbon.2014.07.003

Zhai, L. L., Ling, G. P., & Wang, Y. W. (2008). Effect of nano-Al2O3 on adhesion strength of epoxy adhesive and steel. *International Journal of Adhesion and Adhesives*, *28*(1–2), 23–28. https://doi.org/10.1016/j.ijadhadh.2007.03.005

Zhang, C., Sun, L., Huang, B., Yang, X., Chu, Y., & Zhan, B. (2019). Electrical and mechanical properties of CNT/CB dual filler conductive adhesives (DFCAs) for automotive multi-material joints. *Composite Structures*, *225*(June), 111183. https://doi.org/10.1016/j.compstruct.2019.111183

Zhang, X. M., Yang, X. L., & Wang, K. Y. (2019). Electrical Conductivity Enhancement of Epoxy by Hybrid Carbon Nanotubes and Self-made Silver Nanoparticles. *Fibers and Polymers*, *20*(7). https://doi.org/10.1007/s12221-019-8640-6

Zhang, X., Su, J., Feng, Z., Liu, H., Xia, H., Zhang, Z., Tan, C., Chen, B., & Song, X. (2023). Effect of laser textured patterns on the interfacial characteristics and mechanical properties of 6061Al/GFRTP joints via hot-pressing. *Thin-Walled Structures*, *189*(March), 110916. https://doi.org/10.1016/j.tws.2023.110916

Zhao, S., Schadler, L. S., Duncan, R., Hillborg, H., & Auletta, T. (2008). Mechanisms leading to improved mechanical performance in nanoscale alumina filled epoxy. *Composites Science and Technology*, *68*(14), 2965–2975. https://doi.org/10.1016/j.compscitech.2008.01.009

Zhou, H., Liu, H.-Y., Zhou, H., Zhang, Y., Gao, X., & Mai, Y.-W. (2016). On adhesive properties of nano-silica/epoxy bonded single-lap joints. *Materials & Design*, *95*, 212–218. https://doi.org/10.1016/j.matdes.2016.01.055

Zhou, Z., & Chen, C. (2024). Research advances in the ultrasonic–assisting adhesive bonding. *Journal of Manufacturing Processes*, *110*(December 2023), 134–160. https://doi.org/10.1016/j.jmapro.2023.12.050

Zou, Y., Satou, R., Yamazaki, O., & Xie, H. (2021). Development of a new finishing process combining a fixed abrasive polishing with magnetic abrasive finishing process. *Machines*, *9*(4), 1–14. https://doi.org/10.3390/machines9040081

APPENDICES

Appendix A: Safety data sheet All-purpose component A

Title: Material safety data sheet

Appendix B: Safety data sheet All-purpose component B

Title: Material safety data sheet

REPUBLIC CHEMICAL INDUSTRIES, INC.	SAFETY DATA SHEET (SDS) ALL PURPOSE EPOXY -component A	Revision Number	05
		Revision Date	09/29/17
		Issue Date	09/30/17
		Page Number	Page 1 of 8

SECTION 1: IDENTIFICATION OF THE SUBSTANCE/MIXTURE AND OF THE SUPPLIER

Product Name:	**ALL PURPOSE EPOXY-component A**
Alternative Name/Variants:	Epoxy adhesive
Product Description:	Pioneer All Purpose Epoxy is a two component multipurpose thermosetting plastic material. It will form chemical bonds in many rigid materials like glass-glass, glass-metal, and some metal-metal joints. It is also applicable to joints between these materials and ceramic, concrete, wood and plastics (except PVC, Teflon and Kel-F).
Manufacturer Name:	**Pioneer Adhesives Inc.**
Address:	#127 Progress Avenue, Carmelray Industrial Park 1, Canlubang, Calamba, Laguna, 4037
Telephone Number:	+632 721 5781/ +632 414 1593-95/1800-1888-6263
Emergency Hotline:	+632 488 9999
Fax Number:	+632 414 1596
Website:	www.repchem.com

SECTION 2: HAZARDS IDENTIFICATION

Hazard Class/Symbol	Hazard Category	Signal Word	Hazard Statement
 **Signal word: WARNING**			
a. PHYSICAL HAZARDS			
-none	N/A	N/A	N/A
b. HEALTH HAZARDS			
Acute Toxicity-Oral	Not Classified	N/A	N/A
Acute Toxicity-Dermal	Not Classified	N/A	N/A
Skin Corrosion/Irritation	2	Warning	Causes skin irritation
Serious Eye Damage/Eye Irritation	2B	Warning	Causes eye irritation
Respiratory/Skin Sensitization	1	Warning	May cause an allergic skin reaction
Germ Cell Mutagenecity	Classification not possible		
Carcinogenecity	Classification not possible		
Reproductive Toxicity	Classification not possible		
STOT-Single exposure	Classification not possible		
STOT-Repeated Exposure	Classification not possible		
Aspiration Hazard	Classification not possible		
c. ENVIRONMENTAL HAZARDS			
Hazardous to the Aquatic Environment-Chronic	Not Classified	N/A	N/A
Hazardous to the Ozone layer	Classification not possible		

Continue on the next page

PRECAUTIONARY STATEMENTS:

PREVENTION

Wash skin thoroughly after handling.
Wear protective gloves/clothing/eye and face protection.
Avoid breathing fumes.
Contaminated work clothing should not be allowed out of the workplace.

RESPONSE

If on skin or hair: Wash with plenty of soap and water. Take off contaminated clothing and wash before re-use. If skin irritation or rash occurs, get medical attention
If in eyes: Rinse cautiously with water for several minutes. Remove contact lenses, if present and easy to do. Continue rinsing. If eye irritation persists, get medical advice/attention.
Collect spillage.

STORAGE

Store in a well-ventilated place. Keep cool.
Store locked up.

DISPOSAL

Dispose of contents according to local regulations.

SECTION 3: COMPOSITION/INFORMATION ON INGREDIENTS

Chemical Name/Trade name/Brand name	Chemical Abstract Service (CAS) number	Concentration (%) by mass/volume
Calcium Carbonate	1317-65-3	<70%
Propane, 2,2-bis[p-(2,3-epoxypropoxy)phenyl]-, polymers	25085-99-8	<30%

SECTION 4: FIRST AID MEASURES

Description of necessary first aid measures

Eyes:	Flush eyes thoroughly with water for several minutes. Remove contact lenses after the initial 1-2 minutes and continue flushing for several additional minutes. If effects occur, consult a physician, preferably an ophthalmologist. Suitable emergency eye wash facility should be available in work area.
Skin:	Wash skin with soap and water. Remove and isolate contaminated clothing and shoes.
Inhalation:	Move victim to fresh air. Administer oxygen if breathing is difficult. Get medical assistance if cough or other symptoms occur.
Ingestion:	Rinse mouth. Do not induce vomiting. Call for medical help immediately
Most important symptoms/effects, acute and delayed	Irritation, Headache, Nausea
Indication of immediate medical attention and special treatment needed, if necessary	If seeking medical attention, provide SDS to physician. Physician should treat symptomatically.

Continue on the next page

SECTION 5: FIRE-FIGHTING MEASURES

Suitable Extinguishing media:	For small fire-use dry chemical, CO_2, water spray or regular foam. For large fire- use water spray or regular foam. Do not scatter spilled material with high-pressure water streams. Move container from fire area if it can be done without risk. Dike fire-control water for later disposal.
Specific Hazards Arising from the Chemical:	During a fire, smoke may contain the original material in addition to combustion products of varying composition which may be toxic and/or irritating. Combustion products may include and are not limited to: Phenolics, Carbon monoxide and Carbon dioxide.
Special Protective Actions for fire-fighters:	Wear self-contained respiratory protective device. Keep people away. Isolate fire and deny unnecessary entry. Use water spray to cool fire exposed containers and fire affected zone until fire is out and danger of reignition has passed. Fight fire from protected location or safe distance. Consider the use of unmanned hose holders or monitor nozzles. Immediately withdraw all personnel from the area in case of rising sound from venting safety device or discoloration of the container. Do not use direct water stream. May spread fire. Move container from fire area if this is possible without hazard. Burning liquids may be moved by flushing with water to protect personnel and minimize property damage. Water fog, applied gently may be used as a blanket for fire extinguishment. Contain fire water run-off if possible. Fire water run-off, if not contained, may cause environmental damage.

SECTION 6: ACCIDENTAL RELEASE MEASURES

Personal Precautions, protective equipment and emergency procedures
Isolate area. Keep unnecessary and unprotected personnel from entering the area. Use appropriate safety equipment.
Environmental precautions
Do not allow to enter sewers/surface or ground water.
Methods and materials for containment and cleaning up
Contain spilled material if possible.
Absorb with materials such as: Sand. Polypropylene fiber products. Polyethylene fiber products. Remove residual with soap and hot water. Collect in suitable and properly labeled containers. Residual can be removed with solvent. Solvents are not recommended for clean-up unless the recommended exposure guidelines and safe handling practices for the specific solvent are followed.

SECTION 7: HANDLING AND STORAGE

Precautions for Safe Handling
Avoid prolonged or repeated contact with skin. Avoid contact with eyes, skin, and clothing. Wash thoroughly after handling. Avoid use of electric band heaters.
Conditions for safe storage, including any incompatibilities
Store in a cool location. Keep away from food and beverages. Protect from freezing and physical damage. Provide ventilation for containers. Keep container tightly sealed. Store away from incompatible materials.

Continue on the next page

SECTION 8: EXPOSURE CONTROLS/PERSONAL PROTECTION

Control Parameters
None established.

Appropriate Engineering Controls
Use local exhaust ventilation, or other engineering controls to maintain airborne levels below exposure limit requirements or guidelines. If there are no applicable exposure limit requirements or guidelines, general ventilation should be sufficient for most operations. Local exhaust ventilation may be necessary for some operations.

Individual Protection Measures (PPEs)

General protective and hygienic measures:
Keep away from foodstuffs, beverages and feed. Immediately remove all soiled and contaminated clothing. Wash hands before breaks and at the end of work. Store protective clothing separately.

Respiratory protection:
Respiratory protection should be worn when there is a potential to exceed the exposure limit requirements or guidelines. If there are no applicable exposure limit requirements or guidelines, wear respiratory protection when adverse effects, such as respiratory irritation or discomfort have been experienced, or where indicated by your risk assessment process. For most conditions, no respiratory protection should be needed; however, if material is heated or sprayed, use an approved air-purifying respirator. Use the following CE approved air-purifying respirator: Organic vapor cartridge with a particulate pre-filter, type AP2.

Protection of hands:
Protective gloves

The glove material has to be impermeable and resistant to the product. Selection of the glove material on consideration of the penetration times, rates of diffusion and the degradation.

Material of gloves
The selection of the suitable gloves does not only depend on the material, but also on further marks of quality and varies from manufacturer to manufacturer.

Penetration time of glove material
The exact break through time has to be found out by the manufacturer of the protective gloves and has to be observed.

For the permanent contact gloves made of the following materials are suitable:
Butyl rubber. Ethyl vinyl alcohol laminate ("EVAL"). Nitrile/butadiene rubber ("nitrile" or "NBR"). Neoprene. Polyvinyl chloride ("PVC" or "vinyl"). When prolonged or frequently repeated contact may occur, a glove with a protection class of 6 (breakthrough time greater than 480 minutes according to EN374) is recommended. When only brief contact is expected, a glove with a protection class of 1 or higher (breakthrough time greater than 10 minutes according to EN 374) is recommended.

Eye protection:
Safety glasses with side shields. This should be consistent with EN 166 or equivalent.

Body protection:
Protective clothing should be selected specifically for the working place, depending on concentration and quantity of the hazardous substances handled.

Continue on the next page

SECTION 9: PHYSICAL AND CHEMICAL PROPERTIES

Appearance (*physical state, color, etc)*	Pink, paste	Upper/Lower Flammability or Explosion Limits	Not Applicable
Odor	Odorless to mild	Vapor Pressure	Data not available
Odor Threshold	Data not available	Vapor Density	Data not available
pH	Data not available	Relative Density	1.90
Melting/Freezing Point	Not Applicable	Solubility	Data not available
Initial Boiling Point/Boiling Point Range	Data not available	Partition co-efficient (n-octanol/water)	Data not available
Flash Point	274°C	Auto-ignition temperature	Not Applicable
Evaporation Rate	Data not available	Decomposition temperature	Data not available
Flammability	330°C	Viscosity	1,500,000 cps

SECTION 10: STABILITY AND REACTIVITY

Reactivity	Non-reactive under normal conditions
Chemical Stability	Stable under normal conditions
Possibility of Hazardous Reactions	None under normal processing.
Conditions to Avoid	Generation of gas during decomposition can cause pressure in closed systems. Pressure build-up can be rapid.
Incompatible Materials	Strong oxidizing agents, acids, bases, unintended contact with amines
Hazardous Decomposition Products	CO and CO_2

SECTION 11: TOXICOLOGICAL INFORMATION

VARIOUS TOXICOLOGICAL HEALTH EFFECTS

Acute Toxicity	Oral: LD50> 14,000 mg/kg (rat) Dermal: LD50> 18,000 mg/kg (rat)
Skin Corrosion/irritation	Prolonged contact may cause skin irritation with local redness. Repeated contact may cause skin irritation with local redness.
Serious Eye Damage/Irritation	May cause eye irritation. Corneal injury is unlikely.
Respiratory/Skin Sensitization	Has caused allergic skin reactions in humans.
Germ Cell Mutagenicity	Data not available.
Carcinogenicity	Data not available.
Reproductive Toxicity	Data not available.
STOT-Single exposure	Evaluation of available data suggests that this material is not an STOT-SE toxicant.
STOT-Repeated exposure	Not anticipated to cause significant adverse effects.
Aspiration Hazard	Not likely to be an aspiration hazard.
ROUTES OF EXPOSURE	Data not available.

Continue on the next page

SYMPTOPMS RELATED TO PHYSICAL, CHEMICAL AND TOXICOLOGICAL CHARACTERISTICS	Data not available.
DELAYED, IMMEDIATE AND CHRONIC EFFECTS FROM SHORT AND LONG TERM EXPOSURE	Data not available.

SECTION 12: ECOLOGICAL INFORMATION

Handling Spills	Dike far ahead of liquid spill for later disposal.
Waste Treatment Practices	Dispose according to local regulations.
Summary for Toxicity and other adverse effects	

Data based on Propane, 2,2-bis[p-(2,3-epoxypropoxy)phenyl]-, polymers

Information on toxicity data from tests performed on aquatic and/or terrestrial organisms and relevant data on both acute and chronic aquatic toxicity	**Acute toxicity to fish** Material is toxic to aquatic organisms (LC50/EC50/IC50 between 1 and 10 mg/L in the most sensitive species). LC50, Oncorhynchus mykiss (rainbow trout), semi-static test, 96 Hour, 2 mg/l **Acute toxicity to aquatic invertebrates** EC50, Daphnia magna (Water flea), static test, 48 Hour, 1.8 mg/l **Acute toxicity to algae/aquatic plants** ErC50, Scenedesmus capricornutum (fresh water algae), static test, 72 Hour, Growth rate inhibition, 11 mg/l **Toxicity to bacteria** IC50, Bacteria, 18 Hour, Respiration rates., > 42.6 mg/l **Chronic aquatic toxicity** **Chronic toxicity to aquatic invertebrates** MATC (Maximum Acceptable Toxicant Level), Daphnia magna (Water flea), semi-static test, 21 d, number of offspring, 0.55 mg/l
Test Results on persistence and degredability	**Biodegradability:** Based on stringent OECD test guidelines, this material cannot be considered as readily biodegradable; however, these results do not necessarily mean that the material is not biodegradable under environmental conditions. 10-day Window: Not applicable **Biodegradation:** 12 % **Exposure time:** 28 d **Method:** OECD Test Guideline 302B or Equivalent
Test Results on bioaccumulative potential	**Bioaccumulation:** Bioconcentration potential is moderate (BCF between 100 and 3000 or Log Pow between 3 and 5). **Partition coefficient: n-octanol/water(log Pow):** 3.242 at

Continue on the next page

	25°C Estimated.
Information on Mobility from Related Mobility data	Potential for mobility in soil is low (Koc between 500 and 2000). Given its very low Henry's constant, volatilization from natural bodies of water or moist soil is not expected to be an important fate process. **Partition coefficient(Koc):** 1800 - 4400 Estimated.
Adverse effects on the environment	No further relevant information available.

SECTION 13: DISPOSAL CONSIDERATION

Disposal Containers and Methods	DO NOT DUMP INTO ANY SEWERS, ON THE GROUND, OR INTO ANY BODY OF WATER. All disposal practices must be in compliance with all Federal, State/Provincial and local laws and regulations. Regulations may vary in different locations. Waste characterizations and compliance with applicable laws are the responsibility solely of the waste generator.
Physical/Chemical Properties that may affect disposal options	No further relevant information.
Special Precautions for Incineration or Landfill	Not for sewage disposal.

SECTION 14: TRANSPORT INFORMATION

CLASSIFICATION FOR ROAD AND RAIL TRANSPORT

UN Number	Not classified
UN Proper Shipping Name	Not classified
Transport Hazard Class	N/A
Packing Number	N/A

SECTION 15: REGULATORY INFORMATION

Chemical Control Order List (CCOs)	Not listed
Priority Chemical List (PCL)	Not listed

Continue on the next page

SECTION 16: OTHER INFORMATION

The information contained in this SDS is based on our present knowledge. It is obtained from a variety of sources and is believed to be accurate and current at the stated version date. This data is provided without warranty for the use of this information, application or processing described in this SDS. Users should note the possibility of hazards occurring due to improper use of the product.

Date of preparation of the latest revision of SDS	September 29, 2017
Summary of changes from last revision:	Change in form and SDS content
Department issuing SDS:	Research and Development Department
Contact	Marketing Department

End of SDS

REPUBLIC CHEMICAL INDUSTRIES, INC.	SAFETY DATA SHEET (SDS)	Revision Number	05
	ALL PURPOSE EPOXY -component B	Revision Date	09/29/17
		Issue Date	09/30/17
		Page Number	Page 1 of 6

SECTION 1: IDENTIFICATION OF THE SUBSTANCE/MIXTURE AND OF THE SUPPLIER

Product Name:	**ALL PURPOSE EPOXY-component B**
Alternative Name/Variants:	Curing agent
Product Description:	Pioneer All Purpose Epoxy is a two component multipurpose thermosetting plastic material. It will form chemical bonds in many rigid materials like glass-glass, glass-metal, and some metal-metal joints. It is also applicable to joints between these materials and ceramic, concrete, wood and plastics (except PVC, Teflon and Kel-F).
Manufacturer Name:	**Pioneer Adhesives Inc.**
Address:	#127 Progress Avenue, Carmelray Industrial Park 1, Canlubang, Calamba, Laguna, 4037
Telephone Number:	+632 721 5781/ +632 414 1593-95/1800-1888-6263
Emergency Hotline:	+632 488 9999
Fax Number:	+632 414 1596
Website:	www.repchem.com

SECTION 2: HAZARDS IDENTIFICATION

Hazard Class/Symbol	**Hazard Category**	**Signal Word**	**Hazard Statement**
 **Signal word: WARNING**			
a. PHYSICAL HAZARDS			
-none	N/A	N/A	N/A
b. HEALTH HAZARDS			
Acute Toxicity-Oral	Not Classified		
Acute Toxicity-Dermal	*Classification not possible*		
Skin Corrosion/Irritation	Classification not possible		
Serious Eye Damage/Eye Irritation	Classification not possible		
Respiratory/Skin Sensitization	1	Warning	May cause an allergic skin reaction
Germ Cell Mutagenecity	Classification not possible		
Carcinogenecity	Classification not possible		
Reproductive Toxicity	Classification not possible		
STOT-Single exposure	Classification not possible		
STOT-Repeated Exposure	Classification not possible		
Aspiration Hazard	Classification not possible		
c. ENVIRONMENTAL HAZARDS			
Hazardous to the Aquatic Environment-Chronic	Classification not possible		
Hazardous to the Ozone layer	Classification not possible		

Continue on the next page

PRECAUTIONARY STATEMENTS:

PREVENTION

Wash skin thoroughly after handling.
Wear protective gloves/clothing/eye and face protection.
Avoid breathing fumes.
Contaminated work clothing should not be allowed out of the workplace.

RESPONSE

If on skin or hair: Wash with plenty of soap and water. Take off contaminated clothing and wash before re-use. If skin irritation or rash occurs, get medical attention
If in eyes: Rinse cautiously with water for several minutes. Remove contact lenses, if present and easy to do. Continue rinsing. If eye irritation persists, get medical advice/attention.
Collect spillage.

STORAGE

Store in a well-ventilated place. Keep cool.
Store locked up.

DISPOSAL

Dispose of contents according to local regulations.

SECTION 3: COMPOSITION/INFORMATION ON INGREDIENTS

Chemical Name/Trade name/Brand name	Chemical Abstract Service (CAS) number	Concentration (%) by mass/volume
Calcium Carbonate	1317-65-3	60-80%
Polyamide amine	Trade Secret	20-40%

SECTION 4: FIRST AID MEASURES

Description of necessary first aid measures

Eyes: Flush eyes thoroughly with water for several minutes. Remove contact lenses after the initial 1-2 minutes and continue flushing for several additional minutes. If effects occur, consult a physician, preferably an ophthalmologist. Suitable emergency eye wash facility should be available in work area.

Skin: Wash skin with soap and water. Remove and isolate contaminated clothing and shoes.

Inhalation: Move victim to fresh air. Administer oxygen if breathing is difficult. Get medical assistance if cough or other symptoms occur.

Ingestion: Rinse mouth. Do not induce vomiting. Call for medical help immediately

Most important symptoms/effects, acute and delayed Irritation, Headache, Nausea

Indication of immediate medical attention and special treatment needed, if necessary If seeking medical attention, provide SDS to physician. Physician should treat symptomatically.

Continue on the next page

SECTION 5: FIRE-FIGHTING MEASURES

Suitable Extinguishing media:	For small fire-use dry chemical, CO_2, water spray or regular foam. For large fire- use water spray, for or regular foam. Do not scatter spilled material with high-pressure water streams. Move container from fire area if it can be done without risk. Dike fire-control water for later disposal.
Specific Hazards Arising from the Chemical:	Ammonia gas may be liberated at high temperatures. In case of incomplete combustion an increased formation of oxides of nitrogen (NOx) is to be expected. Incomplete combustion may form carbon monoxide. No special precautions required. Burning produces noxious and toxic fumes.
Special Protective Actions for fire-fighters:	Wear full protective clothing, including helmet, self-contained positive pressure or pressure demand breathing apparatus, protective clothing and face mask. Ventilate closed spaces before entering them. Containers should be cooled with water to prevent vapor pressure build up. Move containers from fire area if you can do it without risk. Evacuate area and fight fire from a safe distance. Prevent runoff from fire control or dilution from entering streams, sewers or drinking water supply.

SECTION 6: ACCIDENTAL RELEASE MEASURES

Personal Precautions, protective equipment and emergency procedures

For non-emergency personnel:

No action shall be taken involving any personal risk or without suitable training. Keep unnecessary and unprotected personnel from entering. Do not touch or walk through spilled material. Put on appropriate personal protective equipment.

For emergency responders:

Avoid inhalation of vapours/spray and contact with skin and eyes. Keep people away from and upwind of spill/leak. Keep out of low areas. Ventilate closed spaces before entering them. Wear protective clothing.

Environmental precautions

Avoid dispersal of spilled material and runoff and contact with soil, waterways, drains and sewers. Inform the relevant authorities if the product has caused environmental pollution (sewers, waterways, soil or air).

Construct a dike to prevent spreading.

Methods and materials for containment and cleaning up

Small Spill: Stop leak if without risk. Move containers from spill area. Dilute with water and mop up if water-soluble. Alternatively, or if water-insoluble, absorb with an inert dry material and place in an appropriate waste disposal container. Dispose of via a licensed waste disposal contractor.

Large Spill: Stop leak if without risk. Move containers from spill area. Prevent entry into sewers, water courses, basements or confined areas. Wash spillages into an effluent treatment plant or proceed as follows. Contain and collect spillage with noncombustible, absorbent material e.g. sand, earth, vermiculite or diatomaceous earth and place in container for disposal according to local regulations. Dispose of via a licensed waste disposal contractor.

SECTION 7: HANDLING AND STORAGE

Precautions for Safe Handling

Put on appropriate personal protective equipment. Eating, drinking and smoking should be prohibited in areas where this material is handled, stored and processed. Workers should wash hands and face before eating, drinking and smoking.

Conditions for safe storage, including any incompatibilities

Store in accordance with local regulations. Store in original container protected from direct sunlight in a dry, cool and well-

Continue on the next page

ventilated area, away from incompatible materials, food and drink. Keep container tightly closed and sealed until ready for use. Containers that have been opened must be carefully resealed and kept upright to prevent leakage. Do not store in unlabeled containers. Use appropriate containment to avoid environmental contamination.

SECTION 8: EXPOSURE CONTROLS/PERSONAL PROTECTION

Control Parameters
None established.
Appropriate Engineering Controls
Good general ventilation should be sufficient to control worker exposure to airborne contaminants.
Individual Protection Measures (PPEs)
General protective and hygienic measures:
Wash hands, forearms and face thoroughly after handling chemical products, before eating, smoking and using the lavatory and at the end of the working period. Ensure that eyewash stations and safety showers are close to the workstation location.

Respiratory protection:
Use a properly fitted, air-purifying or supplied air respirator complying with an approved standard if a risk assessment indicates this is necessary. Respirator selection must be based on known or anticipated exposure levels, the hazards of the product and the safe working limits of the selected respirator.

Protection of hands:
Chemical-resistant, impervious gloves complying with an approved standard should be worn at all times when handling chemical products if a risk assessment indicates this is necessary.

Eye protection:
Safety eyewear complying with an approved standard should be used when a risk assessment indicates this is necessary to avoid exposure to liquid splashes, mists, gases or dusts. If contact is possible, the following protection should be worn, unless the assessment indicates a higher degree of protection: safety glasses with side shields.

Body protection:
Personal protective equipment for the body should be selected based on the task being performed and the risks involved and should be approved by a specialist before handling this product.

SECTION 9: PHYSICAL AND CHEMICAL PROPERTIES

Appearance (*physical state, color, etc)*	Beige, paste	Upper/Lower Flammability or Explosion Limits	Not applicable
Odor	Amine odor	Vapor Pressure	Data not available
Odor Threshold	Data not available	Vapor Density	Data not available
pH	Data not available	Relative Density	1.47
Melting/Freezing Point	Data not available	Solubility	Immiscible
Initial Boiling Point/Boiling Point Range	Data not available	Partition co-efficient (n-octanol/water)	Data not available

Continue on the next page

Flash Point	258°C	Auto-ignition temperature	Data not available
Evaporation Rate	Data not available	Decomposition temperature	Data not available
Flammability	Not applicable	Viscosity	745,000 cps

SECTION 10: STABILITY AND REACTIVITY

Reactivity	Non-reactive under normal conditions
Chemical Stability	Stable under normal conditions
Possibility of Hazardous Reactions	None under normal processing.
Conditions to Avoid	Generation of gas during decomposition can cause pressure in closed systems. Pressure build-up can be rapid.
Incompatible Materials	Strong oxidizing agents and acids
Hazardous Decomposition Products	Nitric Acid, ammonia, Nitrogen oxides, Nitric acid, Carbon monoxide, Carbon Dioxide

SECTION 11: TOXICOLOGICAL INFORMATION

VARIOUS TOXICOLOGICAL HEALTH EFFECTS

Acute Toxicity	***Acute oral toxicity***: LD50 (rat): 12,500 mg/kg
Skin Corrosion/irritation	Causes mild skin irritation.
Serious Eye Damage/Irritation	May cause eye irritation.
Respiratory/Skin Sensitization	May cause nose, throat, and lung irritation. Inhalation of vapors and/or aerosols in high concentration may cause irritation of respiratory system.
Germ Cell Mutagenicity	Data not available.
Carcinogenicity	Data not available.
Reproductive Toxicity	Data not available.
STOT-Single exposure	Data not available.
STOT-Repeated exposure	Data not available.
Aspiration Hazard	Data not available.
ROUTES OF EXPOSURE	Data not available.
SYMPTOPMS RELATED TO PHYSICAL, CHEMICAL AND TOXICOLOGICAL CHARACTERISTICS	Data not available.
DELAYED, IMMEDIATE AND CHRONIC EFFECTS FROM SHORT AND LONG TERM EXPOSURE	Data not available.

SECTION 12: ECOLOGICAL INFORMATION

Handling Spills	Dike far ahead of liquid spill for later disposal.
Waste Treatment Practices	Dispose according to local regulations.
Summary for Toxicity and other adverse effects	
Information on toxicity data from tests performed on aquatic and/or terrestrial organisms and relevant data on both acute and chronic aquatic toxicity	Data not available.

Continue on the next page

Test Results on persistence and degredability	Data not available.
Test Results on bioaccumulative potential	Data not available.
Information on Mobility from Related Mobility data	Data not available.
Adverse effects on the environment	No further relevant information available.

SECTION 13: DISPOSAL CONSIDERATION

Disposal Containers and Methods	DO NOT DUMP INTO ANY SEWERS, ON THE GROUND, OR INTO ANY BODY OF WATER. All disposal practices must be in compliance with all Federal, State/Provincial and local laws and regulations. Regulations may vary in different locations. Waste characterizations and compliance with applicable laws are the responsibility solely of the waste generator.
Physical/Chemical Properties that may affect disposal options	No further relevant information.
Special Precautions for Incineration or Landfill	Not for sewage disposal.

SECTION 14: TRANSPORT INFORMATION

CLASSIFICATION FOR ROAD AND RAIL TRANSPORT

UN Number	Not regulated
UN Proper Shipping Name	N/A
Transport Hazard Class	N/A
Packing Number	N/A
Marine Pollutant:	N/A
Environmentally Hazardous:	N/A

SECTION 15: REGULATORY INFORMATION

Chemical Control Order List (CCOs)	Not listed
Priority Chemical List (PCL)	Not listed

SECTION 16: OTHER INFORMATION

The information contained in this SDS is based on our present knowledge. It is obtained from a variety of sources and is believed to be accurate and current at the stated version date. This data is provided without warranty for the use of this information, application or processing described in this SDS. Users should note the possibility of hazards occurring due to improper use of the product.

Date of preparation of the latest revision of SDS	September 29, 2017
Summary of changes from last revision:	Change in form and SDS content
Department issuing SDS:	Research and Development Department
Contact	Marketing Department

End of SDS

Materials Today: Proceedings 51 (2022) 1437–1443

Contents lists available at ScienceDirect

Materials Today: Proceedings

journal homepage: www.elsevier.com/locate/matpr

Effect of alumina/graphene hybrid nano reinforcement to the adhesion and mechanical properties of adhesively bonded aluminum alloy with epoxy

Mohamad Syaiful Izwan Alies, Nur Zalikha Khalil *

Department of Mechanical Engineering, College of Engineering, University Malaysia Pahang Lebuhraya Tun Razak, 26300 Kuantan, Pahang, Malaysia

ARTICLE INFO

Article history:
Available online 22 December 2021

Keywords:
Adhesive joining
Hybrid nanoparticles
Mechanical properties
Adhesion properties

ABSTRACT

In present work, an attempt has been made to investigate the effect of alumina and graphene nanoplatelets (GNP) hybrid nano reinforcement to the wetting behavior and mechanical property of adhesively joint aluminum alloy with epoxy adhesive. Alumina-GNP hybrid nano adhesive at 1.0 wt% concentration with various weight ratio combination (i.e.: 10:0, 7:3, 5:5, 3:7, 0:10) was adopted into two components structural epoxy adhesive to bond 7075-T6 aluminum alloy. When compared to pristine adhesive, hybrid nano adhesive has shown two distinct trends with regard to the spread area behavior: (i) hybrid nano adhesive at 7:3 and 5:5 wt ratio combination exhibits a reduction of spread area up to 71.59 % and 48.07% respectively while (ii) hybrid nano adhesive at 3:7 wt ratio combination has shown an increase of spread up to 31.58%. It is also observed that the incorporation of hybrid nano reinforcement at 7:3 wt ratio combination has demonstrated highest shear strength up to 42.29% as compared to the pristine adhesive counterpart. Moreover, as compared to specimens with single alumina and GNP nano adhesives (i.e.: 10:0 and 0:10 wt ratio), specimens with hybrid nano adhesive at 7:3 wt ratio demonstrates an improved shear strength up to 61.48% and 101.2%, respectively. In current work, it has been observed that regardless of alumina-GNP weight ratio combination, all fractured specimens demonstrated the combination of adhesive and cohesive fractures behavior.

Selection and peer-review under responsibility of the scientific committee of the 3rd Symposium on Industrial Science and Technology 2021

1. Introduction

Adhesive bonding is one of the simplest and economical alternative which can be used for joining a wide range of materials. Adhesive bonding offers important advantages such as uniform stress transfer mechanism [1], favorable strength to weight ratio property [2], improved damage tolerance [3], aesthetics [4] while offering fewer processing requirements [5]. To date, adhesive joining has been used in many industrial applications which extend to various sectors such as aeronautics [3], electronics and packaging [4] industries. However, adhesive joining's performance is often hindered by relatively low mechanical performance as polymer adhesive is typically weaker than the adherends they join resulting in premature failure at joining ends [5]. To address this issue, researchers have proposed to incorporate nanoparticle into polymer adhesive due to its important attributes. It has been widely reported that adhesive joining utilizing nano adhesive has demonstrated superior mechanical performance as compared to joining specimens with unmodified adhesive [5–7]. The higher bonding performance in specimens with nanoadhesive is associated with nanoparticles filling into existing voids /irregularities on adherend surface which results in bonding strength improvement by mechanical interlocking [5].

Recently, the usage of graphene nanoplatelets (GNPs) as a modification agent has gained significant attention due to its ability to improve functional properties of polymeric material such as mechanical and electrical properties [8–10]. A study conducted by Gültekin et al. [11] has demonstrated that when 1.0 wt% GNP reinforcement was used in epoxy adhesive to join aluminum alloy substrate, the shear strength of the joining specimens have

---

* Corresponding author.
E-mail address: nurzalikhak@ump.edu.my (N.Z. Khalil).

https://doi.org/10.1016/j.matpr.2021.12.087
2214-7853/
Selection and peer-review under responsibility of the scientific committee of the 3rd Symposium on Industrial Science and Technology 2021

increased by 17% as compared to the joining specimens with unmodified epoxy. Similarly, Aradhana et al. [12] has also reported that the tensile shear strength of adhesive specimen has improved up to 50% with 0.5 wt% GNP inclusion as compared to joining specimens with pristine epoxy. The improvement in tensile strength can be associated to the presence of functional group of graphene oxide which may have reacted with epoxy matrix and hardener, leading to strengthening of interfacial bonding [13]. The strengthening effect is further pronounced by the efficient mechanical interlocking mechanism due to the higher surface area of graphene particles.

Alumina nanoparticle on the other hand has also been a preferred nanofiller to be incorporated into polymeric adhesive due to its advantages to such as high hardness [14], chemical inertness/stability [14] and cost effectiveness [15]. Previously, one of the authors [16] has demonstrated that the addition of alumina nanoparticles into a two-part epoxy adhesive has resulted in a considerable increment of joining strength up to 54.2% as compared to that of the pristine epoxy at 1.0 wt% content. In a different work, Gorbatkina et al. [17] have investigated the effect of 1.0 wt% inclusion of alumina into epoxy adhesive where significant improvement of bonding performance up to 9.0% was observed as compared to specimens with pristine epoxy. The higher joining strength is attributed to the increase of interfacial strength due to the improved dispersion stability of alumina nanoparticle into epoxy matrix.

From these literatures, it appears that the addition of certain amount GNP and alumina nanoparticle to epoxy-based adhesive has demonstrated significant improvement in bonding strength as compared to specimens with unmodified adhesive. This has led to the idea of introducing hybrid nanofiller into epoxy matrix to create synergetic enhancements and multi-functional features [14,18,19]. In a recent work, Razavi et al. [20] has demonstrated that the inclusion of silica nanoparticle (SNP) and multi walled carbon nanotube (MWCNT) hybrid nanofiller into epoxy adhesive has resulted in enhanced shear strength of aluminum/epoxy composite joints. In particular, the addition of 0.8 wt% SNP-MWCNT hybrid nanoadhesive at 1:1 wt ratio combination has shown improvement in joining strength up to 28.3% as compared to joining specimen with unmodified epoxy. The improvement is associated with the enhancement of load-bearing capacity for the joining specimens with hybrid SNP-MWCNT. The existence of river-like lines and rough surface of the fractured specimens also suggested that higher energy was required to separate the specimens. Furthermore, physical attributes of nanofiller such as high aspect ratio, may have also contributed to bonding strength improvement through pull-out mechanism by providing high tension to the surrounding matrix [20].

Apparently, the usage of hybrid nanofiller in epoxy system have favorable effect on the mechanical properties joining specimens Nevertheless, to best of author's knowledge, to date, the investigation regarding the effect of hybrid nanoreinforcement towards the mechanical performance of adhesive bonding is rather scarce and its underlying mechanism is not well understood. Therefore, in current work, a study has been carried out to investigate the effect of hybrid nano reinforcement to the adhesion and mechanical properties of adhesive joining. Alumina-GNP hybrid nano adhesive at 1.0 wt% concentration with various weight ratio combination (i.e.: 10:0, 7:3, 5:5, 3:7, 0:10) was adopted into two components epoxy adhesive and subsequently utilized to join aluminum adherends. Subsequently, the effect of hybrid nano reinforcement on the wetting behavior and shear strength of adhesively joined aluminum alloys with epoxy has been investigated. Finally, the fracture behavior of the adhesively bonded specimens was also presented and discussed.

2. Experimental procedures

2.1. Materials

The materials used in this study were aluminum alloys 7075-T6 adherends and two component structural epoxy adhesive (Pioneer epoxy all-purpose structural adhesive) with viscosity 800,000 cps at 25 °C, cures at 8 h supplied by Republic Chemical Industries, Inc (Quezon City, Philippines). Alumina nanoparticles and graphene nanoplatelets (GNP) supplied by Sigma Aldrich were used as the nano reinforcement particles. Fig. 1 illustrates the morphology of the as received alumina nanoparticle and GNP. The alumina nanoparticle and GNP have the average particle size of 13 nm and <2 μm, respectively.

2.2. Preparation of hybrid nano adhesive

Alumina and GNP were measured by weight according to 1.0 wt % nanoparticle content and weight ratio combination as shown in Table 1. Initially, each of alumina nanoparticle and GNP was combined with ethanol in separate beakers for 10 min at ambient temperature (25 °C) using a magnetic stirrer at 1000 rpm. Subsequently, each of the nanoparticles and ethanol solution at 1:10 wt ratio was mixed together by using magnetic stirrer for 10 min at 1000 rpm to form alumina-GNP/ethanol solution. The mixture was carried out by mechanical mixing with magnetic stirrer until both solutions are well dispersed and no visible color difference appeared. It is worth noting that the mixture of each nanoparticle was done in two steps to minimize nanoparticles agglomeration while increasing the dispersion in the solvent. Subsequently, alumina solution with graphene solution were mechanically mixed by using a magnetic stirrer until both solutions are well dispersed and no visible color difference appeared. The alumina-GNP/ethanol solution was then combined with epoxy Part A (<70% Calcium Carbonate as filler, <30 %2,2-bis[p-(2,3-epoxypropoxy) phenyl] propane) with magnetic stirrer at 3000 rpm until all the ethanol is fully evaporated. It is worth noting that the weight of the solution is continuously observed at 10 min interval to measure the weight difference and evaporation rate. The ethanol is considered fully evaporated when the evaporation rate value reaches approximately zero. Finally, the hybrid nano adhesives solution was mixed with hardener part B (<80% Calcium Carbonate as filler, <20% Polyamide amine) by using mechanical stirring for about 1 min before it was applied onto aluminum adherends.

2.3. Preparation of single lap joint specimen

Single lap joint specimens (SLJ) used in this study was fabricated according to ASTM D1002 standard as shown in Fig. 2**.** The adherends were first pre-cleansed with ethanol to eliminate existing contaminants on the surface and was then sandblasted (PanBlast™ Abrasive blasting equipment) for 60 s at a pressure of 621 kPa by using brown aluminum oxide powder with a particle size of 0.65 mm. Subsequently, the aluminum adherends were degreased with ethanol to eliminate debris residue before being dry blown with compressed air. 1 ml drop of hybrid nano adhesive was applied onto pre-treated surface of aluminum adherends by using syringe which was set on a specified height, h using. A customized fixture was utilized to cure SLJ specimens and left to fully cure for 24 h at room temperature. The joint specimens were sticked together using a 1 kg weight to maintain a constant bond line thickness [16]. All specimens are estimated to have an adhesive thickness, t_A approximately 0.86 mm ± 0.02 mm.

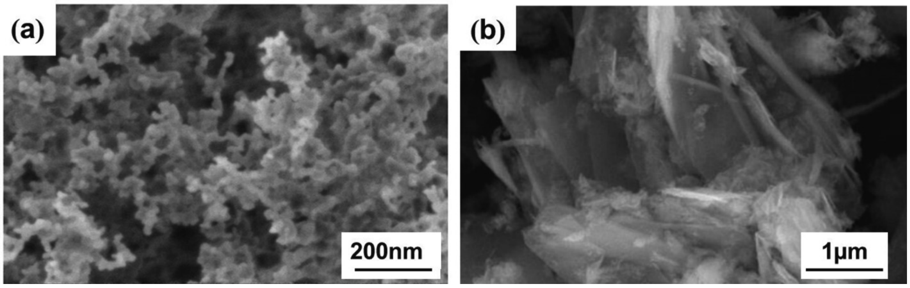

Fig. 1. SEM micrographs of as received (a) alumina nanoparticle and; (b) GNP.

Table 1
Weight ratio combination of hybrid alumina-GNP.

Weight ratio combination (wt%)	
10:0	Alumina-GNP
7:3	
5:5	
3:7	
0:10	

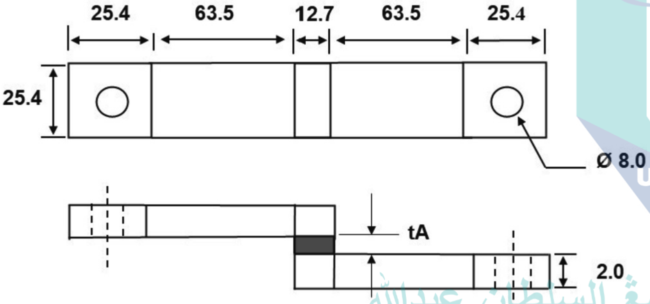

Fig. 2. Configuration of single lap joint specimen.

2.4. Wetting behavior

Spread area measurement was used to assess the wetting behavior of hybrid nano adhesive. 1 ml hybrid nano adhesive was dropped at a fixed distance, *h* = 0.5 mm from the tip syringe to the treated adherends surface as shown in Fig. 3. [16,21,22]. The initial image (after 3 min drop) was used to determine the initial spread area A_i, while the subsequence image (after 5 min drop) was used to determine the final spread area A_f. Adhesive drop images were taken using a smartphone attached with a macro lens at a fixed length from the surface of aluminum alloy, *l* = 50 mm in order to obtain clearer images. The spread area of the images was calculated using ImageJ open-source software [23] by applying spherical approximation technique [16]. Five measurements were made for each alumina-GNP hybrid nano adhesive combination to obtain an average spread area value.

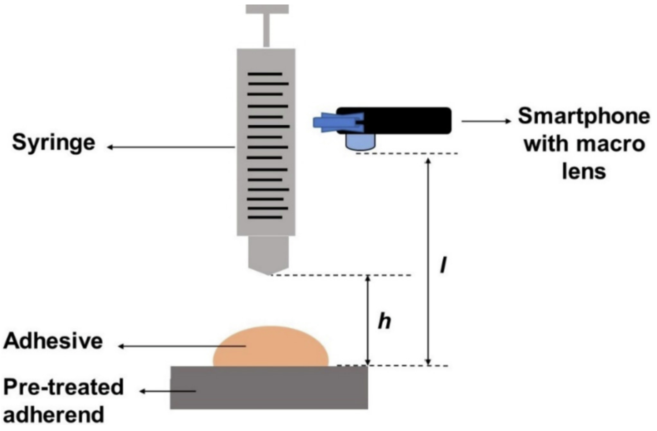

Fig. 3. Spread area measurement setup [16].

2.5. Tensile testing

SLJ specimens' strength was tested at room temperature using a Universal Instron tensile test equipment with a crosshead speed of 1.3 mm/min and a 50 kN load. To establish an average stress value, at least five sets of samples were utilized. Additional holes with 0.8 mm diameter were drilled in the grip region of the specimen (refer Fig. 2) to accommodate the geometry of a customized fixture for tensile shear testing [2,16]. It is worth noting that the usage of customized jig is aimed to minimize possible occurrence of the stress concentration and misalignment in the SLJ specimens [2,16].

3. Results and discussion

3.1. Wetting behavior

Essentially, wettability is a liquid's ability to remain contact with a solid surface. It can be measured by contact angle and spreading area of surface material [16]. Larger spreading area generally indicates a substance has a higher wetting tendency [16]. The wetting behavior was measured for the evaluation of the surface energy of solid and liquid [24]. High surface energy implies a strong molecular interaction, while low surface energy is associated with weaker attractive force between liquid and solid surface. The rise in surface energy increase the wettability and thus enhances the adhesion strength [25].

Fig. 4 shows the representative images of spread area, *A* for hybrid nanoadhesive at various weight ratio combination. The average value of *A* for each weight ratio combination was calculated using five samples of spread area measurement. From the figure, it can be seen that single alumina nanoadhesive (i.e.: 10:0 wt ratio) exhibits the highest spread area with 53.07 mm^2 ± 3.49 mm^2 which represents an increase of 187.58% as compared to pristine adhesive (i.e., 18.45 mm^2 ± 1.50 mm^2). Meanwhile, single GNP nanoadhesive (i.e.: 0:10 wt ratio) exhibits the improvement of spread area up to 30.37 mm^2 ± 4.62 mm^2 representing an increment of 64.59% when compared to pristine epoxy. From these results, it is noted that the addition of single nanoparticles has caused the increment in spread area. This might be attributed to the higher surface free energy of nanoparticle which may have caused improvement in surface interface energy resulting in

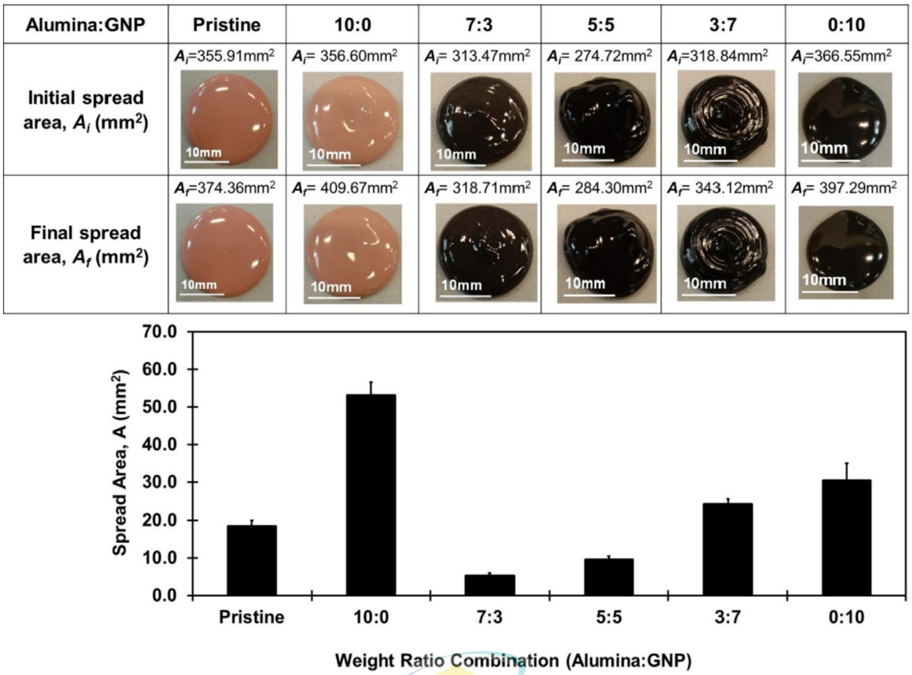

Fig. 4. Representative of spread area, *A* in epoxy adhesive at various weight ratio combination.

hydrophilic in nature and subsequence improvement in wetting behavior [16].

Furthermore, it is also noted that as compared to pristine epoxy, the spread area of hybrid nano adhesive at 7:3, 5:5 wt ratio combination demonstrated a decrease up to 71.59% and 48.07% respectively which imply poor wetting characteristic. Increment of nanoparticle loadings/combinations may have resulted in high viscosity of epoxy system which leads to poor wetting behavior [26].

Meanwhile, it is also observed that the hybrid nano adhesive at 3:7 wt ratio combination shows improvement of spread area (i.e.: 24.28 mm^2 ± 1.39 mm^2), indicating an increase of ~31.58% as compared to pristine epoxy. Possible justification for these result might be inferred by the higher difference in surface and interface free energy for nanoparticle, due to higher surface free energy for the nanoparticle [16]. Increasing the surface energy, promoting the spreading of adhesive onto the surface which in turn increase the wettability [27].

On the other hand, when compared to single alumina nano adhesive (i.e.: 10:0 wt ratio), hybrid nano adhesive at all weight ratio combinations (i.e.: 7:3, 5:5 and 3:7) demonstrates a decrease of spread area to 90.12%, 81.94%, and 54.24% respectively. Similar trend is also observed when comparing hybrid nanoadhesive at all concentrations with single GNP nanoadhesive (i.e.: 0:10 wt ratio) where decrease of spread area in the hybrid nanoadhesive at 7:3, 5:5 and 3:7 wt ratio combinations is observed to be 82.73%, 68.44%, and 20.04% respectively. This may be associated to the presence of many functional groups on the alumina-GNP surface which interact with epoxy monomers causing an imbalance of the epoxy to hardener ratio, increasing the degree of crosslinking [9] and viscosity [28] leading to poor wetting behaviour.

As a summary, in current work, there are several distinct trends observed related to the wetting characteristics of the nanoadhesive. When compared to pristine epoxy,; i) single nano adhesives (i.e.: 10:0 and 0:10 wt ratio) shows an increase of wettability while, ii) hybrid nano adhesive at 7:3 and 5:5 wt ratio combination shows decrease of wetting behavior while hybrid nanoadhesive at 3:7 wt ratio shows improvement of wettability and iii) Hybrid nanoadhesive at every weight ratio combination has demonstrated lower wetting characteristics as compared to single nanoadhesives counterpart (i.e.: 10:0 and 0:10 wt ratio). The variations might have been caused by the interplay of several possible mechanisms in the single/hybrid nanoadhesive as discussed beforehand.

3.2. Tensile shear strength and cohesive failure

Fig. 5 shows the shear strength results of SLJs specimens with hybrid nanoadhesive at various weight ratio combinations. For the purpose, five sets of samples were fabricated, all of which were tested at room temperature. From the figure, it can be observed that SLJ specimens with single alumina nano adhesive (i.e.: 10:0 wt ratio) and single GNP nano adhesive (i.e.: 0:10 wt ratio) have demonstrated shear strength of 6.23 MPa ± 0.71 MPa and 5. 0 MPa ± 0.22 MPa respectively. This corresponds to a decrease of 11.88% and 29.28% respectively as compared specimens with pristine adhesive (i.e.: 7.07 MPa ± 0.46 MPa). Previously, Meguid et al. [29] revealed that the shear strength of adhesive joints were influenced by the nanofillers content, which have significant role in the determining the strength of adhesive substrate interface. Nanofiller generally have large surface areas per unit gram which enables them to fill the any microscopic gaps present in the epoxy and substrate. As the contact point of the adhesive joints increase, the cohesive strength of the adhesive also increases, leading to higher mechanical strength of the interface through the mechanical interlocking mechanism [29]. However, there is a limit on the nanofillers content before the mechanical performance starts to deteriorate. As nanoparticle completely filled the porosities/voids, the excess nanoparticle can no longer interact effectively within the epoxy matrix resulting in poor matrix infiltration [29]. Therefore, the lower bonding strength in adhesive joining with single nano adhesive (i.e.: 10:0 and 0:10 wt ratio) as compared to pristine adhesive at 1.0 wt% content might be attributed to the excess amount of nanofillers which induce poor matrix infiltration resulting in deterioration of joining strength [29].

On the other hand, it is also observed that the SLJ specimens with hybrid nanoadhesive at 7:3 wt ratio combination, shows

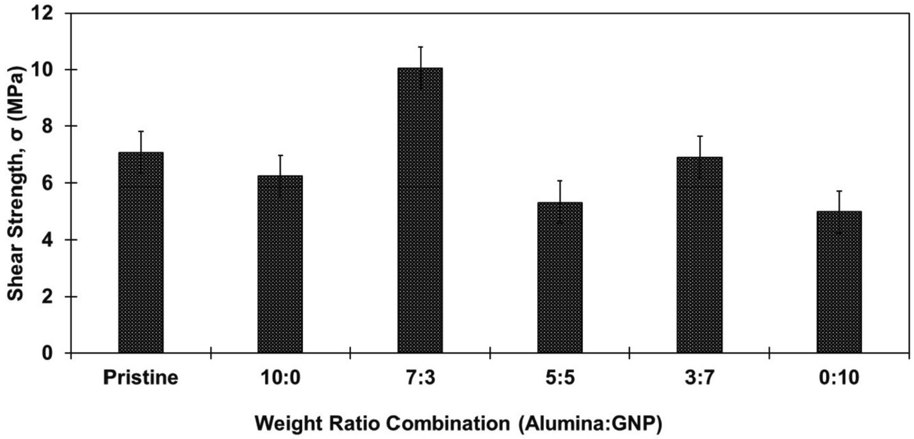

Fig. 5. Tensile shear strength of single lap joint (SLJ) specimens with various hybrid nanoadhesive weight ratio.

higher shear strength as compared specimens with pristine epoxy (i.e.: 10.06 MPa ± 0.74 MPa indicating as an increase of 42.29%. From the previous study by Osman et al. [9] it was reported that the increasing amount of alumina in the hybrid nanoadhesive ratio may have resulted in more alumina nanoparticles to be attached onto GNP surface [9,30], hence improving uniform dispersion of graphene in polymer matrix. Therefore, it is proposed that the higher mechanical strength in the joining specimens with hybrid nanoadhesive might be attributed to the higher alumina content which improve the dispersion of GNP via attachments of alumina nanoparticles. This in turn may have induced higher contact area between nanoparticles and joining adherends resulting in more efficient mechanical interlocking mechanism and improvement of interfacial adhesion. Nevertheless, further investigations are needed to verify the exact mechanism involved.

It is also observed that the shear strength of SLJ specimens with hybrid nano adhesive at 3:7 wt ratio combination indicates more or less similar shear strength results as compared to specimens with pristine epoxy (i.e.: 6.90 MPa ± 0.58 MPa). Meanwhile, at 5:5 wt ratio combination, SLJ specimens with hybrid nanoadhesive shown shear strength of 5.32 MPa ± 0.11 MPa, implying a decrease of 24.75% when compared to specimens with pristine epoxy. Razavi et al. [20] has reported that the aggregation of particles in the adhesive might have been caused by an increase of the weight percent for carbon-based nanoparticles, which results in increased surface energy and subsequent particle aggregation. The high surface energy is attributed to the high surface area and volume ratio of carbon, and therefore the van der Waals interaction between the particles may have caused them to agglomerate to minimize this energy. As a result, the presence of agglomerated GNP may have induced local stress concentration [2] leading to deterioration of joining performance.

Furthermore, when compared to SLJ specimens with single nano adhesives (i.e.: 10:0 and 0:10 wt ratio combination) specimens with hybrid nano adhesive at 7:3 wt ratio combination has demonstrated an improved shear strength up to 61.48% and 101.2% respectively. The significant improvement of shear strength in specimens with hybrid nanoadhesive might be due to the synergistic interactions amongst nanofillers combined with the formation of unique filler networks in polymer matrix [31]. In comparison to polymer systems with single nanofiller, the synergy of carbon based nanofillers in conjunction with inorganic fillers act as a modifying agent of the majority of the characteristics of hybrid polymer composites [32] which may have improved the overall mechanical performance of the joining specimens.

Fig. 6 shows the representative failure surface of the adhesively bonded SLJs specimens. In general, cohesive and adhesive failures are two typical types of failures exist on adhesive joining [2,16,33]. Adhesive failure (AF) occurs when the adhesive layer remains on both surfaces due to an interface bonding failure, while cohesive failure happens when the adhesive layer remains on both surfaces after the fracture. Cohesive failure (CF) in the substrate generally indicates that the adherend fails before the adhesive [5,34] implying a sufficient strength in the adhesive has been achieved. In Fig. 6, the red-colored regions indicate the cohesively fractured regime in the fractured specimens. By altering the color threshold of the fractured specimen's image, open-source software ImageJ was used to evaluate the failure modes in the fractured specimens. The failure mode ratios for each specimen was calculated by dividing the surface area of each failure mode by the overlap surface area [16]. From the figure, it is observed that all fractured specimens have demonstrated the existence of several fracture modes namely; adhesive fracture mode (AF), cohesive fracture mode (CF) or the combination of both modes. It is also noted that initially, SLJ specimen with pristine adhesive has demonstrated a complete AF mode (i.e.: 0% CF). However, with the utilization of nanofiller in the adhesive, it is observed that SLJ specimens has demonstrated an increment of CF mode where the highest CF mode is observed at the specimens with hybrid nano adhesive at 3:7 wt ratio combination.

Fig. 7 Summarizes the relation between shear strength and cohesive failure mode in SLJs specimen with hybrid nanoadhesive at various weight ratio combination. It is well accepted that generally, specimens with larger cohesive (CF) region is associated with higher joining strength due to the ductile characteristics between adhesive and adherends interface [2,26]. Specimen with higher CF mode region usually implies higher energy is required to cause separation in the specimens which results in improved bonding performance [35,36]. Nevertheless, in current work it is observed that the higher CF mode ratio does not corresponds to the higher shear strength in the SLJs specimens as previously discussed. The specimens which pose higher CF mode ratio may indicates the improvement in chemical interaction and surface/contact area between hybrid alumina-GNP and the epoxy matrix, which is may have resulted improvement in interphase adhesion between epoxy adhesive and joining substrate [2]. To summarize, in present work, the lack of correspondence of CF mode and shear strength might be associated with several factors which include dispersion stability of nanofiller in the epoxy matrix combined with chemical interaction between nanofiller and substrate [2]. Nevertheless, a

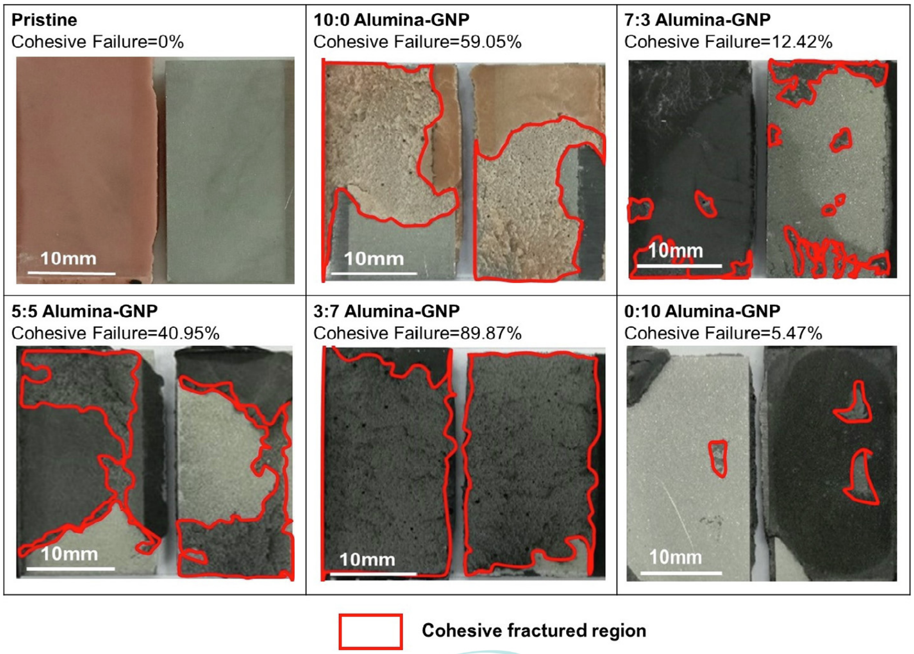

Fig. 6. Representative of fracture surface in single lap joint specimens with various hybrid nanoadhesive weight ratio.

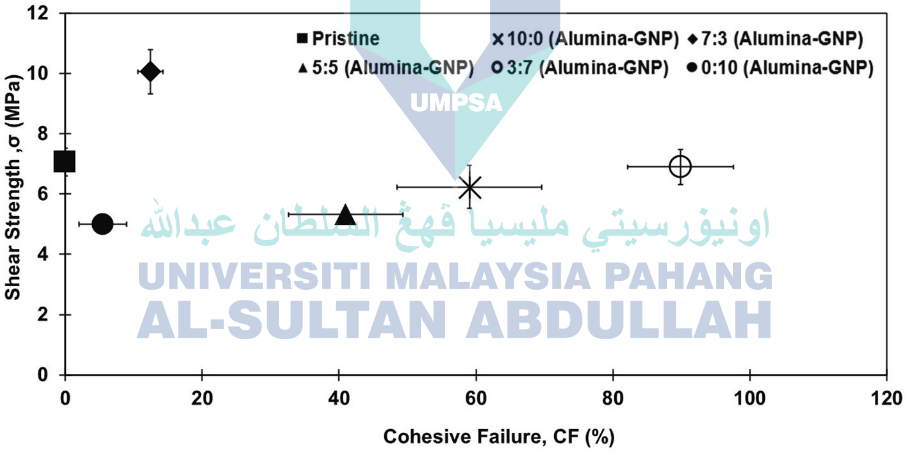

Fig. 7. Relation between shear strength and CF mode in single lap joint (SLJ) specimens at various hybrid nanoadhesive weight ratio combination.

detailed and systematic study is required to elucidate the underlying mechanism.

4. Conclusion

This study has investigated the effect of alumina and graphene nanoplatelets (GNP) hybrid nano reinforcement on the adhesion and adhesively mechanical characteristics of joined aluminum alloys with epoxy adhesive and the following findings are obtained; i) When compared to pristine adhesive, hybrid nano adhesive at 7:3 and 5:5 wt ratio exhibits a reduction of spread area up to 71.59 % and 48.07% respectively while for hybrid nano adhesive at 3:7 wt ratio spread area increased up to 31.58% ii) incorporation of hybrid nano reinforcement at 7:3 wt ratio has resulted in increased shear strength up to 42.29% as compared to pristine adhesive counterpart and iii) the failure modes in the fractured specimens show a mixture of adhesive and cohesive failure modes, regardless of the hybrid nano adhesive with weight ratio combination (i.e.: 10:0, 7:3, 5:5, 3:7, 0:10).

CRediT authorship contribution statement

Mohamad Syaiful Izwan Alies: Investigation. **Nur Zalikha Khalil:** Writing – original draft, Conceptualization, Methodology, Formal analysis, Writing – review & editing, Visualization, Supervision, Funding acquisition, Validation.

Declaration of Competing Interest

The authors declare that they have no known competing financial interests or personal relationships that could have appeared to influence the work reported in this paper.

Acknowledgement

The authors would like to thank the Ministry of Higher Education for providing financial support under Fundamental Research Grant Scheme (FRGS) no. FRGS/1/2019/TK05/UMP/02/11 (University reference RDU1901152) and Universiti Malaysia Pahang under Postgraduate Research Scheme, grant number PGRS2003181.

References

[1] A. Ghumatkar, S. Budhe, R. Sekhar, M.D. Banea, S. de Barros, Lat. Am. J. Solids Struct. 13 (2016) 2356–2370.
[2] N. Kong, N.Z. Khalil, H. Fricke, Polymers (Basel). 13 (2021) 1850.
[3] M.B. Jakubinek, B. Ashrafi, Y. Zhang, Y. Martinez-Rubi, C.T. Kingston, A. Johnston, B. Simard, Compos. Part B Eng. 69 (2015) 87–93.
[4] R. Aradhana, S. Mohanty, S.K. Nayak, Int. J. Adhes. Adhes. 84 (2018) 238–249.
[5] A. Tutunchi, R. Kamali, A. Kianvash, J. Adhes. Sci. Technol. 29 (2015) 195–206.
[6] A. Dorigato, A. Pegoretti, J. Nanoparticle Res. 13 (2011) 2429–2441.
[7] L.L. Zhai, G.P. Ling, Y.W. Wang, Int. J. Adhes. Adhes. 28 (2008) 23–28.
[8] L. Yue, G. Pircheraghi, S.A. Monemian, I. Manas-Zloczower, Carbon N. Y. 78 (2014) 268–278.
[9] A. Osman, A. Elhakeem, S. Kaytbay, A. Ahmed, Mater. Chem. Phys. 257 (2021) 123809.
[10] R. Sun, H. Yao, H. Bin Zhang, Y. Li, Y.W. Mai, Z.Z. Yu, Compos. Sci. Technol. 137 (2016) 16–23.
[11] K. Gültekin, S. Akpinar, A. Gürses, Z. Eroglu, S. Cam, H. Akbulut, Z. Keskin, A. Ozel, Compos. Part B Eng. 98 (2016) 362–369.
[12] R. Aradhana, S. Mohanty, S.K. Nayak, Polymer (Guildf). 141 (2018) 109–123.
[13] Y. Li, J. Tang, L. Huang, Y. Wang, J. Liu, X. Ge, S.C. Tjong, R.K.Y. Li, L.A. Belfiore, Compos. Part A Appl. Sci. Manuf. 68 (2015) 1–9.
[14] A. Kesavulu, A. Mohanty, J. Appl. Polym. Sci. 137 (2020) 49518.
[15] A. Kesavulu, A. Mohanty, Mater. Res. Express 6 (2019) 125329.
[16] N.Z. Khalil, M.F. Johanne, M. Ishak, Compos. Part B Eng. 172 (2019) 9–15.
[17] Y. Gorbatkina, V. Ivanova-Mumzhieva, T. Ulyanova, Polym. Sci. Ser. C 49 (2007) 131–134.
[18] P. Jojibabu, Y.X. Zhang, A.N. Rider, J. Wang, Compos. Part B Eng. 186 (2020) 107813.
[19] I. Ahmad, M. Islam, N. Al Habis, S. Parvez, J. Mater. Sci. Technol. 40 (2020) 135–145.
[20] S.M.J. Razavi, M.R. Ayatollahi, A.N. Giv, H. Khoramishad, Int. J. Adhes. Adhes. 80 (2018) 76–86.
[21] C. Zhang, L. Li, Z. Li, H. Chang, J. Liu, Int. J. Heat Mass Transf. 183 (2022) 122142.
[22] X. Dongxia, L. Xusheng, W. Caiqin, X. Bin, in: 2011 Second Int. Conf. Mech. Autom. Control Eng., 2011, pp. 1706–1708.
[23] J.-J. Han, H.-F. Tan, C. Feng, W.-K. Wee, S.-Y. Tee, S.-M. Tan, Data Br. 6 (2016) 803–810.
[24] W.S. Kang, K.Y. Rhee, S.J. Park, Compos. Part B Eng. 114 (2017) 175–183.
[25] H. Wei, J. Xia, W. Zhou, L. Zhou, G. Hussain, Q. Li, K. (Ken) Ostrikov, Compos. Part B Eng. 193 (2020) 108035.
[26] Z. Ahmadi, Prog. Org. Coatings 135 (2019) 449–453.
[27] D.M.F. Madeira, O. Vieira, L.A. Pinheiro, B. De Melo Carvalho, Int. J. Chem. Eng. (2018) 2018.
[28] J. Ashish, G. Swaroop, K. Balasubramanian, in: Q.-L. Yan, G.-Q. He, P.-J. Liu, M.B. T.-N. in: R.P.S. Gozin (Eds.), Micro Nano Technol., Elsevier, 2019, pp. 299–362.
[29] S.A. Meguid, Y. Sun, Mater. Des. 25 (2004) 289–296.
[30] M.W. Akhtar, Y.S. Lee, D.J. Yoo, J.S. Kim, Compos. Part B Eng. 131 (2017) 184–195.
[31] U. Szeluga, B. Kumanek, B. Trzebicka, Compos. Part A Appl. Sci. Manuf. 73 (2015) 204–231.
[32] S.G. Prolongo, M.R. Gude, J. Sanchez, A. Urena, J. Adhes. 85 (2009) 180–199.
[33] M. May, H.M. Wang, R. Akid, Int. J. Adhes. Adhes. 30 (2010) 505–512.
[34] S. Ebnesajjad, A.H. Landrock, Adhesives Technology Handbook, William Andrew, 2014.
[35] A. Tutunchi, R. Kamali, A. Kianvash, Soft Mater. 14 (2016) 1–8.
[36] A. Dorigato, A. Pegoretti, F. Bondioli, M. Messori, Compos. Interfaces 17 (2010) 873–892.